INFORMATION TO USERS

This dissertation was produced from a microfilm copy of the original document. While the most advanced technological means to photograph and reproduce this document have been used, the quality is heavily dependent upon the quality of the original submitted.

The following explanation of techniques is provided to help you understand markings or patterns which may appear on this reproduction.

1. The sign or "target" for pages apparently lacking from the document photographed is "Missing Page(s)". If it was possible to obtain the missing page(s) or section, they are spliced into the film along with adjacent pages. This may have necessitated cutting thru an image and duplicating adjacent pages to insure you complete continuity.

2. When an image on the film is obliterated with a large round black mark, it is an indication that the photographer suspected that the copy may have moved during exposure and thus cause a blurred image. You will find a good image of the page in the adjacent frame.

3. When a map, drawing or chart, etc., was part of the material being photographed the photographer followed a definite method in "sectioning" the material. It is customary to begin photoing at the upper left hand corner of a large sheet and to continue photoing from left to right in equal sections with a small overlap. If necessary, sectioning is continued again — beginning below the first row and continuing on until complete.

4. The majority of users indicate that the textual content is of greatest value, however, a somewhat higher quality reproduction could be made from "photographs" if essential to the understanding of the dissertation. Silver prints of "photographs" may be ordered at additional charge by writing the Order Department, giving the catalog number, title, author and specific pages you wish reproduced.

University Microfilms

300 North Zeeb Road
Ann Arbor, Michigan 48106

A Xerox Education Company

POLYNUCLEOTIDE STUDIES:

I. Cooperative Binding of Nucleosides

II. Diffusion-Controlled Renaturation

III. Dynamics of Orientational Relaxation of DNA

by

Kenneth S. Schmitz

A dissertation submitted in partial fulfillment

of the requirements for the degree of

DOCTOR OF PHILOSOPHY

UNIVERSITY OF WASHINGTON

1972

Approved by J. Michael Hahn
(Chairman of Supervisory Committee)

Department Chemistry
(Departmental Faculty Sponsoring Candidate

Date Mar 1, 1972

UNIVERSITY OF WASHINGTON

Date: February 16, 1972

We have carefully read the dissertation entitled Polynucleotide Studies: I. Cooperative Binding of Nucleosides; II. Diffusion-Controlled Renaturation; III. Dynamics of Orientational Relaxation of DNA. submitted by Kenneth S. Schmitz in partial fulfillment of the requirements of the degree of Doctor of Philosophy and recommend its acceptance. In support of this recommendation we present the following joint statement of evaluation to be filed with the dissertation.

This thesis is comprised of three distinct parts. In Part One a novel Grand Ensemble method is developed for treating the statistical thermodynamics of cooperative linear binding phenomena, and is applied to data for the binding of adenosine and guanosine by polyuridylic acid. The first determination of the strength of a purine-pyrmidine H-bond association in aqueous solution results from this numerical analysis.

In Part Two a theory for the role of orientation constraints and rotational diffusion in bimolecular solution kinetics is developed, and the viscosity dependence of overall rate constants under a variety of angular constraints is explored by numerical computation. Data for the viscosity dependence of the rate of renaturation of DNA are interpreted in terms of this model.

In Part Three a description is given of an apparatus for the detection and correlation analysis of temporal fluctuations in the intensity of scattered laser light. The theoretical relation between the correlation function for the intensity and that for the corresponding amplitudes of spontaneous fluctuations in solution is derived. This dynamic light scattering technique is employed to determine the T-dependence of the rate of relaxation of $\gamma_{2\pm1}(\Theta,\phi)$ fluctuations in the orientation of calf-thymus DNA segments in the sample through the region of its thermal transition.

DISSERTATION READING COMMITTEE: J Michael Schurr

Robert Vanderkooi

B E Eichinger

Doctoral Dissertation

In presenting this dissertation in partial fulfillment of the requirements for the doctoral degree at the University of Washington, I agree that the Library shall make its copies freely available for inspection. I further agree that extensive copying of this dissertation is allowable only for scholarly purposes. Requests for copying or reproduction of this dissertation may be referred to University Microfilms, 300 North Zeeb Road, Ann Arbor, Michigan 48106, to whom the author has granted "the right to reproduce and sell (a) copies of the manuscript in microform and/or (b) printed copies of the manuscript made from microform."

Signature Kenneth Schmitz

Date March 2, 1972

To Candace, with hope that

she might understand.

TABLE OF CONTENTS

PART I

Cooperative Binding of Nucleosides by Polynucleotides

TABLES

FIGURES

PART II

The Role of Orientation Constraints and

Rotational Diffusion in Bimolecular Solution Kinetics

TABLES

FIGURES

PART III

Dynamic Light Scattering From Solutions of

Calf Thymus DNA

TABLES

FIGURES

ACKNOWLEDGEMENTS

I wish to thank the machinists Howard Fulton, Dick Kair, and Ralph Butterfield for their help in the construction of the light scattering facility. I also want to extend thanks to Sheldon Danielson and Pete Wichern of the electronics shop for designing and building the equipment necessary for filtering and amplifying the signal, and to Ollin Barber for making the special temperature-control sample cells used in the apparatus. Special appreciation goes to Betsy Karess for proof reading the earlier sections of the dissertation. I want to express my gratitude to Mickey Schurr for the interesting, and workable, research projects that are presented in this dissertation.

And, finally, I want to thank my typist, Sharrie Myers, for the time involved in typing this dissertation.

PART I

Cooperative Binding

of Nucleosides by Polynucleotides

"I thought all the trees were whispering to each other, passing news and plots along in an unintelligible language; and the branches swayed and groped without any wind."

from The Lord of the Rings, Part I, by J.R.R. Tolkien

I. Introduction

The biological activity of a macromolecule within the living cell is dependent on the primary, secondary, and tertiary structures of the molecule.[1] The primary structure is defined as the sequential arrangement of the basic building blocks of the molecule, which are the amino acids in the case of proteins and the nucleotides in the base of the nucleic acids. The secondary structure is defined by the three dimensional conformation of the macromolecule. For example, the secondary structure of native deoxyribonucleic acid (DNA) is composed of two intertwining, right-handed helical strands of complementary polynucleotides.[2] The tertiary structure is defined as the three dimensional arrangement of a complex formed from several macromolecules.

Since the complementary strands of native DNA must separate before replication can occur, the binding forces which stabilize the secondary structure must be considerably weaker than those of the primary structure. The resistence to thermal denaturation of DNA is dependent on the base pair composition (adenine-thymine (A-T) or guanine-cytosine (G-C)) of the molecule,[3] therefore one can conclude that the binding forces between the complementary bases are not the same. Attempts to directly measure the binding interaction between complimentary base pairs in aqueous solution fail because of the predominant stacking, or hydrophobic, interaction.[4-10] Infrared and nmr studies of the base pairs in a non-aqueous media, where the stacking interaction is greatly diminished, indicate that the G-C interaction is stronger than the A-T interaction.[11-16] It is not known, however, what the effect of the solvent is on this interaction.

Although chromatographic evidence supporting the Watson-Crick pairing scheme in aqueous solution has been presented,[17] as yet no quantitative

determinations of the strength of any of these hydrogen-bond associations in aqueous solution have been made. However, Miles and coworkers,[18] and also Huang and Ts'o,[19] have independently observed the association of adenosine with polyuridylic acid in aqueous solution to form a 1:2 (purine:pyrimidine) helical structure that possesses an IR spectrum resembling that of the 2polyU + polyA helical complex in the 1500-1700 cm^{-1} range.[18] It seems intuitively apparent that the free energy for the H-bond association of the adenosine with its corresponding pyrimidines on each of the two polyU strands should be contained in the binding data along with the A-A stacking interaction energy,[19] and that this datum is potentially obtainable by appropriate analysis of the data.

In the present study, the grand ensemble formulation of the one-dimensional Ising model is extended to describe the reaction 2polymer + solute = complex. Explicit consideration is given to the sliding and loop degeneracies of the polymer particles, and the polymer-polymer interactions as well as the polymer-solute interactions. A simpler nearest-neighbor model which allows only one solute stack, hence no loop degeneracy, gives simple expressions that relate the characteristic thermodynamic parameters to data obtainable from the experimental solute binding curve. The simple model is applied to the equilibrium dialysis studies of the polyuridylic acid + adenosine,[19] polyuridylic acid + adenosine + guanosine,[20] and the polycytidylic acid + guanosine[21] systems.

II. Review

Under certain experimental conditions, the anomalous behavior of a property of a polymer solution as a function of some thermodynamic variable is attributed to a helix-coil transition of the secondary structure. Some of these properties, such as the dieletric constant,[22] electrophoretic mobility,[23] intrinsic viscosity,[24,25] volume changes of the solution,[26] changes in macroscopic film dimensions,[27] electric birefringence,[36,37] and the buoyant density in Cs_2SO_4,[28] depend on the size and shape of the complex and not on the minute details of the secondary structure. On the other hand, the inference of helical content in a system by optical measurements such as optical absorbance,[29,30] optical rotatory disperson,[31-35] optical rotation,[38] and circular dichroism,[39] is dependent on the microscopic detail of the secondary structure. For example, molecular exciton theory attributes the optical activity of a helical segment to the resonance interactions between $\pi \rightarrow \pi^*$ transitions of the amides in proteins or the bases in polynucleic acids.[40-47] Disruption of these interactions, such as in thermal denaturation, necessarily affects the optical activity of the complex. It should be pointed out that optical measurements alone may not be sufficient in detecting changes in the secondary structure. Indeed, the calorimetric detection of a thermal transition of tropocollagen in a region where the optical activity does not change implies an optically inactive stabilizing interaction other than the amide interaction.[49] Furthermore, the inability of Cassim and Yang[48] to find a crucial negative rotatory band just below the accessible range raises the question of the validity of the molecular exciton theory for explaining the optical activity of the polypeptide helix.

The introduction of hydrogen ions into a solution of polypeptides or polynucleotides induces a helix-to-coil transition of the secondary structure.[23,27,50,51] This isothermal transition is attributed to a competition for the hydrogen bonding sites which help to stabilize the helical structure. The stability of a helical segment is also strongly influenced by the presence of metal cations. These ion-polymer interactions can be specific, such as the interactions of lithium[52,53] and copper(II)[31] with the amide groups of polypeptides, or diffuse, such as the association of magnesium ions with poly(L-glutamic acid).[54] The diffuse ion-polymer interactions are those which can be explained without reference to a particular functional group on the polymer.

Polynucleotides offer two types of sites for specific interactions with ions. There are those sites located on the bases at which metal ion binding tends to destabilize the helical structure, and there are the negatively charged phosphate groups along the backbone of the molecule on which metal ion binding presumably stabilizes the helical structure. The ions of magnesium,[25,55-60] calcium,[55,60] barium,[55,60] manganese(II),[55,60-62,67] cobalt(II),[55,61,67] nickel(II)[55,61] and zinc[55] stabilize the helical DNA structure while the ions of silver,[28,63] copper(II),[31,55,60,68] cadmium,[55] lead(II)[55] and mecury(II)[24,60,64-66] destabilize the helical structure. The classification of ions as stabilizers or destabilizers is clearly a relative classification. For example, copper(II)[60,61] and iron(II)[55] act as stabilizers at low concentrations and destabilizers at higher concentrations. Furthermore, magnesium ions are also found to interact with the base moiety of 5'-ribonucleotides[69] and adenosine phosphates.[70]

Polynucleotides form complexes with nucleosides,[19-21] oligonucleotides,[71] and polynucleotides[29,36] via hydrogen bonds between the complementary purine-pyrimidine pairs. The resulting complex is either a two[19,29,36] or three[19-21,29,36] stranded helix. The thermodynamic parameters are also found to be dependent on the length of the oligomer[71,76] and the relative directions of the sugar-phosphate backbones (i.e., parallel or antiparallel).[76]

Proteins also form complexes with polynucleotides.[30,72,73] The stability of the complex is dependent on whether the polynucleotide is in a helical or random coil configuration and on the code triplet of the polypeptide. If the code triplet contains at least two identical bases, then the complex formed with a homopolymer composed of this coding base and in the random coil configuration is more stable than the complex with the polynucleotide in the helical configuration.[72] Higuchi and Tsuboi[30] suggest four different types of polynucleotide-polylysine complexes, depending on the stoichiometric lysine/nucleotide ratio. Two of the complexes involve the protein molecule wrapping itself around the double helix, either in the helical grove or across the helical grove in a zig-zag pattern, thus shielding the negative charge of the phosphate groups.

Another mode of complex formation with polynucleotides is the intercalation of a portion of the molecule between the bases of the polynucleotide.[20,75,77] In the intercalation mechanism, a portion of the binding molecule interacts with the purine or pyrimidine ring through stacking or hydrophobic interactions and not by hydrogen bonds with the bases. For example, proflavin cations rest on the flat rings of the nucleic acid bases in the complex with calf thymus DNA.[75]

The separation, or "melting," of the component strands in a multi-stranded complex does not occur simultaneously throughout the complex. As a result, loops occur in the secondary structure. The presence of loops affects the physical properties of the complex, as demonstrated by the change in viscosity on ring formation in the poly-decamethylene adipate system.[78] If the polymers are composed of repeating units, then it is possible for the strands of the complex to "slip" with respect to each other. That is, sliding degeneracy can occur if it is possible to displace a fixed configuration of loops and bonds at least one repeating unit along one of the strands in the complex.

A more detailed discussion of the factors that influence the stability of the secondary structure of polynucleotides can be found elsewhere in the literature.[55,77,79]

Since polymer systems are essentially one-dimensional systems, the combinatorial[80] and matrix[81,82] methods of calculating the partition function for one-dimensional systems with nearest-neighbor interactions have been applied directly to the polymer system. More recently, the method of sequence generating functions has been developed for systems of very long polymer chains.[83,84]

In their now classic paper, Zimm and Bragg[85] pointed out the importance of a "nucleation" parameter in describing transition curves of polypeptides. The nucleation parameter was defined as a measure of the degree of difficulty in forming a helical segment from a random coil configuration. At about the same time, Hill discussed the applicability of the generalized one-dimensional Ising model to synthetic polynucleotides, the α-helix, and DNA.[86] The simple model for polypeptide systems has since been extended to include sequences of residue types,[87]

solvent effects,[88,89] two kinds of nucleation,[90] and the kinetics of the helix-coil transition.[91-93]

A theoretical description of the melting of DNA is more complicated than the description of polypeptide melting because of the formation of loops in the secondary structure. The ring weighting factor is generally accepted to be proportional to $(j+1)^{-k}$, where j is the number of broken bonds within the loop and k is dependent on the characteristics of the polymer backbone.[94-100] For example, k has the value 1.5 for a three dimensional random flight model[94] and is estimated to be 1.75 and 2 for the self-avoiding Markovian chain[95] and for calculations of the convergence of the mean square radius of random walks subject to the excluded volume effect,[96] respectively. Klotz has shown that the slope at the midpoint of the transition curve is sensitive to the value of k, hence exact values of the nearest-neighbor interaction energy cannot be obtained unless a precise value of k is known.[101] Because of the computational time involved for very long chains, no exact calculations of the effect of the ring weighting factor have yet been published. The results of several approximate models have been published[101-106] with the general conclusion that the transition profile sharpens with increasing values of k.

The first formal treatment of the effect of different interaction energies for the A-T and G-C pairs is due to Lifson.[107] The major difficulty of the copolymer problem is not knowing the precise sequence of the base pairs in a particular DNA molecule.

Several authors have investigated the copolymer problem as either a Markov distribution,[108-110] regular repeating array,[107,110-112] or a random distribution.[110,113] At one extreme of the distribution spectrum,

where the A-T and G-C pairs alternately occur, the transition profile was found to resemble that of a homogeneous polymer. At the other extreme, where a block of A-T pairs is followed by a block of G-C pairs, the transition profile was found to have two distinct regions corresponding to the two blocks. In general, the profile of the random distribution was found to be flatter and less sharp than that of the regular distribution.[110] Reiss et al[113] discussed the meaning of a randomized sequence in detail and presented criteria for using either the geometric or arithmetic average of the A-T and G-C binding parameters. Their "blended" partition function yeilded a transition profile similar to that of a homogeneous system. They also pointed out that the breadth of the transition curve could be used to theoretically determine the composition of the DNA molecule being studied. Crothers[114] investigated the effect of the form of the partition function (i.e., "solid" lattice versus "liquid" lattice) and concluded that composition fluctuations over a large region of the molecule must be included in the randomized distribution to accurately describe the melting transition.

The first study of the binding of small molecules to proteins was due to Scatchard.[115] He proposed a model which was essentially a Bragg-Williams approximation using an average neighbor interaction with a random distribution of bound molecules. Steiner[116] developed an exact nearest-neighbor model for the titration of a polynucleotide by hydrogen ions. He found that mismatching of the strands within a helical region broadened the transition curve while the preference of the ions for the helical region sharpened the transition. The nearest-neighbor model has been extended to include the binding of oligomers[117-119] and small

molecules which aggregate in solution.[120,121]

The problem of binding molecules of intermediate chain length is conceptually no different from that of binding oligomers or polymers. It is more difficult, however, to obtain a tractable expression for the intermediate chain length problem because an exact nearest-neighbor model would lead to very large matrices and the finite length prevents one from using limiting expressions. Zimm[102] has solved the problem for finite chain lengths in terms of the eigenvalues of the generating matrix, but no calculations were presented nor were the eigenvalues related to the thermodynamic parameters of interest. It is conceivable that certain problems lend themselves to a matrix contraction similar to that of Litan.[122] Laiken and N'emethy approach the ligand binding to proteins as a Markov process with no neighbor interactions.[123]

The effect of chain length has been studied from the kinetics of nucleotide synthesis[124] and helix-coil equilibrium in two-stranded nucleic acids.[125] It was found that chain lengths above a "critical" length favored the growth of the polynucleotide chain[124] and that the degree of bonding became independent of the concentration.[125] Using the smaller chain lengths of oligomers, Applequist and Damle[126] investigated the effect of sliding degeneracy and concluded that the "all or none" model for oligomer binding is good at small chain lengths.

Other problems that have been investigated theoretically are hairpin helics,[127,128] the binding of organic cations around the DNA double helix,[129] the relationship of the cooperativity of the helix-coil transition to hydrodynamic data,[130] and the sequence-generating formalism for multi-stranded polynucleotides.[131]

III. General Description of the Polymer-Solute-Solvent Systems

The multicomponent systems under consideration in this study consist of monodisperse polymers, smaller solute particles, and solvent molecules. Any one particular system is restricted to contain only one type of polymer but may have several different types of smaller solute particles present, therefore the term "solute particles" in the remainder of the text pertains only to the smaller solute particles. In general there is no a priori restriction on the degree of aggregation between the particles in the system. For simplicity, it is assumed that the solute particles exist as monomers in solution and that the polymers aggregate only with the solute and solvent particles. Furthermore, each binding site on the polymer is assumed to be either completely solvated or bound with a solute particle.

The states of the system as a whole are divided into two classes: those states associated with the bound states of the polymer (class I); and those states pertaining to the remaining solution of solute particles (class II). A bound state of a particular binding site is defined by the type of particle bound to the site. Clearly, the bound state of the polymer is defined by the particular arrangement of the states of the sites. For a polymer of N sites, each capable of existing in L states, there are L^N polymer states (configuration states).

In order to establish equilibrium between the bound particles on the polymer (subsystem I) and the particles in solution (subsystem II), it is necessary to be able to exchange particles between these two subsystems. To avoid creating physically unreasonable holes in either subsystem, a particle that is transferred from I to II must be coupled with a transfer of a particle from II to I.

The distinguishing feature of subsystem I is the degree of aggregation that can occur. In addition to the interaction energy resulting from the association of a particle to a polymer site, there are energies of interaction arising from the neighboring bound particles. There is no restriction on the range of interaction with neighboring particles and the range may extend over the entire length of the polymer. The main objective is to calculate the partition function of all possible states for a particular system. Clearly, the complexity of the problem increases with the heterogeneity of the polymer, the number of different types of solute particles present, and the range of interaction between the bound particles.

IV. Thermodynamic Parameters for Two-State, Nearest-Neighbor Interaction System.

Consider a three component system consisting of homogeneous polymers, solute, and solvent particles. Each site on the polymer can exist in either of two states: bound with a solute particle, denoted by 0; or bound with a solvent particle, denoted by 1. There are 2^N configurations for a polymer with N sites. It is further assumed that a bound particle can only interact with adjacent bound particles.

At constant temperature and pressure, the condition for equilibrium between subsystems I and II is the equivalence of the chemical potentials for the two subsystems,

$$\mu_I(\alpha) = \mu_{II}(\alpha) \quad , \qquad (1)$$

where $\alpha = 0,1$ for solute, solvent particles, respectively. If the solution is sufficiently dilute so that the solute particles approximate Henry's Law behavior, one may write for the absolute chemical potential in II

$$\mu_{II}(\alpha) = \mu^o_{II}(\alpha) + RT\ell nX_\alpha \quad , \qquad (2)$$

where, according to Kauzmann,[132] $\mu^o_{II}(\alpha)$ is the molar chemical potential of component α which is fixed (i.e., not allowed to move) in the solution and as a consequence possesses no entropy of mixing, and X_α is the mole fraction of component α. For the present system, we have the approximations

$$\mu_{II}(0) \simeq \mu^o_{II}(0) + RT\ell nX_o \quad , \qquad (3)$$

$$\mu_{II}(1) \simeq \mu^o_{II}(1) \quad . \qquad (4)$$

The standard state of the polymer is defined as the completely solvated polymer. The free energy of binding $\bar{F}(\alpha)$ is the free energy required to transfer one mole of fixed molecules from bulk solution to single isolated sites on the polymer, as defined by the scheme

$$\vdash s + \alpha \text{ (fixed)} = \vdash \alpha + s \text{ (fixed)} \quad , \tag{5}$$

$$\bar{F}(\alpha) = [f'(\alpha) - \mu_{II}^{o}(\alpha)] + [\mu_{II}^{o}(1) - f'(1)]\, s \quad ,$$

where $\vdash$ represents the binding site and s represents the required number of solute molecules to completely solvate the site. For simplicity, we assume only one solvent particle per site. The quantities $f'(\alpha)$ and $f'(1)$ are the absolute chemical potentials of particle α and solvent, respectively, when bound to the single site.

The nearest-neighbor interaction energy is defined in terms of the scheme

$$\begin{matrix} \vdash s \\ \vdash s \end{matrix} + 2\,\alpha \text{ (fixed)} = \begin{matrix} \vdash \alpha \\ \vdash \alpha \end{matrix} + 2\, s \text{ (fixed)} \quad , \tag{6}$$

where the total free energy for this process is

$$\Delta F_a = 2[f'(\alpha) - \mu_{II}^{o}(\alpha)] + 2[\mu_{II}^{o}(1) - f'(1)] \quad , \tag{7}$$

$$+ f(\alpha|\alpha) - f(1|1) = 2\bar{F}(\alpha) + \bar{S}(\alpha,\alpha) \quad ,$$

where $$S(\alpha,\alpha) = f(\alpha|\alpha) - f(1|1) \quad .$$

The quantities $f(\alpha|\alpha)$ and $f(1|1)$ represent the additional interaction with neighboring sites under conditions of uniform bonding. Finally we must consider the effect of nearest-neighbor interaction under conditions of mixed binding according to the scheme

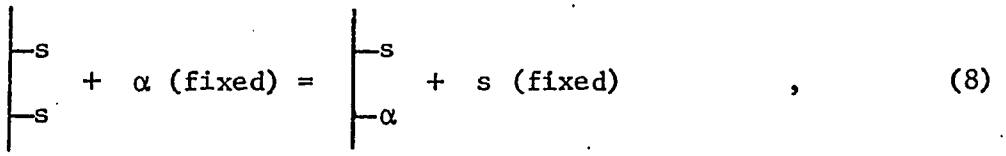

, (8)

for which we have

$$\Delta F_b = [f'(\alpha)-\mu_{II}^{o}(\alpha)] + [\mu_{II}^{o}(1)-f'(1)] + f(\alpha|1) - f(1|1) \quad , \qquad (9)$$

where $f(\alpha|1)$ is the additional interaction energy arising between neighboring sites with mixed binding. It is conceivable that $f(\alpha|1) \neq f(1|\alpha)$ for directional chains.

Eqs.(5), (7), and (9) determine the parameters of interest: the intrinsic association energy $\bar{F}(\alpha)$ of particle α; the nearest-neighbor stacking interaction energy $\bar{S}(\alpha,\alpha) = f(\alpha|\alpha)-f(1|1)$; and the mixed stacking energies $\bar{S}(\alpha,1) = f(\alpha|1)-f(1|1)$ and $\bar{S}(1,\alpha) = f(1|\alpha)-f(1|1)$. For the two-state system, the Boltzmann weighting factors are defined as

$$F_0 = \exp(-\bar{F}(0)/RT) \quad , \qquad (10)$$

$$F_1 = \exp(-\bar{F}(1)/RT) = 1 \quad , \qquad (11)$$

$$S_{00} = \exp(-\bar{S}(0,0)/RT) \quad , \qquad (12)$$

$$S_{01} = \exp(-\bar{S}(0,1)/RT) \quad , \qquad (13)$$

$$S_{10} = \exp(-\bar{S}(1,0)/RT) \quad , \qquad (14)$$

and

$$S_{11} = \exp(-\bar{S}(1,1)/RT) = 1 \quad . \qquad (15)$$

V. The Grand Partition Function for a Two-State Nearest-Neighbor Interaction System

The number of solute particles N_o and solvent particles N_1 can vary in subsystem I, but the total number of particles is subject to the constraint $N_o + N_1 = N$, where N is the total number of sites on the polymer. The grand partition function GPF(N) is defined as[133]

$$GPF(N) = \sum_{N_o=o}^{N} \exp\left(\frac{N_o \mu_I(0)}{RT}\right) \exp\left(\frac{(N-N_o)\mu_I(1)}{RT}\right) Q(N_o,N) \quad , \tag{16}$$

where $Q(N_o,N)$ is the canonical configuration interaction partition function for a system containing N_o bound solute particles, $Q(N_o,N)$ is defined by

$$Q(N_o,N) = \sum_{\alpha=o}^{1} \sum_{\beta=o}^{1} \cdots \sum_{\xi=o}^{1} \exp\left(-\frac{f_1'(\alpha)+f_{12}(\alpha|\beta)+f_2'(\beta)+f_{23}(\beta|\delta)+\ldots+f_N'(\xi)}{RT}\right), \tag{17}$$

where the summation is over all of the states of the sites, $f_i'(\omega)$ is the free energy of association of particle ω at site i and $f_{j,j+1}(\alpha|\phi)$ is the free energy of interaction of particle α at site j with particle ϕ at site j+1. Since the total number of $f'(0)$ terms that appear in Eq.(17) is N_o, the sum over N_o in the grand partition function and the constraint on the sum in $Q(N_o,N)$ can be simultaneously removed with the substitutions

$$f_i(0) \equiv f_i'(0) - \mu_I(0) \quad , \tag{18}$$

and

$$f_i(1) \equiv f_i'(1) - \mu_I(1) \quad . \tag{19}$$

Eq.(16) then becomes

$$GPF(N) = \sum_{\alpha=o}^{1} \sum_{\beta=o}^{1} \cdots \sum_{\xi=o}^{1} \exp\left(-\frac{f_1(\alpha)+f_{12}(\alpha|\beta)+f_2(\beta)+f_{23}(\beta|\gamma)+\ldots+f_N(\xi)}{RT}\right). \tag{20}$$

The subscripts on the quantities appearing in the exponent can be dropped if the individual site summations are separated. Thus, after defining the quantity

$$m(\gamma|\omega) \equiv \exp\left(-\frac{f_{i+1}(\omega) + f_{i,i+1}(\gamma|\omega)}{RT}\right) \quad , \tag{21}$$

Eq.(20) can be expressed as

$$GPF(N) = \sum_{\alpha=o}^{1} \exp\left(-\frac{f_1(\alpha)}{RT}\right)\left(\sum_{\beta=o}^{1} m(\alpha|\beta)\left(\sum_{\gamma=o}^{1} m(\beta|\gamma)\left(\ldots\left(\sum_{\xi=o}^{1} m(\pi|\xi)\right)\right)\ldots\right)\right) . \tag{22}$$

Since the order of summation can be reversed, i.e.,

$$\sum_{\beta=o}^{1} m(\alpha|\beta)\sum_{\gamma=o}^{1} m(\beta|\gamma) = \sum_{\gamma=o}^{1}\left(\sum_{\beta=o}^{1} m(\alpha|\beta)m(\beta|\gamma)\right) \quad , \tag{23}$$

Eq.(22) can be written in the form of a matrix multiplication

$$GPF(N) = \left(\exp\left(-\frac{f(0)}{RT}\right), \exp\left(-\frac{f(1)}{RT}\right)\right) \cdot \underset{\sim}{m}^{N-1} \cdot \begin{pmatrix} 1 \\ 1 \end{pmatrix} \quad , \tag{24a}$$

where the generating matrix $\underset{\sim}{m}$ is defined as

$$\underset{\sim}{m} \equiv \begin{vmatrix} m(0|0) & m(0|1) \\ m(1|0) & m(1|1) \end{vmatrix} \quad . \tag{24b}$$

Since the average number of bound solute particles $\bar{N}_o$ is related to the grand partition function by[134]

$$\bar{N}_o = RT\,\frac{\partial \ell n\ GPF(N)}{\partial \mu_I(0)} = RT\,\frac{\partial \ell n\ GPF(N)}{\partial \mu_{II}(0)} \quad , \tag{25}$$

It is clear that the term $m(1|1)$ is of no consequence to the calculation

of $\bar{N}_o$. Therefore, we can factor the quantity $m(1|1)$ from the matrix in Eq.(24a) to obtain

$$GPF(N) = \exp[-f(1)/RT][m(1|1)]^{N-1}(X_0F_0,1)\cdot\underset{\simeq}{M}^{N-1}\begin{pmatrix}1\\1\end{pmatrix}, \tag{26}$$

where the generating matrix $\underset{\simeq}{M}$ is defined as [cf., Eqs.(10) through (15)]

$$\underset{\simeq}{M} = \begin{vmatrix} X_0F_0S_{00} & S_{01} \\ X_0F_0S_{10} & 1 \end{vmatrix} . \tag{27}$$

In the limit of very long chain lengths, i.e., $N \to \infty$, the grand partition function is proportional to the Nth power of the largest eigenvalue of the generating matrix (cf., Appendix B). Thus, for the particular model under consideration, the fraction of total sites θ that are bound by solute particles is

$$\theta = \frac{\bar{N}_0}{N} = \frac{RT}{}\frac{\partial \ell n\lambda_+}{\partial \mu_{II}(0)} = \frac{\partial \ell n\lambda_+}{\partial \ell n X_0} , \tag{28}$$

where

$$\lambda_+ = \frac{(X_0F_0S_{00} + 1) + [(X_0F_0S_{00} - 1)^2 + 4X_0F_0S_{10}S_{01}]^{\frac{1}{2}}}{2} , \tag{29}$$

is the largest eigenvalue of the generating matrix defined in Eq.(27). One can easily derive the expressions

$$X_0F_0S_{00} = 1 \quad (\theta = \tfrac{1}{2}) , \tag{30}$$

$$\partial\theta/\partial \ell n X_0\big|_{\theta=\frac{1}{2}} = \frac{1}{4}\left(\frac{S_{00}}{S_{10}S_{01}}\right)^{\frac{1}{2}} , \tag{31}$$

and

$$\partial^2\theta/\partial \ell n X_0^{\,2}\big|_{\theta=\frac{1}{2}} = 0 , \tag{32}$$

from Eq.(29). In the case of dilute aqueous solutions, substitution of

$X_0=m/55$ into Eq.(30) leads to the result

$$m_{\theta=\frac{1}{2}} = \frac{55}{F_0 S_{00}} \quad , \qquad (33)$$

where $m_{\theta=\frac{1}{2}}$ is the molality of the solute at the midpoint of the binding curve. It is clear from Eqs.(31) and (33) that the midpoint concentration and the slope at the midpoint obtained from a plot of θ versus $\ln(m)$ cannot uniquely determine the four parameters F_0, S_{00}, S_{10}, and S_{01}.

The possibility that the wings of the transition contain additional information which might enable a unique selection of the parameters was investigated by numerical computations. The values of the midpoint concentration ($\cong 3\times10^{-3}$) and slope at the midpoint ($\cong 30$) were obtained from the equilibrium dialysis curve reported by Huang and Ts'o for the polyuridylic acid-adenosine system. Huang and Ts'o found that the complexes formed in this system follow the stoichiometries,

$$2\ \text{polyU} + \text{A} = \text{poly(2U+A)} \qquad (5^\circ\text{C}) \quad , \qquad (34)$$

and

$$\text{polyU} + \text{A} = \text{poly(U+A)} \qquad (20^\circ\text{C}) \quad , \qquad (35)$$

where polyU denotes polyuridylic acid and A represents adenosine.

The experimental curve at 5°C of Huang and Ts'o is presented in Figure 1 for comparison with the computed curves. The shaded area is bounded by two calculated curves employing the sets of molar energy parameters $\bar{F}(0);\bar{S}(0,0);\bar{S}(1,0) = \bar{S}(0,1)$ of -20,440;+15,000;+10,145 and +19,560;-25,000;-9,855 calories per mole, respectively. The finite width of the shaded area is a consequence of the finite chain length of 500 nucleotide units used in the calculations. It is apparent from these calculations that the midpoint concentration and the slope at the midpoint completely characterize the calculated curves for this simple model. At

Figure 1

A comparison of calculated and experimental curves. The dashed line represents the experimental data of Huang and Ts'o.[19] The shaded region includes all theoretical curves calculated from Eqs. 25 and 26 with parameters that satisfy Eqs. 30 and 31 and that lie in the range ($\bar{F}$ = -20,440, $f_{AA}-f_{ss}$ = +15,000, $f_{As}-f_{ss}$ = +10,145) to ($\bar{F}$ = +19,560, $f_{AA}-f_{ss}$ = -25,000, $f_{As}-f_{ss}$ = -9855). The width of the shaded region at the midpoint arises from the finite chain length.

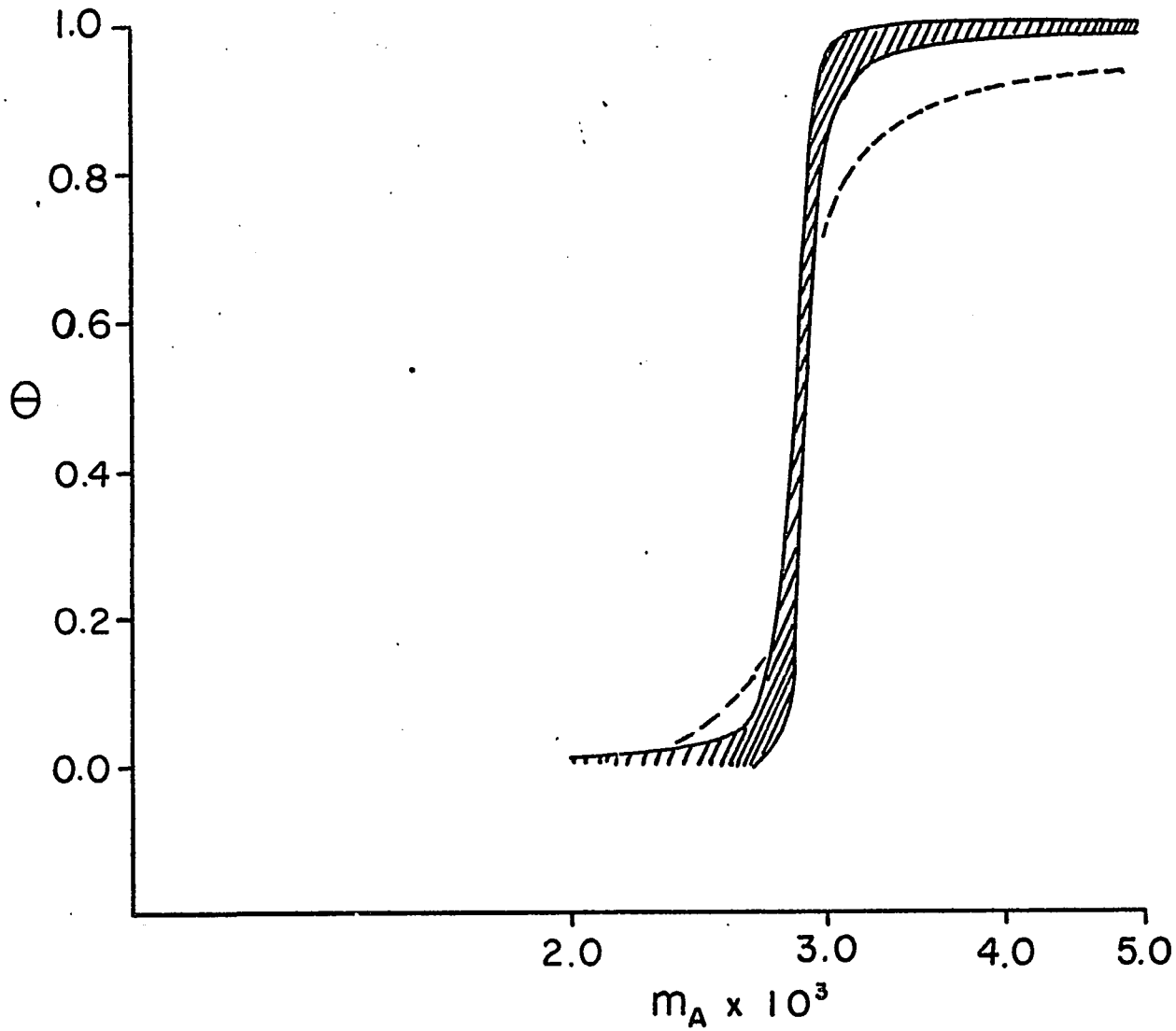
1.0
0.8
0.6
θ
0.4
0.2
0.0
2.0
3.0
4.0
5.0
$m_A \times 10^3$

this point it is assumed that $S_{01} = S_{10} = 1$, which is equivalent to the assumption that a solute particle cannot distinguish between subsystems I and II by solvent-solute interactions alone. All of the subscripts can now be dropped since the problem is reduced to a pseudo one-component system. Eqs.(31) and (33) then define the parameters S and F which characterize the binding curve

$$S = 16\left[(\partial\theta/\partial \ell nm)|_{\theta=\frac{1}{2}}\right]^2 \quad , \tag{36}$$

and

$$F = \frac{55}{Sm}\Big|_{\theta=\frac{1}{2}} \quad . \tag{37}$$

The grand partition function for the simple system becomes

$$GPF(N) = \left(\frac{mF}{55}, 1\right) \cdot \begin{vmatrix} \frac{mFS}{55} & 1 \\ \frac{mF}{55} & 1 \end{vmatrix}^{N-1} \cdot \begin{pmatrix} 1 \\ 1 \end{pmatrix} \quad , \tag{38}$$

where the quantity $\exp(-f(1)/RT)[m(1|1)]^{N-1}$ has been dropped since it does not affect the calculation of $\bar{N}_0$.

VI. Extension of the Simple Model: Inclusion of Sliding Degeneracy for a (2 Polymer + Solute)-Complex

According to the data of Haung and Ts'o,[19] two polyuridylic acid molecules form a complex with adenosine at 5°C. If the two polymer chains are in register over the entire polymer length, i.e., nucleotide i on one chain is adjacent to nucleotide i of the other chain for all $1 \leqslant i \leqslant N$, then the simple model can be directly applied to the process described by Eq.(34). In general, however, the two chains are randomly aligned. The simple model can easily be extended to include the degeneracy due to polymer alignment if the adsorption region, which is defined by the first and last bound solute particle in the complex, is in register. This condition is certainly met by one-solute-stack complexes. Therefore, a sufficient condition is that the number of solute-solute junctions within an adsorption region is much larger than the number of solute-solvent junctions. The cooperativity parameter σ is defined as the ratio of the Boltzmann weighting factors for these two types of junctions

$$\sigma = S_{10}/S_{00} \quad . \tag{39}$$

Thus, the criterion for a one-solute-stack complex is simply

$$\frac{1}{\sigma N} >> 1 \quad , \tag{40}$$

where N is the length of the polymer. If there are n sites within the adsorption region, there are N-n+1 ways of arranging the remaining sites of each polymer, or a degeneracy of $(N-n+1)^2$.

The grand partition function for this extended system is

$$GPFS(N) = 1 + \sum_{n=1}^{N} (N-n+1)^2 \left(\frac{mF}{55},0\right) \cdot \begin{vmatrix} \frac{mFS}{55} & 1 \\ \frac{mF}{55} & 1 \end{vmatrix}^{n-1} \cdot \begin{pmatrix} 1 \\ 0 \end{pmatrix} \quad . \tag{41}$$

The zeros occurring in the row and column vectors eliminate those states of n units bounded at the ends of solvent molecules. From equations (39), (36) and the assumption that $S_{01} = S_{10} = 1$, we have the identity

$$\sigma = 1/S \quad . \tag{42}$$

Huang and Ts'o report that the slope at the midpoint of the solute binding curve for the polyU + adenosine system lies between 30 and 60.[19] Using the minimum value of 30 and a chain length of 500 nucleotide units, we find

$$\frac{1}{N\sigma} = \frac{16(30)^2}{500} = 28.8 \quad . \tag{43}$$

Certainly the polyU + adenosine system meets the criterion for a one-solute-stack system.

It is now profitable to consider the ratio (GPFS(N))/GPF(N) for the states with bound solute particles in the limit of infinite chain length. Using the largest eigenvalues of the generating matrices in Eqs.(38) and (41), we have

$$[GPFS(N \to \infty)]/GPF(N \to \infty) = C_1 \sum_{n=1}^{N} (N-n+1)^2 (1/\lambda_+)^{N-n+1} \quad , \tag{44}$$

where C_1 is a function of m,F, and S and is independent of N (see Appendix B). The change of variables p = N-n+1 leads to the result

$$\frac{GPFS(N \to \infty)}{GPF(N \to \infty)} = C_1 \sum_{p=1}^{\infty} p^2 (1/\lambda_+)^p \quad . \tag{45}$$

For all cases in which $S_{01} \neq 0 \neq S_{10}$, $\lambda_+ > 1$ and the summation in Eq.(45) can be written in the functional form

$$\sum_{p=0}^{\infty} p^2 (1/\lambda_+)^p = \lambda_+(\lambda_+ + 1)/(\lambda_+ - 1)^3 \quad . \tag{46}$$

Since the ratio $(GPFS(N \to \infty))/GPF(N \to \infty)$ is finite and independent of N, substitution of $GPFS(N) \cong C_1\lambda_+(\lambda_+ + 1)GPF(N)/(\lambda_+ - 1)^3$ into the expression for θ leads to the result

$$\theta \cong \frac{\partial \ell n GPF(N\to\infty)}{\partial \ell n m} + \frac{1}{N}\ell n \frac{C_1\lambda_+(\lambda_+ + 1)}{(\lambda_+ - 1)^3} \simeq \frac{1}{N}\frac{\partial \ell n GPF(N\to\infty)}{\partial \ell n m} \quad . \tag{47}$$

A comparison of calculated curves both with and without consideration of the sliding degeneracy for two different chain lengths is presented in Figure 2. It is apparent that the effect of degeneracy decreases as the length of the chain varies from 100 units to 500 units. Therefore, the midpoint conditions defined by Eqs.(36) and (37) can be directly applied to the (2polymer+solute)-complex for very long chains.

Figure 2

A comparison of calculated curves both with and without consideration of the sliding degeneracy. (a) N = 500, no sliding degeneracy, (————————); (b) N = 500, sliding degeneracy, (-----); (c) N = 100, no sliding degeneracy, (—•—•—); (d) N = 100, sliding degeneracy, (·····). All curves computed with $\overline{F}$ = -140, $f_{AA}-f_{ss}$ = -5300, and $f_{As}-f_{ss}$ = 0 cal/mole.

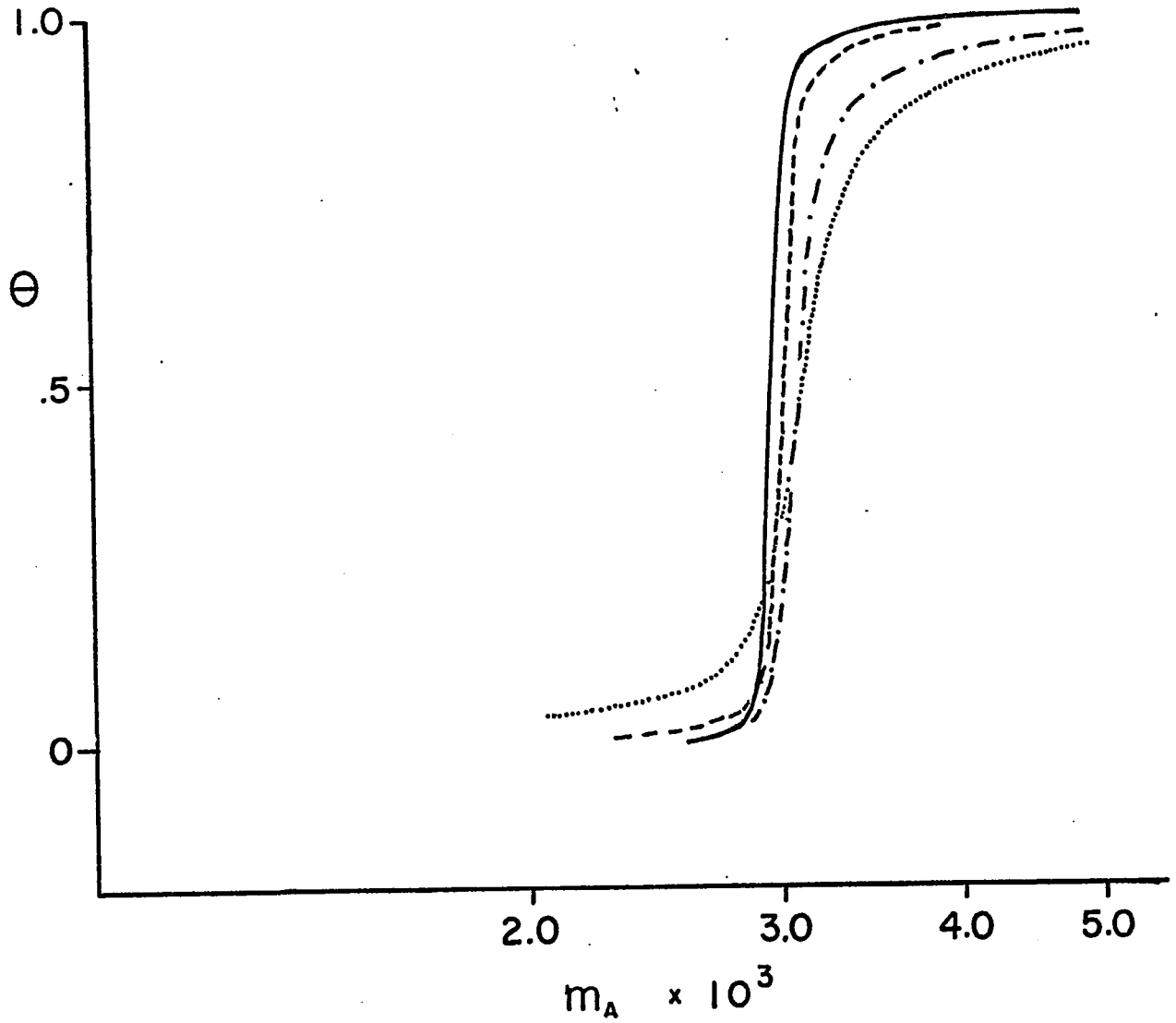
1.0
θ
.5
0
2.0
3.0
4.0
5.0
$m_A \times 10^3$

VII. Extension of the Simple Model: Inclusion of Energy Partitioning Within an Adsorption Unit in a (2Polymer + Solute)-Complex

The two-state model for an adsorption unit is not generally valid for the (2polymer + solute)-complex as described in Eq.(34). In addition to the interactions involving the solute particle A, there may also be interactions between the two polymer molecules. For example, a base on one polymer may form a bond with a base on the other polymer. Assuming a nearest-neighbor model for both the polymer-polymer interactions [denoted by (p-p)] and the polymer-solute interactions [denoted by (p-s)] the four molar energies of interest are schematically defined by

(p-p) association $\bar{P}$

, (48)

(p-p)-(p-p) nearest-neighbor interaction $\bar{W}$

, (49)

(p-s) association $\bar{B}$

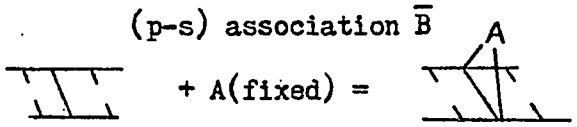

, (50)

and the (p-s)-(p-s) nearest-neighbor interaction $\bar{V}$

, (51)

where the solvent molecules are omitted for simplicity. The corresponding Boltzmann weighting factors P,W,B, and V are defined in a manner analogous to Eqs.(10) through (15). Furtheremore, the model is restricted to one-solute-stack systems. The four possible states for one adsorption unit with their respective weighting factors are given in Figure 3.

Figure 3

State	I	II	III	IV
Weighting factor	$\frac{mBP}{55}$	P	$\frac{mB}{55}$	1

The symbols m, B, and P are defined in the text.

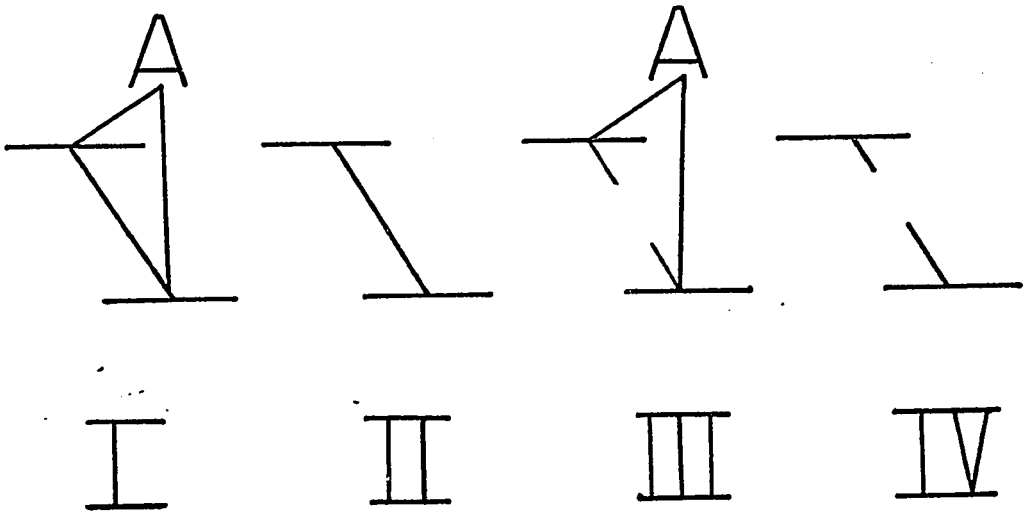
A
A
I
II
III
IV

Representative states of the adsorption region are given in Figure 4.

The grand partition function for a linear system can be calculated by a generating matrix $\underset{\simeq}{M}$ whose elements M(i,j) are the weighting factors for the addition of site k+1 in state j when site k is in state i (cf., Appendix A). In general,

$$GPFS(N) = 1 + \sum_{n=1}^{N} (n-n+1)^2 \underset{\sim}{a} \cdot \underset{\simeq}{M}^{n-1} \cdot \underset{\sim}{b}^{+} = 1 + \sum_{n=1}^{N} (N-n+1)^2 GPF(n) \quad , \tag{52}$$

where $\underset{\sim}{a}, \underset{\sim}{b}^{+}$ are the appropriate row and column vectors, respectively, whose elements reflect the basic assumptions concerning the end sites of the linear system. If the (p-p) and (p-s) sites are mutually independent of each other (i.e., no enhancement of the parameters $\overline{B}, \overline{P}, \overline{W}$, and $\overline{V}$), then all four states described in Figure 3 are accessible to an adsorption unit and the generating matrix is given by

$$\underset{\simeq}{M} = \begin{vmatrix} \frac{mBPVW}{55} & PW & \frac{mBV}{55} & 1 \\ \frac{mBPW}{55} & PW & \frac{mB}{55} & 1 \\ \frac{mBPV}{55} & P & \frac{mBV}{55} & 1 \\ \frac{mBP}{55} & P & \frac{mB}{55} & 1 \end{vmatrix} \quad . \tag{53}$$

The matrix $\underset{\simeq}{M}$ can be written as a tensor product of two matrices which generate the states of the (p-p) sites and (p-s) sites, i.e.,

$$\underset{\simeq}{M} = \begin{vmatrix} PW & 1 \\ P & 1 \end{vmatrix} \otimes \begin{vmatrix} \frac{mBV}{55} & 1 \\ \frac{mB}{55} & 1 \end{vmatrix} \quad . \tag{54}$$

Substitution of Eq.(54) into Eq.(52) leads to the result

$$GPFS(N) = 1 + \sum_{n=1}^{N} (N-n+1)^2 \underset{\sim}{a} \cdot \begin{vmatrix} PW & 1 \\ P & 1 \end{vmatrix}^{n-1} \otimes \begin{vmatrix} \frac{mBV}{55} & 1 \\ \frac{mB}{55} & 1 \end{vmatrix}^{n-1} \cdot \underset{\sim}{b}^{+} \quad , \tag{55}$$

where $\underset{\sim}{a} = (mBP/55,0,mB/55,0)$ and $\underset{\sim}{b} = (1,0,1,0)$. In the limit $n \to \infty$, the GPF(n) can be approximated by the product of the largest eigenvalues of the two generating matrices,

$$GPF(n \to \infty) \simeq (\lambda_{+_{(p-p)}} \lambda_{+_{(p-s)}})^n \quad . \tag{56}$$

Therefore, as one would expect, the solute binding curve is independent of the parameters $\overline{P}$ and $\overline{W}$ in the case of unrestricted binding.

Case 1: Restricted Solute Binding

Consider the case when (p-s) binding is allowed to occur only when (p-p) binding also occurs. In this case, the weighting factor for state III of Figure 3 is zero. According to the rules of formulating the generating matrix, the column corresponding to site k+1 in state III is composed entirely of zeros. The grand partition function is then

$$GPF(n) = \left(\frac{mBP}{55},0,0,0\right) \begin{vmatrix} \frac{mBPVW}{55} & PW & 0 & 1 \\ \frac{mBPW}{55} & PW & 0 & 1 \\ \frac{mBPV}{55} & P & 0 & 1 \\ \frac{mBP}{55} & P & 0 & 1 \end{vmatrix}^{n-1} \begin{pmatrix} 1 \\ 0 \\ 0 \\ 0 \end{pmatrix} \quad . \tag{57}$$

Since the column of zeros effectively eliminates the contribution of the corresponding row, we can substitute zeros for the elements in this row.

Figure 4

Representatives of types of configurations in the adsorption region of the 2polymer + A system

I and II are pure states (homogeneous)

III and IV are mixed states

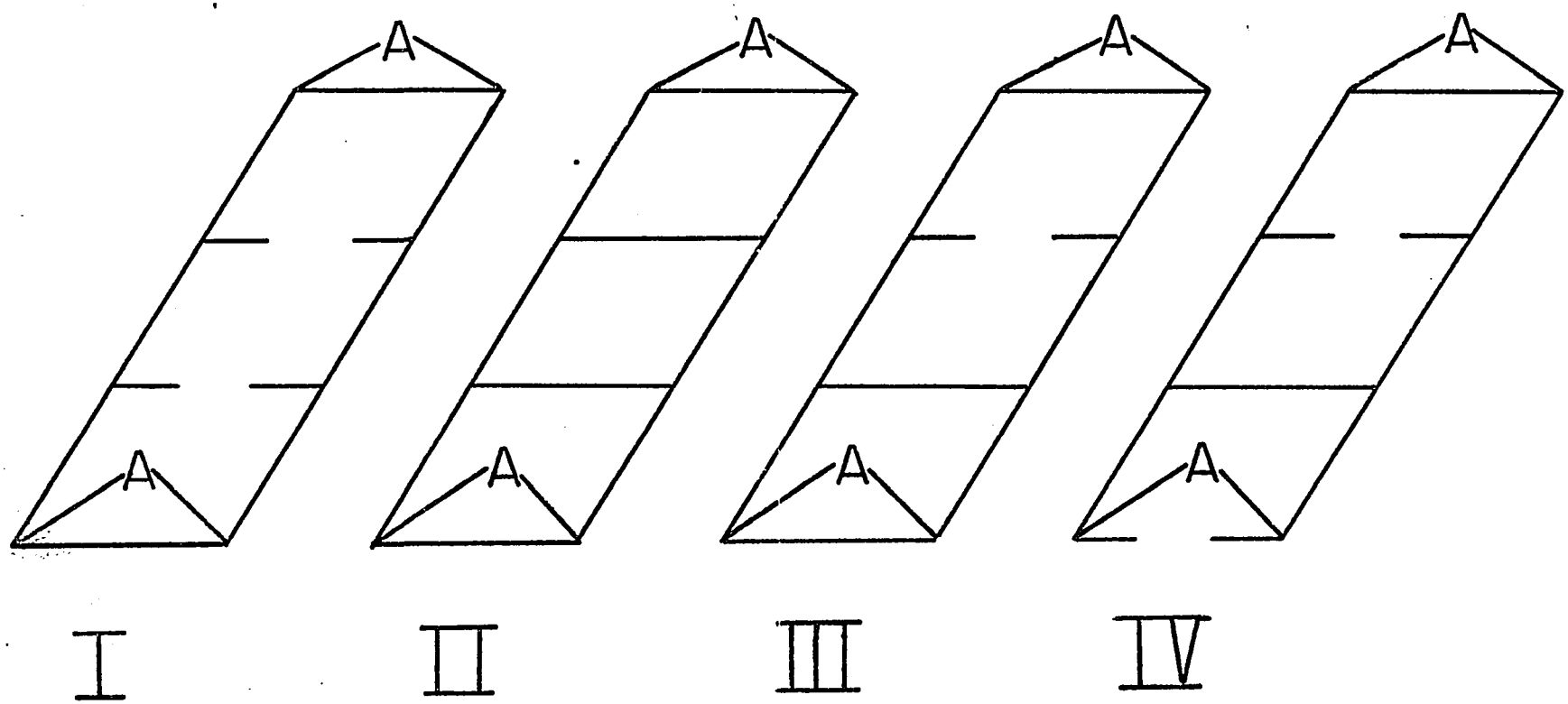
A
A
A
A
A
A
A
A
I
II
III
IV

Interchanging the columns and rows corresponding to states III and IV in Figure 3 brings the matrix $\underline{\underline{M}}$ into block diagonal form. Eq.(57) can then be written as

$$GPF(n) = \left(\frac{mBP}{55},0,0\right) \begin{vmatrix} \frac{mBPVW}{55} & PW & 1 \\ \frac{mBPW}{55} & PW & 1 \\ \frac{mBP}{55} & P & 1 \end{vmatrix}^{n-1} \begin{pmatrix} 1 \\ 0 \\ 0 \end{pmatrix} . \qquad (58)$$

LIMIT OF WEAK NEAREST-NEIGHBOR INTERACTION

Eqs.(55) and (57) can be further reduced in the limit of weak nearest-neighbor interaction, i.e., when PW $\cong$ P. It is known that free uracil does not dimerize to any appreciable extent in aqueous solution,[7,9,34,136] whereas adenosine polymerizes at least to the pentamer.[9] Using the mole fraction standard state, the stacking energies for the uracil dimerization and the adenosine polymerization are -1900 and -3600 calories per mole, respectively.[9] Assuming that the uracil bases are the only significant contributers to $\bar{W}$, the value -1900 calories per mole represents a maximum value for $\bar{W}$. The uracil bases in dinucleotides[136] and trinucleotides,[137] however, are not stacked. Since the maximum interaction between bases occurs when the bases are stacked,[138] the interaction between the uracil bases in the oligomers is less than -1900 calories per mole (i.e., more positive). Using a nearest-neighbor model with mono-and dinucleotide data, Tinoco et. al. showed that the optical rotatory dispersion predicted for the polyU was greater than observed.[139] The interpretation of this result was that the interaction between the uracil bases in the polymer was less than in the dinucleotide. Furthermore, it is not possible to distinguish between

the two-stranded or three-stranded complexes poly(U+A) and poly(2U+A) in the polyU + adenosine system[19,20] or the polyU + polyA[140] system by optical rotation. The implication is that the absolute interaction between the uracil bases in polyU is less attractive than 1900 calories per mole and the change in this interaction on the formation of a complex $\bar{W}$ is much smaller. The neglect of $\bar{W}$ in the polyU + adenosine system appears to be a reasonable first approximation.

Case 2: Unrestricted Solute Binding

It is assumed that the binding of a solute particle is independent of the state at the (p-p) sites in the limit of weak nearest-neighbor interactions is simplified to

$$\begin{vmatrix} P & 1 \\ P & 1 \end{vmatrix}^{n-1} = (P+1)^{n-2} \begin{vmatrix} P & 1 \\ P & 1 \end{vmatrix} \quad . \tag{59}$$

By defining the quantity

$$\underset{\sim}{1} = (1,0) \quad , \tag{60}$$

we can write the GPF(n) for the present case as

$$GPF(n) = \frac{mB}{55} (P\underset{\sim}{1},\underset{\sim}{1})(P+1)^{n-2} \begin{vmatrix} P & 1 \\ P & 1 \end{vmatrix} \otimes \begin{vmatrix} \frac{mBV}{55} & 1 \\ \frac{mB}{55} & 1 \end{vmatrix}^{n-1} (\underset{\sim}{1},\underset{\sim}{1})^{+} \quad , \tag{61}$$

which further simplifies to

$$GPF(n) = \frac{mB}{55} (P+1)^{n}(1,0) \begin{vmatrix} \frac{mBV}{55} & 1 \\ \frac{mB}{55} & 1 \end{vmatrix}^{n-1} \begin{pmatrix} 1 \\ 0 \end{pmatrix} \quad . \tag{62}$$

Case 3: Restricted Solute Binding

In the limit of weak nearest-neighbor interactions, Eq.(57) becomes

$$GPF(n) = \left(\frac{mBP}{55},0,0,0\right) \begin{vmatrix} \frac{mBPV}{55} & P & 0 & 1 \\ \frac{mBP}{55} & P & 0 & 1 \\ \frac{mBPV}{55} & P & 0 & 1 \\ \frac{mBP}{55} & P & 0 & 1 \end{vmatrix}^{n-1} \begin{pmatrix} 1 \\ 0 \\ 0 \\ 0 \end{pmatrix} . \qquad (63)$$

Further simplification can be effected by first defining the quantities

$$\underset{\approx}{B} \equiv \begin{vmatrix} 0 & 1 \\ 0 & 1 \end{vmatrix} , \qquad (64)$$

and

$$\underset{\approx}{A} \equiv \begin{vmatrix} \frac{mBV}{55} & 1 \\ \frac{mB}{55} & 1 \end{vmatrix} , \qquad (65)$$

and then noting the identities

$$\begin{vmatrix} P\underset{\approx}{A} & \underset{\approx}{B} \\ P\underset{\approx}{A} & \underset{\approx}{B} \end{vmatrix}^{n-1} = \begin{vmatrix} (P\underset{\approx}{A}+\underset{\approx}{B})^{n-2} P\underset{\approx}{A} & (P\underset{\approx}{A}+\underset{\approx}{B})^{n-2} \underset{\approx}{B} \\ (P\underset{\approx}{A}+\underset{\approx}{B})^{n-2} P\underset{\approx}{A} & (P\underset{\approx}{A}+\underset{\approx}{B})^{n-2} \underset{\approx}{B} \end{vmatrix} , \qquad (66)$$

and

$$P\underset{\approx}{A} \begin{pmatrix} 1 \\ 0 \end{pmatrix} = (P\underset{\approx}{A} + \underset{\approx}{B}) \begin{pmatrix} 1 \\ 0 \end{pmatrix} . \qquad (67)$$

The grand partition function GPF(n) for the restricted (p-s) binding case then becomes

$$GPF(n) = \frac{mBP}{55}\,(1,0)\,(P\underline{\underline{A}} + \underline{\underline{B}})^{n-1}\begin{pmatrix}1\\0\end{pmatrix}, \qquad (68)$$

which is, explicitly,

$$GPF(n) = (P+1)^n\,\frac{mBP}{55(P+1)}\,(1,0)\begin{vmatrix}\frac{mBPV}{55(P+1)} & 1\\ \frac{mBP}{55(P+L)} & 1\end{vmatrix}^{n-1}\begin{pmatrix}1\\0\end{pmatrix}. \qquad (69)$$

The grand partition function including sliding degeneracy GPFS(N) for the two cases are:

Case 1

$$GPFS(N) = 1 + \sum_{n=1}^{N}(N-n+1)^2\,\frac{mBP}{55}\,(P+1)^n(1,0)\begin{vmatrix}\frac{mBV}{55} & 1\\ \frac{mB}{55} & 1\end{vmatrix}^{n-1}\begin{pmatrix}1\\0\end{pmatrix}; \qquad (70)$$

Case 2

$$GPFS(N) = 1 + \sum_{n=1}^{N}(N-n+1)^2(P+1)^n\frac{mBP}{55(P+1)}(1,0)\begin{vmatrix}\frac{mBVP}{55(P+1)} & 1\\ \frac{mBP}{55(P+1)} & 1\end{vmatrix}^{n-1}\begin{pmatrix}1\\0\end{pmatrix}. \qquad (71)$$

Clearly, the factor $(N-n+1)^2$ is the degeneracy of the polymer chains exterior to the adsorption region, $(P+1)^n$ is the canonical partition function for the (p-p) sites and therefore represents the degeneracy of states interior to the absoprtion region, and $P/(P+1)$ is the probability that a particular (p-p) site within the adsorption region is bound (cf., the Langmuir adsorption isotherm). Defining λ_+ to be the largest eigenvalue of either generating matrix in Eq.(70) or Eq.(71), the ratio $GPFS(N\to\infty)/GPF(N\to\infty)$ is [ignoring the ratio C which occurs in Eq.(44)]

$$\frac{GPFS(N\to\infty)}{GPF\ (N\to\infty)} \cong \frac{\sum_{n=1}^{N}(N-n+1)^2(P+1)^n\lambda_+^{n-1}}{\lambda_+^N}$$

$$= (P+1)^{N+1}\ \frac{(P+1)\lambda_+[(P+1)\lambda_+ +1]}{[(P+1)\lambda_+ -1]^3} \quad . \qquad (72)$$

Since $(P+1)^{N+L}$ is independent of the solute molality and $(P+1)\lambda_+[(P+1)\lambda_+ +1]/[(P+1)\lambda_+ -1]^3$ is independent of N, it can be concluded that the solute binding curve calculated from Eq.(28) is identical to

$$\theta = \frac{1}{N}\frac{\partial \ell n GPFS(N\to\infty)}{\partial \ell n m} = \frac{\partial \ell n \lambda_+}{\partial \ell n m} \quad , \qquad (73)$$

for very large chains. Therefore, the midpoint conditions defined by Eqs.(30), (31), and (32) are applicable to Case 1 and Case 2 if one makes the identities

$$F = B \qquad \text{(Case 2)} \quad , \qquad (74)$$

$$F = \frac{BP}{P+1} \qquad \text{(Case 3)} \quad , \qquad (75)$$

$$S = V \qquad \text{(Both cases)} \quad . \qquad (76)$$

VIII. Results and Discussion

There is no ambiguity in the physical interpretation of the midpoint parameters F and S [cf., Eq.(36) and (37)] for the (polymer + solute)-complex system. The parameter F is simply the intrinsic equilibrium constant for the solute particles in the mole fraction standard state and S is the Boltzmann factor for the solute-solute interaction energy. This interpretation is also valid for the (2polymer + solute)-complex system only if the state of the (p-s) site is completely independent of the state of the (p-p) site [cf., Eq.(56)]. Calculated curves for the restricted solute binding model [cf., Eq.(58)], in which the total interaction energy is $\overline{B} + \overline{P} + \overline{V} + \overline{W} = -540$ calories per mole, are presented in Figure 5. It is quite clear that the slope and midpoint concentration are strongly dependent on the way the total energy of interaction is partitioned among the various parameters. The curves are divided into two groups, according to the total nearest-neighbor interaction energy $\overline{V} + \overline{W}$, and presented in Figure 6. The midpoints of the curves within each group are superimposed to illustrate the effect of energy partitioning on the shape of the curve. The inclusion of sliding degeneracy does not alter the symmetry of the curves about the midpoint of the transition. It is also apparent that the slope of a curve at the midpoint is not a simple function involving the product VW. It is inferred that a solute binding curve which is symmetric about the midpoint concentration is completely characterized by the slope and the solute concentration at the midpoint. Furthermore, the parameters F and S that can be obtained from these characteristic parameters [cf., Eqs.(36) and (37)] do not give unique values of the energies associated with the binding process. The molar quantities $\overline{F}$ and $\overline{S}$ for four systems that form a (2polymer + solute)-complex are listed in Table I.

Figure 5

Calculated binding curves for Case 1. All of the calculations [Eq.(52)] were made with the constraint BPVW = exp(-5440/RT). The quantity $\overline{X}$ (cal/mole) is defined by $X \equiv \exp(-\overline{X}/RT)$, where X = B, P, V, or W.

Curve	$\overline{B}$	$\overline{P}$	$\overline{V}$	$\overline{W}$
-o-o-o-	- 140	0	-5300	0
-x-x-x-	-2140	+2000	-3300	-2000
.....	-2140	+2000	-5300	0
———	-3000	0	-2440	0
- - - -	-3000	0	-4440	+2000

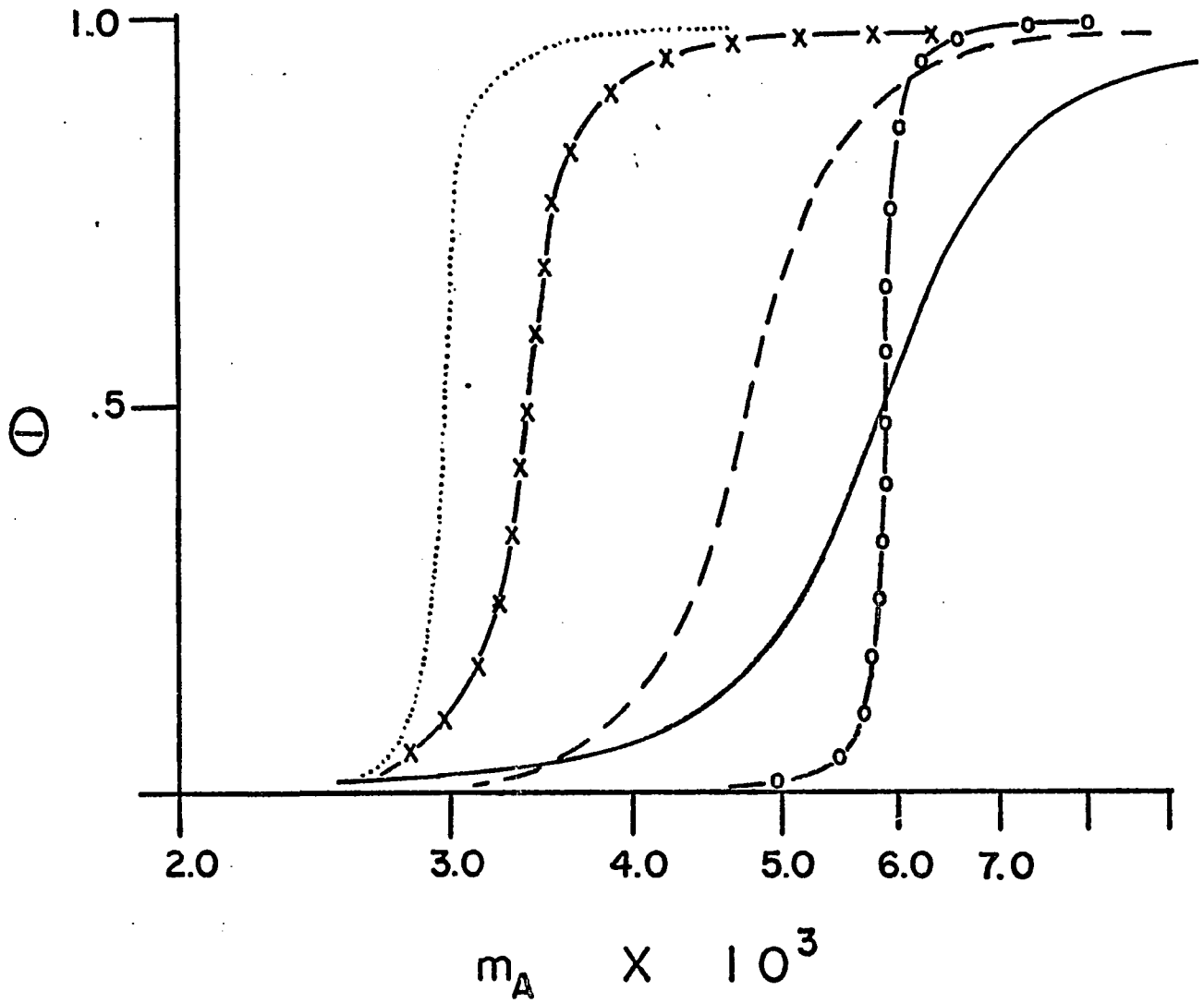
1.0
.5
Θ
2.0
3.0
4.0
5.0
6.0
7.0
$m_A \times 10^3$

Figure 6

Effect of the partitioning of energy on the shape of the binding curves

Group 1 $\bar{V} + \bar{W} = -5300$ cal/mole

Group 2 $\bar{V} + \bar{W} = -2440$ cal/mole

Notation is the same as in Figure 5.

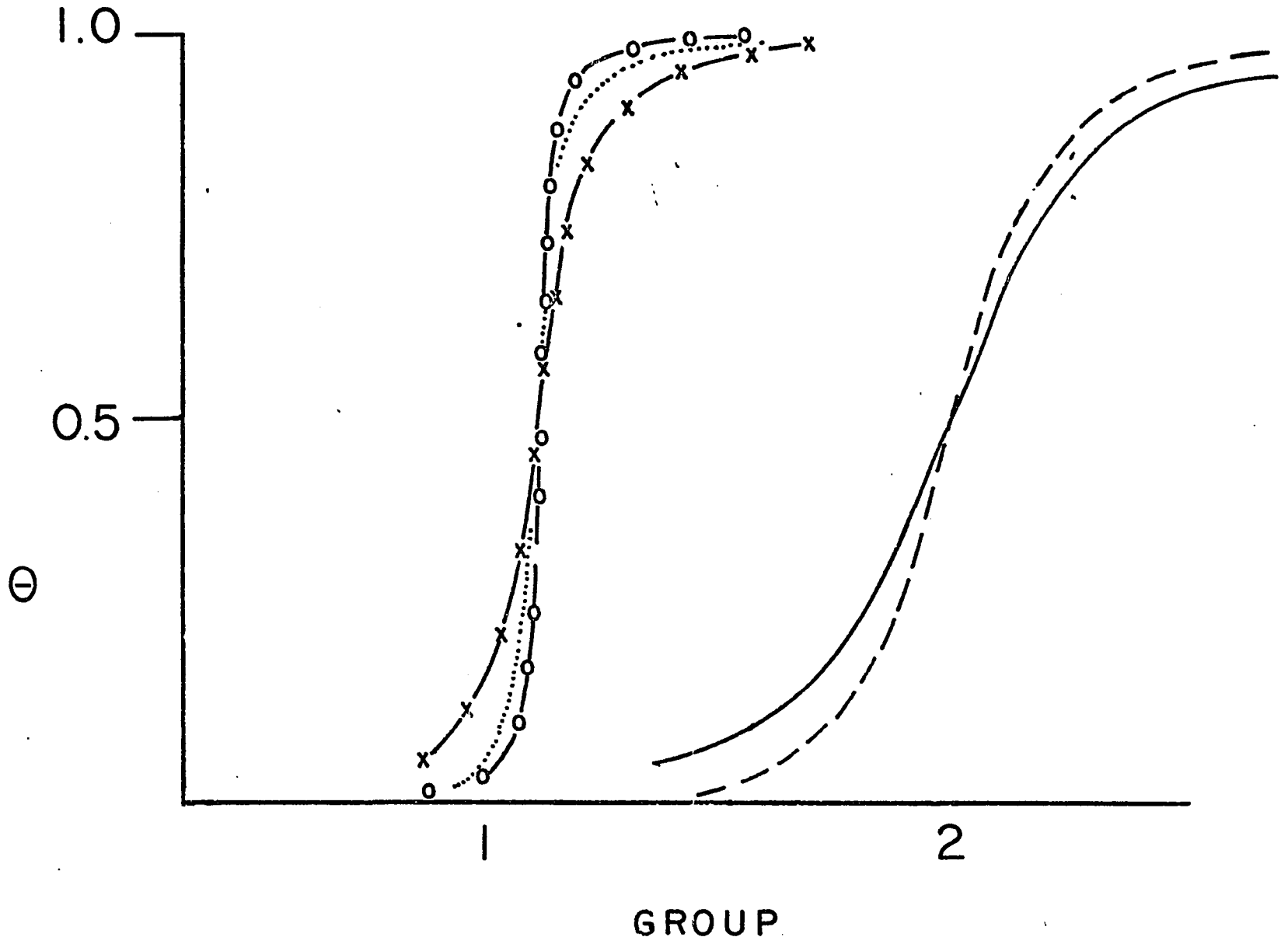
1.0
0.5
Θ
1
2
GROUP

PolyU + Adenosine

The equilibrium dialysis curve of Huang and Ts'o[19] for the (2polyU + adenosine)-complex is presented in Figure 1. They estimate the slope at the midpoint to be in the range 30-60 which corresponds to nearest-neighbor stacking energies of -5300 and -6060 calories per mole, respectively. The values of $\bar{F}$ for these extremes of the estimated slope are given in Table I. One notices that the very small or slightly positive values of the standard binding energy implies a negligible or slightly repulsive hydrogen-bond interaction between a single adenosine and the uridines on the polyU, if this is the only contributor to $\bar{F}$. Since (deoxy) adenosines stack by themselves with an effective equilibrium constant of 12 at 25°C[9], it may be deduced that the effective equilibrium constant is not much greater than 40 at 5°C unless the ΔH for this process is in excess of 5500 calories per mole. This is to be compared with an effective equilibrium constant here of about 3.4×10^2 for the addition of an adenosine to the polyU complex at the midpoint of the transition at 5°C. Thus, the tendency of adenosines to associate on the polyU is about eight times (or more) greater than its tendency toward self-association. Certainly Huang and Ts'o observed no significant amount of self-association of adenosine under their experimental conditions. It is clear from the values of $\bar{F}$ that essentially none of this enhanced association of adenosine with the polyU complex can be attributed to simple hydrogen-bonding of the adenosine to the polyU. One may infer that the quantity $\bar{S}$ cannot simply represent the free energy for stacking of adenosines, but must contain as well one or more of the following contributions: (i) a contribution from stacking of uridines; (ii) a contribution to the A-U and/or U-U hydrogen-bond association

TABLE I

Characteristic Parameters $\bar{F}$ and $\bar{S}$ for (2Polymer + Solute)-Complex Systems

System	Midpoint Concentration	$\bar{F}$ (Cal/Mole)	$\bar{S}$ (Cal/Mole)	Temperature ^{o}K
PolyU + Adenosine	3.1×10^{-3}	- 140.	-5300_a	278
		+ 660	-6060_b	278
PolyC + guanosine	5.3×10^{-4}	-3853	-2800_c	288
PolyC + Guo-3'-P	1.1×10^{-3}	-4349	-2100_c	298
PolyC + Guo-5'OP	7.0×10^{-4}	-3600	-2600_c	275

PolyU = poly uridylic acid

PolyC = polycytidylic acid

Guo-3'-P = guanosine-3'-phosphate

Guo-5'-P = guanosine-5'-phosphate

a) obtained from reported slope of 30[19]

b) obtained from reported slope of 60[19]

c) value reported in literature[21]

energies when the neighboring units are hydrogen bonded and also stacked to this unit; (iii) an extra contribution to the A-A and/or U-U stacking energy that is gained upon hydrogen-bond formation, and which is large enough to compensate for the energetically unfavorable hydrogen bonds that are formed. The argument presented in Section VII for the neglect of the U-U stacking interaction effectively rules out (i). Because of the large ionic strength effect on the binding curve,[19] the repulsive energy between the negatively charged phosphate groups on the different chains apparently contributes significantly to P (or F). Since the two polyU chains do not self-associate to any appreciable extent,[19] it is safe to assume that any hydrogen-bonding that might occur between the uridines is not sufficient to overcome the repulsive nature of the phosphate groups. It is also apparent from the form of Eqs.(74) and (75) that the presence of U-U hydrogen-bonding cannot be deduced from solute binding curves alone. Therefore, the enhancement of adenosine association on the formation of U-U hydrogen bonds must be considered to be a speculation at this point. The prevalent notion that the hydrogen-bond association energies and the stacking energies are simple constants independent of one another is now open to question. Since the complex formed here is multi-stranded, it might be expected that a pre-existing bound site would greatly facilitate the binding at the neighboring sites, as much of the electrostatic work required to join the two polyU chains has already been done in establishing the initial bound site. Indeed, the inability of the theoretical curve which is calculated from the parameters obtained at the midpoint to coincide with the entire experimental curve can be explained in terms of mutual enhancement of the parameters. Furthermore, the value of P, and hence F, changes at higher coverage since there is extensive counter-ion condensation as the two polyU strands are brought together.[141]

It is of interest to compare the values of $\bar{F}$ obtained here with the standard free-energy change for the hydrogen bond dimerization of N-methylacetamide in aqueous solution determined at 25°C by Klotz and Frazen.[142] Since the measured ΔH was found to be zero, the same value of ΔF may be applied at 5°C. After correcting their number for the conversion from a 1.0 molar standard state to a 1.0 mole fraction standard state, one finds $\Delta F = +880$ calories per mole which is somewhat more repulsive than the values obtained here for $\bar{F}$. Infra-red studies by Klotz and Franzen on urea indicate that dimerization of urea by hydrogen-bonding does not proceed to a significant extent, certainly not with the equilibrium constant calculated by Schellman[142] from the vapor pressure data of Scatchard, Hamer and Wood,[143] so that Schellman's free energy for dimerization of urea in aqueous solution $\Delta F = -730$ calories per mole (converted to 1.0 mole fraction standard state at 5°C) is at present a doubtful quantity. In any case these two previous values bracket the extreme values of $\bar{F}$, and thereby serve to reinforce the conclusion that the association energy of the three-stranded complex is not drastically different from more conventional associations involving hydrogen bonds.

It should also be noted that Applequist and Damle[126] attempted to determine thermodynamic parameters equivalent to $\bar{F}$ and $\bar{S}$ from the temperature dependence of the hypochromicity of oligomers of adenylic acid. Unfortunately, the temperature dependence of the hydrogen bonding equilibrium constant for the first bond between two chains could not be determined with any reasonable certainty, although the absolute magnitude of this constant at the midpoint (~50°C) was obtained with satisfactory precision. Thus, their data is not readily translated to 5°C. However, if a temperature coefficient of zero is arbitrarily assumed then a standard free energy

$\Delta F = -570$ calories per mole is deduced at $5^{\circ}C$ for 1.0 mole fraction standard state. This number is not too far out of line with those considered above.

PolyU + Adenosine + Guanosine

The simultaneous binding of guanosine and adenosine to polyuridylic acid studied by Pitha, Huang, and Ts'o[20] potentially contains the difference of binding energies of A and G for the primary sites on the polyU chains. The GPF(N) is calculated by

$$GPF(N) = \left[m_A F_A/55, m_G F_G/55, 1\right] \cdot \begin{vmatrix} \frac{m_A F_A S_{AA}}{55} & \frac{m_G F_G S_{AG}}{55} & 1 \\ \frac{m_A F_A S_{GA}}{55} & \frac{m_G F_G S_{GG}}{55} & 1 \\ \frac{m_A F_A}{55} & \frac{m_G F_G}{55} & 1 \end{vmatrix}^{N-1} \cdot \begin{pmatrix} 1 \\ 1 \\ 1 \end{pmatrix}, \qquad (77)$$

where $$F_i \equiv \exp(-\bar{F}_i/RT),\ i = A, G, \text{ or } s$$

$$S_{ij} \equiv \exp\left[-(f_{ij} - f_{ss})/RT\right] = \exp(-\bar{S}_{ij}/RT) \quad ,$$

and it is assumed that $S_{As} = S_{sA} = S_{Gs} = S_{sG} = 1$.

The added feature to the computation is the requirement of a constant total concentration of the guanosine molecules. The details of the

computational procedure are given in Appendix C.

The parameters $\bar{F}_A$ and $\bar{S}_{AA}$ were chosen to provide an optimum fit of the calculated adenosine binding curve to the experimental data. This optimum curve is displayed along with the experimental isotherm in Figure 7. It is notable that the optimum values of $\bar{F}_A$ and $\bar{S}_{AA}$ of -4000 and -1550 calories per mole, respectively, differ drastically from those obtained from the data of Huang and Ts'o[19] (-140 and -5300 calories, respectively). Even so, the sum $\bar{F}_A + \bar{S}_{AA}$, which determines the midpoint of the binding curve, in this case is -5550 calories per mole, which agrees fairly well with the -5440 calories per mole found for the earlier data. For some unknown reason the binding curves are very much less steep in this sample.

After the parameters characterizing the adenosine binding had been established, trial and error computations of guanosine binding were carried out for various values of $\bar{F}_G$, $\bar{S}_{GG}$, and $\bar{S}_{AG} = \bar{S}_{GA}$. When the absolute magnitude of the free energy change for A addition exceeds that for G addition one finds that the curves of % G bound versus $\ln(m_A)$ always exhibit maxima at about the same value of m_A corresponding to 70% binding on the A adsorption isotherm. Typical calculated curves are compared with the experimental data in Figure 7. If hydrogen bond association dominates the G binding, the maxima in the G binding curves may be found at much lower values of m_A, but they always occur. It is simply not possible to find parameters $\bar{F}_G$, $\bar{S}_{GG}$, and $\bar{S}_{AG}$ that exhibit simultaneously the delayed onset of G binding and the absence of any maximum in G binding near the middle-binding region of the A isotherm, even without any consideration of the magnitudes of the numbers involved.

Having established that the primary mode of G binding is not a competition with A for the hydrogen-bonding sites on the polyU, it is

Figure 7

The simultaneous binding of A and G to polyU as a function of m_A. The solid curves A and G represent the experimental data of Pitha, Huang and Ts'o for A- and G-binding, respectively. The crosses (x x x x) denote the values for A-binding calculated using a binding energy $\overline{F}_A = -4000$, and a stacking energy $f_{AA} - F_{ss} = -1550$ cal/mole. The A-binding curves employ the left-hand ordinate, while the G-binding curves utilize the one on the right. The circles (o o o o), squares (■ ■ ■ ■), and dots (. . . .) are all G-binding values calculated using the above parameters for A-binding and also stacking energies $f_{AG} - f_{ss} = f_{GG} - f_{ss} = -1550$ cal/mole. These G-binding curves differ only in their binding energies: (i) for the circles $\overline{F}_G = -3400$ cal/mole; (ii) for the squares $\overline{F}_G = -2800$ cal/mole; (iii) for the dots $\overline{F}_G = -1500$ cal/mole. The experimental data were taken in a solution containing 0.4 M NaCl, 0.01 tris buffer, 1.5×10^{-2} M $r(U)_n$, and $1.1 - 1.2 \times 10^{-5}$ M guanosine at 5°C. The calculations were performed using a value $m_G = 1.0 \times 10^{-5}$ M, and an assumed chain length of 500 nucleotides.

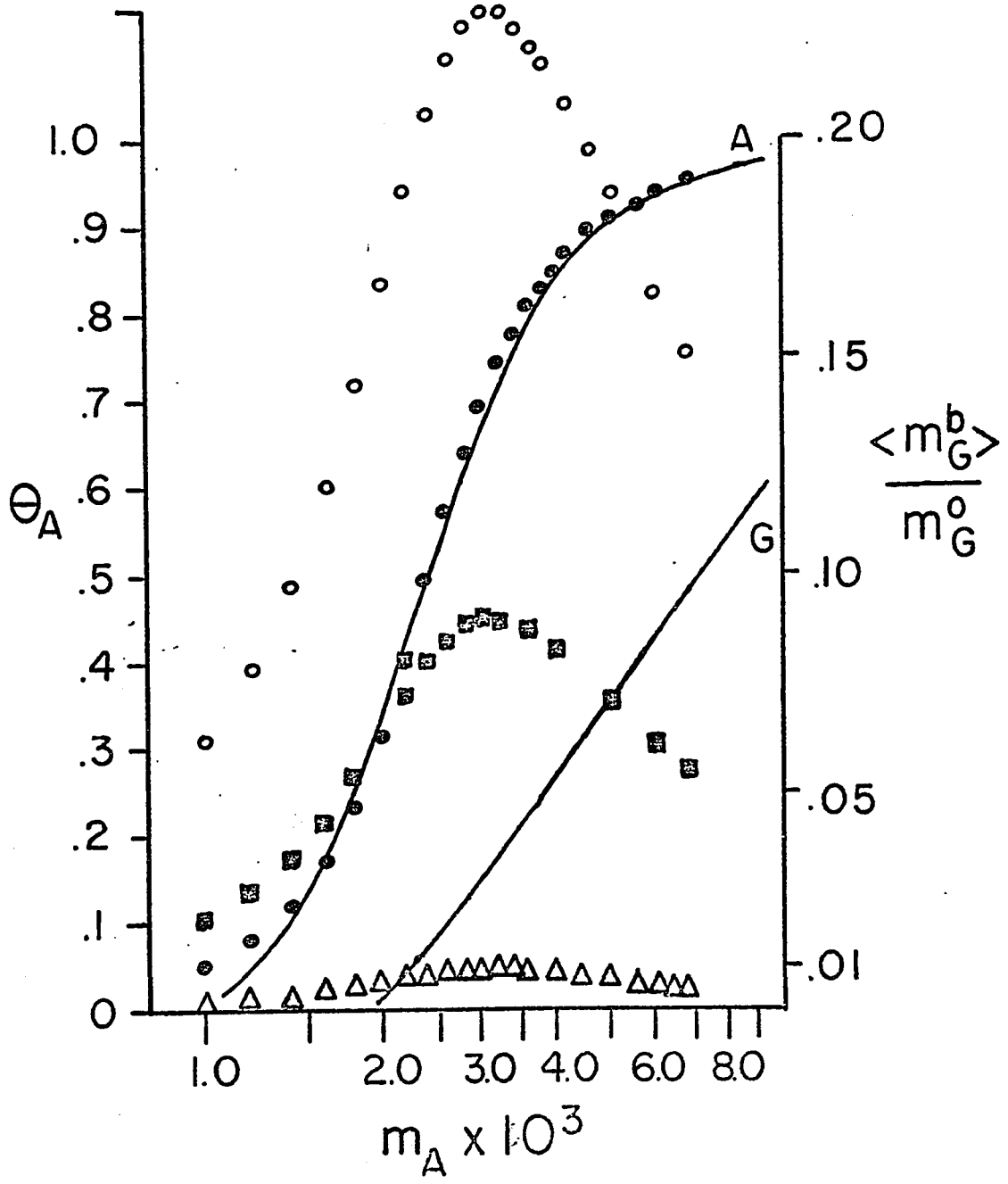
1.0
.9
.8
.7
.6
.5
.4
.3
.2
.1
0
Θ_A
A
G
.20
.15
.10
.05
.01
$\frac{\langle m_G^b \rangle}{m_G^o}$
1.0
2.0
3.0
4.0
6.0
8.0
$m_A \times 10^3$

desirable to establish an upper limit for the extent of competitive binding. In other words, suppose we assume that a small component of the total binding proceeds according to the competitive model and ask how large this component could be and still escape detection. The more precise question to ask is, "what is the largest possible value of the ratio of bound guanosine to total guanosine $< m_G^b >/m_G^o$ at the maximum of any competitive binding curve that could escape detection?" Presumably this value is .01 (1%) or less. The long initial rise of all the competitive curves in contrast to the steep ascent of the experimental curve insures that any competitive binding amounting to 1% or more would have been readily detected, especially since a resolution of at least 0.5% is indicated by the authors.[20] Now, setting all stacking parameters equal to $\bar{S}_{AA} = -1550$ calories per mole, a unique value for the binding parameter $\bar{F}_G$ may be found that just satisfies the condition $<m_G^b>/m_G^o = .011$ at the maximum of the isotherm. For the optimum parameters, it was found that $\bar{F}_G = -1600$ calories per mole. Since there is some evidence from the stacking of free nucleosides that $S_{AG} > S_{AA}$, it may be inferred that -1600 represents a lower bound to the free energy for G binding (exclusive of stacking) on the primary uracil sites. The difference in binding energies $\bar{F}_G - \bar{F}_A = +2400$ calories per mole is, then, likewise a lower limit.

Calculations were also performed for a hypothetical case in which $\bar{F}_A = -1000$ and $\bar{S}_{AA} = -4550$ calories per mole. Retaining the difference in $\bar{F}_G - \bar{F}_A = +2400$ and the equivalence of the stacking parameters to $\bar{S}_{AA}$, the ratio $<m_G^b>/m_G^o$ was found to be equal to .016. The maximum occurred at a somewhat lower value of m_A owing mainly to the enhanced sharpness of the transition. Thus, it is seen that a difference in binding free energy of +2400 calories per mole between incorrect and correct bases leads to

a maximum competitive G binding of 1-2%, quite irrespective of the relative magnitudes of the binding and stacking free energies.

It is felt that, if the actual difference in binding free-energies between the incorrect (G) and correct (A) bases were +2400 calories per mole or smaller, then the competitive binding would have been large enough to have been detected. One is forced to conclude that the difference in binding free energies is greater than +2400 calories per mole. This corresponds to a specificity of at least $\exp(+2400/RT) = 80{:}1$ in favor of A at 5°C.

Although the A adsorption isotherm in the present study is apparently not as steep as that reported by Huang and Ts'o,[19] it is intriguing to consider the possibility that the result here for the difference in binding free energy also applies to the steeper case. In that eventuality, the free energy $\overline{F}_G$ for G binding would be required to be substantially positive, since $-140 < \overline{F}_A < +620$ calories per mole for the steeper curve. A positive $\overline{F}_G$ (for the 1.0 mole fraction standard state) implies an effective repulsion of incorrect bases. At the present it would appear that such repulsion is the only means of achieving the observed genetic specificity[144] of $\sim 10^9$ from a purely equilibrium molecular specificity, since the observed strengths of association of correct pairs are in fact rather weak.[12-16]

Achieving specificity through strong repulsion of incorrect bases, rather than via strong attraction of correct bases, offers the advantage of a much more rapid kinetics. With the 1.0 mole fraction standard state a completely neutral affinity of incorrect bases for one another would be characterized by an equilibrium constant $K_X^{inc} = 1.0$, so that a specificity of 10^9 could only come from a strong association of correct bases with a

$K_X^{corr} = 10^9$. For the 1.0 M standard state this equilibrium constant $K_M^{corr} = 10^9/55.5 = 1.8\times10^7\ M^{-1}$. Since there is an upper limit of $\vec{k} \cong 10^9\ M^{-1}\ sec^{-1}$ for the bimolecular association rate constant, the dissociation rate constant cannot be larger than $\overleftarrow{k} = 55\ sec^{-1}$ which is an order of magnitude too small to accommodate the observed replication rate of $> 10^3$ nucleotides/sec. That is, the DNA chains could not possibly separate rapidly enough if all of the specificity were vested in the stability of correct pairs relative to neutral incorrect pairs. However, if the association of correct pairs remains weak and specificity is achieved via repulsion of incorrect pairs, then there is no problem with the kinetics since K_M^{corr} may be as small as .018 (neutral affinity), which lies within the limits set by the free-energies found from the data of Huang and Ts'o, and $\overleftarrow{k}$ could be as large as $5.5\times10^6\ sec^{-1}$ which can certainly accommodate the observed replication rate.

We now want to consider the possibility that the guanosine and adenosine form a complex in solution and that this complex competes for the primary sites on the polyU. The reaction for the formation of the complex is

$$A + G = C \quad , \tag{78}$$

with an effective equilibrium constant

$$K = m_C/m_A m_G \quad . \tag{79}$$

The complex C can now be treated simply as a third solute particle in solution, thus providing another possible state for a site on the polymer. Solving Eq.(79) for m_C, the GPF(N) is then calculated by the matrix multiplication which is similar in form to that of Rawlings and Schneider,[120]

$$GPF(N) = \left(\frac{m_A F_A}{55}, \frac{m_G F_G}{55}, 1, \frac{m_A m_G K F_C}{55}\right) \begin{vmatrix} \frac{m_A F_A S_{AA}}{55} & \frac{m_G F_G S_{AG}}{55} & 1 & \frac{m_A m_G K F_C S_{AC}}{55} \\ \frac{m_A F_A S_{GA}}{55} & \frac{m_G F_G S_{GG}}{55} & 1 & \frac{m_A m_G K F_C S_{GC}}{55} \\ \frac{m_A F_A}{55} & \frac{m_G F_G}{55} & 1 & \frac{m_A m_G K F_C}{55} \\ \frac{m_A F_A S_{CA}}{55} & \frac{m_G F_G S_{CG}}{55} & 1 & \frac{m_A m_G K F_C S_{CC}}{55} \end{vmatrix}^{N-1} \begin{pmatrix} 1 \\ 1 \\ 1 \\ 1 \end{pmatrix} . \quad (80)$$

It is clear that C is not bound by having both A and G bind to adjacent polyU sites since this would be equivalent to having A and G compete independently for the primary sites. By having the complex form in solution with subsequent competitive binding for one primary site, we provide a mechanism for increasing the bound guanosine particles beyond the 70% bound adenocine isotherm. For simplicity, we assume that K = 1 (or that K is absorbed in the parameter F_C) and $S_{AG} = S_{GA} = S_{AA}$ and employ the optimum parameters $\overline{F}_A = -4000$ and $\overline{S}_{AA} = -1550$ calories per mole. In view of the results of guanosine binding to primary sites, the parameter $\overline{F}_G = -1000$ calories per mole was assumed in order to supress the maximum in the guanosine binding at the primary sites. The parameters $\overline{F}_C$ and $\overline{S}_{AC} = \overline{S}_{CA} = \overline{S}_{GC} = \overline{S}_{CG} = \overline{S}_{CC}$ were assumed adjustable. Two of the calculated curves are presented in Figure 8 along with the experimental A and G binding isotherms. It is quite clear that the calculated G curves are not linear but approach a plateau.

It should be pointed out that Eq.(80) is valid for a model in which only the guanosine molecules are allowed to intercalate between the primary polyU sites subject to the restriction that at least one of the neighbors be adenosine. This is quite clear if the mode of binding the complex C is via hydrogen bonding of the adenosine to the uracil while the guanosine

Figure 8

Intercalation model for guanosine binding by polyU. The experimental curves were reported by Pitha, Huang, and Ts'o.[20] The computed curves employed the parameters $\overline{F}_A$ = -4000 cal/mole, $\overline{F}_G$ = -1550 cal/mole, and $\overline{N}$ = 500. The adjustable parameters are $\overline{F}_C$ and $\overline{S}_{AC} = \overline{S}_{CA} = \overline{S}_{GC} = \overline{S}_{CG} = \overline{S}_{CC}$.

(———) experimental isotherm for adenosine binding

(- - -) experimental isotherm for guanosine binding

(x-x-x) $\overline{F}_C$ = 0; $\overline{S}_{CC}$ = -4600 cal/mole

(o-o-o) $\overline{F}_C$ = -4200 cal/mole; $\overline{S}_{CC}$ = -2350 cal/mole

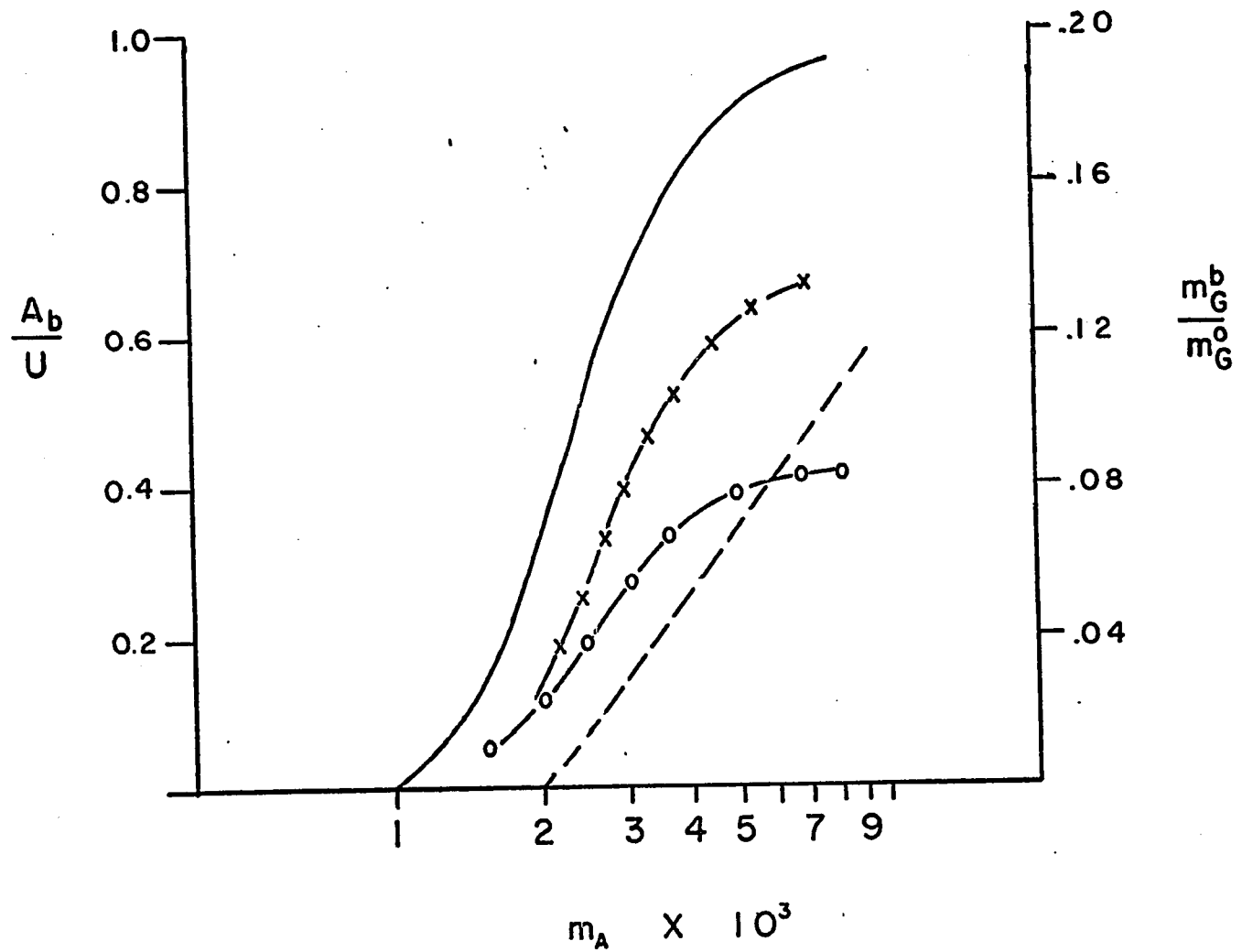
1.0
0.8
0.6
0.4
0.2
$\frac{A_b}{U}$
.20
.16
.12
.08
.04
$\frac{m_G^b}{m_G^o}$
1
2
3
4
5
7
9
$m_A \times 10^3$

"stacks" with the adenosine. Allowing the guanosine to complex with another guanosine, hence intercalation between neighboring guanosines on primary sites, is of no advantage since guanosine is "squeezed off" the primary sites at higher adenosine concentration.

Polycytidylic Acid + Guanylic Monomers

Equilibrium dialysis studies of the interaction between polycytidylic acid and guanylic monomers (i.e., guanosine, guanosine-5'-phosphate, and guanosine-3'-phosphate) were recently completed by Sarocchi, Courtois, and Guschlbauer.[21] They analyzed their data by making Hill plots (θ versus $\ln(m_G^f)$, where θ is the fraction of sites bound and m_G^f is the molality of free G) and Scatchard plots $[\ln(r/m_G^f(n-r))$-versus r where r/n is the fraction of sites bound]. The values that they obtained from these plots are presented in Table II.

TABLE II

Monomer	Temperature °C	Nearest-neighbor energy (cal/mole) (Hill)	(Scatchard)	Intrinsic equilibrium constant (Scatchard)
guanosine	15	-2800	-2700	170
guo-5'-P	2	-2600	-2700	170
guo-3'-P	25	-2100	-2500	110

It is clear from the values of the nearest-neighbor energy obtained from the Hill plot [identical to Eq.(36)] that a single stack model is not valid for this system. For example, if we assume that the chain length of polyC is 500 units, then the test for a one-solute-stack complex is

$$\frac{1}{\sigma N} = \frac{S}{N} = \frac{\exp(2800/576)}{500} \simeq \frac{129}{500} < 1 \quad , \qquad (81)$$

which does not meet the criterion [cf., Eq.(40)]. A model is presented in Appendix E which includes the formation of loops, but no tractable expressions have yet evolved that are as simple as Eqs.(36) and (37).

It is shown in Appendix D that the exact nearest-neighbor model and the average-neighbor model (Bragg-Williams model) give equivalent midpoint expressions only in the limit of weak neighbor interactions ($S/2RT \ll 1$). Furthermore, if one does a Scatchard-type plot with parameters obtained with the exact nearest-neighbor model, one obtains a curve that is almost linear in the 20-80% bound region (cf., Figs. 9 and 10). Therefore, extrapolation of this apparently linear region to zero bound solute particles does not give the "true" intrinsic association constant as predicted by Scatchard's theory. Since Scatchard-type plots are used extensively in the analysis of small-molecule binding to polymers,[21,24,25,59,63] it may be of interest to compare the exact nearest-neighbor model with the Bragg-Williams model at the midpoint. Guschlbauer's Eq.(2)[21] has the same mathematical form as obtained from the Bragg-Williams model,

$$(r/m_G)\exp(2Er/kT) = k_o(n-r) \quad , \qquad (82)$$

where E is the average-neighbor energy, k_o is the intrinsic equilibrium constant, m_G is the molality of free guanosine, and r/n is the fraction of sites occupied. At the midpoint, we have $r/n = 1/2$. Guschlbauer[21] found that $n = 1/2$ the systems that his group studied, which implies that only half of the total available sites are used in the formation of the complex, i.e., a two-stranded complex with respect to the polyC. Therefore, $r = 1/4$ and Eq.(82) becomes,

$$m_G k_o \exp(-E/2kT) = 1 \quad , \qquad (83)$$

If we now equate the molar average interaction energy $\bar{E}$ with the exact nearest-neighbor energy $\bar{S}$, then comparison of the midpoint condition for the exact model

$$m\exp(-\bar{F}/RT)\exp(-\bar{S}/RT) = 1 \quad , \qquad (84)$$

with Eq.(83) leads to the identity

$$k_o = \exp(-\bar{F}/RT)\exp(-\bar{S}/2RT) \quad . \qquad (85)$$

In other words, extrapolation of a Scatchard-type plot through the midpoint region to zero concentration yields an "apparent" intrinsic constant

$$k_{app} = k_{in}\exp(+\bar{S}/2RT) \quad , \qquad (86)$$

where

$$k_{in} = \exp(-\bar{F}/RT) \quad , \qquad (87)$$

is the "true" intrinsic binding constant.

Guschlbauer's reported values of k_o are presented in Table III along with the values calculated by the empirical equation

$$k_o = \exp(-\bar{F}/RT)\exp(-\bar{S}/2RT)/55 = \exp(+\bar{S}/2RT)/m_G \quad , \qquad (88)$$

where m_G is the concentration of free G at the midpoint of the transition [cf., Eq.(82)]. The calculation employed the reported Hill value for $\bar{S}$ and the estimated midpoint concentration which was obtained from the published binding curves.[21]

TABLE III

Comparison of the Reported and Calculated Values of k_o

Monomer	Estimated Midpoint Concentration	k_o	
		Reported	Calculated
guanosine	5.3×10^{-4}	170	165
Guo-3'-P	11.0×10^{-4}	110	152
Guo-5'-P	7.0×10^{-4}	170	133

If one takes into consideration the fact that the experimental value of k_o was not obtained from an extrapolation of the slope at the midpoint, the agreement between the calculated and experimental values of k_o is quite good. But, this now presents a dilemma, since the average nearest-neighbor interaction at the midpoint should not be equivalent to the exact nearest-neighbor interaction energy. Scatchard plots were made on the data obtained from exact nearest-neighbor calculations and presented in Figures 9 and 10. It is apparent from these figures that the region most accessible to experiment, i.e., from 20-80% bound, is almost linear as predicted by Scatchard's theory. Experimental curves presented by other authors[24,59,63] also have data points at the extremes of the transition region which do not fall on the linear plot. Sander and Ts'o[59] specifically point out the presence of such points in their data and attempt to fit the data by introducing an "apparent" equilibrium constant, which is the Scatchard constant k_o modified by an "interference" factor (i.e., $k_{app} = k_o \exp(-\phi\upsilon)$, where ϕ is the interference factor and υ is the fraction of sites occupied). On closer inspection, Scatchard plots do become linear

Figure 9

Scatchard plots using exact nearest-neighbor parameters and computed values of θ at $T = 278^{o}$ and $N = 500$.

(.....) $\overline{F}$ = -4000 cal/mole; $\overline{S}$ = -1550 cal/mole

(- - -) $\overline{F}$ = -4000 cal/mole; $\overline{S}$ = -1440 cal/mole

(x-x-x) $\overline{F}$ = -3000 cal/mole; $\overline{S}$ = -2440 cal/mole

(—•—•—) $\overline{F}$ = 0; $\overline{S}$ = -5550 cal/mole

Actual value of k_o = exp(-3000/RT)/55

Actual value of k_o = exp(-4000/RT)/55

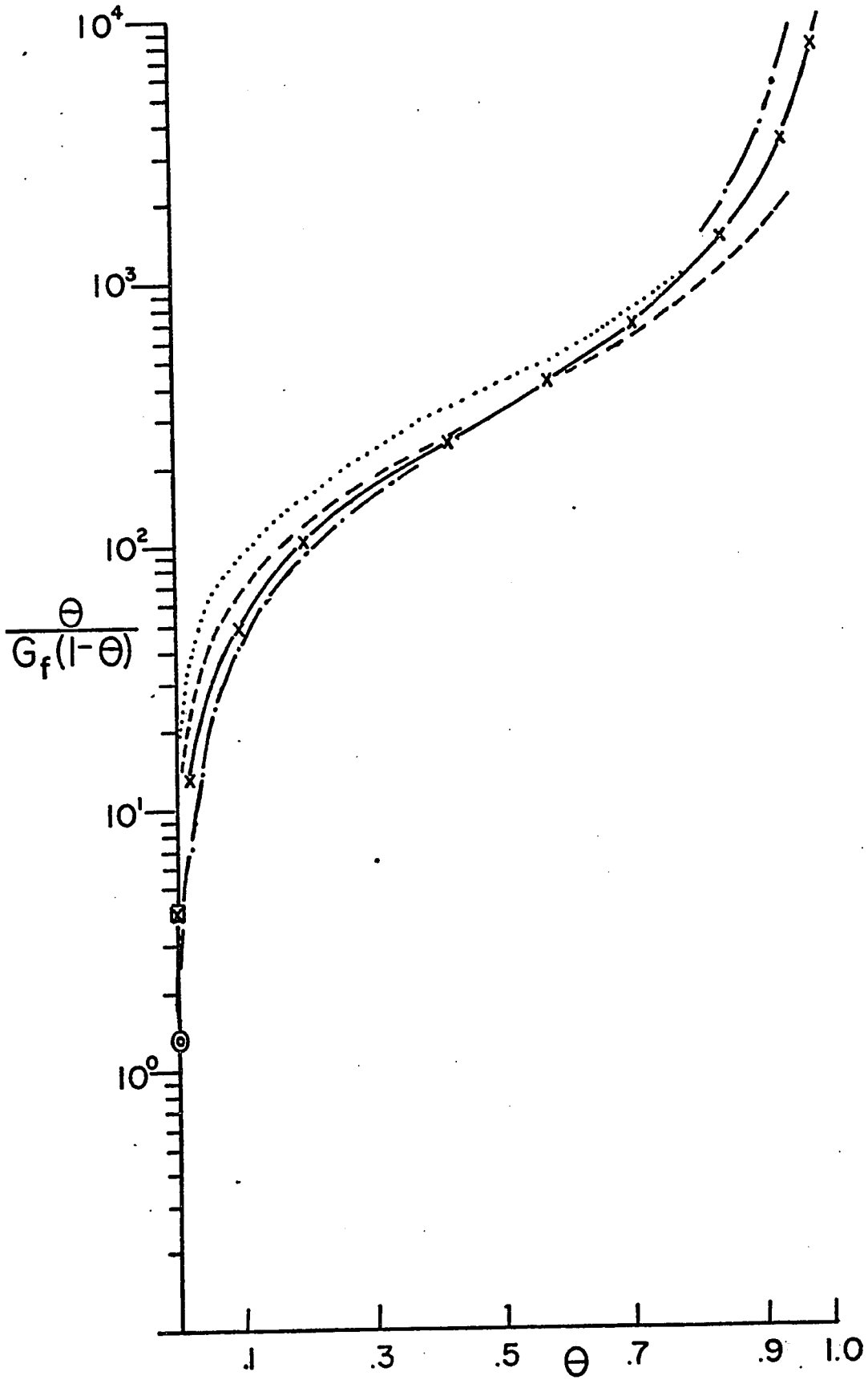
10^4
10^3
10^2
10^1
10^0
$\frac{\Theta}{G_f(1-\Theta)}$
.1
.3
.5
Θ
.7
.9
1.0

Figure 10

Scatchard plot using exact nearest-neighbor parameters and computed values of θ. Notation is the same as in Figure 9.

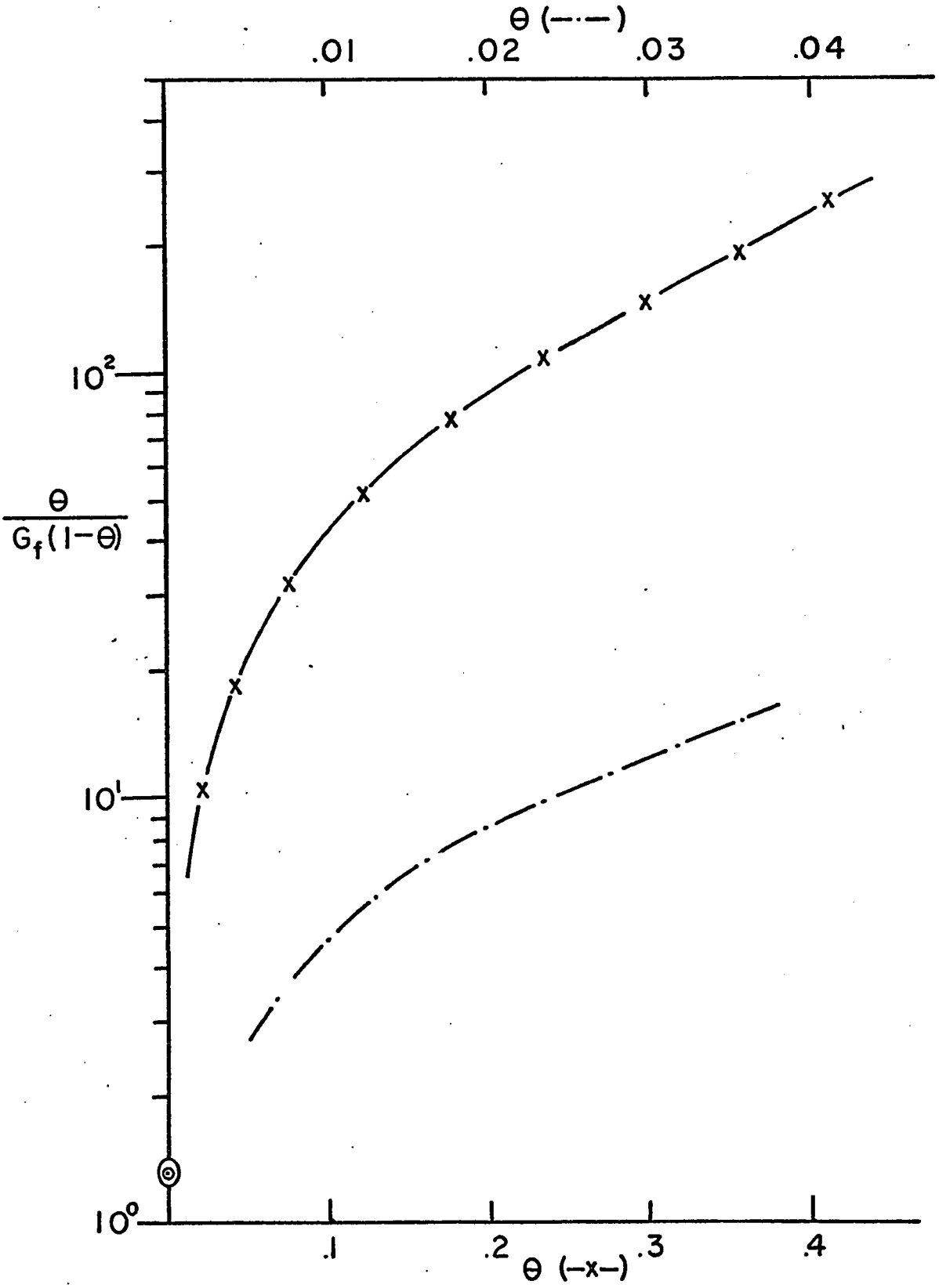
θ (-·-·-)
.01
.02
.03
.04
10^2
10^1
10^0
$\frac{\theta}{G_f(1-\theta)}$
.1
.2
.3
.4
θ (-x-)

in the region of low coverage (cf., Figure 10). This result is not entirely unexpected since in the low coverage region the assumption of random adsorption of the solute molecules is valid. Unfortunately, this region is not always subject to study with any degree of accuracy.

"TRUE" PHASE TRANSITIONS IN ONE DIMENSION

Within the past few years, interest has been shown in the possibility of the (mathematical) occurrence of a first-order phase transition in a one-dimensional system.[97-100,145-148,95,119] The usual criterion for the presence of an nth order phase transition in the mathematical models is the discontinuity of the nth derivative of some thermodynamic function, which was first proposed by Ehrenfest.[149] As pointed out by Baur and Nosano,[145] the conventional proofs for the non-existence of a "true" first-order phase transition assume the interaction energies are of finite range and finite strength. Higher-order phase transitions can (mathematically) occur in a two-stranded complex such as DNA if the ring weighting exponent k (cf., Appendix E) is allowed to have values greater than 2.[97,99]

The matrix formulation of the partition function offers another definition of a phrase transition which is more suited to our purpose, namely the equivalence of two eigenvalues at some particular value of a thermodynamic variable.[81,145] The eigenvalues for the generating matrix defined in Eq.(38) are (cf., Appendix B)

$$\lambda_{+} = \frac{(mF/55+1) + [(mFS/55+1)^2 - 4(mFS/55-mF/55)]^{\frac{1}{2}}}{2}, \qquad (88)$$

$$\lambda_- = \frac{(mF/55+1) - [(mF/55+1)^2 - 4(mFS/55-mF/55)]^{\frac{1}{2}}}{2} . \qquad (89)$$

The difference between the two eigenvalues evaluated at the midpoint of the transition is

$$\lambda_+ - \lambda_- = 2/S^{\frac{1}{2}} , \qquad (90)$$

where the condition $mFS/55 = 1$ is utilized. The nearest-neighbor interaction energy is related to the separation of the two eigenvalues at the midpoint and therefore should influence the breadth of the transition region. In the special case of an infinitely large attractive interaction energy, the two eigenvalues coalesce and a "true" phase transition occurs. On defining the quantities

$$s = mFS/55 , \qquad (91)$$

and

$$\sigma = 1/S , \qquad (92)$$

The generating matrix of Eq.(38) can be written in a form identical to that of Zimm and Bragg,[85]

$$\underset{\sim}{M} = \begin{vmatrix} s & 1 \\ \sigma s & 1 \end{vmatrix} . \qquad (93)$$

As the attractive interaction energy becomes very large, and assuming s remains finite, the generating matrix takes on the form

$$\underset{\sim}{M} = \begin{vmatrix} s & 1 \\ 0 & 1 \end{vmatrix} . \qquad (94)$$

The grand partition function for this special case can then be written

in the simplified form

$$GPF(N) = \left(\frac{mF}{55},1\right) \begin{vmatrix} s^{N-1} & \sum_{n=0}^{N-2} s^n \\ 0 & 1 \end{vmatrix} \begin{pmatrix} 1 \\ 1 \end{pmatrix} \quad , \qquad (95)$$

or

$$GPF(N) = 1 + \frac{mF}{55} \sum_{n=0}^{N-1} s^n \quad . \qquad (96)$$

It should be noted that the terms in the sum correspond to all of the possible states in a system which nucleate at one end of the polymer and "grow" toward the other end. We can convert this "zipper" model into a "melting" model by simply factoring out s^N from the sum, i.e.,

$$(mF/55) \sum_{n=0}^{N-1} s^n = s_1 \sum_{n=0}^{N-1} (1/s)^{N-n} \quad , \qquad (97)$$

where $s_1 = (mF/55)s^N$, which corresponds to a completely bound polymer of N+1 units. We choose to rewrite the sum as

$$s_1 \sum_{n=0}^{N-1} (1/s)^{N-n} = s_1(x + \sum_{j=1}^{\infty} x^{j+1}) = s_1 G(x) \quad , \qquad (98)$$

where $x = 1/s$ and the chain length is allowed to go to infinity. If we do not allow the polymer to melt from the ends, but rather from the middle, then a loop is formed. In this case, each term in the sum must have another factor to account for the ring weighting, i.e.,

$$\sum_{j=1}^{\infty} x^{j+1} \rightarrow \sum_{j=1}^{\infty} w_j x^{j+1} \quad , \qquad (99)$$

where $w_j = b/(j+1)^k$, b is the Boltzmann factor for the nearest-neighbor interaction energy, and k is the ring weighting exponent. To completely

change the notation from the model of binding solute particles to that of melting a double helix, we reinterpret the factor s_1. Certainly we are no longer interested in the concentration of solute particles since these no longer exist in the model. Since the goal of this exercise is to show the mathematical equivalence of the matrix method with the generating sequence method, we change both the notation and the interpretation of the characteristic parameters to coincide with existing theories, i.e.,

$$\frac{mF}{55}\,\frac{S}{S} = s\chi \quad , \qquad (100)$$

where χ represents a factor containing the entropy and end effect.[119] Multiplying Eq.(100) by the polymer concentration yields the new definition of s_1,

$$s_1 = cs^{N+1}\chi \quad , \qquad (101)$$

still keeping in mind that N+1 is the chain length. We now observe that Eqs.(101) and (98) are precisely the definitions of s_1 and $G(x)$ used by Applequist[99,147] and Damle[119] in their extension of the theory of Lifson and Zimm.[106] It is also true that the eigenvalues of Eq.(95) correspond to the two regions of the transition mentioned by Applequist,[147] i.e.,

$$\lambda = 1 \equiv 1/X_1 \qquad (s < s_c) \quad , \qquad (102)$$

$$\lambda = s \equiv 1/X_2 \qquad (s > s_c) \quad . \qquad (103)$$

Thus far, the inclusion of more than one ring has been simply to raise the function $s_1G(x)$ to the power corresponding to the number of rings and then sum over all possible numbers of rings.[106,147] This approximation appears to be valid in the infinite chain length limit since the states

which correspond to overlapping of rings are negligible compared to the states of widely separated rings. Furthermore, larger rings tend to grow at the expense of smaller rings, i.e., $(j + j')^k < (jj')^k$ when $j,j' > 2$, which tends to decrease the weight of a polymer state containing many rings if the interaction energy between neighboring sites is attractive. In the finite chain length case, however, the restriction on the number of sites within and without the loop is crucial. That is, the sum in Eq.(98) cannot be allowed to go to infinity. Fortunately, as shown in Appendix E, if $N^{3/2} \leq SW$ where N is the chain length and SW is the effective Boltzmann weighting factor for the total nearest-neighbor interaction energy, then multiple loop contributions are negligible.

APPENDIX A: DERIVATION OF THE GENERALIZED GENERATING MATRIX

It is assumed that L-1 dilute species in addition to the solvent molecules have the capacity to bind to the N sites in subsystem I. Furthermore, it is assumed that the interaction of the state at site i extends over a range of 2p+1 sites, i.e., from site i-p to site i+p. All sites are assumed to interact pairwise with all others with a potential which depends only on the species bound at the sites and the relative displacement as measured by the intervening number of sites r-1. The interaction energy of order r, $f_{i-r,i}(\alpha|\beta)$ is the energy of interaction of site i-r occupied by species α with site i occupied by species β. This quantity is assumed to be independent of the value of i so long as i-r > 0 and may be denoted by $f(r|\alpha|\beta)$. The range of r may be extended to include r=0 if we set

$$f(0|\alpha|\beta) = f(\alpha)\delta_{\alpha,\beta} \quad , \tag{A1}$$

where $f(\alpha) = f'(\alpha) - \mu(\alpha)$ and $\delta_{\alpha,\beta}$ is the Kronecker delta function. If we first set

$$W(r|\alpha|\beta) = \exp[-f(r|\alpha|\beta)/RT] \quad , \tag{A2}$$

then for an adsorption region of N sites the grand partition function becomes

$$GPF(N) = \sum_{\alpha=0}^{L-1} W(0|\alpha|\alpha) \sum_{\beta=0}^{L-1} W(0|\beta|\beta)W(1|\alpha|\beta) \sum_{\gamma=0}^{L-1} W(0|\gamma|\gamma)W(1|\beta|\gamma)W(2|\alpha|\beta)$$
$$\ldots \sum_{\xi=0}^{L-1} W(0|\xi|\xi)W(1|\rho|\xi) \ldots W(N-2|\beta|\xi)W(N-1|\alpha|\xi) \quad \ldots \quad , \tag{A3}$$

An appreciable simplification of the grand partition function can only be achieved when the interaction between sites is negligible for sites

separated by more than p-1 intervening sites, where p-1 << N. Assuming that this is the case, we note that the first p site of subsystem I taken as a group can exist in any one of L^p configurations. The corresponding L^p different energies result from the particular configurations of this set of p sites. Using the convention that (L-1) implies a solvent bound at a particular site, while 0,1,...,(L-2) denotes a particular molecular type of the remaining (L-1) dilute species, the configurations of the p sites can be represented by p-digit L-nary (i.e., base L) numbers:

State \ Site	1	2	3.....p-2	p-1	p
1	0	0	0 ... 0	0	0
2	0	0	0 ... 0	0	1
3	0	0	0 ... 0	0	3
...	...	...	... ...	...	...
L	0	0	0 ... 0	0	L-1
...	...	...	... ...	...	...
L^2	0	0	0 ... 0	L-1	L-1
...	...	...	... ...	...	...
L^2+2	0	0	0 ... 1	0	1
...	...	...	... ...	...	...
L^p	L-1	L-1	L-1 ... L-1	L-1	L-1

We now construct a vector whose components are numbered by the ordered p-digit L-nary numbers characterizing the configurations. The Boltzmann statistical weighting factor of a particular configuration is recorded in the corresponding position of the statistical weight vector. For

example, in the case where only 3 species can bind (i.e., L = 3) and interactions only up to the fourth nearest neighbor are allowed (i.e., p = 4), the initial row vector is

$$\underset{\sim}{I}^{o} = [S(0000),S(0001),S(0002),S(0010),\ldots,S(2221),S(2222)] , \qquad (A5)$$

where S(klmn) is the statistical weight of a chain 4 units long in the configuration klmn. Addition of the site p+1 in conjunction with all possible states of the previous p-1 sites simply regenerates the L^p configurations of the first p sites. This new stastical weight vector can be generated by multiplying the initial weight vector by an appropriate $L^p \times L^p$ matrix $\underset{\simeq}{M}$ whose rows and columns are also labeled by the ordered p-digit L-nary indices and whose matrix elements are given by

$$M(\alpha\beta\gamma\ldots\pi,\alpha'\beta'\gamma'\ldots\xi'\pi') = \delta_{\beta\alpha'}\delta_{\alpha\beta'}\ldots\delta_{\pi\xi'}V(\alpha\alpha'\beta'\ldots\pi'), \qquad (A6)$$

where

$$V(\alpha\alpha'\beta'\ldots\pi')=W(0|\pi'|\pi)W(1|\xi'|\pi')\ldots W(p-\alpha|\beta'|\pi')W(p-1|\alpha'|\pi')W(p|\alpha|\pi'), \qquad (A7)$$

is the contribution to the statistical weight obtained by addition of a site in state π' to a pre-existing state of p-1 sites in the configuration $\alpha'\beta'\gamma'\ldots\xi'$. For the particular case L=3, p = 4, $\underset{\simeq}{M}$ is a matrix of the form

Site Label in Sequence 1 2 3 4	5	4	3	2	1
	0	0	0	0	2
0 0 0 0	V(00000)	V(00001)	0	0	0
0 0 0 1	0	0	0	0	0
.....	...	...	...	...	...
0 1 0 0	0	0	0	V(01000)	0
.....	...	...	...	...	...
1 0 1 0	0	0	V(10100)	0	0
.....	...	...	...	...	...
2 0 0 0	V(20000)	0	0	0	0
.....	...	...	...	...	...
2 2 2 2	0	0	0	0	V(22222)

Since the terminal p-1 sites of the new row index must be identical to the initial p-1 sites of the column index, there are <u>at most</u> L non-zero elements in any column. It is possible that a particular model may have fewer than L non zero elements. For example, if it is physically impossible for two bulky solute particles to occupy adjacent binding sites then the corresponding nearest-neighbor interaction energy is effectively infinite and the Boltzmann weighting factor is zero.

Each matrix element has a value which depends upon its corresponding column index that represents the configuration of the terminal p sites of the chain (now p+1 units in length). Multiplying the initial row vector $\underset{\sim}{I}^{o}$ on the left into the matrix $\underset{\simeq}{M}$ results in a new row vector $\underset{\sim}{I}^{1}$ whose positions (i.e., columns) are labeled by the column indices of $\underset{\simeq}{M}$. In

general there are L non-vanishing products which are summed to form the element of $\underset{\sim}{I}^1$. The important feature is that the non-vanishing row elements in a particular column of the matrix M are located such that only the elements in $\underset{\sim}{I}^0$ whose indices contain a terminal sequence of p-1 digits matching the initial sequence of p-1 digits in the column index of $\underset{\approx}{M}$ give non-vanishing contributions. For the particular case L = 3, p = 4 the multiplication gives us

$$\begin{aligned}\underset{\sim}{I}^1 = \underset{\sim}{I}^0\underset{\approx}{M} = &[S(0000)V(00000)+S(1000)V(10000)+S(2000)V(20000)] , \\ &[S(0000)V(00001)+S(1000)V(10001)+S(2000)V(20001)] , \\ \ldots , &[S(0001)V(00010)+S(1001)V(10010)+S(2001)V(20010)] , \ldots , \\ &[S(0222)V(02222)+S(1222)V(12222)+S(2222)V(22222)] .\end{aligned} \qquad (A9)$$

The value of an element in $\underset{\sim}{I}^1$ is just the statistical weight of all possible sequences of the p+1 sites whose terminal p sites have the configuration specified by the index (i.e., column) of that element. Repeated multiplication by $\underset{\approx}{M}$ generates new vectors whose elements correspond to all possible configurations whose terminal p sites correspond to the index of the vector component. The sum over the statistical weights of all possible allowed configurations is the grand partition function,

$$GPF(N) = \underset{\sim}{I}^0 \cdot \underset{\approx}{M}^{N-p} \cdot \underset{\sim}{1}^+ \qquad , \qquad (A10)$$

where $\underset{\sim}{1}$ is a row vector whose elements are either unity or zero depending on the restrictions imposed on the terminal p sites of the chain of length N.

APPENDIX B: SIMPLIFICATION OF THE GRAND PARTITION FUNCTION IN THE INFINITE CHAIN LENGTH LIMIT.

Consider the general case in which the grand partition function is calculated by the matrix multiplication

$$GPF(N) = \underset{\sim}{a} \cdot \underset{\simeq}{M}^{N} \cdot \underset{\sim}{b}^{+} \quad , \qquad (B1)$$

where $\underset{\sim}{a}, \underset{\sim}{b}^{+}$ are appropriate row and column vectors, respectively, and M is the generating matrix for a sequence of N sites. If $\underset{\simeq}{T}^{-1}$ and $\underset{\simeq}{T}$ are matrices which diagonalize $\underset{\simeq}{M}$, i.e.,

$$\underset{\simeq}{T}^{-1} \cdot \underset{\simeq}{M} \cdot \underset{\simeq}{T} = \underset{\simeq}{\Lambda} \quad , \qquad (B2)$$

and subject to the condition

$$\underset{\simeq}{T}^{-1} \cdot \underset{\simeq}{T} = \underset{\simeq}{T} \cdot \underset{\simeq}{T}^{-1} = \underset{\simeq}{E} \quad , \qquad (B3)$$

where $\underset{\simeq}{E}$ is the identity matrix, then Eq.(B1) can be written in the form

$$GPF(N) = \underset{\sim}{a} \cdot \underset{\simeq}{T} \cdot \underset{\simeq}{\Lambda}^{N} \cdot \underset{\simeq}{T}^{-1} \cdot \underset{\sim}{b}^{+} \quad , \qquad (B4)$$

If it is assumed that the largest element of $\underset{\simeq}{\Lambda}$ occupies the (1,1) position and that it is non-degenerate, then as N approaches infinity

$$\lambda_1^N \begin{vmatrix} 1 & 0 & 0 \ldots \\ 0 & (\lambda_2/\lambda_1)^N & 0 \ldots \\ 0 & 0 & (\lambda_3/\lambda_1)^N \end{vmatrix} \cong \lambda_1^N \begin{vmatrix} 1 & 0 & 0 \ldots \\ 0 & 0 & 0 \ldots \\ 0 & 0 & 0 \ldots \\ \vdots & \vdots & \vdots \end{vmatrix} \quad . \qquad (B5)$$

In this limit Eq.(B4) simplifies to the expression

$$GPF(N \to \infty) = \lambda_1^N GH \quad , \tag{B6}$$

where

$$G \equiv (\underset{\sim}{a} \cdot \underset{\approx}{T})_1 \quad , \tag{B7}$$

and

$$H \equiv (\underset{\approx}{T}^{-1} \cdot \underset{\sim}{b}^{+})_1 \quad . \tag{B8}$$

For the general case when $\underset{\approx}{M}$ is a 2x2 matrix of the form

$$\underset{\approx}{M} = \begin{vmatrix} A & B \\ C & 1 \end{vmatrix} \quad , \tag{B9}$$

we have the eigenvalue equation

$$\begin{vmatrix} A & B \\ C & 1 \end{vmatrix} \begin{pmatrix} X_1 \\ X_2 \end{pmatrix} = \begin{vmatrix} \lambda & 0 \\ 0 & \lambda \end{vmatrix} \begin{pmatrix} X_1 \\ X_2 \end{pmatrix} \quad , \tag{B10}$$

whose solutions are

$$\lambda_+ = \frac{(A+1) + \left[(A+1)^2 - 4(A-BC)\right]^{1/2}}{2} \quad , \tag{B11}$$

and

$$\lambda_- = \frac{(A+1) - \left[(A+1)^2 - 4(A-BC)\right]^{1/2}}{2} \quad , \tag{B12}$$

where $\lambda_+ > \lambda_-$. Requirement of normalization of the eigenvectors (x_1, x_2) and (x_1', x_2') corresponding to the eigenvalues λ_+ and λ_-, respectively, leads to the matrices $\underset{\approx}{T}$ and $\underset{\approx}{T}^{-1}$

$$\underset{\approx}{T} = \begin{vmatrix} x_1 & x_1' \\ x_2 & x_2' \end{vmatrix} = \begin{vmatrix} \frac{-B}{D_+} & \frac{-B}{D_-} \\ \frac{(A-\lambda_+)}{D_+} & \frac{(A-\lambda_-)}{D_-} \end{vmatrix} \quad , \tag{B13}$$

and
$$\underline{\underline{T}}^{-1} = \frac{1}{\lambda_+ - \lambda_-} \begin{vmatrix} \frac{-D_+(A-\lambda_-)}{B} & -D_+ \\ \frac{D_-(A-\lambda_+)}{B} & D_- \end{vmatrix} , \tag{B14}$$

where
$$D_\pm \equiv [B^2 + (A-\lambda_\pm)^2]^{1/2} . \tag{B15}$$

The quantity C_1 introduced in Eq.(44) can now be evaluated. The generating matrices for the GPF(N) and GPFS(N) are identical [cf., Eqs.(38) and (41)], therefore the corresponding values of G and H as defined in Eqs.(B7) and B8), respectively, are found to be

$$H[GPF(N)] = T^{-1}(1,1) + T^{-1}(1,2) , \tag{B16}$$

$$G[GPF(N)] = T(1,1) , \tag{B17}$$

$$H[GPFS(N)] = T^{-1}(1,1) , \tag{B18}$$

and
$$G[GPFS(N)] = \frac{mF}{55} T(1,1) . \tag{B19}$$

The ratio C_1 is

$$C_1 = \frac{H[GPFS(N)]G[GPFS(N)]}{H[GPF(N)]G[GPF(N)]} = \frac{mFT^{-1}(1,1)}{55[T^{-1}(1,1) + T^{-1}(1,2)]} . \tag{B20}$$

Substituting the values A = mFS/55 and B = 1 into Eqs.(B13) and B(14) and noting $mFS/55 - \lambda_- = \lambda_+ - 1$, we arrive at the expression

$$C_1 = \frac{mFS(\lambda_+ - 1)}{55[3\lambda_+ - (mFS/55) - 1]} . \tag{B21}$$

APPENDIX C: THE COMPUTATION

The fraction of sites that are occupied by component i on the polyU chain of N units is given by

$$\theta_i = \frac{1}{N} \frac{\partial \ell n GPF(N)}{\partial \ell n m_i} \quad , \qquad (C1)$$

for the single stack model, where GPF(N) is defined by Eq.(38).

At a particular value of m_A, the GPF(N) was first computed for the values $(1 + \delta)m_A$ and $(1 - \delta)m_A$ which were then used to approximate the derivative by the finite difference

$$\left.\frac{\partial n GPF(N)}{\partial \ell n m_A}\right|_{m_A} \cong \frac{\ell n GPF(N)\big|_{m=(1+\delta)m_A} - \ell n GPF(N)\big|_{m=(1-\delta)m_A}}{\ell n(1+\delta)m_A - \ell n(1-\delta)m_A} \quad . \qquad (C2)$$

The values $\delta = .01$ and $\delta = .001$ did not result in significantly different curves. Most of the computations, however, employed $\delta = .001$.

According to Eq.(38), the generating matrix is raised to the (N-1)th power. The actual computation did not involve N-1 matrix multiplications. N-1 was broken down into sums and products involving only 2 and 1. For example,

$$500 = 2X2X(2X2X(2X(2X(2X(2+1)+1)+1)+1)+1) \quad . \qquad (C3)$$

Thus, the actual multiplication involved only thirteen matrix multiplications when N = 501. If degeneracy is included [cf., Eq.(41)], then it is clear that each multiplication must be done independently.

Although Eq.(C1) is valid for the calculation of the fraction of sites occupied by guanosine in the studies by Pitha, Huang, and Ts'o,[20] the situation is complicated by the fact that the concentration m_G of free

guanosine is not directly given, but rather the total concentration is fixed at $m_G^o = 1.0 \times 10^{-5} M$. We have then

$$m_G^o = < m_G^b > + m_G^f \quad , \qquad (C4)$$

where m_G^f is the molality of free guanosine, and m_G^b is the total average (over solutions both inside and outside the dialysis membrane, where $m_G^b = 0$) molality of bound guanosine. It is clear that

$$< m_G^b > = \theta_G \frac{< m_U >}{2} \quad , \qquad (C5)$$

where m_U is the total average (inside and outside the dialysis membrane) molality of the uracils. In this calculation an iterative procedure was employed in which a trial value $m_G^f(i)$ was selected, and θ_G then calculated using the appropriate analogue of Eq.(C1) after which $< m_G^b(i) >$ was calculated from Eq.(C5). At the end of each iteration step the sum $[m_G^f(i) + < m_G^b(i) >]$ was compared with m_G^o [cf., Eq.(C4)], and the trial value $m_G^f(i+1)$ adjusted in such a way as to improve the agreement at the end of the subsequent (i+1)th iteration. This stepwise procedure was repeated until for some i the condition

$$\left| \frac{< m_G^b(i) > + m_G^f(i)}{m_G^o} - 1 \right| \leqslant 10^{-4} \quad , \qquad (C6)$$

was met, and the prevailing $m_G^f(i)$ and $< m_G^b(i) >$ were adopted as the average molalities of, respectively, free and bound G.

Once a value of m_G^f satisfying Eq.(C6) had been found, this value was then used in a final iteration step in which the sliding degeneracy was included [cf., Eq.(41)]. It was found that after this final iteration

$$\left| \frac{< m_G^b > + m_G^f}{m_G^o} - 1 \right| \leq 10^{-2} \quad , \qquad (C7)$$

so that conservation [cf., Eq.(C4)] was adequately satisfied.

The use of GPF(N) rather than GPFS(N) for all iterations except the last was dictated by the much smaller amount of computer time required for evaluating GPF(N).

APPENDIX D: CONDITION FOR MIDPOINT EQUIVALENCE OF BRAGG-WILLIAMS AND NEAREST-NEIGHBOR MODELS FOR LINEAR ADSORPTION

The Bragg-Williams approximation assumes that the average interaction energy can be substituted for the actual interaction energy and that the solute particles are randomly bound to the potential surface. For the random distribution, the probability that any one site is bound is b/N, where b is the number of bound solute particles and N is the number of sites. If $\bar{S}$ is the molar nearest-neighbor interaction energy, then the average interaction energy is

$$< \bar{S} > = c(b/N)b\bar{S}/2 = b^2\bar{S}/N \quad , \qquad (D1)$$

where the coordination number c is equal to 2 in the linear system and the factor $\frac{1}{2}$ corrects for counting the pairs twice. The cannoical partition function then becomes

$$Q(b,V,T) = \frac{N!}{b!(N-b)!} \exp(-\frac{\bar{F}b}{RT})\exp(-\frac{b^2\bar{S}}{NRT}) \quad , \qquad (D2)$$

where $\bar{F}$ is the molar binding energy. Making use of the relationship

$$\bar{F}_b^o = -RT\ell nQ(b,V,T) \quad , \qquad (D3)$$

where $\bar{F}_b^o$ is the free energy of one mole of lattice particles containing b bound species in their infinite dilution standard state. The chemical potential of an ideal solution of lattice particles with the bound species is

$$\mu_b = \bar{F}^o + RT\ell nX_b \quad , \qquad (D4)$$

where X_b is the mole fraction of lattice particles with b bound species. The chemical potential of the free solute species is

$$\mu_f = \mu_f^o + RT\ell nX_f \quad , \qquad (D5)$$

where the subscript f denotes the free solute species. The free energy for the reaction (G = solute monomer)

$$P + bG = PG_b \quad , \qquad (D6)$$

is given by

$$\Delta F/RT = \frac{\mu_b - \mu_f b}{RT} \quad , \qquad (D7)$$

$$= \ell n(X_b/X_b X_f^b) - \ell n(N!/(N-b)!b!) + \frac{b\overline{F}}{RT} + b^2\overline{S}/NRT \quad . \qquad (D8)$$

Expressing Eq.(D8) in terms of molalities,

$$\frac{F}{RT} = \ell n(m_b/m_o m_f^b) - \ell n(N!/(N-b)!b!) + \frac{\overline{F}b}{RT} - b\ell n55 + \frac{b^2\overline{S}}{NRT} \quad , \qquad (D9)$$

and noting Scatchard's Eq.(1)

$$(\Delta F)_\upsilon/RT = \ell n c_\upsilon/C_o C_A^\upsilon + \ell n\upsilon!(n-\upsilon)!/n! - \upsilon\ell nk + \omega\upsilon^2 \quad , \qquad (D10)$$

we have the identities

$$\omega = \overline{S}/NRT \quad , \qquad (D11)$$

$$k = \exp(-\overline{F}/RT)/55 \quad , \qquad (D12)$$

and

$$c_\upsilon \simeq m_\upsilon \quad . \qquad (D13)$$

The equation of interest, however, is Scatchard's Eq.(4),

$$\ell nk'c = \ell n\frac{\bar{\upsilon}}{n-\bar{\upsilon}} + 2\omega'\bar{\upsilon} \quad , \qquad (D14)$$

where $k' = k\exp(\omega)$, $\omega' = (1+1/n)^{\omega}$, and $\bar{\upsilon}$ is the average association. Comparison of Eq.(D14) with Guschlbauer's Eq.(2),[21]

$$\frac{r}{m_G}e^{2Er/kT} = k_o(n-r) \quad , \qquad (D15)$$

implies the identities

$$r = \bar{\upsilon}/2N \quad , \qquad (D16)$$

$$n = N/2N = .5 \quad , \qquad (D17)$$

$$k_o = ke^{\omega} = (55)^{-1}\, e^{-\bar{F}/RT} e^{+\bar{S}/NRT} \quad , \qquad (D18)$$

and

$$E/kT = 2N\omega - 2\bar{S}/RT \quad . \qquad (D19)$$

Substitution of Eqs.(D18) and (D19) into Eq.(D15) and then evaluation at the midpoint $\upsilon = N/2$ results in the expression

$$\frac{m_G}{55}\, e^{-\bar{F}/RT} e^{-\bar{S}/RT} e^{\bar{S}/NRT} = 1 \quad . \qquad (D20)$$

In the infinite chain length limit, Eq.(D20) becomes identical to Eq.(33). Defining the fraction of sites bound as $\theta = r/n$, Eq.(D15) becomes

$$k_o m_G = \frac{\theta}{1-\theta}\, e^{2\bar{S}\theta/RT} \quad , \qquad (D21)$$

or

$$\ell nk_o + \ell nm_G = \ell n\theta - \ell n(1-\theta) + 2\bar{S}\theta/RT \quad , \qquad (D22)$$

Differentiating Eq.(D22) with respect to ℓnm_G and then solving for $\partial\theta/\partial\ell nm_G$, we obtain

$$\frac{\partial\theta}{\partial \ell n m_G} = \frac{1}{\frac{1}{\theta} + \frac{1}{1-\theta} + \frac{2\bar{S}}{RT}} \qquad (D23)$$

At the midpoint, $\theta = \frac{1}{2}$ and

$$\frac{\partial\theta}{\partial \ell n m_G}_{\theta=\frac{1}{2}} = \frac{1}{2\bar{S}/RT} \quad , \qquad (D24)$$

For $\bar{S}/2RT \ll 1$, Eq.(D24) takes the form

$$\frac{\partial\theta}{\partial \ell n m_G}_{\theta=\frac{1}{2}} = \frac{1}{4}\left(\frac{1}{1+\bar{S}/2RT}\right) = \frac{1}{4}(1-\bar{S}/2RT+\ldots) \simeq \frac{1}{4}\exp(-\bar{S}/2RT). \qquad (D25)$$

Eq.(D25) is identical to Eq.(36) in the limit of weak interactions. This result is not entirely unexpected since all models involving neighbor interactions should reduce to the ideal case in the limit of weak interactions.

APPENDIX E: INCLUSION OF RING FORMATION IN COMPLEXES OF FINITE CHAIN LENGTH

It is clear from Eq.(40) that the assumption of only one solute stack is not valid for very long chains or particles with repulsive or weakly attractive interactions. Under these conditions, an accurate description of the solute binding curve must include the possibility of forming one or more loops. Since the solute particles are monomers, loop formation is only meaningful in terms of the polymer configuration of the complex. For one loop containing j non-bonded bases, the infinite chain length limit ring weighting factor, or interuption parameter, is[101,104,119]

$$\sigma_j = 2^k(j+1)/w(j+2)^k \quad , \qquad (E1)$$

where j+1 is the ring degeneracy factor, W is the Boltzmann weighting factor as defined by Eq.(49), and k has a value between 1.5 and 2. The factor j+1 cannot be included when the chains are of finite length since this amounts to the transfer of sites from one polymer to the other. This is obvious for two chains that are attached at the terminal sites. We now define the ring weighting factor for a single ring of fixed configuration, i.e., m non-bonded bases from chain p and m' non-bonded bases from chain p', as

$$R_{m,m'} = [2/(m+m' + 2)]^k/W \quad . \qquad (E2)$$

Consider an adsoprtion region which is defined by the first and last bound particle.. It is assumed that:

(1) the thermodynamic paramters depend only on the state of the solute binding sites;

(2) no loops can form within a bound solute stack.

The effect of assumption 1 is the simplification of the mathematics, since Eqs.(56),(74), and (75) imply that a one stack region is essentially a two parameter problem. Assumption 2 is a reflection of the monomeric nature of the solute particles. It does not seem to be physically reasonable to force a "kink" in the polymer structure to simultaneously accommodate a uniform structure of the solute stack. For this reason, there must be at least one polymer site from each polymer in every loop that is formed. In terms of the ring degeneracy factor for the infinite chain length limit, j+1 is replaced by j-1.

We adopt the notation that m_i and m_i' represent the number of non-bonded bases in loop i from the chains p and p', respectively. Then the total number L of non-bonded bases in a given configuration of the adsorption region is

$$L = \ell + \ell' \quad , \qquad \text{(E3)}$$

where

$$\ell = \sum_i m_i \quad , \qquad \text{(E4)}$$

$$\ell' = \sum_i m_i' \quad . \qquad \text{(E5)}$$

We now ask what the degeneracy is for a fixed configuration of loops. Clearly, we can adjust the arrangement of the bonded solute particles within the adsorption region by simply "sliding" the interfacial solute particles from one side of the loop to the other side of the same loop. This "abacus" effect is nothing more than the arrangement of balls in boxes since at least one solute particle must remain to separate the two adjacent loops. The degeneracy factor is simply

$$A_{n,b} = (b-1)!/n!(b-1-n)! \quad , \qquad \text{(E6)}$$

TABLE E1

Representative Portions of the Calculated Solute Binding Curves*

	(b/N) x 100				
$mx10^3$	A	B	C	D	E
1.5	15.37	22.79	22.85	24.49	23.29
2.0	19.32	27.80	27.89	30.00	28.65
2.5	24.80	33.15	33.25	35.90	34.39
3.0	31.73	38.61	38.71	41.84	40.19
4.0	47.15	48.81	48.87	52.50	50.75
4.5	54.77	53.37	53.40	56.96	55.30
5.0	61.43	57.43	57.44	60.78	59.25
7.0	77.62	69.07	69.03	71.01	70.61
9.5	85.65	77.14	77.09	77.58	77.43
12.0	89.39	81.86	81.81	81.29	81.63
15.0	91.88	85.46	85.41	84.10	84.85
16.0	97.74	86.37	86.32	84.81	85.66

Notation	Model (Chain length = 11 units)
A = GPFS(N)	Single solute stack only (with sliding degeneracy)
B = GPFS(N) + GPF1(N)	Single solute stack and single loop (exact)
C = GPFR(N)	Single solute stack and multiple loops (exact)
D = GPFS(N) + GPFS1(N)	Single solute stack and integrated single loop ring weighting factor
E = GPFS(N) + GPFA(N)	Single solute stack and average single loop size

* parameters used in these calculations:

$\bar{F}$ = -5490 cal/mole ; $\bar{S}$ = 50 cal/mole ; $\bar{W}$ = 50 cal/mole

where b is the total number of bound solute particles and n is the number of loops. The sliding degeneracy, i.e., the arrangement of non-bonded polymer sites exterior to the adsorption region, is given by

$$D_{N,b,\ell\ \ell'} = (N-b-\ell+1)(N-b-\ell'+1) \quad , \qquad (E7)$$

where N is the length of the polymer. The grand partition function can be found in the following manner. Assume that the entire adsorption region is bound by solute particles, i.e., only one stack. The Boltzmann weighting factor for a single stack of b solute particles is $(mF/55)^b S^{b-1}$, where m,F, and S are defined in Section IV. The introduction of a single loop within the solute stack changes the Boltzmann weighting factor to $(mF/55)^b S^{b-2}$. In general, the introduction of n loops into a stack of b solute particles results in a Boltzmann weighting factor of $(mF/55)^b S^{b-1-n}$. The contribution to the partition function of a fixed configuration of loops $C\{m_i,m_i'\}$, i.e., a particular set of numbers $\{m_i,m_i'\}$, is given by

$$C\{m_i,m_i'\} = (mF/55)^b S^{b-1-} \ A_{n,b}\ D_{N,b,\ell,\ell'} \ \prod_{i=1}^{n} R_{m_i,m_i'} \ . \qquad (E8)$$

We have not yet considered the abacus effect of the non-bonded sites within the loop. Clearly, the factor $(m+m'+2)^{-k}$ prevents one from writing a simple expression analogous to Eq.(E6). At this point of the development, no simplifying expression has been found for the abacus effect of the loops. The contribution to the partition function for a fixed set $\{\ell,\ell'\}$ is the summation of Eq.(E8) over all possible sets of $\{m_i,m_i'\}$, i.e.,

$$C\{\ell,\ell'\} = \sum_{\{m_i,m_i'\}} C\{m_i m_i'\} \quad . \qquad (E9)$$

Explicitly, $C\{\ell,\ell'\}$ is

$$C\{\ell,\ell'\} = (mF/55)^b S^{b-1-n} A_{n,b} D_{N,b,\ell,\lambda'} G_{\ell,\ell',n} \quad , \qquad \text{(E10)}$$

where

$$G_{\ell,\ell',n} = \sum_{\{m_i,m_i'\}} \prod_{i=1}^{n} R_{m_i,m_i} = \quad , \qquad \text{(E11)}$$

$$\left(\frac{2k}{W}\right)^n \sum_{m_1=1}^{\ell-n+1} \sum_{m_1=1}^{\ell'-n+1} \sum_{m_2=1}^{\ell-n+2-m_1} \sum_{m_2'=1}^{\ell'-n+2-m_1'} \cdots \sum_{m_{n-1}=1}^{\ell-1-\sum_{i=1}^{n-1} m_i} \sum_{m_{n-1}'=1}^{\ell'-1-\sum_{i=1}^{n-1} m_i'} \prod_{i=1}^{n} (m_i+m_i'+2)^{-k} \quad , \qquad \text{(E12)}$$

and it is understood that

$$m_n \equiv \ell - \sum_{i=1}^{n-1} m_i \quad , \qquad \text{(E13)}$$

and

$$m_n' = \ell' - \sum_{i=1}^{n-1} m_i' \quad . \qquad \text{(E14)}$$

The grand partition function with rings GPFR(N) can be written as

$$GPFR(N) = 1 + \sum_{b=1}^{N} \frac{mF}{55}^b S^{b-1} \left[(N-b+1)^2 + \sum_{\ell=1}^{N-b} \sum_{\ell'=1}^{N-b} \frac{2^k(b-1)}{SW} \frac{(N-b-\ell+1)(N-b-\ell'+1)}{(\ell+\ell'+2)^k}\right]$$

$$+ \sum_{n=2}^{(N-1)/2} \sum_{b=n+1}^{N-n} \sum_{\ell=n}^{N-b} \sum_{\ell'=n}^{N-b} (mF/55)^b S^{b-1-n} A_{n,b} D_{N,b,\ell,\ell'} G_{\ell,\ell',n} \quad . \qquad \text{(E15)}$$

The first two summations represent the contributions to the partition function of the single solute stack and single loop configurations, while the last expression represents the multiple loop contributions.

Single Loop Contributions for Long Chains

The contributions of the single loop configurations are

$$GPF1(N) = \sum_{b=1}^{N} \sum_{\ell=1}^{N-b} \sum_{\ell'=1}^{N-b} \left(\frac{mF}{55}\right)^b S^{b-2} \frac{(b-1)2^k}{W} \frac{(N-b-\ell+1)(N-b-\ell'+1)}{(\ell+\ell'+2)^k} , \qquad (E16)$$

$$= \sum_{b=1}^{N} \left(\frac{mF}{55}\right)^b S^{b-2} \frac{(b-1)2^k}{W} \sum_{\ell=1}^{N-b} \sum_{\ell'=1}^{N-b} \frac{(N-b-\ell+1)(N-b-\ell'+1)}{(\ell+\ell'+2)^k} . \qquad (E17)$$

We now assume that the summations over ℓ and ℓ' can be replaced by integrals when $N-b \gg 1$, i.e.

$$\sum_{\ell=1}^{N-b} \sum_{\ell'=1}^{N-b} \frac{(N-b-\ell+1)(N-b-\ell'+1)}{(\ell+\ell'+2)^k} \simeq \int_1^{N-b} (N-b-\ell+1)\,d\ell \int_1^{N-b} \frac{(N-b-\ell'+1)\,d\ell'}{(\ell+\ell'+2)^k} . \qquad (E18)$$

If we ignore any small integers occuring with N-b, the largest term after integration becomes

$$I_{k,N,b} \simeq \frac{(N-b)^{4-k}(2^{4-k}-10+2k)}{(4-k)(3-k)(2-k)(1-k)} , \qquad (E19)$$

For the random flight model of the polymers (k=1.5), Eq.(E19) becomes

$$I_{3/2,N,b} \simeq 1.44(N-b)^{5/2} . \qquad (E20)$$

The grand partition function for the one stack and one loop contributions can then be approximated by

$$GPFS1(N) \simeq \sum_{b=1}^{N} \left(\frac{mF}{55}\right)^{b} S^{b-1}\left[(N-b+1)^2 + \frac{2^{3/2}(1.44)(b-1)(N-b)^{5/2}}{SW}\right]. \qquad (E21)$$

It follows directly from Eq.(E21) that the formation of loops can be ignored if

$$\frac{2.88N^{3/2}}{SW} << 1 \quad , \qquad (E22)$$

when $b = N/2$ and $N/2 >> 1$.

Now consider the average loop size for a fixed number of bound solute particles. The distribution function for the total number of states is defined as

$$\rho_{b,\ell,\ell'} \equiv (b-1)(N-b-\ell+1)(N-b-\ell'+1) \quad . \qquad (E23)$$

The average number of non-bonded bases from chain p in the single loop configuration is given by $(N-b >> 1)$

$$<\ell> \equiv \int_{1}^{N-b} \rho_{b,\ell,\ell'} \ell d\ell \Big/ \int_{1}^{N-b} \rho_{b,\ell,\ell'} d\ell \quad , \qquad (E24)$$

$$= \int_{1}^{N-b} (N-b-\ell+1)\ell d\ell \Big/ \int_{1}^{N-b} (N-b-\ell+1) d\ell = \frac{(N-b)}{3} \quad . \qquad (E25)$$

A similar result is obtained for $<\ell'>$, hence

$$<\ell> + <\ell'> = \frac{2}{3}(N-b) \quad . \qquad (E26)$$

The grand partition function for the average chain length model for single stack and single loop contributions is then

$$GPFA(N) = \sum_{b=1}^{N} \left(\frac{mF}{55}\right)^b S^{b-1} \left((N-b+1)^2 + \frac{\rho_b 2^k}{SW[2(N-b)/3+2]^k} \right) , \qquad (E27)$$

where

$$\rho_b = (b-1) \int_1^{N-b} \int_1^{N-b} (N-b-\ell+1)(N-b-\ell'+1) d\ell d\ell' \simeq \frac{(b-1)(N-b)^4}{4} , \qquad (E28)$$

This result can also be derived from the direct summation

$$\begin{aligned} \sum_{\ell=1}^{N-b} (N-b-\ell+1) &= (N-b) + (N-b-1) + \ldots + 2 + 1 \quad , \\ &= (N-b+1) + (N-b+1) + \ldots \quad , \\ &= (N-b+1)(N-b)/2 \quad , \end{aligned} \qquad (E29)$$

with a similar expression for the summation over ℓ'. When $k = 1.5$ and $b - N/2$, the criterion for neglecting single loop contributions is

$$\frac{.48N^{3/2}}{SW} \ll 1 \quad . \qquad (E30)$$

The calculated results for binding curves using GPFS(N) [cf., Eq.(41)], GPFS(N) + GPF1(N), GPFR(N), GPFS(N) + GPFS1(N), and GPFS(N) + GPFA(N) are presented in Table E1. In place of the matrix multiplication occurring in GPFS(N) the factor $(mF/55)^b S^{b-1}$ was used. Since the computation time required to calculate GPFR(N) was large, the chain length was restricted to 11 units (i.e., 5 loops). It is clear from Table E1 that the largest contribution to the partition function is from the introduction of the first loop while other loops do not significantly alter the calculated binding

Figure 11

Numerical evaluation of

$$\rho_{exact} = \sum_{\ell=1}^{N-b} \sum_{\ell'=1}^{N-b} (b-1)(N-b-\ell+1)(N-b-\ell'+1)$$

where the number of bound particles $N_b = b$ and the total number of sites on a single chain is $N = 11$.

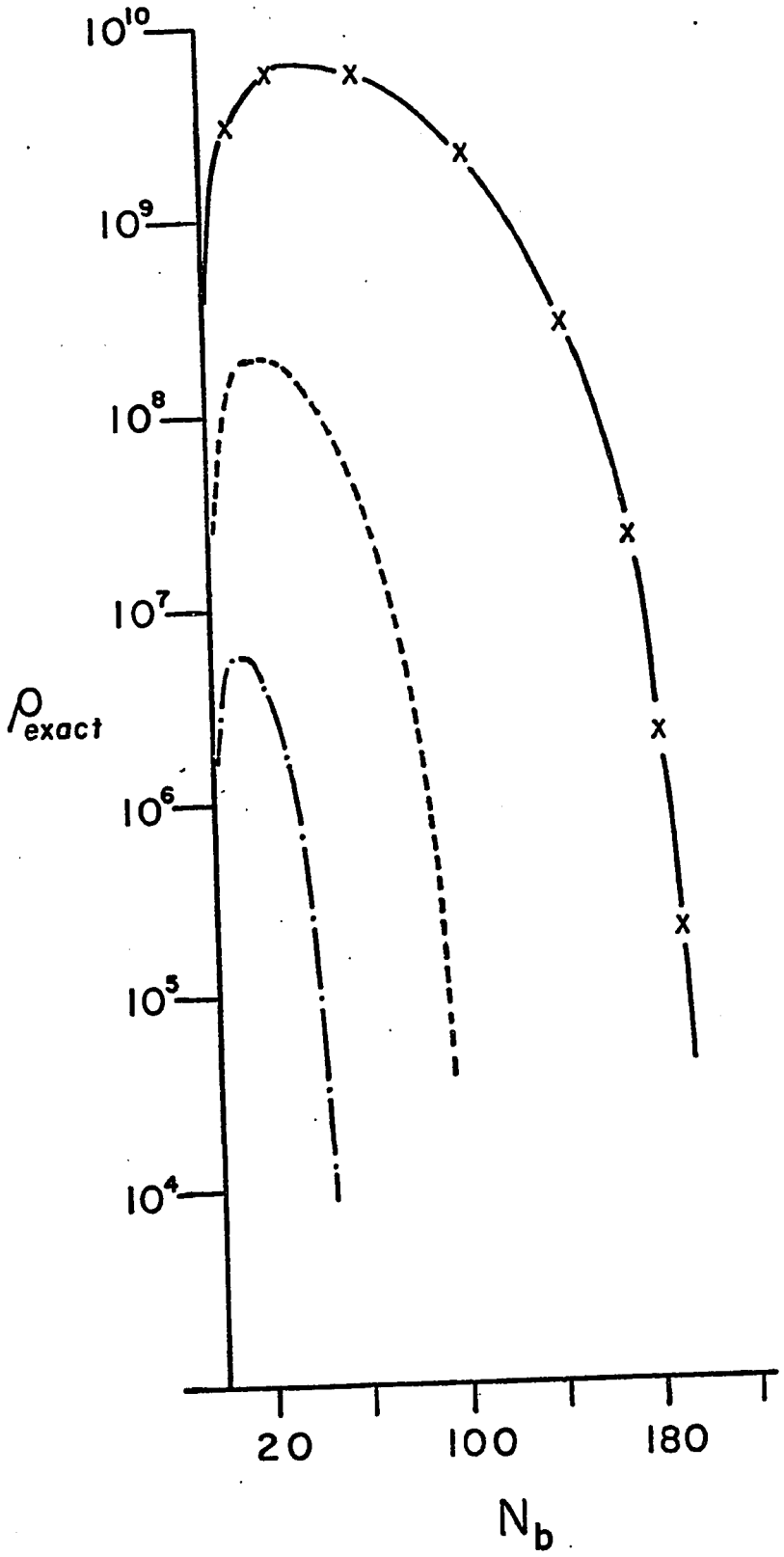
10^{10}
10^{9}
10^{8}
10^{7}
10^{6}
10^{5}
10^{4}
ρ_{exact}
20
100
180
N_b

Figure 12

Fraction R of states counted in the approximation given in Eq.(E28), where

$$R = \frac{(b-1)(N-b)^2}{4\rho_{exact}}$$

where ρ_{exact} is defined in Figure 11.

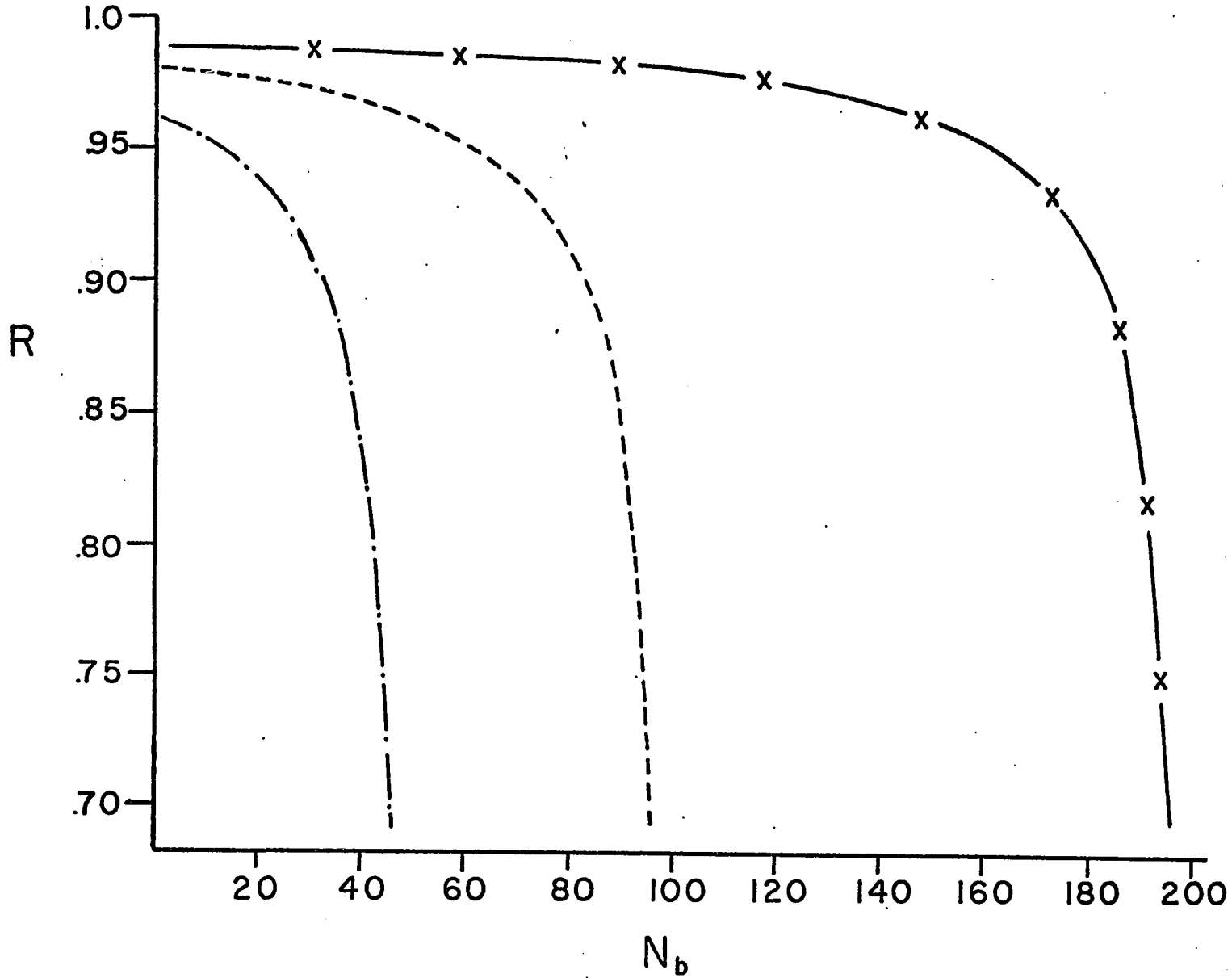
1.0
.95
.90
.85
.80
.75
.70
R
20
40
60
80
100
120
140
160
180
200
N_b

curve. The reason for the apparent excellent agreement between the exact single loop contributions and the integrated forms becomes clear with inspection of Figures 11 and 12, where the density of states function defined by Eq.(E28) is evaluated and compared with the exact values. These figures indicate that more than 95% of the states are accounted for by the density function over the range of states that give significant contributions to the grand partition function. Furthermore, if the stacking parameters S and W are sufficiently attractive such that

$$N^{3/2} \leqslant SW \quad , \qquad \text{(E31)}$$

then the agreement between the three methods vastly improves since the importance of the single loop configurations has correspondingly decreased.

The effect of the formation of loops when the criterion defined in Eq.(E31) is not met is illustrated in Figure 13. Numerical calculations of the coefficients in Eq.(E15) indicate that the grand partition function for N = 11 and b = 6 is

$$GPFR(11) = 1 + (mF/55)^6 S^5 [36 + 211/SW + 1.52/(SW)^2 + .228/(SW)^3 + .01/(SW)^4 + .00008/(SW)^5] \quad . \qquad \text{(E32)}$$

One can now explicitly determine the particular value of SW which is required in order to significantly alter the weight of a particular loop configuration. The effect of repulsive values for $\overline{W}$ is shown in Figure 13. By matching the midpoints, the effect on the shape of the transition curve is illustrated in Figure 14. It is clear that the inclusion of five loops introduces an asymmetry in the calculated curve since the coefficients pertaining to the different numbers of loops are not symmetric about the value b = N/2. The numerical values of the coefficients are given in Table E2.

Figure 13

Effect of loop degeneracy on the solute binding curve for N = 11. All four curves employ the parameters $\overline{F}_A$ = -5490 cal/mole and $\overline{S}_{AA}$ = +50 cal/mole.

(———) no loops

(.....) 1 loop, $\overline{W}$ = +2137 cal/mole

(- - -) 5 loops, $\overline{W}$ = +1093 cal/mole

(x-x-x) 5 loops, $\overline{W}$ = +2137 cal/mole

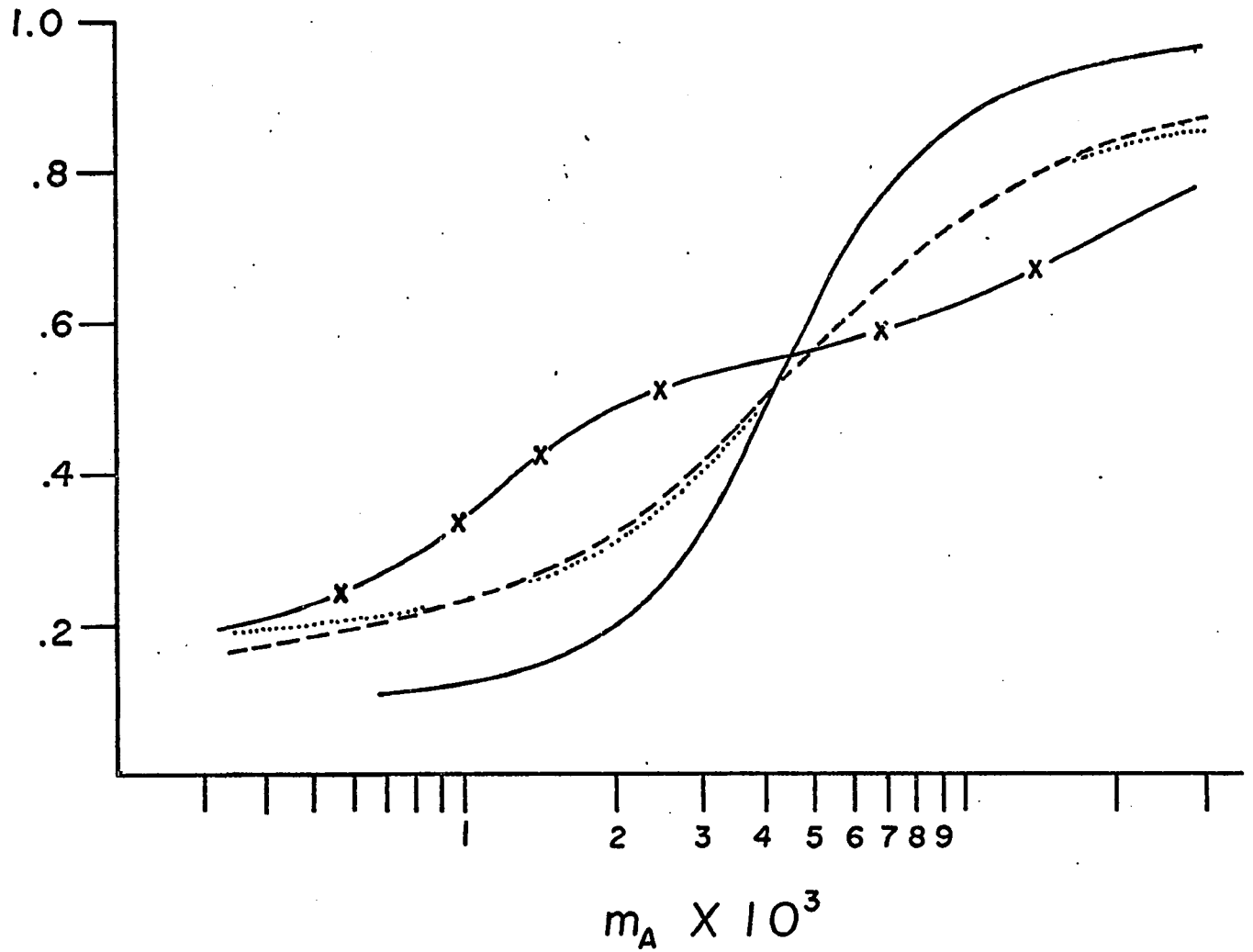
1.0
.8
.6
.4
.2
1
2
3
4
5
6
7
8
9
$m_A \times 10^3$

Figure 14

Effect of loop degeneracy on the shape of the curve. The notation is the same as in Figure 13.

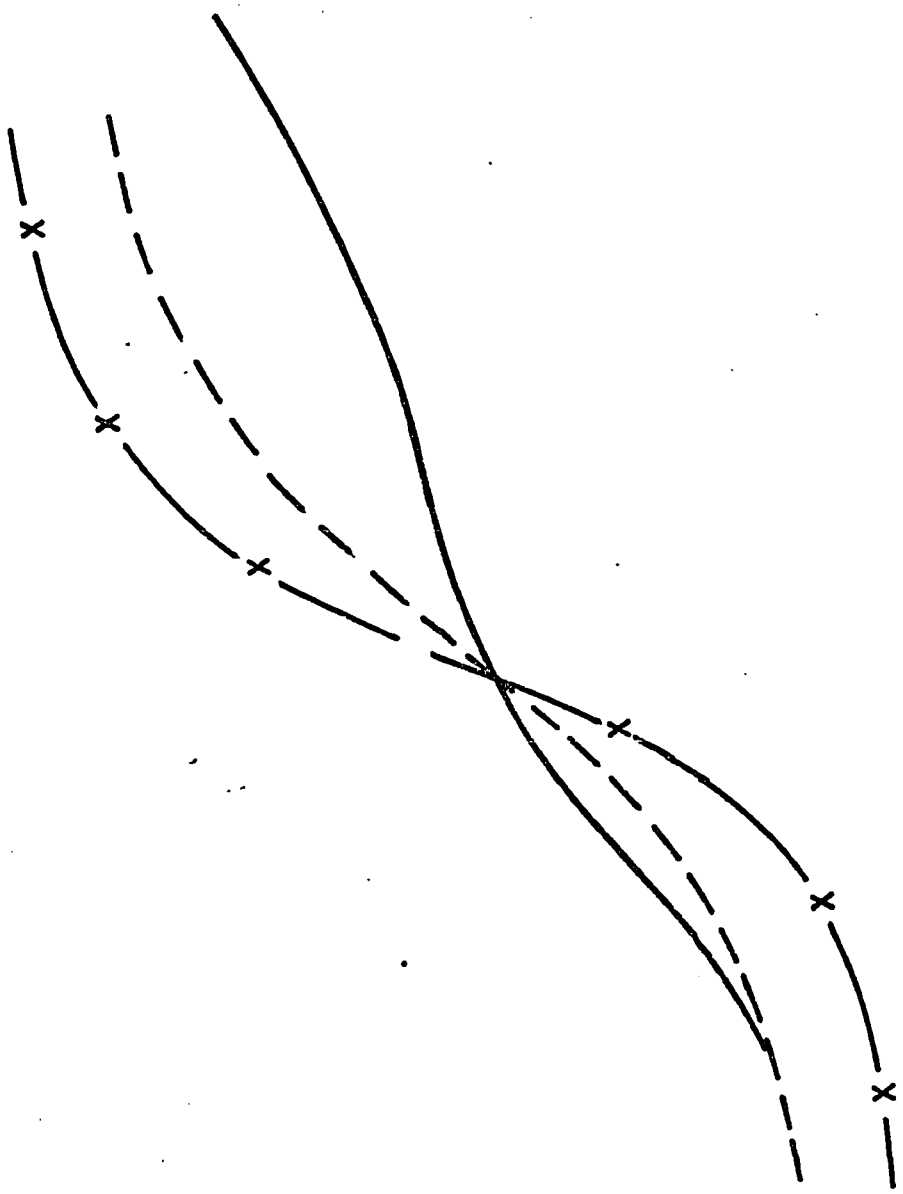

TABLE E2

Numerical Values of Loop Configuration Coefficients as a Function of the Number of Bound Solute Particles (N=11)

Number of Bound Particles	Number of Loops in Configuration			
	2	3	4	5
1	0	0	0	0
2	0	0	0	0
3	5.71	0	0	0
4	4.01	1.37	0	0
5	2.61	.628	.059	0
6	1.52	.228	.010	8.6×10^{-5}
7	.745	.055	6.9×10^{-4}	0
8	.264	.0055	0	0
9	.044	0	0	0
10	0	0	0	0
11	0	0	0	0

REFERENCES

1. G. D. Watson, Molecular Biology of the Gene, W. A. Benjamin, Inc., New York, 1965.

2. J. D. Watson and F. H. Crick, Proc. Roy. Soc. (London), 223A, 80 (1954).

3. J. Marmur and P. Doty, Nature, 183, 1427 (1959).

4. A. D. Broom, M. P. Schweizer, and P. O. P. Ts'o, J. Am. Chem. Soc., 89, 3612 (1967).

5. S. I. Chan and J. H. Nelson, J. Am. Chem. Soc., 91, 168 (1969).

6. M. P. Schweizer, S. I. Chan, and P. O. P. Ts'o, J. Am. Chem. Soc., 87, 5241 (1965).

7. P. O. P. Ts'o and S. I. Chan, J. Am. Chem. Soc., 86, 4176 (1964).

8. P. O. P. Ts'o, I. S. Melvin, and A. C. Olson, J. Am. Chem. Soc., 85, 1289 (1963).

9. T. N. Solie and J. A. Schellman, J. Mol. Biol., 33, 61 (1968).

10. S. I. Chan, M. P. Schweizer, P. O. P. Ts'o, and G. K. Helmkamp, J. Am. Chem. Soc., 86, 4182 (1964).

11. R. M. Hamlin, R. C. Lord, and A. Rich, J. Am. Chem. Soc., 89, 496((1967).

12. R. M. Hamlin, R. C. Lord, and A. Rich, Science, 148, 1734 (1965).

13. Y. Kyogoku, R. C. Lord, and A. Rich, Science, 154, 518 (1966).

14. R. Shoup, H. T. Miles, and E. D. Becker, Biophys. Biochem. Res. Comm., 23, 194 (1966).

15. L. Katz and S. Penman, J. Mol. Biol., 15, 220 (1966).

16. E. Kuchler and J. Derkosch, Z. Naturforsch, 218, 209 (1966).

17. H. Tuppy and E. Kuchler, Biochem, et Biophys. Acta, 80, 669 (1964).

18. F. B. Howard, J. Frazier, M. F. Singer, and H. T. Miles, J. Mol. Biol., 16, 415 (1966).

19. W. M. Huang and P. O. P. Ts'o, J. Mol. Biol., 10, 523 (1966).

20. P. M. Pitha, W. M. Huang, and P. O. P. Ts'o, Proc. Nat. Acad. Sci., 61, 332 (1968).

21. M. T. Sarocchi, Y. Courtois, and W. Guschlbauer, Eur. J. Biochem., 14, 411 (1970).

22. S. Takashima, Biopolymers, 4, 663 (1966).

23. L. Costantino and V. Vitagliano, Biopolymers, 4, 521 (1966).

24. T. Yamane and N. Davidson, J. Am. Chem. Soc., 83, 2599 (1961).

25. A. M. Willemsen and G. A. J. Van Os, Biopolymers, 10, 945 (1971).

26. F. Hughes and R. F. Steiner, Biopolymers, 4, 1081 (1966).

27. H. Noguchi, Biopolymers, 4, 1105 (1966).

28. R. H. Jensen and N. Davidson, Biopolymers, 4, 17 (1966).

29. C. L. Stevens and G. Felsenfeld, Biopolymers, 2, 293 (1964).

30. S. Higuchi and M. Tsuboi, Biopolymers, 4, 837 (1966).

31. H. Takesada, Y. Yamazaki and A. Wada, Biopolymers, 4, 713 (1966).

32. J. T. Yang, Tetrahedron, 13, 143 (1961)

33. J. N. Vournakis, H. A. Scheraga, G. W. Rushizky and H. A. Sober, Biopolymers, 4, 3341 (1966).

34. D. Poland, J. N. Vournakis and H. A. Scheraga, Biopolymers, 4, 223 (1966).

35. A Blake and A. R. Peacocke, Biopolymers, 4, 1091 (1966).

36. S. Z. Jakabhazy and S. W. Fleming, Biopolymers, 4, 793 (1966).

37. P. J. Oriel and J. A. Schellman, Biopolymers, 4, 469 (1966).

38. G. K. Helmkamp and P. O. P. Ts'o, Biochim. et Biophys. Acta., 55, 601 601 (1962).

39. J. Brahms and W. F. H. M. Mommaerts, J. Mol. Biol., 10, 73 (1964).

40. D. F. Bradley, I. Tinoco, Jr., and R. W. Woody, Biopolymers, 1, 239 (1963).

41. W. Moffitt, J. Chem. Phys., 25, 467 (1956)

42. I. Tinoco, Jr., J. Chem. Phys., 33, 1332 (1960).

43. I. Tinoco, Jr., J. Am. Chem. Soc., 86, 297 (1964).

44. I. Tinoco, Jr., R. W. Woody and J. Bradley, J. Chem. Phys., 38, 1317 (1963).

45. I. Tinoco, Jr., J. Am. Chem. Soc., 82, 4785 (1960).

46. W. Rhodes, J. Am. Chem. Soc., 83, 3609 (1961).

47. G. Felsenfeld and S. Z. Hirschman, J. Mol. Biol., 13, 407 (1965).

48. J. Y. Cassim and J. T. Yang, Biopolymers, 9, 1475 (1970).

49. P. L. Privalov and E. I. Tiktopulo, Biopolymers, 9, 127 (1970).

50. C. H. Zimmer and H. Venner, Biopolymers, 4, 1073 (1966).

51. C. H. Zimmer and H. Venner, J. Mol. Biol., 7, 603 (1963).

52. G. Barons, V. Crescenzi and F. Quadrifoglio, Biopolymers, 4, 529 (1966).

53. J. S. Franzen, C. Bobik and J. B. Harry, Biopolymers, 4, 637 (1966).

54. N. Kono and A. Ikegami, Biopolymers, 4, 823 (1966).

55. G. L. Eichhorn, Nature, 194, 474 (1962).

56. A. Goldberg, J. Mol. Biol., 15, 663 (1966).

57. J. W. Lyons and L. Kotin, J. Am. Chem. Soc., 87, 1670 (1965).

58. J. Skerjanc and U. P. Strauss, J. Am. Chem. Soc., 90, 3081 (1968).

59. C. Sander and P. O. P. Ts'o, J. Mol. Biol., 55, 1 (1971).

60. H. Venner and C. H. Zimmer, Biopolymers, 4, 321 (1966).

61. J. Eisinger, R. G. Shulman and B. M. Szymunski, J. Chem. Phys., 36, 1721 (1962).

62. J. Eisinger, F. Fawaz-Estrup and R. G. Schulman, J. Chem. Phys., 42, 43 (1965).

63. M. Daune, C. A. Dekker and H. K. Schachman, Biopolymers, 4, 51 (1966).

64. S. Katz, Biochim, Biophys. Acta, 68, 240 (1963).

65. U. S. Nandi, J. C. Wang and N. Davidson, Biochemistry, 4, 1687 (1965).

66. T. Yamane and N. Davidson, Biochim. Biophys. Acta, 55, 609 (1962).

67. R. G. Schulman, H. Sternlicht and B. J. Wyluda, J. Chem. Phys., 43, 3116 (1965).

68. G. L. Eichhorn and P. Clark, Proc. Natl. Acad. Sci., U.S., 53, 586 (1965).

69. K. Hotta, J. Brahms, and M. Morales, J. Am. Chem. Soc., 83, 997 (1961).

70. A. Epp, T. Ramasarma and L. R. Wetter, J. Am. Chem. Soc., 80, 725 (1958).

71. M. Eigen and D. Pörschke, J. Mol. Biol., 53, 123 (1970).

72. W. Szor and S. Ochoa, J. Mol. Biol., 8, 823 (1964).

73. E. O. Akinrimisi, J. Bonner and P. O. P. Ts'o, J. Mol. Biol., 11, 128 (1965).

74. L. S. Lerman, J. Mol. Biol., 3, 18 (1961).

75. D. S. Drummond, H. J. Pritchard, V. F. W. Simpson-Gildemeister and A. R. Peacock, Biopolymers, 4, 971 (1966).

76. R. B. Gennis and C. R. Cantor, Biochemistry, 9, 4714 (1970).

77. M. Tsubio, Bull. Chem. Soc. Japan, 37, 1514 (1964).

78. H. Jacobson, C. O. Beckmann, and W. H. Stockmayer, J. Chem. Phys., 18, 1607 (1950).

79. J. Marmur, R. Rownd, and C. L. Schildkraut, Progress in Nucleic Acid Research, Vol. I, Academic Press, New York and London, 1963, pp. 231-300.

80. E. Ising, Z. Phys., 31, 253 (1925).

81. E. W. Montroll, J. Chem. Phys., 9, 706 (1941).

82. H. A. Kramers and G. H. Wannier, Phys. Rev., 60, 252 (1941).

83. S. Lifson, J. Chem. Phys., 40, 3705 (1964).

84. D. M. Gray and I. Tinoco, Jr., Biopolymers, 9, 223 (1970).

85. B. H. Zimm and J. K. Bragg, J. Chem. Phys., 31, 526 (1959).

86. T. L. Hill, J. Chem. Phys., 30, 383 (1959).

87. M. Fixman and D. Zeroka, J. Chem. Phys., 48, 5223 (1968).

88. M. Bixon and S. Lifson, Biopolymers, 4, 815 (1966).

89. J. H. Gibbs and E. A. DiMarzio, J. Chem. Phys., 30, 271 (1959).

90. M. Bixon and S. Lifson, Biopolymers, 5, 509 (1967).

91. G. Schwarz, Biopolymers, 6, 873 (1968).

92. G. Schwarz, J. Mol. Biol., 11, 64 (1965).

93. R. Ullman, Biopolymers, 9, 471 (1970).

94. H. Jacobson and W. H. Stockmayer, J. Chem. Phys., 18, 1608 (1950).

95. M. E. Fisher, J. Chem. Phys., 45, 1469 (1966).

96. F. T. Wall, L. A. Miller, Jr., and W. F. Atchinson, J. Chem. Phys., 23, 2314 (1955).

97. D. Poland and H. A. Scheraga, J. Chem. Phys., 45, 1464 (1966).

98. J. Applequist, J. Chem. Phys., 50, 609 (1969).

99. J. Applequist, J. Chem. Phys., 50, 600 (1969).

100. D. Poland and H. A. Scheraga, J. Chem. Phys., 45, 1456 (1966).

101. I. C. Klotz, Biopolymers, 7, 265 (1969).

102. B. H. Zimm, J. Chem. Phys., 33, 1349 (1960).

103. B. E. Eichinger and M. Fixman, Biopolymers, 9, 205 (1970).

104. D. M. Crothers and B. H. Zimm, J. Mol. Biol., 9, 1 (1964).

105. D. M. Crothers, N. R. Kallenbach, and B. H. Zimm, Jr. Mol. Biol., 11, 802 (1965).

106. S. Lifson and B. H. Zimm, Biopolymers, 1, 15 (1963).

107. S. Lifson, Biopolymers, 1, 25 (1963).

108. S. Lifson and G. Allegra, Biopolymers, 2, 65 (1964).

109. H. K. Frensdorff and R. Pariser, J. Chem. Phys., 39, 2303 (1963).

110. E. W. Montroll and N. S. Goel, Biopolymers, 4, 855 (1966).

111. S. Strassler, J. Chem. Phys., 46, 1037 (1967).

112. D. M. Crothers and N. R. Kallenbach, J. Chem. Phys., 45, 917 (1966).

113. H. Reiss, D. A. McQuarries, J. P. McTague, and E. R. Cohen, J. Chem. Phys., Phys., 4567 (1966).

114. D. M. Crothers, Biopolymers, 4, 1025 (1966).

115. G. Scatchard, Ann. N. Y. Acad. Sci., 51, 660 (1949).

116. R. F. Steiner, J. Chem. Phys., 32, 215 (1960).

117. W. S. Magee, Jr., J. H. Gibbs, and B. H. Zimm, Biopolymers, 1, 133 (1963).

118. W. S. Magee, Jr., J. H. Gibbs, and G. F. Newell, J. Chem. Phys., 43, 2115 (1965).

119. V. N. Damle, Biopolymers, 9, 353 (1970).

120. P. K. Rawlings and F. W. Schneider, J. Chem. Phys., 52, 946 (1970).

121. V. N. Damle, Biopolymers, 9, 1437 (1970).

122. A. Litan, J. Chem. Phys., 49, 2294 (1968).

123. N. Laiken and G. N'emethy, J. Phys. Chem., 74, 4421 (1970).

124. M. V. Volkenstein and S. N. Fishman, Biopolymers, 4, 77 (1966).

125. J. Applequist and V. N. Damle, J. Chem. Phys., 39, 2719 (1963).

126. J. Applequist and V. N. Damle, J. Am. Chem. Soc., 87, 1450 (1965).

127. J. R. Fresco, B. M. Alberts, and P. Doty, Nature, 188, 98 (1960).

128. P. G. DeGennes, Biopolymers, 6, 715 (1968).

129. D. F. Bradley and M. K. Wolf, Proc. Natl. Acad. Sci. U.S., 45, 944 (1959).

130. G. Hagnauer and W. G. Miller, Biopolymers, 9, 589 (1970).

131. A. Litan and S. Lifson, J. Chem. Phys., 42, 2528 (1965).

132. W. Kauzmann, Adv. Prot. Chem., 14, 1 (1959).

133. T. L. Hill, Introduction to Statistical Thermodynamics, Addison-Wesley Publishing Co., Reading, Mass., 1960, Sec. 1-5.

134. Ibid., Sec. 1-4.

135. A. Messiah, Quantum Mechanics, Vol. 1, John Wiley & Sons, Inc., New York, 1965, p. 279.

136. M. M. Warshaw and I. Tinoco, Jr., J. Mol. Biol., 13, 54 (1965).

137. C. R. Cantor and I. Tinoco, Jr., J. Mol. Biol., 13, 65 (1965).

138. H. Devoe and I. Tinoco, Jr., J. Mol. Biol., 4, 500 (1962).

139. C. R. Cantor, S. R. Jaskunas, and I. Tinosc, Jr., J. Mol. Biol., 20, 39 (1966).

140. P. K. Sarkar and J. T. Yang, J. Biol. Chem., 240, 2088 (1965).

141. T. Ohnishi, Biophysical J., 3, 459 (1964).

142. I. M. Klotz and J. S. Franzen, J. Am. Chem. Soc., 84, 3461 (1962).

143. G. Scatchard, W. Hamer, and S. Wood, J. Am. Chem. Soc., 60, 3061 (1938).

144. E. Freese, J. Theoret. Biol., 3, 82 (1962).

145. M. E. Baur and L. H. Nosano, J. Chem. Phys., 37, 153 (1962).

146. G. A. Baker, Jr., Phys. Rev., 122, 1477 (1961).

147. J. Applequist, J. Chem. Phys., 45, 3459 (1966).

148. M. Kac, G. E. Uhlenbeck, and P. C. Hemmer, J. Math. Phys., 4, 216 (1963).

149. P. Ehrenfest, Koninkl. Ned. Akad. Wetenschap. Proc., 36, 153 (1933).

PART II

The Role of Orientation Constraints and Rotational Diffusion in Bimolecular Solution Kinetics

"'How fast is he going?' asked Pipin. 'Fast by the wind, but very smooth. And how light his footfalls are!'

'He is running now as fast as the swiftest horse could gallop,' answered Gandalf; 'but that is not fast for him.'"

from The Lord of the Rings, Part II, by J.R.R. Tolkien

I. Introduction

The classical theory of diffusion in bimolecular solution kinetics, as formulated by Smoluchowski,[1] Debye,[2] Collins and Kimball,[3] Noyes,[4] and Schurr,[5] is strictly applicable only to spherical particles that are uniformly reactive over their entire surface. For this special case the theory is now fairly complete in the sense that the steady-state forward and reverse rate constants are known, even in the presence of spherically symmetric interparticle potentials, and moreover the frequency-response spectrum of such a reaction has also been obtained.[5] More recently, a general theory of the kinetics of a diffusion-controlled reaction between two chemically asymmetric molecules has been presented.[16] Only the formalism was developed in this study and no calculations were performed. The authors correctly concluded that angular constraints lead to factors, less than unity, which multiply Smoluchowski's ideal diffusion-controlled expression, but erroneously inferred the impossibility of drawing any definite conclusions about the nonuniformity at the surface from the steady-state rate constants alone. A simpler model, which results in more tractable expressions, is developed in the present study.

Of special interest is the effect of orientation constraints on the maximum diffusion-controlled bimolecular rate constant. A fairly large number of enzyme-substrate association rate constants are known to lie in a range 10^6 - 5×10^8 M^{-1} sec^{-1}, which is sufficiently far below the value of 8×10^9 predicted by the Smoluchowski formula that the possibility of diffusion-control has generally been dismissed. At least for some of these enzyme-substrate pairs the substrate is sufficiently large that its orientation probably proceeds by a process closely akin to classical rotational diffusion. Such pairs certainly include Old Yellow Enzyme with

flavin mononucleotide;[7] and the H_2O_2-horseradish peroxidase complex with cytochrome c[8], and may also include β-amylase with amylose,[9] and liver alcohol dehydrogenase with diphosphopyridine nucleotide.[10] It is the main thesis of this study that moderate angular constraints imposed on reactants that orient by rotational diffusion produce rather drastic decreases in the maximum diffusion-controlled rate constant. Thus, it is entirely possible that reactions previously thought to be far from the diffusion-controlled range in fact are strongly viscosity dependent. Furthermore, a knowledge of the maximum diffusion-controlled rate constant may permit a rational estimate of the allowed angular tolerance for the chemical reaction.

II. The Model

The microscopic process treated here is the reaction of orientable spheres of hydrodynamic radius R_H suspended in an infinite half-space of solution with localized sites on a bounding plane (cf. Figure 1). Each sphere is assumed to have only one localized reactive site. We define the orientation vector as the vector originating from the center of the sphere and passing through the center of the reacting site on the surface of the sphere. The orientation of this vector is characterized by the polar angle θ with respect to the downward normal into the plane and the azimuthal angle ϕ with respect to an arbitrary vector in the plane.

Each reaction site on the plane can be associated with a set of coordinate axes. Since the distance of closest approach of the center of the sphere to the plane is the hydrodynamic radius R_H, it is convenient to place the origin at a point located directly above the reaction site at a distance R_H from the surface. If the distances between neighboring reaction sites are large compared to the extents of the diffusion gradients at the sites, then the entire collection of sites may be thought of as an ensemble describing a reduced system, the reaction at one site. We can then superimpose all of the origins and define only one set of coordinate axes. The z-axis is defined to be the downward normal into the plane and α is the polar angle with respect to this axis. The azimuthal angle β is measured with respect to an arbitrary x-axis. The distance of any arbitrary point in the allowed solution half-space from the origin is defined as r. The allowed ranges for the polar coordinates are $0 \leq r \leq \infty$, $\pi/2 \leq \alpha \leq \pi$, and $0 \leq \beta \leq 2\pi$.

Because the extents of concentration gradients associated with neighboring sites do not overlap, the concentration of spheres is essentially

Figure 1

Schematic diagram of the model for reaction between a mobile, orientable sphere bearing a reactive site and a localized, stationary site on the plane. In order for reaction to occur the center of the sphere must lie on the small hemisphere, and θ must be less than or equal to some θ_o.

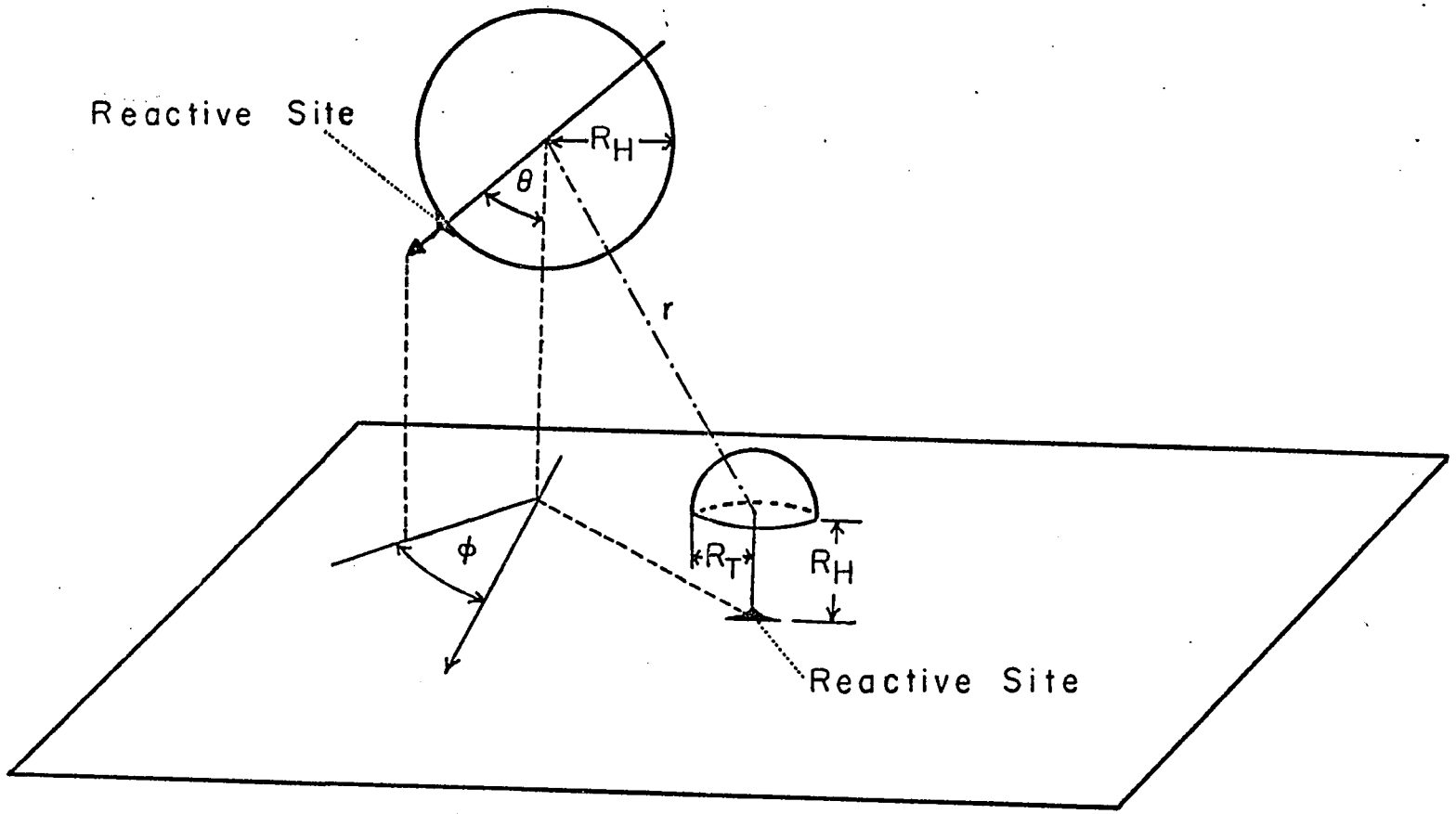
Reactive Site
R_H
θ
r
ϕ
R_T
R_H
Reactive Site

constant at large values of r in the reduced system. Furthermore, all orientations are assumed to be equally probable in the limit $r \to \infty$. It is clear from the symmetry of the problem that the distribution function describing the concentration of the spheres at the point r, α, β with orientation θ, ϕ is independent of $\alpha, \beta,$ and ϕ. Let $c(r,\theta)2\pi r^2 \sin\theta dr d\theta/2$ be the number of spheres between r and $r + dr$ with orientations in the range θ and $\theta + d\theta$ in the infinite half-space. The continuity equation for spheres in the steady-state limit is

$$\frac{\partial c(r,\theta)}{\partial t} = 0 = D\nabla_r^2 c(r,\theta) + \circledR \nabla_\theta^2 c(r,\theta) \quad , \qquad (1a)$$

where the Laplacian operators are defined as

$$\nabla_r^2 = \left(\frac{1}{r^2}\right)\frac{\partial(r^2 \partial/\partial r)}{\partial r} \quad , \qquad (1b)$$

$$\nabla_\theta^2 = \left(\frac{1}{\sin\theta}\right)\frac{\partial(\sin\theta \partial/\partial\theta)}{\partial\theta} \quad , \qquad (1c)$$

and D and $\circledR$ are the translational and rotational diffusion coefficients, respectively.

In order for two reacting sites to interact, the center of the sphere must come within a target radius R_T of the origin associated with the site on the plane. A reaction hemisphere is obtained by sweeping a vector of length R_T through all allowed values of α and β. The projection lines of the base of the reaction hemisphere onto the surface of the plane define a reaction cylinder. In order for a reaction to occur, the center of the diffusing sphere must lie within the reaction hemisphere and the site on the sphere must be within the reaction cylinder. The maximum allowed angular tolerance for the orientation vector is defined as the critical angle θ_o.

Consideration of the boundary conditions completes the description of the model. Since the concentration of spheres becomes constant as $r \to \infty$, we have

$$\lim_{r \to \infty} c(r) = \lim_{r \to \infty} \int_0^{\pi} c(r,\theta)\sin\theta d\theta/2 = c_o \quad , \tag{2a}$$

where $c(r)$ is the total concentration of spheres of all orientations between r and r + dr. It is required that, at the surface of the reaction hemisphere of area $2\pi R_T^2$, the total inward current is equivalent to the net rate of reaction. If there are N_b bound sites and N_e empty sites on the bounding plane, the net rate of reaction per empty site with spheres of a particular orientation θ is

$$2\pi R_T^2 D \partial c(r,\theta)/\partial r\big|_{r=R_T} = k_a^o X(\theta) c(R_T,\theta) - k_d^o X(\theta) N_b/N_e \quad , \tag{2b}$$

where k_a^o, k_d^o are the intrinsic association and dissociation rate constants, respectively, and $X(\theta)$ for the present model is the step function

$$X(\theta) = \begin{cases} 1 & (0 \leqslant \theta \leqslant \theta_o) \\ 0 & (\theta_o < \theta \leqslant \pi) \end{cases} \quad , \tag{2c}$$

that defines the range of θ over which a reaction may occur. Integration of Eq.(2b) over all orientations of the spheres leads to the total rate of reaction per empty site,

$$J = 2\pi R_T^2 D \int_0^{\pi} \partial c(r,\theta)/\partial r\big|_{r=R_T} \sin\theta d\theta/2 \quad . \tag{2d}$$

Eqs.(2a) and (2b) constitute the boundary conditions for this model and Eq.(2d) is an auxiliary equation that defines the total rate J.

III. The Formal Solution

Separation of variables in Eq.(1a) leads to an expression for $c(r,\theta)$ in terms of a series expansion in Legendre polynomials,

$$c(r,\theta) = \sum_{n=0}^{\infty} b_n(r) P_n(\cos\theta) \quad . \tag{3}$$

Substitution of Eq.(3) into Eq.(1a) and subsequent multiplication by $P_m(\cos\theta)\sin\theta d\theta/2$ followed by integration over the allowed values of θ leads to the differential equation for $b_m(r)$,

$$\frac{[D/r^2]\partial[r^2 \partial b_m(r)/\partial r]}{\partial r} - \Theta m(m+1) b_m(r) = 0 \quad . \tag{4}$$

Thus, we have the solutions

$$b_0(r) = -A + B/r \qquad (m = 0) \quad , \tag{5a}$$

$$b_m(r) = C_m \exp(-\kappa_m r)/r \qquad (m \neq 0) \quad , \tag{5b}$$

where $\kappa_m = [m(m+1)\Theta/D]^{1/2}$ and A, B, and C_m are constants. From the boundary condition expressed in Eq.(2a), the corresponding positive exponential solutions are forbidden and

$$A = c_o \quad . \tag{6}$$

Since $P_0(\cos\theta) = 1$, substitution of Eq.(5a) into the auxiliary condition [Eq.(2d)] gives directly,

$$B = -J/2\pi D \quad . \tag{7}$$

The only problem that remains is finding an expression for the coefficients C_m. Substitution of Eq.(3) into the boundary condition given by Eq.(2b), multiplication on the left by $P_m(\cos\theta)\sin\theta d\theta/2$, and subsequent evaluation of the integral leads to the expression

$$\frac{-C_m \exp(-\kappa_m R_T)(\kappa_m + 1/R_T)}{2m+1} =$$

$$[Q(A + B/R_T)-P]X_{mo} + \sum_{n=1}^{\infty} \frac{QC_n \exp(-\kappa_n R_T)X_{mn}}{R_T} \quad , \qquad (8a)$$

where $m = 1,2,3,\ldots$

$$X_{mn} \equiv \int_0^{\pi} P_m(\cos\theta)X(\theta)P_n(\cos\theta)\frac{\sin\theta d\theta}{2} \quad , \qquad (8b)$$

$$Q \equiv k_a^o/2\pi R_T D \quad , \qquad (8c)$$

and

$$P \equiv k_d^o(N_b/N_e)/2\pi R_T D \quad . \qquad (8d)$$

Eq.(8a) can be written in the matrix form

$$\underset{\sim}{\underset{\sim}{G}}\,\underset{\sim}{C} = \underset{\sim}{L}_o \quad , \qquad (9)$$

where the elements of the column vector C are just the coefficients

$$(\underset{\sim}{C})_m = C_m \quad , \qquad (10)$$

and the vector $\underset{\sim}{L}_o$ is defined by

$$(\underset{\sim}{L}_o)_m \equiv [Q(A + B/R_T)-P]X_{mo} \quad . \qquad (11)$$

The matrix $\underset{\sim}{\underset{\sim}{G}}$ is defined by

$$G_{mn} \equiv \frac{-Q\exp(-\kappa_n R_T)X_{mn}}{R_T} - \exp(-\kappa_m R_T)(\kappa_m + \frac{1}{R_T})\frac{\delta_{m,n}}{2m+1} \quad , \qquad (12)$$

where $\delta_{m,n}$ is the Kronecker delta function. The coefficients C_m can be obtained directly from Eq.(9),

$$\underset{\sim}{C} = \underline{\underline{G}}^{-1}\underset{\sim}{L}_0 \quad . \tag{13}$$

In the event that a computer program for finding the inverse of a non-symmetric matrix is not available, a procedure for finding the C_m's by first symmetrizing $\underline{\underline{G}}$ is presented in Appendix A.

J is determined by multiplying Eq.(2b) by $P_0(\cos\theta)\sin\theta d\theta/2$ and then integrating over the allowed values of θ, thus obtaining

$$J = \int_0^{\pi} k_a\left[c(R_T,\theta) - (k_d^0/k_a^0)(N_b/N_e)\right]X(\theta)\sin\theta d\theta/2 \quad . \tag{14}$$

Substitution of Eqs.(13), (11), (7), and (6) into Eq.(14) gives the expression

$$J = \left[k_a\left(c_o - \frac{J}{2\pi DR_T}\right) - k_d^0(N_b/N_e)\right]X_{00}$$

$$+k_a^0\left[Q\left(c_o - \frac{J}{2\pi DR_T}\right)-P\right]\sum_{m=1}^{\infty}(\underline{\underline{G}}^{-1}\underset{\sim}{X}_0)_m\left[\exp(-\kappa_m R_T)/R_T\right]X_{mo} \quad . \tag{15}$$

Rearrangement of Eq.(15) and multiplying by N_e leads to the total reaction rate

$$\Phi = JN_e = \frac{k_a^0(2\pi R_T D)c_o N_e - k_d^0(2\pi R_T D)N_f}{(2\pi R_T D/SUM) + k_a^0} \quad , \tag{16}$$

where $$SUM \equiv X_{00} + \frac{k_a^0}{2\pi R_T D}\sum_{m=1}^{\infty}(\underline{\underline{G}}^{-1}\underset{\sim}{X}_0)_m\left[\exp(-\kappa_m R_T)/R_T\right]X_{mo}$$

and $$(\underset{\sim}{X}_0)_m = X_{mo} \quad . \tag{17}$$

The effective association rate constant is

$$\vec{k} = \frac{k_a^\circ(2\pi R_T D)}{(2\pi R_T D/SUM) + k_a^\circ} \qquad (cm^3\ molec^{-1}\ sec^{-1}) \quad , \tag{18}$$

and the effective dissociation rate constant is

$$\overleftarrow{k} = \frac{k_d^\circ(2\pi R_T D)}{(2\pi R_T D/SUM) + k_a^\circ} \quad . \tag{19}$$

Apart from the factor SUM in the denominator, these expressions are equivalent to those obtained for spheres that are uniformly reactive over their entire surface, provided only half of the allowed solid angle is accessible.

IV. The Numerical Computation

The molar forward rate constant k_M is defined as

$$k_M = N_A \vec{k}/1000 \qquad (\ell \text{ mole}^{-1} \text{ sec}^{-1}) \quad , \tag{20a}$$

where N_A is Avagadro's number. Since the main objective is the investigation of the diffusion-controlled limit for the association reaction, the results are presented only for the molar forward rate constant k_{eff} in the diffusion-controlled region

$$k_{eff} = k_M \qquad (Q > 1) \quad , \tag{20b}$$

where k_a' is the molar intrinsic association rate

$$k_a' = k_a^0 N_A/1000 \quad . \tag{21}$$

In the calculations presented here k_a' is chosen such that $(Q \geq 10)$

It is possible to ascertain the effect of rotational constraints by comparison with the corresponding diffusion-controlled rate constant for uniformly reacting spheres. The diffusion-controlled rate constant for the reaction of such spheres in infinite half-space solution with an identical sphere rigidly attached to the plane at a bottom tangent is

$$k_{diff} = N_A 2\pi(2R_H)D/1000 \qquad (\ell \text{ mole}^{-1} \text{ sec}^{-1}), \tag{22}$$

where $2R_H$ is now the target radius. If Stokes Laws are employed for the friction factors associated with translational and rotational motions of the spheres, then the diffusion coefficients may be written as

$$D = kT/6\pi\eta R_H \quad , \tag{23}$$

$$\Theta = kT/8\pi\eta R_H^3 \quad , \qquad (24)$$

where η is the solvent viscosity, k is Boltzmann's constant, and T is the absolute temperature. The quantity k_{diff} is independent of R_H, and at $T = 300^0K$, $\eta = .008$ poise,

$$k_{diff} = 2.08 \times 10^9 \qquad (\ell \text{ mole}^{-1} \text{ sec}^{-1}) \quad . \qquad (25)$$

Substitution of Eqs.(23) and (24) into Eq.(12) leads to the result that every term in the matrix $\underline{\underline{G}}$ can be written as a function of R_T/R_H, $(R_T)^{-1}$, and θ_0. Furthermore, according to Eq.(17), SUM is a function simply of R_T/R_H and θ_0. Thus, at constant η and T, the effective rate constants of Eqs.(18) and (19) are functions of R_T/R_H and θ_0 only. The ratio k_{eff}/k_{diff} provides a direct measure of the effectiveness of the radial and orientational constraints in reducing the maximum theoretical rate constant below that value expected for uniformly reactive spheres. Computed values of k_{eff}/k_{diff} are plotted against the allowed reactive angular range θ_0 in Figure 2 for three values of R_T/R_H. The limiting values at $\theta_0 = \pi$ give the effect of the radial constraint alone.

Consider a sphere whose center is exactly a distance R_H from the surface of the plane and with its orientation vector normal to the plane. The reaction condition allows the center of the sphere a translational tolerance of $2R_T$. The orientation vector, however, is not required to be normal to the plane for a reaction to occur. For spheres rotated to the critical angle θ_0, the projection of the center of the reaction site onto the surface of the plane has an additional tolerance of $2\theta_0 R_H$ for small θ_0. It seems probable that in reality the reaction tolerance for spatial deviation of the site on the sphere is the same, whether originating

from translation or rotation of the sphere. Therefore, the relation

$$2\theta_0 R_H = 2R_T \quad , \tag{26}$$

is maintained for the remainder of the calculations. It follows that $\vec{k}$, $\overleftarrow{k}$, and k_{eff} are functions of R_T/R_H, T, and η. A "universal" curve of k_{eff}/k_{diff} as a function of θ_0 is presented in Figure 3, where $\theta_0 = R_T/R_H$.

Because of the inverse relationship between the size of the angular tolerance and the number of polynomials that are needed in the computation, the storage capacity of the computer limited the choice of a minimum value for θ_0. Since the quantities X_{mn} were calculated by numerical integration in the event a different functional form of $X(\theta)$ may be employed, cost consideration dictated that the following set of arbitrary rules be used to determine the number of polynomials used for a particular angle θ_0.

number of polynomials	angular tolerance (radians)
140	.05 to .8
80	.8 to 1.6
40	1.6 to 3.14

To illustrate that these rules lead to a value for SUM [cf. Eq.(17)] that has sufficiently converged so no gross error is introduced, the quantities SUM-X_{00} and k_M/k_{diff} at $\theta_0 = .05$ as a function of the number of polynomials is presented in Figure 4. In all calculations, the number of points interior to the range of the angular tolerance in performing the numerical integration was 200. All calculations were performed on a CDC 6400 computer.

Figure 2

Computed values of $k_{eff}/k_{diff} = k_{eff}/2.08\times10^{9}$ as a function of the allowed angular reaction range θ_0. For the triangles (Δ) $R_H/R_T = 4.0$, $k'_a = 2.6\times10^{9}\ M^{-1}\ sec^{-1}$; for the filled circles ($\bullet$) $R_H/R_T = 7.0$, $k'_a = 1.49\times10^{9}\ M^{-1}sec^{-1}$; for the open circles (O) $R_H/R_T = 10$; $k'_a = 1.04\times10^{9}\ M^{-1}sec^{-1}$. For all calculations T = 300 k, η = .008 poise.

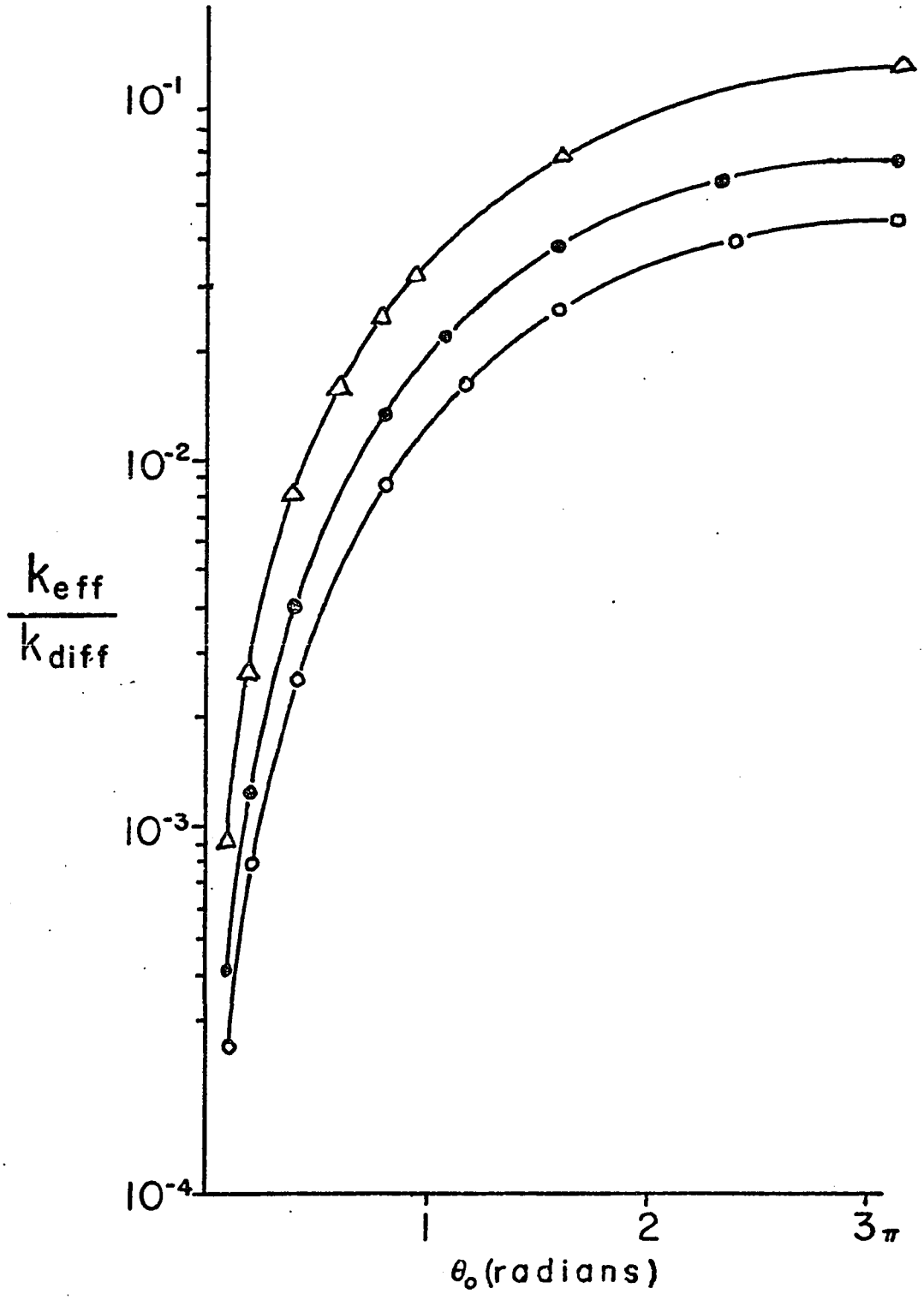
10^{-1}
10^{-2}
10^{-3}
10^{-4}
$\frac{k_{eff}}{k_{diff}}$
1
2
3π
θ_o (radians)

Figure 3

Computed values of k_{eff}/k_{diff} as a function of $\theta_0 = R_T/R_H$. The value of k_a^o was chosen so that $Q = k_a^o/2\pi R_H D = 10.0$ for each point calculated. The range of k_a' values was from 5×10^8 - 3×10^9 $M^{-1}sec^{-1}$. For these calculations $T = 300^oK$, $\eta = .008$.

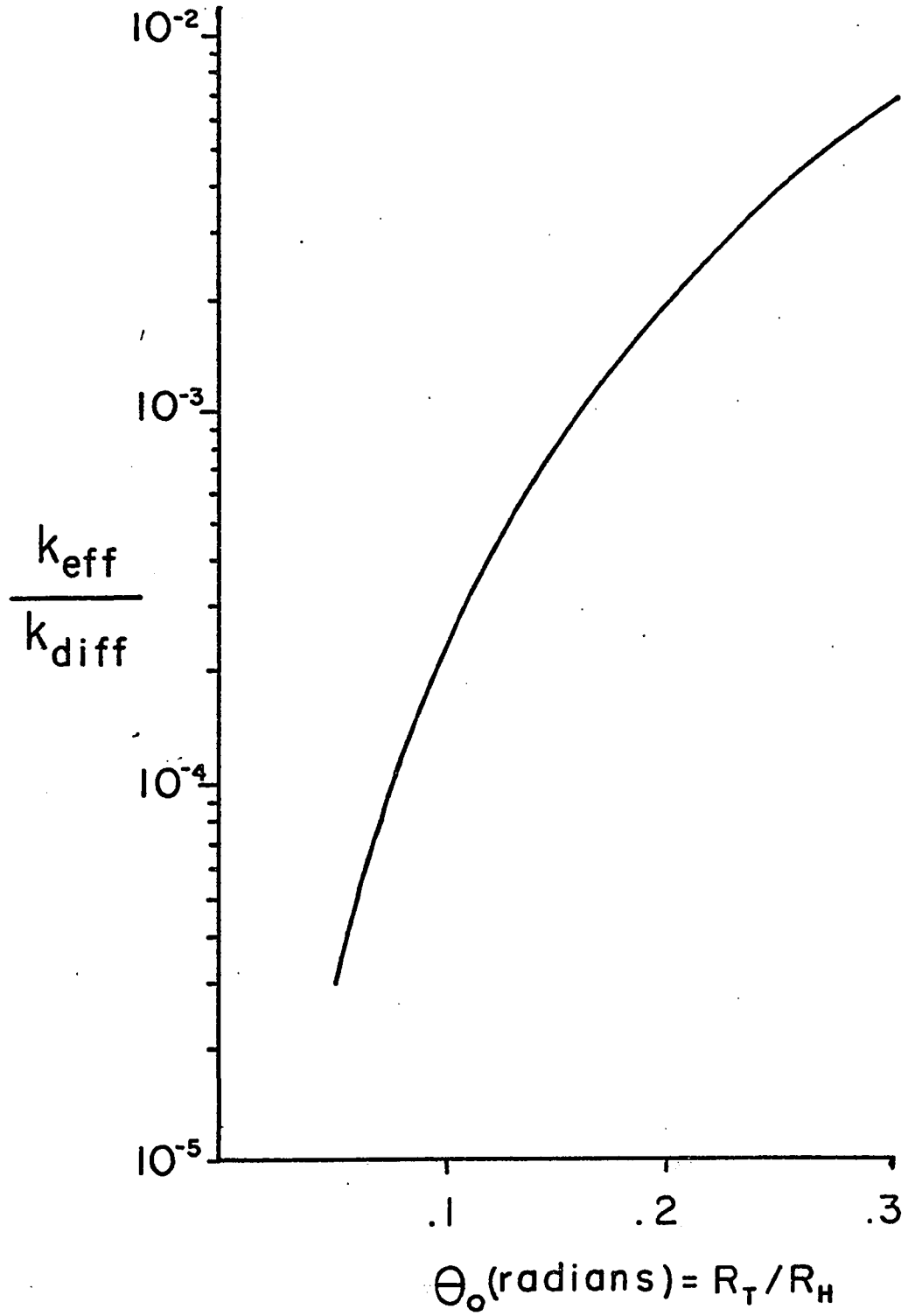
10^{-2}
10^{-3}
10^{-4}
10^{-5}
$\frac{k_{eff}}{k_{diff}}$
.1
.2
.3
θ_o(radians) = R_T/R_H

Figure 4

Convergence of SUM - X_{00} and (k_M/k_{diff}) as a function of the number of Legendre polynomials used in the calculation. In all cases, $X_{00} = 6.2518 \times 10^{-4}$ and $\theta_0 = .05$ radians.

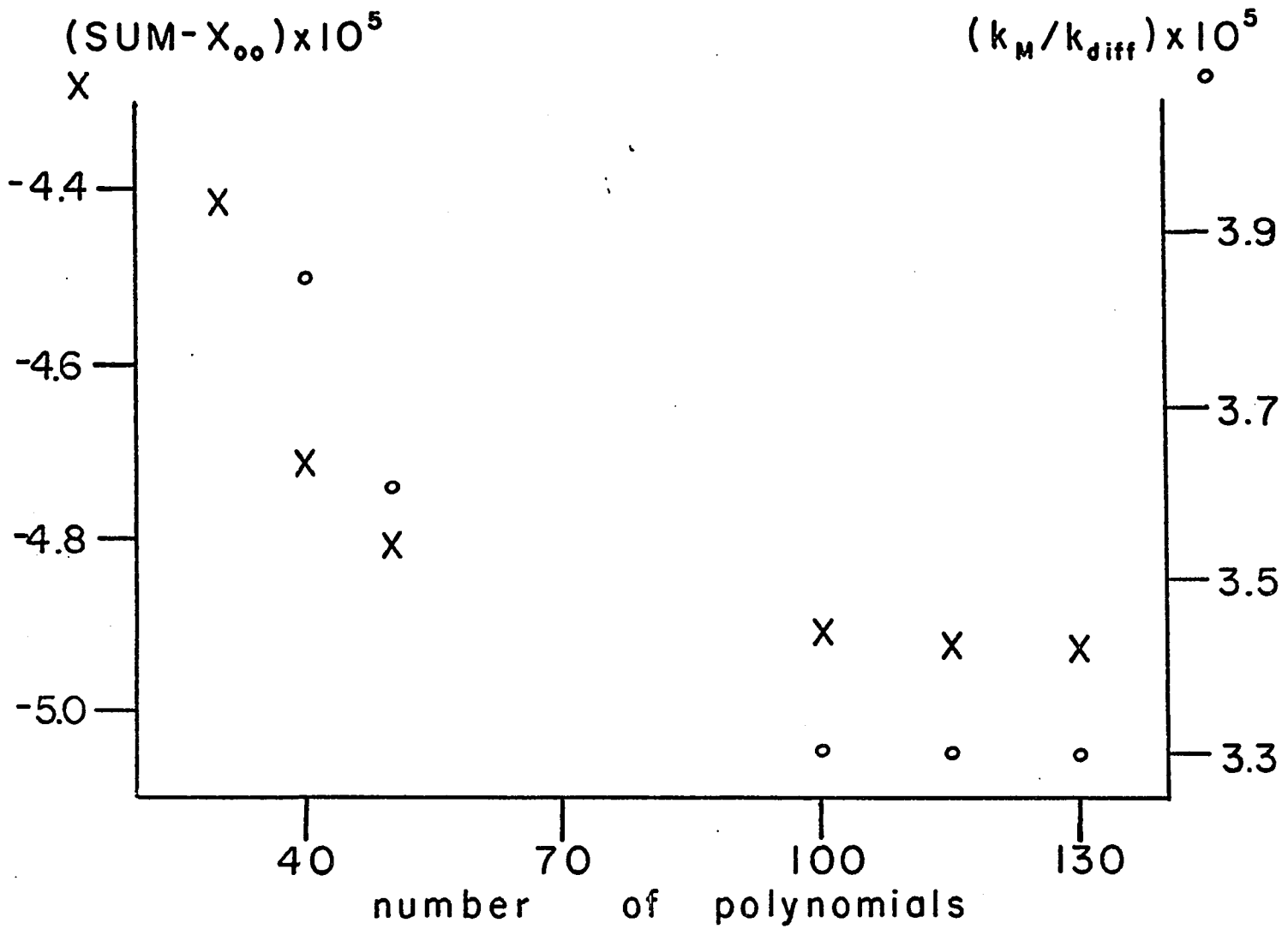
(SUM-X$_{oo}$)x10^5
(k$_M$/k$_{diff}$)x10^5
-4.4
-4.6
-4.8
-5.0
3.9
3.7
3.5
3.3
40
70
100
130
number of polynomials

V. Viscosity Dependence

It is known that the reciprocal of the effective association rate constant for uniformly reacting spheres is a linear function of the solvent viscosity. For the reaction of uniformly reacting spheres in the infinite solution half space with uniformly reacting spheres of radius R_H fixed to the bounding plane, we have the relationship

$$1/k_{eff} = 1/k'_a + 1500\eta/N_A kT \quad , \qquad (27)$$

where we have used $R_T = 2R_H$. Rearrangement of Eq.(18) for the corresponding reaction of spheres bearing localized reaction sites gives

$$1/k_M = \frac{1}{k'_a SUM} + \frac{3000\eta R_H}{N_A k T R_T} \quad . \qquad (28)$$

Since it is not possible, at this time, to obtain an analytical expression for SUM as a function of viscosity, the functional dependence is deduced from numerical calculations. A plot of the reciprocal of k_M, as calculated by Eq.(18), as a function of viscosity results in a curve which only slightly deviates from linearity over several orders of magnitude in the viscosity. It is concluded, therefore, that

$$\frac{1}{SUM} \cong A\eta + B \quad , \qquad (29)$$

where A and B are constants and the corrections for curvature are neglected. Substitution of Eq.(29) into Eq.(28) leads to the result

$$1/k_M = \frac{B}{k'_a} + \eta\left(\frac{3000}{N_A kT}\frac{R_H}{R_T} + \frac{A}{k'_a}\right) \quad . \qquad (30)$$

Since SUM $\to 1$ as $\theta_0 \to \pi$, it is required that $A \to 0$ and $B \to 1$ in this limit to retain the equivalence of Eqs.(30) and (28).

Defining the quantity

$$W \equiv \sum_{m=1}^{\infty} (\underline{\underline{G}}^{-1} \underline{X}_0)_m \frac{\exp(-\kappa_m R_T)}{R_T} X_{m0} \quad , \qquad (31)$$

Eq.(17) becomes

$$\frac{1}{SUM} = \frac{1}{X_{00} + QW} = \frac{1}{X_{00}} \left(\frac{1}{1 + QW/X_{00}} \right) \quad , \qquad (32)$$

where Q is defined in Eq.(8c). It is necessarily true that

$$0 \geq \frac{W}{X_{00}} > -1 \quad . \qquad (33)$$

For example, at $\theta_0 = .05$ radians, $W = -4.59 \times 10^{-5}$ and $X_{00} = 5.82 \times 10^{-4}$. Furthermore, $0 < QW < 1$ in the diffusion-controlled region. Eq.(32) can then be expressed as a power series

$$\frac{1}{SUM} = \frac{1}{X_{00}} + \frac{1}{X_{00}} \left(\sum_{n=1}^{\infty} \left| \frac{QW}{X_{00}} \right|^n \right) \quad , \qquad (34)$$

where the vertical lines denote the absolute value. Since only the second term on the right hand side of Eq.(34) is viscosity dependent, Eq.(29) can be written as

$$\frac{1}{SUM} = \frac{1}{X_{00}} + \frac{1}{X_{00}} (A' \eta + B') \quad . \qquad (35)$$

The quantity B' is determined as follows. In the limit $\eta \to 0$ according to Eq.(12),

$$G_{mn} \to \frac{\delta_{m,n}}{R_T(2m+1)} \quad , \qquad (36)$$

hence $QW \to 0$ since Q is directly proportional to the viscosity.

In this limit, Eq.(32) becomes

$$\frac{1}{SUM} = \frac{1}{X_{00}} \quad , \tag{37}$$

which implies that $B' = 0$. As a result, Eq.(28) becomes

$$1/k_M = \frac{1}{X_{00}k'_a} + \eta\left(\frac{A'}{X_{00}k'_a} + \frac{3000R_H}{N_A kTR_T}\right) \quad . \tag{38}$$

For this particular case where $X(\theta)$ is a step function,

$$X_{00} = \int_0^{\theta_0} \frac{\sin\theta d\theta}{2} = \frac{(1-\cos\theta_0)}{2} \quad . \tag{39}$$

Therefore, we arrive at the desired expression

$$1/k_M = \frac{2}{(1-\cos\theta_0)k'_a} + \eta\left(\frac{2A'}{(1-\cos\theta_0)k'_a} + \frac{3000R_H}{N_A kTR_T}\right) \quad . \tag{40}$$

Since both the uniformly reacting spheres and the localized reacting site spheres give a linear dependence of $1/k_M$ as a function of solvent viscosity, the question arises as to how they might be distinguished from each other experimentally. If there is a very stringent angular requirement, it is obvious from Eq.(40) that the intercept should be noticeably different from zero (i.e., usually $1/k'_a \ll 1$ in the diffusion-controlled region). Furthermore, it can be demonstrated by numerical calculations that the slope is strongly dependent on the angular constraint. Consider two systems which are identical in every respect except one system, which we define to be the "real" system, has an angular constraint on the reaction. It is assumed that we perform experiments on the "real"system and obtain the slope S from $1/k_M$ as a function of viscosity. We now try to interpret S in terms of the "model" system of uniformly reacting spheres. In the

limit $\theta \to \pi$, Eq.(40) becomes

$$\lim_{\theta_0 \to \pi} 1/k_M = 1/k_a' + \eta(3000R_H/N_A kTR_T) \quad . \qquad (41)$$

The "effective" R_H/R_T ratio that we would then calculate for the "real" system is simply

$$R_H/R_T = (N_A kT/3000)S \quad . \qquad (42)$$

For a "real" system in which $\theta_0 = 1/7$, $T = 300^oK$, and $k_a' = 1.48 \times 10^7$, it is found that $S = .656 \times 10^{-4}$. The calculated curves for both the "real" and "model" systems are presented in Figure 5. Furthermore, from the knowledge of R_H/R_T used in the calculation, we find that

$$3000R_H/N_A kTR_T = 8.4 \times 10^{-7} \quad , \qquad (43)$$

hence the contribution to the slope due to the angular constraint is

$$\frac{2A'}{(1-\cos\theta_0)k_a'} = S - (3000R_H/N_A kTR_T) = 657.6 \times 10^{-7} \quad . \qquad (44)$$

It can be concluded from Eqs.(43) and (44) that the angular constraint gives the predominant contribution to the slope for this case. Thus, a definite non-zero intercept or an unusually large R_H/R_T ratio obtained from the slope of $1/k_M$ as a function of η is indicative of an angular constraint.

Now consider a reaction with an angular constraint that is not in the diffusion-controlled region (i.e., $k_a' \lesssim k_{diff}$). According to Eq.(40), we should expect a definite non-zero intercept and an unreasonable estimate of the effective R_H/R_T ratio. The magnitude of the limit

Figure 5

The reciprocal $(k_M)^{-1}$ of the computed bimolecular rate constant as a function of viscosity η. For the filled triangles (▲) $R_T/R_H = \theta_0 = 1/7$, $k_a' = 1.4 \times 10^7$; for the open circles (○) $R_T/R_H = \theta_0 = .37$, $k_a' = 1.53 \times 10^7$; for the filled squares (■) $R_T/R_H = \theta_0 = 1/7$, $k_a' = 1.48 \times 10^9$; for the filled circles (●) $R_T/R_H = 1/555$, $\theta_0 = \pi$, $k_a' = 1.48 \times 10^7$; for the open triangles (△) $R_T/R_H = 1/3$, $k_a' = 3.46 \times 10^7$. The k_a' above are given in units of M^{-1} sec^{-1}. For all of the calculations $T = 300^{\circ}K$. The filled circles represent a special case which is defined in Section V.

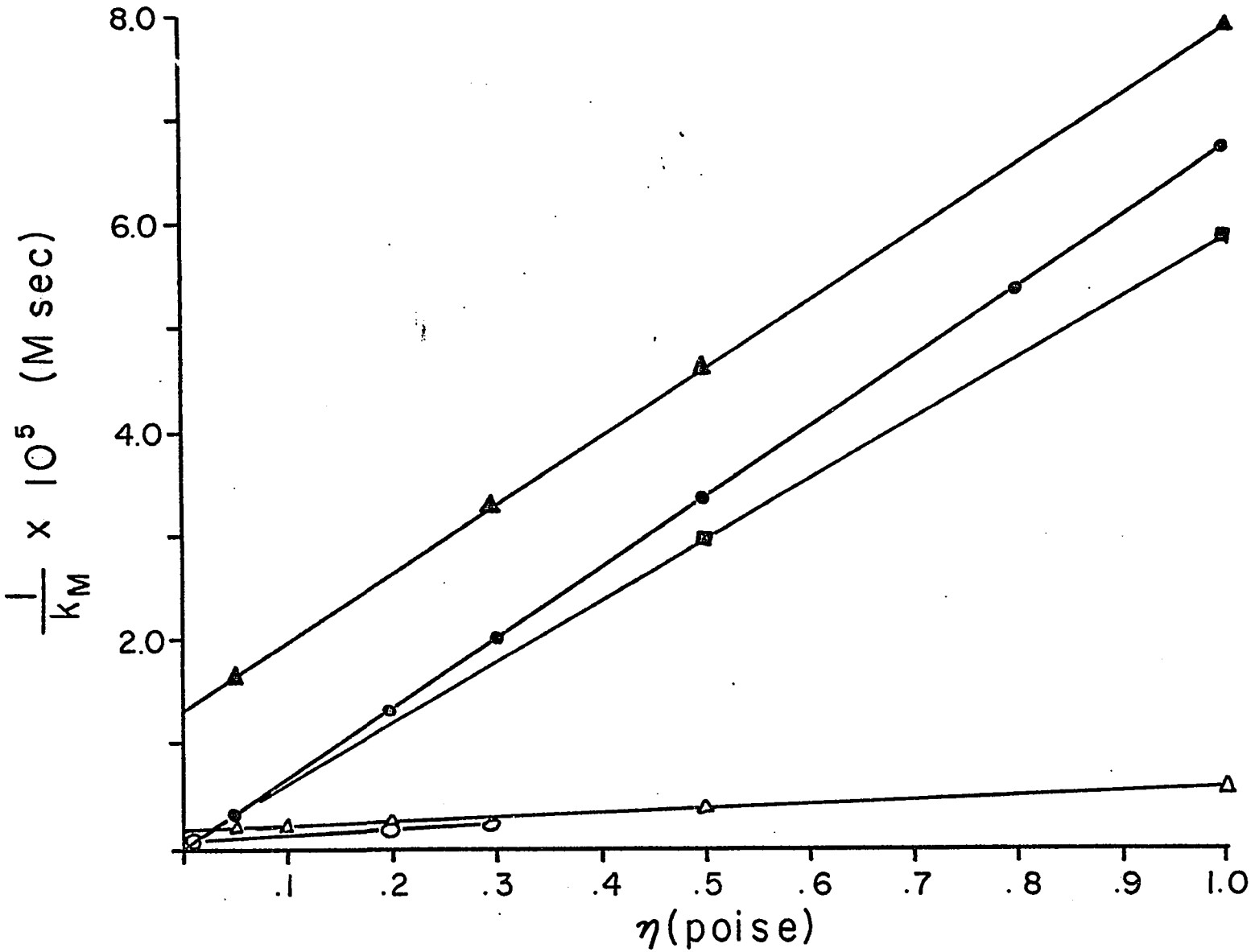
8.0
6.0
4.0
2.0
$\frac{1}{k_M} \times 10^5$ (M sec)
.1
.2
.3
.4
.5
.6
.7
.8
.9
1.0
η(poise)

$\lim_{\eta \to 0} 1/k_M = 1/k_M^o$ is to be considered in order to distinguish between the two regions when no "extreme" orientation restriction is imposed on the reaction (i.e., where $1-\cos\theta_0 \to 0$). Clearly, a reasonable orientation constraint only acts to increase the intercept by two or three orders of magnitude at the most. For example, $1-\cos\theta_0 \cong 1.4\times10^{-3}$ when $\theta_0 = 3^o$. Since $k_a' > k_{diff} \simeq 10^8$, the intercept for the diffusion-controlled region should have an upper limit on the order of 10^{-5}. On the other hand, there is no restriction on the intercept in the non-diffusion control region. As illustrated in Section VI in which the data of Wetmur and Davidson is reinterpreted, the intercept can be used to determine the degree of diffusion control for a reaction.

Since the factor pertaining to the orientation constraint, $2A'/(1-\cos\theta_0)$, and the reciprocal of the intrinsic rate constant occur as a product in the expression for the slope, it is not possible to deduce anything about the degree of diffusion control due to the presence of the unknown quantity A'. As discussed in the paragraph preceding Eq.(44), which is valid for all magnitudes of k_a', the slope can be used to indicate the presence of angular constraints on the reaction being studied.

VI. Results and Discussion

It is quite clear from Figures 2 and 3 that a moderate orientation constraint leads to a drastic reduction in k_{eff}/k_{diff}. For example, a reduction in the maximum rate constant of four and a half orders of magnitude is effected with an angular constraint of $\theta_0 = .05$ radians = 2.86 degrees. This is not an extremely stringent constraint since the total angle subtended by the reaction cone is $2\theta_0$. Furthermore, it can be expected that molecules which have an azimuthal requirement would exhibit a more drastic reduction in the maximum rate constant. The values of k_{eff}/k_{diff} at $\theta_0 = \pi$ exhibit a reduction in the rate constant from the radial constraint because R_T is used in place of $2R_H$. Due to the choice of a finite value of k_a', the limiting values of k_{eff}/k_{diff} at $\theta_0 = \pi$ are not exactly equal to $R_T/2R_H$. Thus, the k_{eff} value is approximately 10% below its maximum value since $k_a'/k_{eff} \cong 10$.

1. Reaction of the H_2O_2-Horseradish Peroxidase Complex with Cytochrome c

Farwell and Ackerman[8] have examined the viscosity dependence of the rate of association of H_2O_2-horseradish peroxidase with cytochrome c. The bimolecular rate constant for this association was observed to become viscosity dependent when the viscosity was about ten times that of water, and the rate constant had the value $k_M = 5\times10^5\ M^{-1}sec^{-1}$. In water, presumably, the rate constant has its low viscosity limiting value. According to Eq.(40), in the limit $\eta \to 0$,

$$\lim_{\eta \to 0} k_M = \frac{k_a'(1-\cos\theta_0)}{2} \quad . \qquad (45)$$

The problem is to select a k_a' and a $\theta_0 = R_T/R_H$ such that the following two conditions are approximately satisfied:

$$k_a'(1-\cos\theta_0)/2 = 5\times10^5\ M^{-1}\ sec^{-1} \quad , \qquad (46)$$

and the rate constant k_M becomes viscosity dependent when $\eta \cong 0.05$ poise. Inspection of the expressions for $\underset{\sim}{G}$ and SUM indicates that increasing the viscosity will begin to affect the rate constant when $k_a' \simeq (.25)(2\pi R_T DN_A/1000) = (kTN_A/3000)(.25)\theta_0$. If we now specify that this relation shall obtain when $\eta \simeq .05$, then we find

$$k_a' \simeq 4.2\times10^7\theta_0 \quad , \qquad (47)$$

which together with Eq.(46) permits determination of both k_a' and θ_0, whose values are

$$\theta_0 \simeq .37 \text{ radians} \quad , \qquad (48)$$

and

$$k_a' \simeq 1.5\times10^7\ M^{-1}\ sec^{-1} \quad . \qquad (49)$$

Values of k_M computed using Eqs.(48) and (49) are plotted against the inverse viscosity in Figure 6. The experimental data of Farwell and Ackerman are also shown for comparison. A curve computed using $\theta_0 = .143$ radians and $k_a' = 1.48\times10^7\ M^{-1}\ sec^{-1}$ is also shown to indicate the sensitivity of the result to choice of angular constraint.

2. <u>The Effect of Viscosity on the Rate of Renaturation of DNA</u>

Wetmur and Davidson[11] have presented a thorough study of the renaturation rate of various DNA's as a function of complexity, chain-length, temperature, and viscosity. The observed complexity and chain-length dependence were summarized concisely in their Eq.(20) as follows:

$$k_2 = 3.5\times10^5 L^{\frac{1}{2}}/N \quad , \qquad (50)$$

Figure 6

The bimolecular rate constant k_M for the association of the H_2O_2-horseradish peroxidase complex with cytochrome c as a function of the reciprocal viscosity $1/\eta$. The filled circles (●) represent the data of Farwell and Ackerman (cf., ref. 8). Solid line A is the theoretical curve computed with $R_T/R_H = \theta_0 = .37$, $k_a' = 1.5 \times 10^7\ M^{-1}\ sec^{-1}$. Solid line B is a theoretical curve computed with $R_T/R_H = \theta_0 = .143$, $k_a' = 1.48 \times 10^7\ M^{-1} sec^{-1}$.

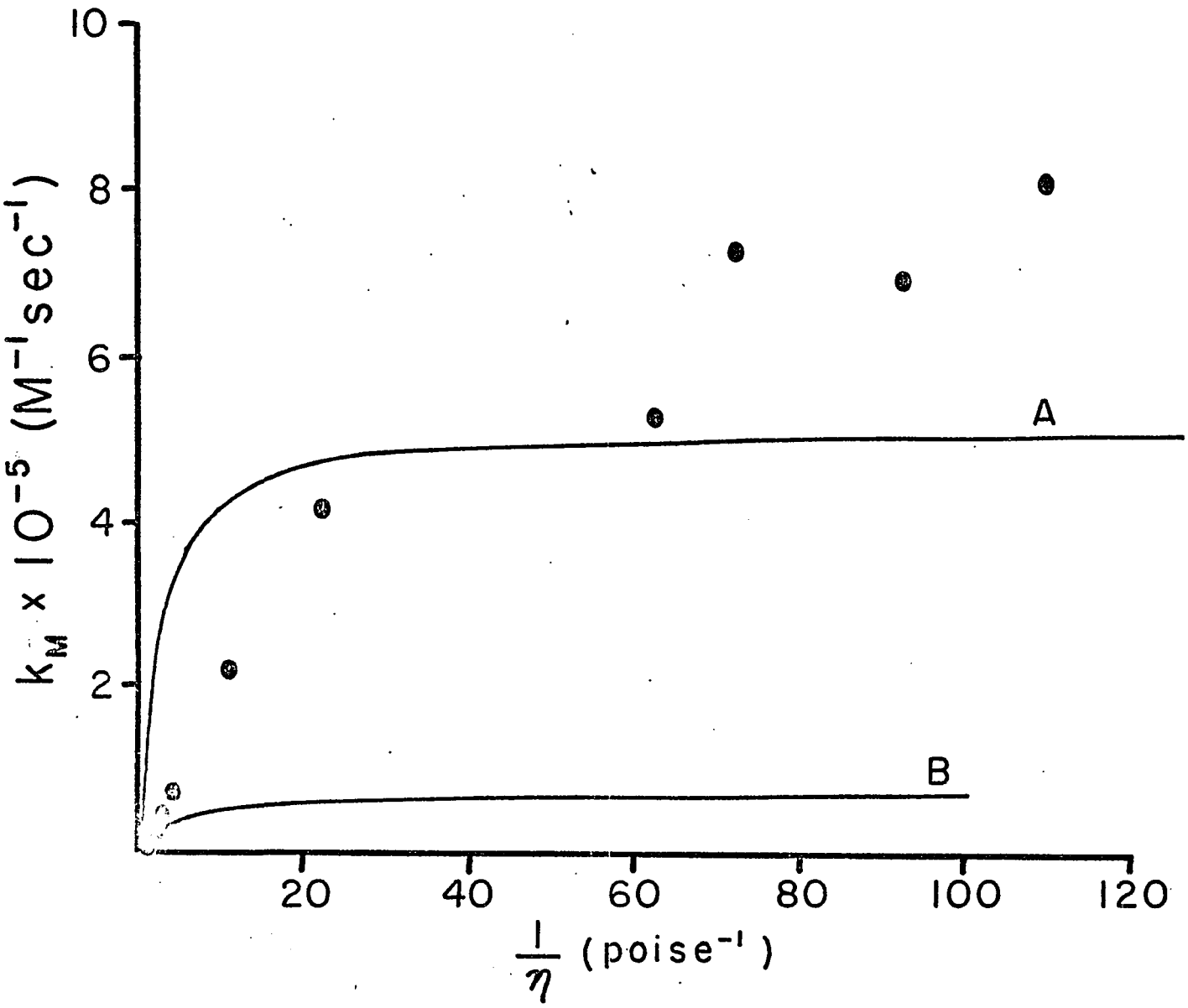
10
8
6
4
2
$k_M \times 10^{-5}$ ($M^{-1}sec^{-1}$)
A
B
20
40
60
80
100
120
$\frac{1}{\eta}$ (poise^{-1})

where k_2 is the second order rate constant calculated from $V_2 = k_2 P^2/4$, V_2 being the molar rate of base pair formation and P the denatured DNA phosphorus concentration; L is the average number of bases per single-stranded DNA molecule; and N is the complexity, or number of base pairs in non-repeating sequences for a given biological species. The rate constant k_2 applies at a temperature 25 degrees below the melting temperature, $(T_m-25)^oC$, and $[Na^+] = 1.0M$ in aqueous solution in the neutral pH range. Furthermore, the rate constant was strongly viscosity dependent. The constant k_2 also exhibited a moderately broad maximum as a function of (T_m-T) with the maximum occuring some 20-30°C below T_m.

The linearity of the second-order rate plots of the optical density over 75% of the renaturation range certainly argues that the bimolecular step is rate-limiting. Furthermore, the $L^{\frac{1}{2}}$ dependence of k_2 and its sharp viscosity dependence strongly suggests that this bimolecular step is diffusion-controlled. On the basis of general theoretical arguments (neglecting diffusion-control) Wetmur and Davidson showed that k_2 should be proportional to L, since this is the number of base-pairs formed in the rapid zippering reaction immediately following each bimolecular recognition, or nucleation, step. Since the diffusion coefficient for a non-draining random coil has the form $D \propto TL^{-1/2}\eta^{-1}$, it is apparent that, if the reaction were diffusion-controlled, one might expect to find $k_2 \propto L^{1/2}$ as was observed. All of these considerations were carefully made by Wetmur and Davidson, who nonetheless rejected diffusion-control of the bimolecular step primarily on the grounds that the absolute rate constant calculated according to the formula of Smoluchowski $k_2 = 4\pi(2D)R_T$ would be far too large for any reasonable choice of reaction radius R_T. From the previous calculations in Section V it is easily shown that a cylindrically

symmetric orientation constraint of $\theta_0 = .05$ radians (or an allowed fraction of total solid angle $f(.05) = 6.3\times10^{-4}$) will reduce the diffusion-controlled rate by three orders of magnitude, quite apart from the small target effect (i.e., $R_T <$ twice the effective hydrodynamic radius = $2kT/6\pi\eta D$) already considered by Wetmur and Davidson. Removal of cylindrical symmetry by including an azimuthal constraint will reduce the diffusion-controlled rate constant even further below the value predicted by the Smoluchowski equation. Such constraints for the alignment of strands during the nucleation step are not unreasonable. Presumably a number of base-pairs must be nearly aligned so that they can react almost simultaneously. A single hydrogen bond could not hold such large particles against their Brownian motion. If the polar axis from which θ_0 is measured is taken along the molecular axis, then a reaction cone constraint of $\theta_0 = 3°$ for the axis of the complimentary strand is not unreasonable. Furthermore, it is difficult to see how more than a quarter of the azimuthal angular range of the other strand could permit reaction to occur, since the bases of the two parallel chains must be pointing toward one another.

It is possible to assess the role of rotational diffusion by considering the hypothetical case in which no rotational diffusion occurs but the orientation constraint is still retained. Assuming random orientations, the fraction of molecules with the correct orientation is given by

$$f(\theta_0) = \int_0^{\theta_0} \frac{\sin\theta d\theta}{2} = \frac{1-\cos\theta_0}{2} \quad , \qquad (51)$$

which is equivalent to X_{00} for the case when $X(\theta)$ is a step function [cf., Eq.(2b)]. For mutually diffusing spherical particles in total solution space, i.e., 4π and $2D$ will occur in k_{diff} instead of 2π and D in Eq.(22), the effective diffusion-controlled rate constant is

just the Smoluchowski result with a modified concentration

$$k_{\theta_0} = \frac{4\pi R_T(2D)[f(\theta_0)N_A]}{1000} \quad , \qquad (52)$$

since only those molecules with the proper orientation can react. Assuming an azimuthal constraint (arising from the cylindrical shape of the molecules) introduces another factor of $\frac{1}{4}$ into Eq.(52) in accord with the preceding paragraph, then one can expect an effective second order diffusion-controlled rate constant of the form

$$k(\theta_0,\phi_0) = \frac{3x10^{-4}4\pi(2D)R_TN_A}{4(1000)} \quad , \qquad (53)$$

when $\theta_0 = .05$ radians.

The argument that Wetmur and Davidson present for rejection of diffusion-control is summarized as follows. Since the renaturation process is bimolecular, it is assumed that a certain fraction of sites β function as nucleating sites for the reaction. If N is the complexity of the chain and P is the denatured phosphate concentration, then the concentration of any one unique nucleation site is $\beta P/2N$. If k_N is the average rate constant for nucleation, then the rate of nucleation per site is $k_N(\beta P/2N)^2$, or the total rate of nucleation for βN sites is $k_N(\beta P/2N)^2\beta N$. However, if the strands are exactly complimentary, then L base pairs are formed for each nucleation, hence

$$V = k_N\beta^3(L/4N)P^2 \quad . \qquad (54)$$

Comparison of Eq.(54) with the experimental rate expression $V = k_2P^2/4$ leads to the identity

$$k_2 = \beta^3k_N(L/N) \quad . \qquad (55)$$

If the nucleation step is truly diffusion-controlled, then $k_N = 4\pi(2D)R_T(N_A/1000)$. Therefore, the target radius is

$$R_T = \frac{k_2\ (N/L)}{4\pi(2D)\beta^3}\ \frac{1000}{N_A} \quad . \qquad (56)$$

Substitution of $L = N, D = 1.9\text{x}10^{-8}\ cm^2\ sec^{-1}$, and $k_2 = 1800M^{-1}\ sec^{-1}$ into Eq.(56) for T7 phage, Wetmur and Davidson arrived at their Eq.(23)

$$R_T = 6\text{x}10^{-12}\beta^{-3}cm \quad . \qquad (57)$$

For $\beta = 1/20$, they find that $R_T = 5\text{x}10^{-8}cm$, which is a reasonable value. Their computer calculations, however, suggest that every site may be a nucleation site (i.e., $\beta = 1$), which leads to the unreasonable value $R_T = 6\text{x}10^{-12}cm$. Furthermore, they argue, the inclusion of segmental diffusion acts to decrease the value of β (i.e., one nucleating site per 20 nucleotides) needed to obtain a reasonable value of R_T. From this argument, Wetmur and Davidson conclude that the rate determining step is not diffusion-controlled. Substitution of Eq.(53) for k_N in Eq.(55) and using the parameters for T7 phage, one finds

$$R_T = 2\text{x}10^{-8}\beta^{-3}\ cm \quad . \qquad (58)$$

It becomes obvious that the inclusion of rotational diffusion leads to reasonable estimates for both R_T and β.

Wang and Davidson[15] have argued that segment diffusion will increase the reaction rate by a factor of 100 above that due to translational diffusion alone. Their estimate hinges in a crucial way on the value of the segmental diffusion coefficient and the interpretation of its role in determining the encounter frequency. The segmental diffusion coefficient was estimated from the shortest relaxation time in the electric

birefringence spectrum, and used in Smoluchowski's formula to compute the segment encounter rate. Although this procedure may give a crude estimate of the dynamics of segments engaged in low amplitude, small-displacement motions, it is hardly adequate to describe diffusion along a steep and extensive diffusion gradient varying as R_T/r, where $r \geq R_T$ can be as large as the dimensions of the entire polymer molecule. Surely the effective segmental diffusion coefficient for diffusion into a sink is very much smaller than that applicable to the relaxation of small distortions of the radial distribution function. For this reason the conjectured rate enhancement by a factor of 100 due to segmental diffusion appears to be an overestimate. Furthermore, the coulombic repulsion of the strands will act to reduce the rate constant below the value predicted by Smoluchowski's formula.

In any event, the mechanism advanced by Wetmur and Davidson to account for the $L^{\frac{1}{2}}$ dependence of the bimolecular rate constant, the excluded volume effect, is inconsistent with their contention that the bimolecular step is not diffusion-controlled. It simply isn't possible to impose a large scale geometric constraint (i.e., excluded volume) to reduce the rate of reaction of these flexible, freely-diffusing, single-strand molecules without introducing a concommitment "diffusion-control" of that reaction. Only if these polymers were highly branched, or formed metastable bonds so as to inhibit free diffusion, would such a conclusion require modification. The imposition of a large scale geometric constraint is capable only of reducing the diffusion rate constant. Since the extent of diffusion-control depends upon the relative competion of the intrinsic rate constant and the diffusion rate constant, the decrease in the diffusion rate constant will either leave the rate unchanged or decrease it

[cf. Eq.(18)]. Clearly an excluded volume effect of such a magnitude as to make itself felt in the rate constant implies a large degree of diffusion-control of the reaction (i.e., $k_a' >> k_{diff}$).

A feature of the renaturation reaction that is difficult to reconcile with complete diffusion-control is the bell-shaped temperature dependence of the bimolecular rate constant k_2. It is possible to examine the question of the degree of diffusion control by plotting $1/k_2$ versus η/T. As is apparent from Figure 5, one expects a nearly straight line for any reaction, irrespective of the degree of diffusion-control. However, the relative magnitudes of k_M and its low viscosity limit $k_M^o = \frac{k_a'(1-\cos\theta_0)}{2}$ [cf. Eq.(40)] provide a measure of the degree of diffusion-control d defined by

$$d = 1 - \vec{k}_M/k_M^o \quad ; \quad 0 \leqslant d \leqslant 1 \qquad . \qquad (59)$$

Thus, any reciprocal plot of $1/k_M$ as a function of viscosity for which the intercept $1/k_M^o$ is significantly different from zero cannot represent a completely diffusion-controlled reaction (i.e., $d < 1$ which implies $k_a' \not\gg k_{diff}$). A modification of the reciprocal plot that may be employed when the temperature is not held constant is to graph $1/k_M$ as a function of $(\eta/T)_{rel}$, where $(\eta/T)_{rel}$ is defined to be the value of η/T for the actual solvent at the temperature of renaturation divided by η/T for an aqueous solution with the same salt concentration at the temperature specified. This type of plot has not been investigated numerically, but it is expected to deviate but slightly from linearity if k_a' is only weakly temperature dependent over the same interval. Such plots for the data of Wetmur and Davidson are given in Figures 7 and 8, in which the $\Delta T = T_m - T$ values associated with each point are also presented. Examining Figure 7 for the ethylene glycol data first, it is observed that

Figure 7

Reciprocal plot of $1/k_2$ vs $(\eta/T)_{rel}$ for the renaturation of mechanically sheared T4 DNA in 0.4 M-sodium ion in phosphate buffer, pH 7, containing ethylene glycol to enhance the viscosity. These data were reported by Wetmur and Davidson (ref. 11). The values of (T_m-T_r) associated with each measurement are indicated in the figure. T_m is the melting point of DNA in a solution of the given composition, and T_r is the temperature at which the kinetics of the reaction were observed.

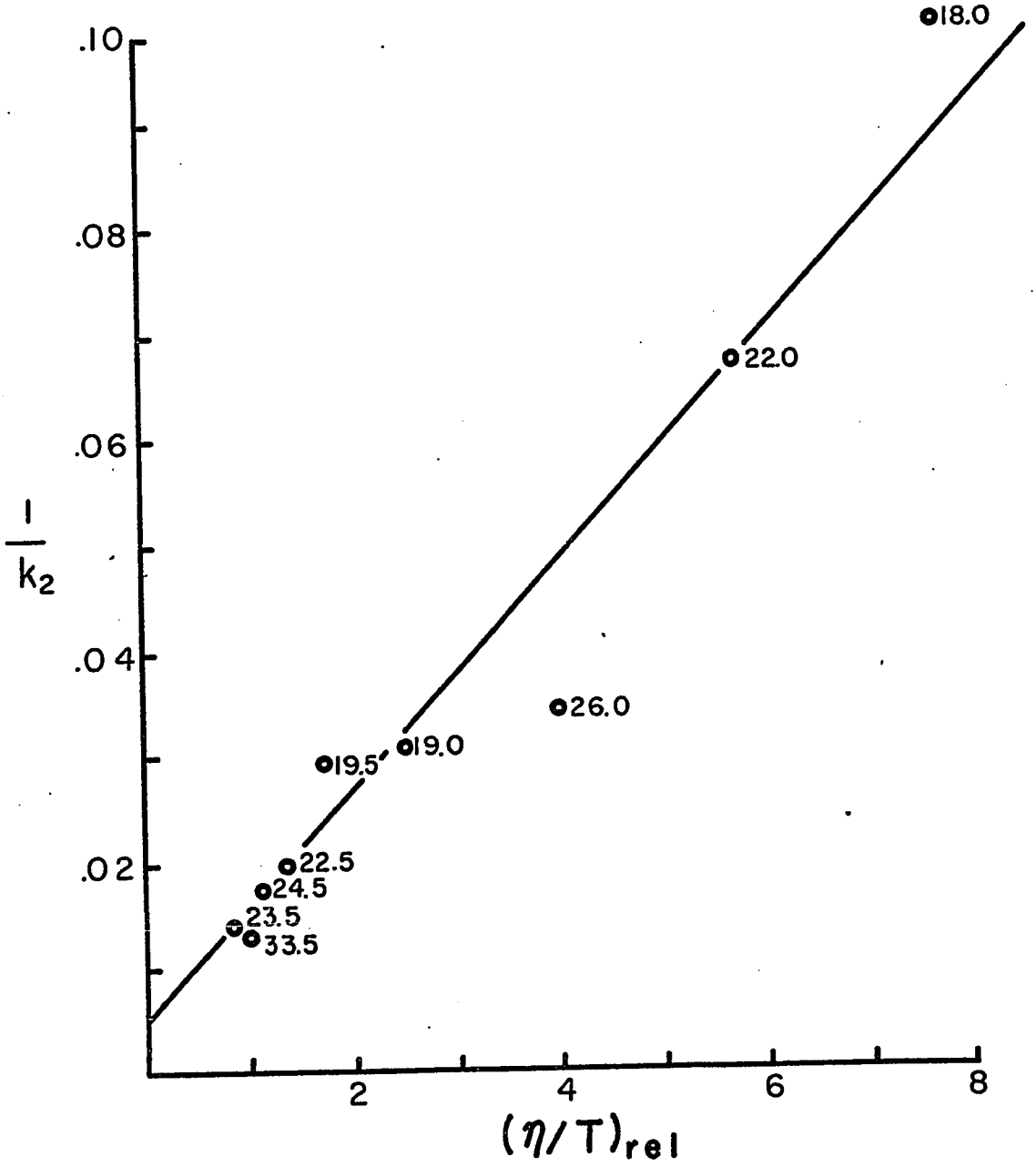
.10
.08
.06
.04
.02
1/k2
18.0
22.0
26.0
19.0
19.5
22.5
24.5
23.5
33.5
2
4
6
8
(η/T)rel

Figure 8

Reciprocal plot of $1/k_M$ vs $(\eta/T)_{rel}$ for the renaturation of mechanically sheared T4 DNA in 0.4 M-sodium ion (●), and in 1.0 M-sodium ion (△), in phosphate buffer, pH 7.0, containing sucrose to enhance the viscosity. These data were reported by Wetmur and Davidson (see ref. 11). The values of $(T_m - T_r)$ associated with each measurement are indicated in the figure; see legend of Figure 7 for explanation.

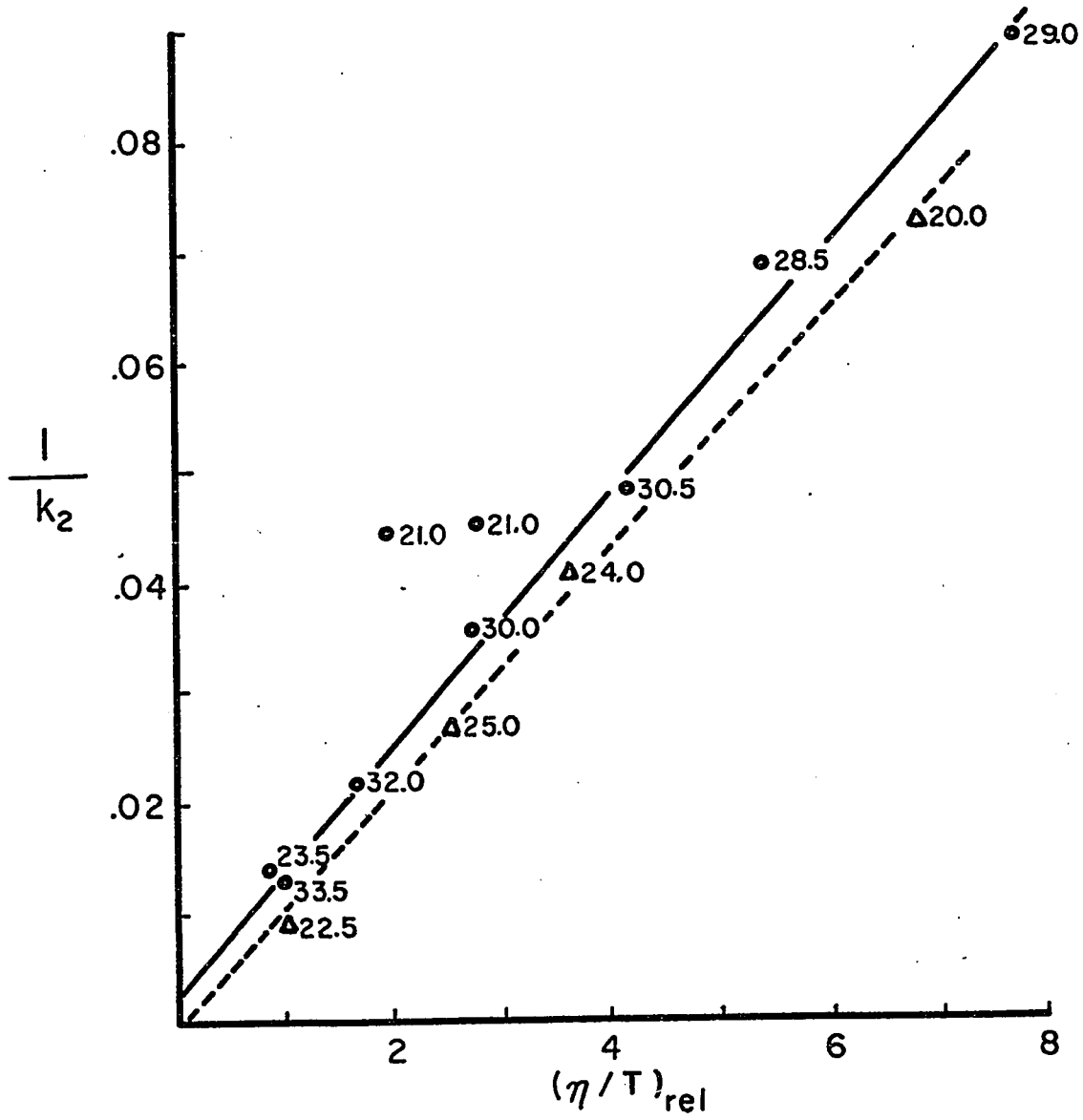
29.0
28.5
Δ20.0
.08
.06
1/k2
21.0
21.0
30.5
Δ24.0
.04
30.0
Δ25.0
32.0
.02
23.5
33.5
Δ22.5
2
4
6
8
(η/T)rel

the data taken in the range $\Delta T = 19 - 33.5$ give a good straight line with a significant positive intercept. Furthermore, the $\Delta T = 18$ point lies above this line while the 26 and 33.5 points lie below this line. If the intrinsic molar rate constant k_a' increases with decreasing temperature, then one would expect points of smaller ΔT to lie above, and the points of larger ΔT to lie below, as observed. Taking the intercept in Figure 7 to be $1/k_M = .005$ one finds at $[Na^+] = 0.4$ M a degree of diffusion-control for $(\eta/T)_{rel} = 1$ of approximately

$$d = 1 - 50(.005) = .75 \quad . \qquad (60)$$

The corresponding data for the sucrose solutions in 0.4 M and 1.0 M Na^+ ion are plotted in Figure 8. The data for the 1.0 M Na^+ solutions apparently have an intercept that is not significantly different from zero. The data for the 0.4 M Na^+ solutions appear to have an intercept somewhat different from zero, but its significance is more open to question than it was for the ethylene glycol data. However, if one specifies that only points in the range $\Delta T = 29 - 33.5$ are to be considered, then a reasonable straight line and intercept are obtained. Again, points with ΔT less than the "main" range of values lie above the line drawn, as expected if k_a' increases with decreasing temperature below T_m. Although rather less accuracy can be claimed in this instance, the degree of diffusion-control at $\Delta T \simeq 31^\circ$ and $[Na^+] = 0.4M$ for $(\eta/T)_{rel} = 1$ is found to be (taking $1/k_M^\circ = .022$)

$$d \simeq 1 - (45.6)(.022) = .90 \quad . \qquad (61)$$

The degree of diffusion-control at $\Delta T \simeq 25^\circ$ and $[Na^+] = 1.0M$ is evidently $d = 1$ for all values of $(\eta/T)_{rel}$ for which the data were obtained. The

implication is that the intrinsic rate constant k_a' is fast enough in the presence of the extra salt so that the rate constant is essentially completely diffusion-controlled in aqueous solution. A reciprocal plot of the $NaClO_4$ data of Wetmur and Davidson produced a negative intercept. This is probably a consequence of the effect of the salt either on k_a' directly, or on the intermolecular potential. It certainly would not be surprising to discover that the intrinsic rate constant k_a' was in general enhanced by increased salt. It may well prove possible by working at lower ionic strengths to obtain rate constants with smaller degrees of diffusion-control than those found by Wetmur and Davidson.

If it may be assumed that the intrinsic rate constants and orientation constraints at the nucleation sites are unaffected by the solutes used to enhance the viscosity, whether sucrose or ethylene glycol, then the estimated values of the intercepts may be employed to obtain the ratio of the intrinsic rate constants at the two values of ΔT

$$k_a'(31)/k_a'(21) \simeq 455/200 \simeq 2.3 \quad . \qquad (62)$$

There now arises the interesting possibility that k_a' does not have a bell-shaped temperature dependence at all, at least in this region, and that instead it is monotonically increasing function of ΔT. The observed decline in the value of k_2 (or k_M) with decreasing T could then be interpreted as the onset of diffusion-control of the overall rate constant in the plateau region.

The proposed reaction mechanism of Wetmur and Davidson is based on the assumption that the reaction is not diffusion-controlled. Their proposed mechanism, briefly, is the diffusion of two polymer molecules towards each other until one nucleotide unit on one chain is within a radius

R_T of the second chain. This initiating step is followed by a nucleation step in which a single bond is formed between these nucleotides. The remaining step is simply the zippering of adjacent complimentary base units until a sequence of N base pairs is attained. The mechanism is represented by

$$A + A' \underset{k_{0,-1}}{\overset{k_{-1,0}}{\rightleftharpoons}} C_0 \underset{k_{1,0}}{\overset{k_{0,1}}{\rightleftharpoons}} C_1 \underset{k_{2,1}}{\overset{k_{1,2}}{\rightleftharpoons}} C_2 \cdots \underset{k_{N,N-1}}{\overset{k_{N-1,N}}{\rightleftharpoons}} C_N \quad , \tag{63}$$

where C_i is the species containing i bonded base pairs. The equilibrium constants for the three major steps in the mechanism are,

$$k_{-1,0}/k_{0,-1} = 4\pi R_T^3/3 \quad , \tag{64}$$

$$k_{0,1}/k_{1,0} = \sigma s \quad , \tag{65}$$

$$k_{i,i+1}/k_{i+1,i} = s_{i+1} > 1 \quad , \tag{66}$$

(since C_N is favored at equilibrium)

where σ constitutes a nucleation parameter measuring the degree of difficulty for the nucleating step. If σ is divided up into contributions from the forward and reverse steps, then one can write

$$k_{0,1} = \sigma_f k_f \quad , \tag{67}$$

$$k_{1,0} = k_f/s\sigma_b \quad , \tag{68}$$

$$\sigma_f \sigma_b = \sigma \quad . \tag{69}$$

For a system not too close to equilibrium, their steady state analysis leads to the equation

$$k_N = \frac{(4\pi/3)R_T^3 \; k_f(N_A/1000)}{(k_f R_T^3/3D) + \frac{1}{\sigma_f} + \left(\frac{1}{\sigma}\right)\left(\frac{1}{s_1} + \frac{1}{s_1 s_2} + \cdots + \frac{1}{s_1 s_2 \cdots s_{N-1}}\right)} \quad , \tag{70}$$

where D is twice the diffusion coefficient of one polymer molecule. Based on the conclusion that k_N is not diffusion-controlled and the assumption that the dissociation of the first unstacked base pair is more rapid than the others, Wetmur and Davidson conclude that the third term in the denominator of Eq.(70) is the dominant term,

$$k_N \simeq \frac{(4/3)R_T\, k_f\, (N_A/1000)}{\frac{1}{s_1} + \frac{1}{s_1 s_2} + \frac{1}{s_1 s_2 s_3} + \cdots + \frac{1}{s_1 s_2 \cdots s_{N-1}}} \quad , \qquad (71)$$

which is proportional to k_f.

Wetmur and Davidson explain the bell shaped temperature dependence of k_N by noting the formal equivalence of k_N [cf. Eq.(71)] with that obtained by Sanders and Ross.[17] The observed chain length and viscosity dependence is explained, in their final analysis, by postulating that the stabilization reaction (i.e., the formation of the first ten or twenty bonds) takes place by first stretching the coil without translational or rotational motion of the molecule as a whole through the solvent. The steric hindrance mechanism would then explain the chain length dependence. The viscosity dependence is then explained by assuming k_f for the rate determining step is viscosity dependent.

It is clear that the proposed mechanism is postulated to obtain compatable parameters for R_T and β in Eq.(57) since the net effect of the mechanism is to substitute the diffusion of small molecules (i.e., k_f is assumed to be viscosity dependent) for the diffusion of large molecules [cf. Eq.(64)]. It is crucial in the argument of Wetmur and Davidson that the bonds participating in the stabilization reaction are already pre-aligned so that no motion of the polymer as a whole is involved in the rate determining step. If an orientation constraint is assumed to be present in this reaction then

$$k_{-1,0} = \vec{k} \quad , \tag{72}$$

and

$$k_{0,-1} = \overleftarrow{k} \quad , \tag{73}$$

where $\vec{k}$ and $\overleftarrow{k}$ are defined by Eqs.(18) and (19), respectively. It should be emphasized that Eqs.(72) and (73) do not represent the total rate expressions since the zippering mechanism is not included. The ratio of these quantities replaces the expression given in Eq.(64). In this instance the steady-state analysis, in molar quantities, is

$$-\frac{1}{A^2}\frac{\partial A}{\partial t} = \frac{(k_M/\overleftarrow{k})k_f}{\frac{k_f}{\overleftarrow{k}} + \frac{1}{\sigma_f} + \frac{1}{\sigma}\left(\frac{1}{s_1} + \frac{1}{s_1 s_2} + \cdots + \frac{1}{s_1 s_2 \cdots s_{N-1}}\right)} \quad , \tag{74}$$

which may be reduced exactly to

$$-\frac{1}{A^2}\frac{\partial A}{\partial t} = \frac{k_D k_a'}{k_a^o + k_D\left(\frac{1}{SUM} + \frac{k_d^o}{k_f}\left(\frac{1}{\sigma_f} + \frac{1}{s_1} + \frac{1}{s_1 s_2} + \frac{}{2} \cdots + \frac{1}{s_1 s_2 s_3 \cdots s_{N-1}}\right)\right)} \quad , \tag{75}$$

where $k_D = 2\pi R_T D$ is the diffusion-controlled rate constant with both polar and azimuthal constraints [cf. Eq.(53)] and $s_1' = \sigma s_1$. If the zippering reaction rates are to affect the overall rate of reaction in the absence of diffusion-control of the bimolecular step as suggested by Wetmur and Davidson, then 1/SUM in Eq.(75) must be negligible compared to the other terms in the brackets. Therefore, the bimolecular association rate constant can be written as

$$-\frac{1}{A^2}\frac{\partial A}{\partial t} = \frac{k_D k_a'/\gamma}{k_D + k_a^o/\gamma} \quad , \tag{76}$$

where $$\gamma = \frac{k_d}{k_f}\left[\frac{1}{\sigma_f} + \frac{1}{s_1'} + \frac{1}{s_1' s_2} + \cdots + \frac{1}{s_1' s_2 s_3 \cdots s_{N-1}}\right] \quad .$$

Clearly, if k_f is proportional to the diffusion coefficient of the nucleotide units, then $-(1/A^2)\partial A/\partial t$ should always be inversely proportional to the viscosity, so that a reciprocal plot of k_M as a function of viscosity will always have a zero intercept. Although the experimental data presented in Figures 7 and 8 are not unequivical, they do not appear to substantiate a zero intercept. The mechanism proposed by Wetmur and Davidson to account for the viscosity dependence of the overall bimolecular rate constant is evidently not supported by their data.

In order for the steady-state assumption to be valid for an intermediate step, its logarithmic time derivative must be small (in absolute value) compared to the logarithmic time derivative of the concentration of reactants. This condition is certainly not met for those intermediates participating in the rapid zippering reaction which follows the rate determining step. The steady-state approximation employed by Wetmur and Davidson is applicable, therefore, only to the C_0 component of the process described by Eq.(63). A more reasonable model would entail the assignment of a cooperativity parameter to each of the steps in the stabilization reaction. Thus, provided that diffusion-control of the bimolecular step is accepted, the mechanism proposed by Wetmur and Davidson might still be employed to account for the increase in the overall rate constant with decreasing T over at least part of the observed range. Using the definitions:

(i) $N \equiv P$, the number of intermediates involved in the stabilization reaction ;

(ii) $k_{i,i+1} \equiv \sigma_{nf} k_f$, $i = 0,\ldots,P-1$;

(iii) $k_{i+1,i} \equiv k_f/s\sigma_{nb}$, $i = 0,\ldots,P-1$;

(iv) $\sigma_{nf}\sigma_{nb} \equiv \sigma_n$;

(v) $k_{i,i+1}/k_{i+1,i} \equiv s\sigma_n$;

(vi) $(\sigma_n)^{P-1} \equiv \sigma$,

where σ is the cooperativity parameter for overall helical stability, the steady-state treatment of the states 0 to P-1 leads to

$$-\frac{1}{A^2}\frac{\partial A}{\partial t} = \frac{k_D k'_a}{k_a^o + k_D \frac{1}{SUM}\frac{k_d^o}{k_f \sigma_{nf}} 1 + \frac{1}{\bar{s}} + \left(\frac{1}{\bar{s}}\right)^2 + \cdots + \left(\frac{1}{\bar{s}}\right)^{P-1}} \quad ; \qquad (77)$$

where $\bar{s} = \sigma_n s$. Eq. (77) can be further reduced to the concise form

$$-\frac{1}{A^2}\frac{\partial A}{\partial t} = \frac{k_D k'_a}{k_a^o + k_D \frac{1}{SUM} + \frac{k_d^o}{k_f \sigma_{nf}} \frac{1 - (1/\bar{s})^P}{1 - 1/\bar{s}}} \quad . \qquad (78)$$

The success of Eq.(70) in predicting the unusual temperature behavior is the similarity in form to a valid steady-state approximation, such as given in Eq.(77). A plot of $\left(-\frac{1}{A^2}\frac{\partial A}{\partial t}\right)^{-1}$ as a function of viscosity has an intercept

$$k_M^o = \left(\frac{2}{k_a^o(1-\cos\theta_0)} + \frac{k_d^o}{k_f \sigma_{nf}} \frac{1-(1/\bar{s})^P}{1 - 1/\bar{s}}\right)^{-1} \frac{N_A}{1000} \quad , \qquad (79)$$

in which the source of the temperature dependence is manifested explicitly.

3. Comparison with Model of Solc and Stockmayer

The model proposed by Solc and Stockmayer[16] for the reaction between two chemically asymmetric molecules is primarily the diffusion of a spherical particle with two orientation vectors toward a fixed sphere that is uniformly reactive over the entire surface. One of the orientation vectors on the diffusion sphere represents the transposed orientation vector of the fixed sphere. Thus, for a collision to occur between spheres A and B, the center of the diffusing sphere having a relative diffusion coefficient $D = D_A + D_B$ must fall within a collision radius $r = r_A + r_B$, where r_A and r_B are the radii of sphere A and B, respectively. For a reaction to occur as a result of the collision, the orientation vectors

$\underset{\sim}{A}$ and $\underset{\sim}{B}$ must be properly aligned. The general solution to the diffusion equation for this model, which Solc and Stockmayer find by the method of Laplace transformation, consists of a series solution involving modified Bessel functions of the third kind, spherical harmonics, and "unknown" constants of six indices in addition to the transformation variable. Since analytical solutions to their diffusion equation do not exist, Solc and Stockmayer proceed to study the limiting cases for short and long times. They find that, at short times, the rate constant k(t) is independent of the rotational diffusion coefficient and is simply Smoluchowski's result multiplied by the fractional active surface area. This is the same result for non-rotating spheres as expressed in Eq.(52). In the long time limit, however, Solc and Stockmayer did not find an explicit solution. Their Eq.(20) for this limit is

$$k(t) = 4\pi a D c_0 \left[2\pi^{1/2}\alpha_0(000)+2(a^2/Dt)^{1/2}(\alpha_0(000)+\alpha_1(000))\right] + O(t^{-3/2}), \quad (80)$$

where $D = D_A + D_B$, a is the effective collision radius, c_0 is the initial total volume concentration of spheres with the two orientation vectors, and $\alpha_0(000), \alpha\alpha_1(000)$ are the first two unknown coefficients of the expansion in their Eq.(B8)

$$\underset{\sim}{\alpha}(ik_1k_2;p) = \sum_{n=0}^{\infty} \alpha_n(ik_1k_2)\left(\frac{a^2}{D}\right)^{1/2} p^{(n-2)/2} \quad , \quad (81)$$

where p is the Laplace transformation variable.

Clearly, in the limit $t \to \infty$, Eq.(80) reduces to the steady-state rate constant

$$k(t \to \infty) = 4\pi a D c_0 2\pi^{1/2}\alpha_0(000) \quad . \quad (82)$$

To make the theory of Solc and Stockmayer coincident with the present

study, Eq.(18) is modified to account for total solution space

$$\vec{k} = \frac{k_a^o(4\pi R_T D)}{4\pi R_T D/SUM + k_a^o} \quad , \tag{83}$$

where $D = D_A + D_B$. Unfortunately, the term SUM has a complicated functional dependence on k_a^o [cf. Eqs.(8c), (31), and (34)] and a simple expression for the diffusion-controlled rate constant ($k_a^o \to \infty$) cannot be obtained at this time. If one retains the usual functional form for the diffusion-controlled rate constant k_D by defining an "effective" target radius R_T^*

$$R_T^* = R_T k_a / (4\pi R_T D/SUM + k_a^o) \quad , \tag{84}$$

we find that R_T is related to a by

$$R_T = k_a 2\pi^{1/2} a\alpha_0(000) / [(k_a^o - 8\pi^{3/2} aD\alpha_0(000))SUM] \quad . \tag{85}$$

In the absence of numerical calculations, Solc and Stockmayer state that no definite conclusion can be drawn about the heterogeneity of the reacting surface unless there is a gross discrepancy between the reactive cross section and the known dimensions of the molecule. In view of Eq.(85), this appears to be a reasonable conclusion. But the weaknesses of this argument are the necessity of an a priori knowledge of the hydrodynamic radius and the lack of a quantitative interpretation of "gross discrepancy."

Perhaps a more sensitive method for detecting the presence of an angular constraint is measuring the slope of $1/k_M$ as a function of viscosity. As implied by the numerical calculation in Section V, the slope is greatly affected by the angular constraint. Furthermore, this method is not limited to diffusion-controlled reactions and does not require an a priori knowledge of the hydrodynamic radius. Value judgments pertaining to "gross

discrepancies" are replaced by the more quantitative measure of $(R_H/R_T)_{eff}$, which can be calculated from the slope.

It is possible to assess the effect of rotational diffusion on the rate of reaction in the following manner. The rate constant for non-rotating spheres with a reaction site on a plane can be obtained by multiplying k_{θ_0} [cf. Eq.(52)] by $\frac{1}{4}$. The ratio $4k_{eff}/k_{\theta_0}$ represents the enhancement factor due to rotational diffusion.

In the region of small angles, Eq.(51) is approximated by the expansion

$$1-\cos\theta_0 = 1-\sum_{n=0}^{\infty}\frac{(i\theta_0)^{2n}}{(2n)!} \simeq \frac{\theta_0^2}{2} \qquad . \qquad (86)$$

Substituting Eq.(86) into Eq.(20) and noting the restriction imposed on R_T [cf. Eq.(26)] predicts that k_{eff} is roughly proportional to θ_0^3 for small angles.

As indicated in Table I, the effective diffusion controlled rate constant is enhanced by a factor of approximately 2 at small angles over the rate constant in which no rotation is allowed to occur. The implication is that rotational diffusion is simply not fast enough to alleviate the angular constraint. If R_T is independent of the choice of θ_0, then k_{eff} would be approximately proportional to the fraction of molecules with the proper orientation. For small angles, this would be approximately $\frac{\theta_0^2}{2}$ as indicated in Eq.(86). It does not seem physically reasonable, however, to impose a rigid angular constraint while simultaneously allowing a large uncertainty in the translational position.

TABLE I

EFFECT OF ROTATIONAL DIFFUSION ON THE DIFFUSION-CONTROLLED RATE CONSTANT

θ_0 (radians)	R_H/R_T	η (poise)	$k_{eff}(M^{-1}sec^{-1})$	$4k_{eff}/k_{\theta_0}$
1.04	1	.008	4.3×10^8	1.65
.30	3.33	.008	1.39×10^7	1.975
.20	5.0	.008	4.13×10^6	1.988
.149	6.72	.008	1.74×10^6	2.04
.143	7.0	.008	1.53×10^6	2.06
.098	10.0	.008	5.19×10^5	2.12
.048	20.0	.008	6.18×10^4	2.23

APPENDIX A: FINDING THE INVERSE OF THE MATRIX $\underset{\simeq}{G}$

The matrix $\underset{\simeq}{G}$ is defined to be

$$G_{mn} = \frac{-Q\exp(-\kappa_n R_T) X_{mn}}{R_T} - \exp(-\kappa_m R_T)(\kappa_m + 1/R_T)\frac{\delta_{m,n}}{2m+1} , \qquad (A1)$$

Since $X_{mn} = X_{nm}$, the only term preventing the matrix $\underset{\simeq}{G}$ from being symmetric is $\exp(-\kappa_n R_T)$. This term can be symmetrized by multiplying G_{mn} by $\exp[-R_T(\kappa_m - \kappa_n)/2]$, with the result

$$G_{mn} = \frac{-Q\exp[-(\kappa_m+\kappa_n)R_T/2] X_{mn}}{R_T} - \exp(-\kappa_m R_T)(\kappa_m + 1/R_T)\frac{\delta_{m,n}}{2m+1} . \qquad (A2)$$

The term containing $\delta_{m,n}$, which occurs only in the diagonal elements, is unaffected by this multiplication. Therefore, we define the matrices

$$(\underset{\simeq}{\xi}^{1/2})_{mn} \equiv \exp(-\kappa_m R_T/2)\delta_{m,n} , \qquad (A3)$$

$$\xi^{-1/2}_{mn} \equiv \exp(+\kappa_m R_T/2)\delta_{m,n} , \qquad (A4)$$

and write Eq.(A2) in matrix form

$$(\underset{\simeq}{\xi}^{1/2}\underset{\simeq}{G}\underset{\simeq}{\xi}^{-1/2})_{ij} = \sum_{k,l}(\underset{\simeq}{\xi}^{1/2})_{ik} G_{kl} (\underset{\simeq}{\xi}^{-1/2})_{lj} = -Q\exp[-R_T(\kappa_i+\kappa_j)/2]X_{ij} , \qquad (A5)$$

for $i \neq j$. Multiplication of Eq.(9) in the text on the left by results in

$$\underset{\simeq}{\xi}^{1/2}\ \underset{\simeq}{G}\ \underset{\sim}{C} = \underset{\simeq}{\xi}^{1/2}\ \underset{\simeq}{G}\ \underset{\simeq}{\xi}^{-1/2}\ \underset{\simeq}{\xi}^{1/2}\ \underset{\sim}{C} = \underset{\simeq}{\xi}^{1/2}\ \underset{\sim}{L}_o , \qquad (A6)$$

We now solve for $\underset{\sim}{C}$,

$$\underset{\sim}{C} = \underset{\simeq}{\xi}^{-1/2}(\underset{\simeq}{\xi}^{1/2}\ \underset{\simeq}{G}\ \underset{\simeq}{\xi}^{-1/2})^{-1}\underset{\simeq}{\xi}^{1/2}\ \underset{\sim}{L}_o . \qquad (A7)$$

Because $\underset{\simeq}{\xi}^{\frac{1}{2}}\ \underset{\simeq}{G}\ \underset{\simeq}{\xi}^{-\frac{1}{2}}$ is symmetric, it is now a simple matter to diagonalize the resulting product with the transformation

$$\underset{\simeq}{S}(\underset{\simeq}{\xi}^{\frac{1}{2}}\underset{\simeq}{G}\ \underset{\simeq}{\xi}^{-\frac{1}{2}})\underset{\simeq}{S}^{-1} = \underset{\simeq}{\Lambda} \quad , \tag{A8}$$

where the product $\underset{\simeq}{S}\ \underset{\simeq}{S}^{-1}$ gives the identity matrix, Eq.(A7) then becomes

$$\underset{\sim}{C} = \underset{\simeq}{\xi}^{-\frac{1}{2}}(\underset{\simeq}{S}^{-1}\ \underset{\simeq}{\Lambda}\ \underset{\simeq}{S})^{-1}\underset{\simeq}{\xi}^{\frac{1}{2}}\underset{\sim}{L}_0 \tag{A9}$$

$$= \underset{\simeq}{\xi}^{-\frac{1}{2}}\underset{\simeq}{S}\ \underset{\simeq}{\Lambda}^{-1}\underset{\simeq}{S}^{-1}\underset{\simeq}{\xi}^{\frac{1}{2}}\underset{\sim}{L}_0$$

The problem now becomes one of finding $\underset{\simeq}{S}$ and $\underset{\simeq}{\Lambda}$, since $(\underset{\simeq}{S})_{mn} = (\underset{\simeq}{S}^{-1})_{nm}$ and $(\underset{\simeq}{\Lambda}^{-1})_{m,n} = \delta_{m,n}/(\underset{\simeq}{\Lambda})_{m,n}$. There are several numerical routines available, such as the Jacobi method, for finding the eigenvalues and eigenvectors of a symmetric matrix.

GLOSSARY OF k TERMS

k	Boltzmann's constant.
k_a^o	Intrinsic association constant (cm^3 $molec^{-1}$ sec^{-1})[cf. Eq.(2b)].
k_d^o	Intrinsic unimolecular dissociation constant [cf. Eq.(2b)].
k_a'	Intrinsic association constant (ℓ $mole^{-1}$ sec^{-1})[cf. Eq.(21)].
$\vec{k}$	General bimolecular association rate constant (cm^3 $molec^{-1}$ sec^{-1}) [cf. Eq.(18)].
$\overleftarrow{k}$	General dissociation constant [cf. Eq.(19)].
k_M	General bimolecular association rate constant (ℓ $mole^{-1}$ sec^{-1}) [cf. Eq.(20a)].
k_{eff}	Bimolecular association rate constant (ℓ $mole^{-1}$ sec^{-1}) in diffusion-control region ($Q > 1$)[cf. Eq.(20b)].
k_D	Diffusion-controlled rate constant ($k_a' \to \infty$) with both polar and azimuthal constraints [cf. Eq.(75)].
k_{diff}	Diffusion-controlled rate constant for uniformly reactive spheres [cf. Eq.(22)].
k_{θ_0}	Diffusion-controlled rate constant for a reaction with an angular constraint but the spheres cannot rotate [cf. Eq.(52)].
$k(\theta_0,\phi_0)$	Diffusion-controlled rate constant for a system with both polar and azimuthal angular constraints [cf. Eq.(53)].
k_2	Diffusion-controlled rate constant of Wetmur and Davidson [cf. Eq.(50)].
k_N	Renaturation rate constant for DNA of Wetmur and Davidson [cf. Eq.(70)].
$k(t)$	Time-dependent bimolecular association rate constant of Solc and Stockmayer [cf. Eq.(80)].

REFERENCES

1. M.V. Smoluchowski, J. Phys. Chem., 92, 129 (1917).
2. P. Debye, Trans. Electrochem. Soc., 82, 265 (1942).
3. F. C. Collins and G. E. Kimball, J. Colloid Sci., 4, 425 (1949).
4. R. M. Noyes, in Progress in Reaction Kinetics, 1, 131 (1961).
5. J. M. Schurr, Biophys. J., 10, 700 (1970).
6. M. Eigen and G. G. Hammes, in Adv. in Enzymology, 25, 1 (1963).
7. H. Theorell and A. Nygaard, Acta Chem. Scand. 8, 1649 (1954).
8. R. W. Farwell and E. Ackermann, Biophys. J., 3, 479 (1963).
9. L. Peller and R. A. Alberty, J. Am. Chem. Soc., 81, 5907 (1959).
10. (a) V. Bloomfield, L. Peller and R. A. Alberty, J. Am. Chem. Soc., 84, 4375 (1962); (b) H. Theorell and J. S. M. McKee, Acta Chem. Scand., 15, 1797, 1811, 1834 (1961).
11. J. G. Wetmur and N. Davidson, J. Mol. Biol., 31, 349 (1968).
12. A. Einstein, Investigations on the Theory of Brownian Movement, p. 17, Dover Publications (1956).
13. P. Debye, Polar Molecules, p. 85, Dover Publications (1929).
14. J. M. Schurr, Biophys. J., 10, 717 (1970).
15. J. C. Wang and N. Davidson, J. Mol. Biol., 19, 469 (1966).
16. K. Solc and W. H. Stockmayer, J. Chem. Phys., 54, 2981 (1971).
17. M. Sanders and P. D. Ross, Biochem. Biophys. Res. Comm., 3, 314 (1960).

PART III

Dynamic Light Scattering

from Solutions of Calf Thymus DNA

"It drew now to evening by the hour, and the light was so dim that even far-sighted men upon the Citadel could discern little clearly upon the fields, save only the burnings that ever multiplied, and the lines of fire that grew in length and speed. At last, less than a mile from the City, a more ordered mass of men came into view, marching not running, still holding together."

from The Lord of the Rings, Part III, by J.R.R. Tolkien

I. Introduction

It has been known for many years that fluctuations in the polarizability of dense media give rise to scattered light.[1-4] Since the advent of continuous gas lasers, the theoretical foundation for dynamic light scattering from macromolecules in solution has been rapidly developing. A theory of spectral broadening of light scattered from dynamic fluctuations of macromolecules by translational diffusion was developed[5] and subsequently the phenomenon was experimentally observed.[6-8] A theory for dynamic light scattering associated with the decay of concentration fluctuations of species by rapid chemical reaction was recently developed[9-11] and has already been realized in ionic[12] and helix-coil reactions.[13] The decay of fluctuations in polarization by rotational diffusion of optically anisotropic molecules has been investigated theoretically[14] and experimentally observed in solutions of tobacco mosaic virus[15] and lysozyme.[16] The prediction of simultaneous contributions of rotational and translational diffusion of rigid rods whose length is comparable to that of the incident radiation[17] has been experimentally verified.[18]

Conventional methods for studying relaxation processes involve the technique of imposing a sudden change of condition on the equilibrium system. The change must be large enough so that one can monitor some observable quantity, such as the optical absorbance. It is conceivable that in some cases the size of the applied perturbation may exceed the limits of validity for application of a linear response theory. In contrast, light scattering techniques probe the temporal decay of the much smaller spontaneous fluctuations of the equilibrium parameters.

Until recently, both the theoretical formulation and experimental analysis have been carried out in the frequency domain. In the present study, a theoretical formulation for the autocorrelation function of the phototube current due to the scattered light is developed in Section III. The general formulation is applied to the special cases of translational diffusion of polymers and rotational diffusion of optically anisotropic particles. The case when two types of particles are present, one being much larger than the other, is also discussed. The experimental appartus is described in detail in Section IV and the stepwise alignment procedure is presented in Section V. Section VI is devoted to the preparation and characterization of the calf thymus DNA used in this study.

Figure 1

The incident radiation $\underset{\sim}{E}_{in}(\underset{\sim}{r},t)$ is scattered from the point $\underset{\sim}{r}$ and detected at point $\underset{\sim}{R}$. The dashed lines represent to total illuminated volume, with the origin of the laboratory reference frame located at its center.

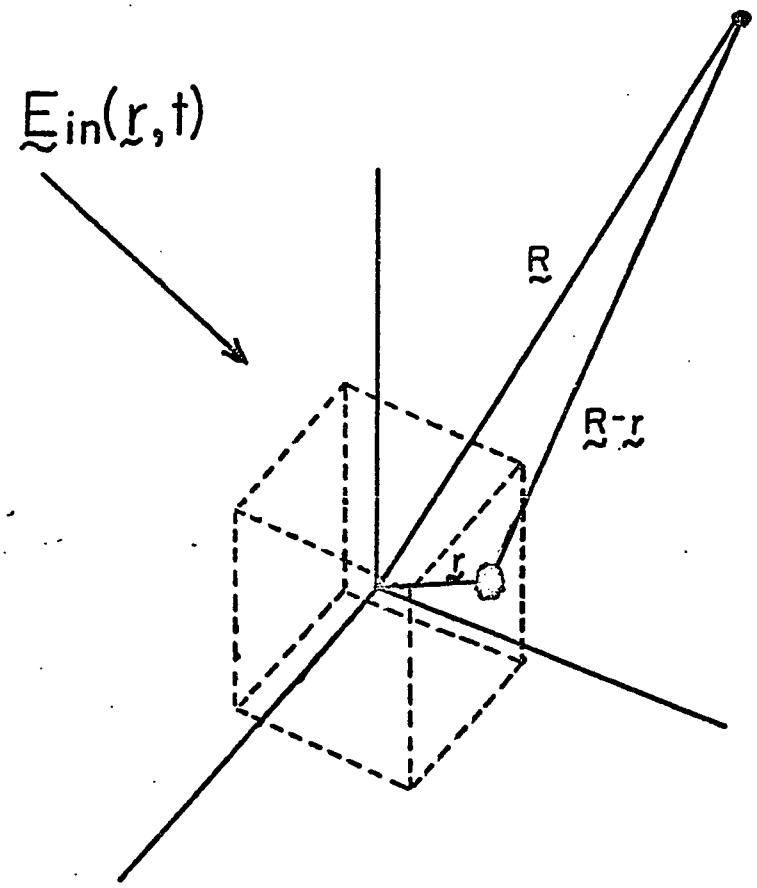
$\underset{\sim}{E}_{in}(\underset{\sim}{r},t)$
$\underset{\sim}{R}$
$\underset{\sim}{R}-\underset{\sim}{r}$
$\underset{\sim}{r}$

II. The Scattered Field

It is assumed that the total scattered electric field which is detected at some point in space arises entirely from a small portion of a total solution. This illuminated region is assumed to be small enough so that the intensity of the incident radiation is effectively constant at any particular instant in time but large enough to consider the medium as a classical continuum. It is further assumed that the scattered region is a rectangular parallelopiped of dimensions L_x, L_y, L_z. The position of any point in space is measured with respect to a set of coordinate axes that are parallel to the edges of the parallelopiped and whose origin is located at the center of the parallelopiped (cf., Figure 1). This particular set of coordinates axes is referred to as the laboratory reference frame.

The incident electric field $\underset{\sim}{E}_{in}(\underset{\sim}{r},t')$ at time t' at a point $\underset{\sim}{r}$ within the scattering region induces a polarization $\underset{\sim}{P}(\underset{\sim}{r},t')$ according to the equation

$$\underset{\sim}{P}(\underset{\sim}{r},t') = \underset{\sim}{\alpha}(\underset{\sim}{r},t') \; \underset{\sim}{E}_{in}(\underset{\sim}{r},t') \quad , \tag{1}$$

where $\underset{\sim}{\alpha}(\underset{\sim}{r},t')$ is the instantaneous polarizability tensor at $\underset{\sim}{r}$. The incident electric field drives the induced polarization which then generates the scattered field. If the point of observation $\underset{\sim}{R}$ in the medium is in the radiation zone (i.e., $\underset{\sim}{R}-\underset{\sim}{r} \cong \underset{\sim}{R}$), then the field $d\underset{\sim}{E}_s(\underset{\sim}{R},\omega)$ radiated by induced oscillations in the polarization in the volume element $d^3\underset{\sim}{r}$ and with frequency ω is given by the expression[19]

$$d\underset{\sim}{E}_s(\underset{\sim}{R},\omega) = -\left(\frac{\omega}{C_m}\right)^2 \frac{\underset{\sim}{R}x\underset{\sim}{R}x\underset{\sim}{P}(\underset{\sim}{r},\omega)\exp[i\omega\, \underset{\sim}{R}-\underset{\sim}{r}\, /C_m]d^3\underset{\sim}{r}}{|\underset{\sim}{R}|^3} \quad , \tag{2}$$

where C_m is the speed of light in the medium. It is assumed that the medium extends out to the detector to avoid any ambiguity regarding the index of refraction appropriate to the wave vector of the scattered field. The light intensity, or the Poynting vector, at the detector does not depend upon the location of the boundary between the sample and the air, except for a small time delay, so long as the scattered beam traverses the boundary at normal incidence. This ambiguity does not arise if the pertubation solution of Maxwell's equations inside the sample is employed.[5]

Our main concern, however, is with the time dependence of the scattered field. We define the symmetrical time Fourier transform of the scattered field by

$$d\underset{\sim}{E}_s(\underset{\sim}{R},t) \equiv \frac{1}{(2\pi)^{\frac{1}{2}}} \int_{-\infty}^{+\infty} \exp(-i\omega t)\, d\underset{\sim}{E}_s(\underset{\sim}{R},\omega)\, d\omega \quad . \tag{3}$$

If we write the incident field with frequency ω_o as

$$\underset{\sim}{E}_{in}(\underset{\sim}{r},t') = \underset{\sim}{E}^o_{in}(\underset{\sim}{r})\exp(-i\omega_o t') \quad , \tag{4}$$

and substitute this expression into Eq.(1) and then take the inverse Fourier transform, we arrive at the expression

$$\underset{\sim}{P}(\underset{\sim}{r},\omega) = \underset{\sim}{E}^o_{in}(\underset{\sim}{r})\alpha(\underset{\sim}{r},\omega-\omega_o) \quad , \tag{5}$$

in which it is assumed that the medium is isotropic, and where we have defined

$$\alpha(\underset{\sim}{r},\omega-\omega_o) \equiv \frac{1}{(2\pi)^{\frac{1}{2}}} \int_{-\infty}^{+\infty} \exp[i(\omega-\omega_o)t']\alpha(\underset{\sim}{r},t')\, dt' \quad . \tag{6}$$

If the only significant amplitude of the Fourier transform defined in Eq.(6) occurs when $\omega \simeq \omega_o$, then the Fourier transform of Eq.(2) becomes

$$d\underset{\sim}{E}_s(\underset{\sim}{R},t) = -\left(\frac{\omega_o}{C_m}\right)^2 \frac{\underset{\sim}{R}x\underset{\sim}{R}x}{(2\pi)^{\frac{1}{2}}|\underset{\sim}{R}|^3}$$

$$\left[\int_{-\infty}^{+\infty} \exp(-i\omega t)\underset{\sim}{P}(\underset{\sim}{r},\omega)\exp(i|\underset{\sim}{R}-\underset{\sim}{r}|\omega/C_m)\,d\omega\right] d^3\underset{\sim}{r} \quad . \tag{7}$$

We now substitute Eq.(6) into Eq.(3) to obtain

$$d\underset{\sim}{E}_s(\underset{\sim}{R},t) = -\left(\frac{\omega_o}{C_m}\right)^2 \frac{\underset{\sim}{R}x\underset{\sim}{R}x\underset{\sim}{E}^o_{in}(\underset{\sim}{r})d^3\underset{\sim}{r}}{|\underset{\sim}{R}|^3(2\pi)^{\frac{1}{2}}}$$

$$\int_{-\infty}^{+\infty} \exp(-i\omega t)\exp(+i|\underset{\sim}{R}-\underset{\sim}{r}|\omega/C_m)\alpha(\underset{\sim}{r},\omega-\omega_o)\,d\omega \quad . \tag{8}$$

Factoring the quantity $\exp[i\omega_o(|\underset{\sim}{R}-\underset{\sim}{r}|/C_m - t)]$ from the integral in Eq.(8), we arrive at the expression

$$d\underset{\sim}{E}_s(\underset{\sim}{R},t) = -\left(\frac{\omega_o}{C_m}\right)^2 \frac{\underset{\sim}{R}x\underset{\sim}{R}x\underset{\sim}{E}^o_{in}(\underset{\sim}{r})d^3\underset{\sim}{r}}{|\underset{\sim}{R}|^3}$$

$$\exp[+i\omega_o(|\underset{\sim}{R}-\underset{\sim}{r}|/C_m - t)]\alpha(\underset{\sim}{r},t-|\underset{\sim}{R}-\underset{\sim}{r}|/C_m) \quad , \tag{9}$$

where

$$\alpha(\underset{\sim}{r},t-|\underset{\sim}{R}-\underset{\sim}{r}|/C_m) = \frac{1}{(2\pi)^{\frac{1}{2}}}\int_{-\infty}^{+\infty} \alpha(\underset{\sim}{r},\omega-\omega_o)\exp[-i(\omega-\omega_o)(t-|\underset{\sim}{R}-\underset{\sim}{r}|/C_m)]\,d\omega \quad . \tag{10}$$

It is clear that the quantity defined by Eq.(10) is the polarizability at the point $\underset{\sim}{r}$ at the time of scattering, i.e., $t' = t-|\underset{\sim}{R}-\underset{\sim}{r}|/C_m$. The total scattered field in this approximation is simply obtained by integrating Eq.(9) over the scattering volume,

$$\underset{\sim}{E}_s(\underset{\sim}{R},t) = -\left(\frac{\omega_o}{C_m}\right)^2 \frac{\underset{\sim}{R}x\underset{\sim}{R}x}{|\underset{\sim}{R}|^3}$$

$$\int_V \underset{\sim}{E}^o_{in}(\underset{\sim}{r})\exp[i\omega_o(|\underset{\sim}{R}-\underset{\sim}{r}|/C_m - t)]\alpha(\underset{\sim}{r},t-|\underset{\sim}{R}-\underset{\sim}{r}|/C_m)\,d^3\underset{\sim}{r} \quad . \tag{11}$$

We now write the cross products in Eq.(11) as

$$\frac{\underset{\sim}{R}x\underset{\sim}{R}x\underset{\sim}{E}^{o}_{in}(\underset{\sim}{r})}{|R|^3} = \frac{\underset{\sim}{n}}{|\underset{\sim}{R}|}\sin\phi|\underset{\sim}{E}_{in}|\exp(i\underset{\sim}{k}_o\cdot\underset{\sim}{r}) \quad , \tag{12}$$

and define $\underset{\sim}{k}_s$ by

$$\frac{\omega_o}{C_m}|\underset{\sim}{R}-\underset{\sim}{r}| = \underset{\sim}{k}_s\cdot(\underset{\sim}{R}-\underset{\sim}{r}) \quad , \tag{13}$$

where $\underset{\sim}{n}$ is the unit vector lying in the plane of $\underset{\sim}{E}_{in}(\underset{\sim}{r},t')$ and $\underset{\sim}{R}$ and perpendicular to $\underset{\sim}{R}$, $\underset{\sim}{k}_s$ and $\underset{\sim}{k}_o$ are the wave vectors of the Rayleigh scattered and incident fields, respectively, and ϕ is the angle between $\underset{\sim}{R}$ and $\underset{\sim}{E}_{in}$. Substitution of Eqs.(13) and (13) into Eq.(11) and subsequent rearrangement leads to the expression

$$\underset{\sim}{E}_s(\underset{\sim}{R},t) = -\underset{\sim}{n}\left(\frac{\omega_o}{C_m}\right)^2\frac{\sin\phi|E_{in}|\exp(i\underset{\sim}{k}_s\cdot\underset{\sim}{R})\exp(-i\omega_o t)}{|\underset{\sim}{R}|}\alpha(\underset{\sim}{K},t-|\underset{\sim}{R}-\underset{\sim}{r}|/C_m) \quad , \tag{14}$$

where the scattering vector $\underset{\sim}{K}$ is defined by

$$\underset{\sim}{K} \equiv \underset{\sim}{k}_s - \underset{\sim}{k}_o \quad , \tag{15}$$

and the inverse space Fourier transform of the polarizability is recognized as

$$\alpha(\underset{\sim}{K},t-|\underset{\sim}{R}-\underset{\sim}{r}|/C_m) = \int_V d^3\underset{\sim}{r}\exp(-i\underset{\sim}{K}\cdot\underset{\sim}{r})\alpha(\underset{\sim}{r},t-|\underset{\sim}{R}-\underset{\sim}{r}|/C_m) \quad . \tag{16}$$

Since the integration in Eq.(16) is over a finite volume of solution, the space Fourier transform is a sum over the allowed wave vectors $\underset{\sim}{K}'$

$$\alpha(\underset{\sim}{r},t-|\underset{\sim}{R}-\underset{\sim}{r}|/C_m) = \frac{1}{V}\sum_{\underset{\sim}{K}'}\alpha(\underset{\sim}{K}',t-|\underset{\sim}{R}-\underset{\sim}{r}|/C_m)\exp(+i\underset{\sim}{K}'\cdot\underset{\sim}{r}), \tag{17}$$

where the components of $\underset{\sim}{K}'$ are $k'_x = 2\pi n'_x/L_x$, etc., and V is the scattering volume.

If the polarizability can be written as the sum of a space average part $\langle\alpha\rangle$ and a fluctuating part $\delta\alpha(\underset{\sim}{r},t-|\underset{\sim}{R}-\underset{\sim}{r}|/C_m)$, then Eq.(16) can be written as

$$\alpha(\underset{\sim}{K},t-|\underset{\sim}{R}-\underset{\sim}{r}|/C_m) = \langle\alpha\rangle\int_V d^3\underset{\sim}{r}\exp(-i\underset{\sim}{K}\cdot\underset{\sim}{r})+\int_V d^3\underset{\sim}{r}\delta\alpha(\underset{\sim}{r},t-|\underset{\sim}{R}-\underset{\sim}{r}|/C_m)\exp(-i\underset{\sim}{K}\cdot\underset{\sim}{r}). \quad (18)$$

It is clear from Eq.(18) that the space average part does not contribute to the scattered light (except at $\underset{\sim}{K} = 0$) and that only fluctuations in the polarizability with wave vector $\underset{\sim}{K}$ as defined in Eq.(15) contribute to the scattered field at $\underset{\sim}{R}$.

In addition to the preceeding assumptions about the scattering region, it is assumed that the fluctuations in the polarizability, or index of refraction, arise primarily from the fluctuations in the concentration, orientation, and configuration of dissolved macromolecules in dilute solution. It is also assumed that the intensity of scattered light is sufficiently large that the scattered electric field at the detector is a well-behaved classical quantity and that quantum statistics are unimportant. Finally, it is assumed that only a small fraction of the incident field is scattered on a single passage through the sample, so that multiple scattering may be neglected.

III. The Autocorrelation Function

In the experiment described here, the scattered light at a point $\underset{\sim}{R}$ is detected by a phototube. The intensity of light at this point at time t is

$$I(\underset{\sim}{R},t) = \frac{C_m}{4\pi}|E(\underset{\sim}{R},t)|^2 = \frac{C_m}{4\pi} F_o[\alpha^*(\underset{\sim}{K},t')\alpha(\underset{\sim}{K},t')] \quad , \tag{19}$$

where

$$F_o = \frac{|E_{in}|^2 \sin^2\phi}{|\underset{\sim}{R}|^2}\left(\frac{\omega_o}{C_m}\right)^4 \quad , \tag{20}$$

and t' is the time when light was scattered from the sample. Since the instantaneous phototube current J(t) is proportional to the intensity of the scattered field at the detector, one may write

$$J(t) = A\alpha^*(\underset{\sim}{K},t')\alpha(\underset{\sim}{K},t') \quad . \tag{21}$$

The a.c. component of the phototube current (see below) is then relayed to a capacitor in an analog channel of a PDP-12 laboratory computer. The digitized voltage over 25 microsecond intervals is then stored on tape and the autocorrelation function of the phototube current. (See Section VII for details of computation.) The autocorrelation function of the phototube current is, in general,

$$\langle J(t)J(t+\tau)\rangle_t = A^2\langle\alpha^*(\underset{\sim}{K},t)\alpha(\underset{\sim}{K},t)\alpha^*(\underset{\sim}{K},t+\tau)\alpha(\underset{\sim}{K},t+\tau)\rangle_t \quad . \tag{22}$$

It is not possible to determine the components of the autocorrelation function from the present form of Eq.(22). In order to obtain this information, we write the polarizability of the scattering region as

$$\alpha(\underset{\sim}{r},t) = \alpha \sum_{i=1}^{N} \delta[\underset{\sim}{r}-\underset{\sim}{r}_i(t)] \quad , \tag{23}$$

where we have assumed that there are N independent infinitesimal scattering centers within the scattering region. The Fourier transform of Eq.(28) gives [cf., Eq.(16)]

$$\alpha(\underset{\sim}{K},t) = \alpha \sum_{i=1}^{N} \exp[-i\underset{\sim}{K}\cdot\underset{\sim}{r}_i(t)] \quad . \tag{24}$$

Substitution of Eq.(24) into Eq.(22) and equating the time average to the ensemble average leads to the result

$$\langle J(o)J(\tau)\rangle_t = A^2\alpha^4 \sum_i \sum_j \sum_k \sum_\ell \langle \exp(i\underset{\sim}{K}\cdot[r_i(o)-r_j(o)+r_k(\tau)-r_\ell(\tau)])\rangle_{ens} . \tag{25}$$

Since the term in the brackets in Eq.(25) is an ensemble average, the terms with subscripts occurring an odd number of times vanish. Similarly, the terms with i=k≠j=1 also vanish. There remain N terms of unity when i=j=k=1, N(N-1) terms of unity when i=j≠k=1, and N(N-1) terms when i=1≠j=k. The autocorrelation function of the phototube current for a system of N independent scattering centers is

$$\langle J(o)J(\tau)\rangle_t = A^2\alpha^4 \left(N^2 + \sum_{i\neq j} \sum \langle \exp(i\underset{\sim}{K}\cdot[r_i(o)-r_i(\tau)+r_j(\tau)-r_j(o)])\rangle_{ens} \right) . \tag{26}$$

In general, the autocorrelation function for the phototube current has a time-independent (d.c.) component and a time-dependent (a.c.) component.

THE PHOTOTUBE AUTOCORRELATION FUNCTION DUE TO TRANSLATIONAL DIFFUSION OF POLYMERS

Let us assume that each of the N polymers in solution have μ scattering centers of polarizability α_o. The polarizability of the scattering region can then be written as

$$\alpha(\underset{\sim}{r},t) \equiv \alpha_o \sum_{r=1}^{N} \sum_{\beta=1}^{\mu} \delta[\underset{\sim}{r}-\underset{\sim}{R}_I(t)-\underset{\sim}{r}_I^{\beta}(t)] \quad , \tag{27}$$

where $\underset{\sim}{R}_I(t)$ is the position of the center of mass of the I^{th} polymer measured from the origin of the laboratory reference frame and $\underset{\sim}{r}_I^{\beta}(t)$ is the position of the β^{th} scattering center on the I^{th} polymer measured in the molecular-fixed coordinates of the I^{th} polymer. The autocorrelation function for the phototube current is

$$\left\langle J(o)J(\tau)\right\rangle = A^2\alpha^o \sum_{I=1}^{N}\sum_{J=1}^{N}\sum_{K=1}^{N}\sum_{L=1}^{N}\sum_{\beta=1}^{\mu}\sum_{\gamma=1}^{\mu}\sum_{\delta=1}^{\mu}\sum_{\zeta=1}^{\mu}$$

$$\left\langle \exp[i\underset{\sim}{K}\cdot(\underset{\sim}{R}_I(o)+\underset{\sim}{r}_I^{\beta}(o)-\underset{\sim}{R}_J(o)-\underset{\sim}{r}_J^{\gamma}(o)+\underset{\sim}{R}_K(\tau)+\underset{\sim}{r}_K^{\delta}(\tau)-\underset{\sim}{R}_L(\tau)-\underset{\sim}{r}_L^{\zeta}(\tau))]\right\rangle \quad , \tag{28}$$

where the angular brackets denote the ensemble average.

On defining the quantity

$$B_j(t) \equiv \sum_{\varepsilon=1}^{\mu} \exp[i\underset{\sim}{K}\cdot\underset{\sim}{r}_j^{\varepsilon}(t)] \quad , \tag{29}$$

where j = I,J,K, or L, we can rewrite Eq.(28) in the simpler form

$$\left\langle J(o)J(\tau)\right\rangle = A^2\alpha^4 \sum_{I}\sum_{J}\sum_{K}\sum_{L}$$

$$\left\langle \exp(iK\cdot[R_I(o)-R_J(o)+R_K(\tau)-R_L(\tau)])B_I(o)B_J^{*}(o)B_K(\tau)B_L^{*}(\tau)\right\rangle . \tag{30}$$

If the internal motions of the polymers are independent of the motion of the center of mass, then the average of products in Eq.(30) can be written as the product of averages,

$$\langle J(o)J(\tau)\rangle = A^2\alpha^4 \sum_I \sum_J \sum_K \sum_L$$

$$\left\langle \exp(i\underset{\sim}{K}\cdot[\underset{\sim}{R}_I(o)-\underset{\sim}{R}_J(o)+\underset{\sim}{R}_K(\tau)-\underset{\sim}{R}_L(\tau)])\right\rangle \langle B_I(o)B_J^*(o)B_K(\tau)B_L^*(\tau)\rangle \quad . \tag{31}$$

In view of the discussion in the preceeding section, the only nonzero contributions to Eq.(31) come from the terms I=J=K=L, I=J≠K=L, and I=L≠J=K.

When I=J≠K=L for a system of independent molecules, we have the identities

$$\langle B_I(o)B_J^*(o)B_K(\tau)B_L^*(\tau)\rangle = \langle B_I(o)B_I^*(o)\rangle\langle B_K(\tau)B_K^*(\tau)\rangle = \langle B(o)B^*(o)\rangle^2. \tag{32}$$

The quantity $P(\underset{\sim}{K})$, defined as

$$P(\underset{\sim}{K}) = \frac{1}{\mu^2}\langle B(o)B^*(o)\rangle \quad , \tag{33}$$

is the usual interference factor due to the internal structure of the polymer. Since there are N(N-1) terms of this type, the total contribution to the d.c. component of the autocorrelation function of the phototube current is

$$\langle J(o)J(\tau)\rangle_{d.c.} = A^2N(N-1)\alpha_o^4\mu^4P^2(\underset{\sim}{K}) \quad (I=J\neq K=L). \tag{34}$$

When I=J=K=L we have the time-dependent "self" term contributions due to the internal motions of the polymer,

$$D^{int}(\underset{\sim}{K},\tau) = \sum_{I=1}^{N}\sum_{\beta=1}^{\mu}\sum_{\gamma=1}^{\mu}\sum_{\delta=1}^{\mu}\sum_{\zeta=1}^{\mu}\left\langle \exp(i\underset{\sim}{K}\cdot[\underset{\sim}{r}_I^{\beta}(o)-\underset{\sim}{r}_I^{\gamma}(\tau)-\underset{\sim}{r}_I^{\delta}(o)+\underset{\sim}{r}_I^{\zeta}(\tau)])\right\rangle . \tag{35}$$

Since the molecules are assumed to be independent, $D^{int}(\underset{\sim}{K},\tau)$ is proportional to the number of polymers N.

When I=L≠K=J we have the time-dependent term which depends on both the motion of the center of mass and the internal motions of the polymer,

$$\langle J(o)J(\tau)\rangle\,(I=L\neq K=J) = \sum_{I}\sum_{J}$$

$$\left\langle \exp(i\underset{\sim}{K}\cdot[\underset{\sim}{R}_I(0)-\underset{\sim}{R}_T(\tau)]\exp[i\underset{\sim}{K}\cdot(\underset{\sim}{R}_J(\tau)-\underset{\sim}{R}_J(0)]\right\rangle \left\langle B_I(0)B_I^*(\tau)B_J^*(0)B_J(\tau)\right\rangle \quad . \tag{36}$$

Since the molecules are independent and their internal and external motions are uncorrelated, we can write Eq.(36) as the product of averages,

$$\langle J(o)J(\tau)\rangle\,(I=L\neq K=J) = [C^{ext}(\underset{\sim}{K},\tau)]^*C^{ext}(\underset{\sim}{K},\tau)[C^{int}(\underset{\sim}{K},\tau)]^*C^{int}(\underset{\sim}{K},\tau), \tag{37}$$

where the correlation functions for the center of mass $C^{ext}(\underset{\sim}{K},\tau)$ and the internal motions $C^{int}(\underset{\sim}{K},\tau)$ are defined, respectively,

$$C^{ext}(\underset{\sim}{K},\tau) \equiv \sum_{I=1}^{N}\left\langle \exp(i\underset{\sim}{K}\cdot[\underset{\sim}{R}_I(o)-\underset{\sim}{R}_I(\tau)])\right\rangle \quad , \tag{38}$$

and

$$C^{int}(\underset{\sim}{K},\tau) \equiv \left\langle B^*(o)B(\tau)\right\rangle \quad . \tag{39}$$

The complete expression for the autocorrelation function of the phototube current due to translational and internal motions of polymers in dilute solution is

$$\langle J(o)J(\tau)\rangle = A^2\alpha_o^4\{\mu^4N(N-1)P^2(\underset{\sim}{K})+[C^{ext}(\underset{\sim}{K},\tau)C^{int}(\underset{\sim}{K},\tau)]^2+D^{int}(\underset{\sim}{K},\tau)\}. \tag{40}$$

In order to evaluate $C^{ext}(\underset{\sim}{K},\tau)$, we assume that the concentration of polymers at the point $\underset{\sim}{r}$ at time t is described by the distribution function

$c(\underset{\sim}{r},t)$ which satisfies the diffusion equation,

$$\frac{\partial c(\underset{\sim}{r},t)}{\partial t} = D\nabla^2 c(\underset{\sim}{r},t) \quad , \tag{41}$$

where D is the translational diffusion coefficient and ∇^2 is the spatial Laplacian operator. The autocorrelation function then involves an integration over the volume element at the two different times,

$$C^{ext}(\underset{\sim}{K},\tau) = \left\langle \int_V \int_V \exp[-i\underset{\sim}{K}\cdot(\underset{\sim}{r}-\underset{\sim}{r}')]c(\underset{\sim}{r},o)c(\underset{\sim}{r}',\tau)d^3\underset{\sim}{r}d^3\underset{\sim}{r}' \right\rangle . \tag{42}$$

The double integral in Eq.(42) is recognized as the spatial Fourier transform as defined in Eq.(16) at the two different times. The inverse space Fourier transform,

$$c(\underset{\sim}{r},t) = \frac{1}{V}\sum_{K'} c(\underset{\sim}{K}',t)\exp(i\underset{\sim}{K}'\cdot\underset{\sim}{r}) \quad , \tag{43}$$

is inserted into Eq.(41) and yields the expressions,

$$\sum_{\underset{\sim}{K}'} \frac{\partial c(\underset{\sim}{K}',t)}{\partial t} = \sum_{\underset{\sim}{K}'} -DK'^2 c(\underset{\sim}{K}',t) \quad , \tag{44}$$

and

$$C^{ext}(\underset{\sim}{K},\tau) = \left\langle c^*(\underset{\sim}{K},o)c(\underset{\sim}{K},o)\right\rangle \exp(-K^2D\tau) \quad , \tag{45}$$

where we have used the solution to Eq.(44)

$$c(\underset{\sim}{K},t) = c(\underset{\sim}{K},o)\exp(-K^2Dt) \quad , \tag{46}$$

in Eq.(45).

The task now remains to find an expression for $\left\langle c(\underset{\sim}{K},o)^* c(\underset{\sim}{K},o)\right\rangle$ in terms of known quantities of the system. Since Eq.(15) can be interpreted either as a Bragg reflection or a conservation of momentum equation, the

magnitude of the scattering vector $\underset{\sim}{K}$ is simply (cf., Figure 2)

$$|\underset{\sim}{K}| = 2|\underset{\sim}{k}_o|\sin(\theta/2) \quad , \tag{47}$$

where θ is the scattering angle. Since the uniform distribution of scattering centers does not contribute to the scattered field except at $\underset{\sim}{K}=0$, the quantity $\langle c(\underset{\sim}{K},0)^* c(\underset{\sim}{K},0)\rangle$ is simply a measure of the probability of a flucuation occurring with the wave vector $\underset{\sim}{K}$. We assume that the time average and the ensemble average of this amplitude are equivalent,

$$\langle c(\underset{\sim}{K},0)^* c(\underset{\sim}{K},0)\rangle_t = \langle c(\underset{\sim}{K},0)^* c(\underset{\sim}{K},0)\rangle_{ens} \quad . \tag{48}$$

In order to average over all possible initial conditions at constant temperature and pressure, it is assumed that the probability of observing any particular fluctuation state of the system relative to the uniform, or equilibrium, state is

$$\frac{P[\delta c(\underset{\sim}{r},0)]}{P(c_o)} = G\exp\frac{-\Delta F[\delta c(\underset{\sim}{r},0)]}{kT} \quad , \tag{49}$$

where G is a proportionality constant and $\Delta F[\delta c(\underset{\sim}{r},0)]$ is the Gibbs free energy change associated with the fluctuation. For a system of non-interacting particles, the exponential argument simply becomes $\Delta S[\delta c(\underset{\sim}{r},0)]/k$, where $\Delta S[\delta c(\underset{\sim}{r},0)]$ is the entropy change associated with the fluctuations. To proceed, we first divide the total volume of solution into smaller volumes ΔV. The concentration c_i in cell i can then be expressed as

$$c_i = (n_i^o + \delta n_i)/\Delta V \quad , \tag{50}$$

where $n_i^o = N/M$ is the number of particles in the uniform distribution of the system of N particles and M cells. The probability of observing the most probable distribution is proportional to the number of ways

Figure 2

Relationship between the incident wave vector $\underset{\sim}{k}_o$, scattered wave vector $\underset{\sim}{k}_s$, and the scattering vector $\underset{\sim}{K}$ of the fluctuation.

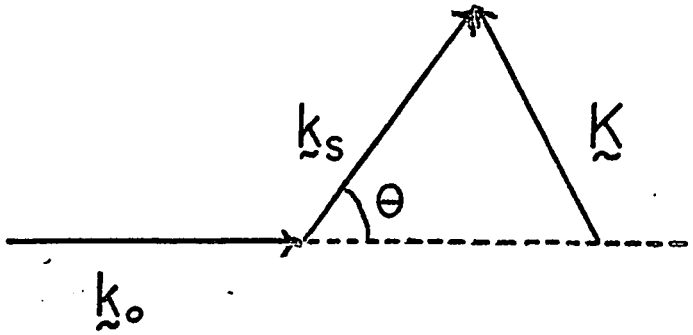

$$|\underset{\sim}{k}_s| = |\underset{\sim}{k}_o|$$

$$\frac{|\underset{\sim}{K}|}{2} = |\underset{\sim}{k}_o| \sin(\theta/2)$$

of achieving this distribution,

$$P_{most} \alpha \frac{N!}{n_1^o! n_2^o! \ldots n_\mu^o!} \Big/ W_{tot} \quad , \tag{51}$$

where W_{tot} is the total number of possible arrangements of the distribution of particles. The probability of observing any other distribution is also proportional to the number of ways of achieving that distribution,

$$P_{other} \alpha \frac{N!}{n_1! n_2! \ldots n_\mu!} \Big/ W_{tot} \quad , \tag{52}$$

which leads to the relative probability

$$P_R = \frac{n_1^o! n_2^o! n_3^o! \ldots n_\mu^o!}{n_1! n_2! n_3! \ldots n_\mu!} \quad . \tag{53}$$

We now use Stirling's approximation in taking the logarithm of P_R and retain only the first two terms of the logarithmic expansion of $\ln(1+\delta n_i/n_i^o)$ to obtain

$$\ell n P_R = \sum_i \left(-\delta n_i \ell n n_i^o - \frac{(\delta n_i)^2}{2n_i^o} + \frac{1}{2} \frac{(\delta n_i)^3}{(n_i^o)^2} \right) \quad . \tag{54}$$

If the last term inside the summation can be neglected, we find that the relative probability for a fluctuation to occur is simply a Guassian,

$$P_R = \exp\left(- \frac{(\delta n_i)^2}{2n_i^o} \right) = \exp\left(- \frac{1}{2c_i^o} \sum_i \delta c_i(\underset{\sim}{r},0)^2 \Delta V \right) \quad . \tag{55}$$

If the summation over the volume elements in Eq.(55) can be replaced by an integration over the total volume, then the probability of observing a fluctuation $P[\delta c(\underset{\sim}{r},0)]$ then becomes

$$P[\delta c(\underset{\sim}{r},0)] = B\exp\left(-\frac{1}{2c_o}\int_V [\delta c(\underset{\sim}{r},0)^* \delta c(\underset{\sim}{r},0)]d^3\underset{\sim}{r}\right) \quad , \tag{56}$$

where B is the normalization constant. Substitution of the Fourier transform of $\delta c(r,0)$ [cf., Eq.(43)] into the integral leads to the expansion

$$\int_V [\delta c(\underset{\sim}{r},0)]^2 d^3\underset{\sim}{r} =$$

$$\frac{1}{V^2}\int_V d^3\underset{\sim}{r}\left(\sum_{\underset{\sim}{K}}\sum_{\underset{\sim}{K}'} c^*(\underset{\sim}{K},0)\delta c(\underset{\sim}{K}',0)\exp[-i(\underset{\sim}{K}-\underset{\sim}{K}')\cdot r]\right) = \frac{1}{V}\sum_{\underset{\sim}{K}} |c(\underset{\sim}{K},0)|^2. \tag{57}$$

Therefore, the probability of observing a particular amplitude in the $\underset{\sim}{K}$ modes is

$$P[\delta c(\underset{\sim}{K}_1,0),\delta c(\underset{\sim}{K}_2,0),\delta c(\underset{\sim}{K}_3,0),\ldots\delta c(\underset{\sim}{K}_\infty,0)] \;\alpha\; \exp\left(-\frac{1}{2Vc_o}\sum_{\underset{\sim}{K}} |\delta c(\underset{\sim}{K},0)|^2\right) . \tag{58}$$

Since each $\underset{\sim}{K}$ mode has a Gaussian probability which is independent of the other $\underset{\sim}{K}$ modes, we finally arrive at the desired expressions

$$\left\langle c^*(\underset{\sim}{K},0)c(\underset{\sim}{K},0)\right\rangle = Vc_o \quad , \tag{59}$$

and

$$C^{ext}(\underset{\sim}{K},\tau) = Vc_o\exp(-K^2D\tau) \quad . \tag{60}$$

THE AUTOCORRELATION FUNCTION FOR ROTATIONAL DIFFUSION OF OPTICALLY ANISOTROPIC POLYMERS

Assume that the parallelopiped described in Section II is oriented in such a way that the incident beam propagates along the y-axis with a polarization along the z-axis. We define this set of coordinate axes as the laboratory reference frame. The incident electric field $\underset{\sim}{E}_{in}(\underset{\sim}{r},t)$

$$\underset{\sim}{E}_{in}(\underset{\sim}{r},t) = |E_z| \exp[i(k_y y - \omega_o t)] \quad , \tag{61}$$

where $|k_y| = 2\pi/\lambda_m$, λ_m being the wavelength of light in the medium. If the scattering region is anisotropic, then the interaction of the z-component of the polarizability with the incident driving electric field results in an x-component in the scattered field.

Every polymer is assumed to be made up of a sequence of μ scattering centers of identical length, each possessing the same excess polarizability tensor (with respect to the solvent). The polarizability tensor is assumed to be cylindrically symmetric about the long axis of the particular segment and may be expressed in dyadic form as

$$\underset{\sim}{\alpha} = \alpha_o \hat{\underset{\sim}{i}}\hat{\underset{\sim}{i}} + \alpha_o \hat{\underset{\sim}{j}}\hat{\underset{\sim}{j}} + \alpha_{||} \hat{\underset{\sim}{k}}\hat{\underset{\sim}{k}} \quad , \tag{62}$$

where the unit vector $\hat{\underset{\sim}{k}}$ lies along the directional segment axis and $\hat{\underset{\sim}{i}}$, $\hat{\underset{\sim}{j}}$ are any pair of mutually perpendicular vectors in the transverse plane. A segment with arbitrary orientation relative to the laboratory frame is illustrated in Figure 3. The induced polarizations of segment j on polymer I along the laboratory z and x axes are, respectively,

$$P_z(y_j^I,t') = [\alpha_o + (\alpha_{||} - \alpha_o)|\cos\theta(y_j^I,t')|]E_z \exp[i(k_y y - \omega_o t')] \quad , \tag{63a}$$

$$P_x(y_j^I,t') = [\alpha_o + (\alpha_{||} - \alpha_o)\cos\theta(y_j^I,t')\cos\chi(y_j^I,t')]E_z \exp[i(k_y y - \omega_o t')] , \tag{63b}$$

Figure 3

Relationship between the anisotropic polarizability vector $\alpha_{11}-\alpha_o$, the incident field E_z with the wave vector k_y, and the laboratory coordinate system. The angles θ and χ define the orientation of the anisotropic vector with respect to the z and x axes, respectively.

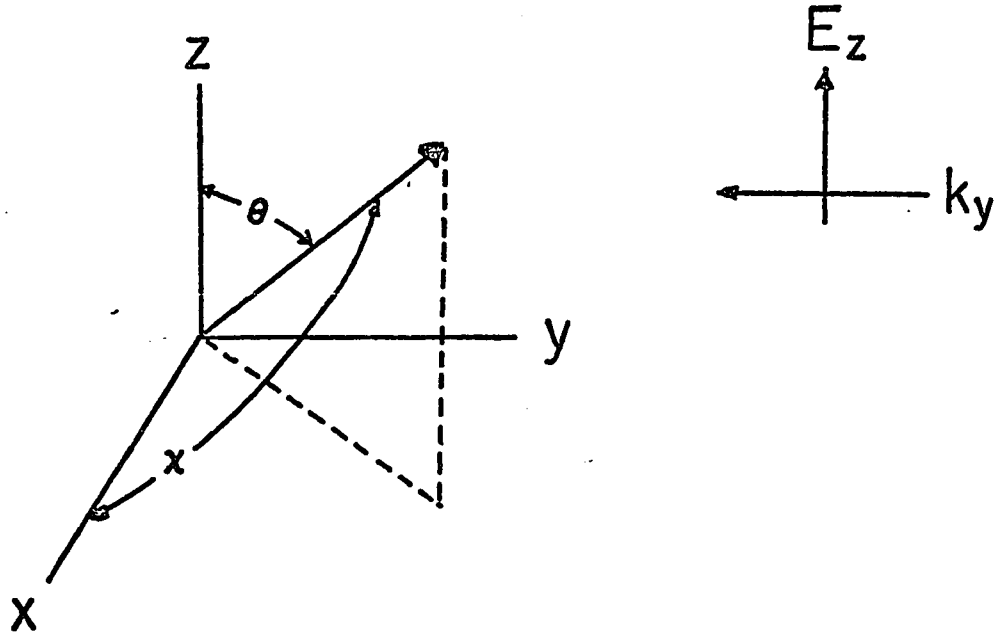
z
θ
y
x
x
E_z
k_y

where $E_z \exp([i(k_y y - \omega_o t')]$ is the instantaneous electric field associated with the light wave, and $\cos\theta(y_j^I, t')$ and $\cos\chi(y_j^I, t')$ are the projections of the directional segment axis j of polymer I on the laboratory z and x axes at time t', respectively. The depolarized component of the forward scattered light is radiated by the x-component of the induced polarization, which arises entirely from the anisotropy of the segment polarizability. The contribution of segment j of polymer I to the scattered field detected at Y at time t is simply

$$E_x(Y,t) = \frac{1}{YC_m^2} \frac{\partial^2 P_x(y_j^I, t')}{\partial t^2} \Bigg|_{t' = t - \frac{|Y - y_j^I|}{C_m}} , \qquad (64)$$

where it is assumed that the detector is in the radiation zone. According to Eq.(63b) there are two sources of time dependence in $P_x(y_j^I, t')$; (i) the projections $\cos\theta$, $\cos\chi$ vary in time, and (ii) the external driving field oscillates in time with angular frequency ω_o. When the projections $\cos\theta$, $\cos\chi$ are only weakly time-dependent in the sense that their Fourier components are significant only for values of the angular frequency that are very small compared to ω_o, then Eq.(64) becomes

$$E_x(Y,t) = \frac{\omega_o^2}{YC_m^2}(\alpha_{\shortparallel} - \alpha_o)\cos\theta(y_j^I, t')\cos\chi(y_j^I, t')E_z \exp[i(k_y Y - \omega_o t)]. \qquad (65)$$

The total scattered field is the sum of such contributions from every segment of every molecule in the scattering region. When the scattering region is small in dimension compared with the distance to the detector Y, one finds for the scattered intensity of depolarized light at the detector

$$I_x(t) = \frac{C_m}{4\pi} |E_x(Y,t)|^2$$

$$= (E_z^o)^2 \frac{\omega_o^4}{4\pi C_m^3} \frac{(\alpha_{\parallel} - \alpha_o)^2}{Y^4} \left(\sum_{I=1}^{N} \sum_{j=1}^{\mu} \cos\theta(y_j^I, t') \cos\chi(y_j^I, t') \right)^2 . \qquad (66)$$

The correlation function of interest is

$$\left\langle I_x(t) I_x(t+\tau) \right\rangle_t = \frac{E_z^{o\,4} \omega_o^8}{Y^4 16\pi^2 C_m^6} (\alpha_{\parallel} - \alpha_o)^4$$

$$\left\langle \left(\sum_J \sum_i \cos\theta(y_i^J, t') \cos\chi(y_i^J, t') \right)^2 \left(\sum_I \sum_j \cos\theta(y_j^I, t'+\tau) \cos\chi(y_j^I, t'+\tau) \right)^2 \right\rangle_t , \qquad (67)$$

where $\langle \ldots \rangle_t$ denotes a time average.

We make the usual assumption that the time average is equal to an origin-independent ensemble average, and also we assume that the rotational motions of different molecules are uncorrelated. In view of the discussion for independent particles preceeding Eq.(26), we have three contributions to the ensemble average

$$N(N-1) \left\langle g^*(\theta,\phi,o) g(\theta,\phi,o) \right\rangle^2 \quad (i=j\neq k=l) \quad , \qquad (68a)$$

$$N \left\langle \left| g^*(\theta,\phi,o) g(\theta,\phi,\tau) \right|^2 \right\rangle \quad (i=j=k=l) \quad , \qquad (68b)$$

and

$$N(N-1) \left\langle g^*(\theta,\phi,o) g(\theta,\phi,\tau) \right\rangle^2 \quad (i=l\neq j=k) \quad , \qquad (68c)$$

where we have defined

$$g(\theta,\phi,t) \equiv \int_{\theta} \int_{\phi} \delta c(\theta,\phi,t) \cos\theta \cos\chi \, d(\cos\theta) \, d\phi \quad , \qquad (69)$$

where $\delta c(\theta,\phi,t)$ is the distribution function for the orientations of the segments which gives the fraction of segments per unit solid angle with directional segment axes in the element of solid angle θ,ϕ at time t. This distribution function may be expanded in the complete set of spherical harmonics,

$$\delta c(\theta,\phi,t) = \sum_{\ell,m} b_{\ell m}(t) Y_{\ell m}(\theta,\phi) \quad . \tag{70}$$

Substitution of Eq.(70) into Eqs.(68) and subsequent substitution into E.(67) leads to the result

$$\left\langle I_x(t) I_x(t+\tau) \right\rangle = \frac{(E_z^o)^4 \omega_o^8}{Y^4 16\pi^2 C_m^6} (\alpha_{//} - \alpha_o)^4 N^2 \mu^2$$

$$\left\{ \left(\sum_{\ell,m} \sum_{p,q} I^*_{\ell m} I_{pq} \left\langle b^*_{\ell m}(0) b_{pq}(0) \right\rangle \right)^2 + \left(\sum_{\ell,m} \sum_{p,q} I^*_{\ell m} I_{pq} \left\langle b^*_{\ell m}(0) b_{pq}(\tau) \right\rangle \right)^2 \right\} \quad , \tag{71}$$

where we have retained only the quadratic terms in N and defined the integrals $I_{\ell,m}$ by

$$I_{\ell,m} = \int_\theta \int_\phi Y_{\ell,m}(\theta,\phi) \cos\theta \cos\chi \, d(\cos\theta) \, d\phi \quad . \tag{72}$$

To evaluate the integral, we use the addition theorem of Legendre polynomials to express $\cos\chi$ as

$$\cos\chi = P_1(\cos\chi) = (4\pi/3) \sum_{m'=-1}^{+1} Y^*_{1,m'}(\theta,\phi) Y_{1,m'}(\pi/2,0). \tag{73}$$

The integral now has the form

$$\int_\theta \int_\phi Y_{\ell,m}(\theta,\phi) \cos\theta \cos\chi \, d(\cos\theta) \, d\phi =$$

$$\frac{4\pi}{3} \sum_{m'=-1}^{+1} \int_\theta \int_\phi Y_{\ell,m}(\theta,\phi) Y_{1,m'}(\theta,\phi) Y_{1,m'}(\pi/2,0) \cos\theta \, d(\cos\theta) \, d\phi. \tag{74}$$

It is clear from Eq.(74) that the ϕ integration gives 2π when $m = m' = 0$, ± 1 and zero otherwise. The term $Y_{1,m'}(\pi/2,0)$ is non-zero when $m' = \pm 1$

with the result that the only non-vanishing integrals are

$$I_{2,\pm 1} = \mp\sqrt{\frac{4\pi}{30}} = I^*_{2,\pm 1} \quad . \tag{75}$$

The intensity autocorrelation function becomes finally

$$\begin{aligned}\langle I_x(t)I_x(t+\tau)\rangle &= \frac{(E_z^o)^4\omega_o^8}{Y^4 16\pi^2 C_m^6}(\alpha_{\parallel}-\alpha_o)^4N^2\mu^2\,\frac{16\pi^2}{900} \\ &\Big\{\Big(\langle|b_{2,1}(0)|^2\rangle - \mathrm{Re}\langle b^*_{2,1}(0)b_{2,-1}(0)\rangle\Big)^2 \\ &+ \Big(\langle b^*_{2,1}(0)b_{2,1}(\tau)\rangle - \mathrm{Re}\langle b^*_{2,1}(0)b_{2,-1}(\tau)\rangle\Big)^2\Big\} \quad . \end{aligned} \tag{76}$$

For a polymer whose length is very long compared to its persistence length it is expected that the crossterm $\mathrm{Re}\langle b^*_{2,1}(0)b_{2,-1}(\tau)\rangle$ is negligible compared to the direct term $\langle b^*_{2,1}(0)b_{2,1}(\tau)\rangle$. Thus, the time-varying part of the phototube current $J_{ac}(t)$ arising from the depolarized intensity has a correlation function essentially proportional to the square of the autocorrelation function for the amplitude of $Y_{2,1}(\theta,\phi)$ [or equivalently $Y_{2,-1}(\theta,\phi)$] fluctuations in the angular distribution of segments, i.e.,

$$\langle J_{ac}(t)J_{ac}(t+\tau)\rangle \cong G\langle b^*_{2,1}(0)b_{2,1}(\tau)\rangle^2 \quad , \tag{77}$$

where

$$G = \frac{(E_z^o)^4\omega_o^8}{Y^4 16\pi^2 C_m^6}(\alpha_{\parallel}-\alpha_o)^4N^2\mu^2\,\frac{16\pi^2}{900}\,Q \quad , \tag{78}$$

and Q is the efficiency of the phototube.

In order to proceed from Eq.(77), we must adopt a model for the reorientation of the polymer molecules. Let us assume that the long axes for the molecules behave like independent rigid rods. The development of

the probability function for an arbitrary distribution of points on a unit sphere (i.e., the tips of the orientation vectors) is identical to that which led to Eq.(55). At this point, however, the integration is carried out over all initial angle orientations [$\delta c(\theta,\phi,t=0) = \delta c(\theta,\phi)$] instead of the spatial volume of the solution, using the appropriate probability weighting function

$$\exp\left(-\sum_i \frac{(\delta n_i)^2}{2n_i^o}\right) = \exp\left(-\frac{1}{2c_o}\int_\theta\int_\phi [\delta c(\theta,\phi)]^2 d(\cos\theta)d\phi\right) . \tag{79}$$

The quantity $\delta c(\theta,\phi,t)$ is governed by the rotational diffusion equation of Debye

$$\frac{\partial \delta c(\theta,\phi,t)}{\partial t} = D_\Omega \nabla_\Omega^2 \delta c(\theta,\phi,t) \quad , \tag{80}$$

where ∇_Ω^2 is the Laplacian operator over the surface of a sphere

$$\nabla_\Omega^2 = \frac{1}{\sin\theta}\frac{\partial}{\partial\theta}\left(\sin\frac{\partial}{\partial\theta}\right) + \frac{1}{\sin^2\theta}\frac{\partial^2}{\partial\phi^2} \quad , \tag{81}$$

and D_Ω is the rotational diffusion coefficient. Substitution of Eq.(70) into Eq.(81) leads to the equation for $b_{l,m}(t)$,

$$\frac{\partial}{\partial t} b_{\ell,m}(t) = -\ell(\ell+1)D_\Omega b_{\ell,m}(t) \quad , \tag{82}$$

with the solution

$$b_{\ell,m}(t) = b_{\ell,m}(0)\exp[-\ell(\ell+1)D_\Omega t] \quad . \tag{83}$$

The distribution function for the orientation fluctuations $\delta c(\theta,\phi,t)$ is

$$\delta c(\theta,\phi,t) = \sum_{\ell,m} b_{\ell,m}(0)\exp[-\ell(\ell+1)D_\Omega t]Y_{\ell,m}(\theta,\phi) \quad . \tag{84}$$

Substituting Eq.(70) into Eq.(79) and using the orthogonality property of the spherical harmonics, we have for the probability weighting function at t = 0,

$$\exp\left(-\iint_{\theta\phi}\frac{\delta c(\theta,\phi)^2 d(\cos\theta)\,d\phi}{2c_o}\right) = \exp\left(-\frac{\sum_{\ell,m}|b_{\ell,m}(0)|^2}{2c_o}\right). \tag{85}$$

The normalized probability function then takes on the form

$$P_N = P(b_{1,-1},b_{1,0},b_{1,1}\cdots)db_{1,-1}db_{1,0}db_{1,1}\cdots = \prod_{\ell,m}\frac{\exp(-\frac{2\pi}{N}|b_{\ell,m}|^2)}{\sqrt{N/2}}, \tag{86}$$

where $N/4\pi$ is the uniform concentration c_o of points over the solid angle. We then have the following averages for the manifestly Gaussian distribution of amplitudes

$$\left\langle b_{\ell,m}(0)\right\rangle = \int P_N b_{\ell,m}(0)db_{1,-1}db_{1,0}db_{1,1}\cdots = 0\ , \tag{87}$$

and

$$\left\langle b_{\ell,m}(0)b_{\ell',m'}(0)\right\rangle = \int P_N b_{\ell,m}(0)b_{\ell',m'}(0)db_{1,-1}db_{1,0}db_{1,1}\cdots$$

$$= (N/4\pi)\delta_{\ell,\ell'}\delta_{m,m'}\ . \tag{88}$$

Therefore, the ℓ,m and ℓ',m' modes are uncorrelated on the average and Eq.(76) reduces exactly to Eq.(77) which now has the form

$$\left\langle J_{ac}(t)J_{ac}(t+\tau)\right\rangle = \frac{GN}{4\pi}\exp(-12D_\Omega\tau)\ . \tag{89}$$

THE AUTOCORRELATION FUNCTION OF THE PHOTOTUBE CURRENT WHEN TWO TYPES OF PARTICLES ARE PRESENT

It is conceivable that the sample one uses in a dynamic light scattering experiment is not perfect in the sense that only one type of particle is present in solution. For example, some molecules may form high molecular weight aggregates or dust particles may be present in the solution. We assume, therefore, that the sample contains two species of macromolecules; one which is very much larger than the other. In a unit volume of solution there are N_S of the smaller molecules each made up of μ segments, or scattering centers, with excess polarizability α_S. There are also N_L of the larger species each containing υ segments of excess polarizability α_L. The instantaneous polarizability of the point $\underset{\sim}{r}$ in solution is

$$\alpha(\underset{\sim}{r},t) = \alpha_S \sum_{j=1}^{\mu N_S} \delta[\underset{\sim}{r}-\underset{\sim}{r}_j(t)] + \alpha_L \sum_{k=1}^{\upsilon N_L} \delta[\underset{\sim}{r}-\underset{\sim}{r}_k(t)] \quad , \tag{90}$$

with the Fourier transform [cf., Eq.(24)]

$$\alpha(\underset{\sim}{K},t) = \alpha_S \sum_{j=1}^{\mu N_S} \exp[-i\underset{\sim}{K}\cdot\underset{\sim}{r}_j(t)] + \alpha_L \sum_{k=1}^{\upsilon N_L} \exp[-i\underset{\sim}{K}\cdot\underset{\sim}{r}_k(t)] \quad . \tag{91}$$

The position $\underset{\sim}{r}_i(t)$ of the β^{th} segment in the m^{th} molecule may be expressed in terms of the center of mass $\underset{\sim}{R}_m$ of the molecule and the relative displacement $\underset{\sim}{r}_m$ therefrom,

$$\underset{\sim}{r}_i(t) = \underset{\sim}{R}_m(t) + \underset{\sim}{r}_m^{\beta}(t) \quad . \tag{92}$$

When Eq.(92) is substituted into Eq.(91), which in turn is employed in Eq.(22), the following expression results,

$$\left\langle J(t)J(t+\tau)\right\rangle = \sum_{k,\ell,m,n}\sum\sum\sum\sum \sum_{\alpha,\beta,\gamma,\delta}\sum\sum\sum\sum \alpha_k\alpha_\ell\alpha_m\alpha_n$$

$$\text{esp}(i\underset{\sim}{K}\cdot[\underset{\sim}{R}_k(0)+\underset{\sim}{r}_k^{\alpha}(0)+\underset{\sim}{R}_m(\tau)+\underset{\sim}{r}_m^{\beta}(\tau)-\underset{\sim}{R}_\ell(\tau)-\underset{\sim}{r}_\ell^{\gamma}(\tau)-\underset{\sim}{R}_n(0)-\underset{\sim}{r}_n^{\delta}(0)] \quad . \tag{93}$$

In view of the discussion preceding Eq.(40), the autocorrelation function for the phototube current becomes

$$\begin{aligned}\left\langle J(0)J(\tau)\right\rangle = A^2\Big\{&\alpha_S^4N_S(N_S-1)(\mu^2P_S(\underset{\sim}{K}))^2 + \alpha_L^4N_L(N_L-1)(\upsilon^2P_L(\underset{\sim}{K}))^2 \\ &+ 2\alpha_S^2\alpha_L^2N_SN_L\mu^2\upsilon^2P_S(\underset{\sim}{K})P_L(\underset{\sim}{K}) + \alpha_S^4[C_S^{ext}(\underset{\sim}{K},\tau)]^2[C_S^{int}(\underset{\sim}{K},\tau)]^2 \\ &+ \alpha_L^4[C_L^{ext}(\underset{\sim}{K},\tau)]^2[C_L^{int}(\underset{\sim}{K},\tau)]^2 + 2\alpha_S^2\alpha_L^2C_L^{ext}(\underset{\sim}{K},\tau)C_L^{int}(\underset{\sim}{K},\tau)C_S^{ext}(\underset{\sim}{K},\tau)C_S^{int}(\underset{\sim}{K},\tau) \\ &+ \alpha_S^4D_S^{int}(\underset{\sim}{K},\tau) + \alpha_L^4D_L^{int}(\underset{\sim}{K},\tau)\Big\} \quad ,\end{aligned} \tag{94}$$

where $P(\underset{\sim}{K})$, $D^{int}(\underset{\sim}{K},\tau)$, $C^{ext}(\underset{\sim}{K},\tau)$, and $C^{int}(\underset{\sim}{K},\tau)$ are derined by Eqs.(33), (35), (38), and (39), respectively, for the molecules S or L. Since the $D^{int}(\underset{\sim}{K},\tau)$ terms in Eq.(94) contain only a single sum over the molecules, while the remaining terms contain double sums over the molecules, the former terms may be expected to be exceedingly small compared to the latter under essentially all experimental conditions, and they will henceforth be ignored. Retaining only the terms which are quadratic in the numbers of molecules, Eq.(94) can be written as

$$\begin{aligned}\left\langle J(0)J(\tau)\right\rangle = A^2\ &[\alpha_S^2N_S\mu^2P_S(\underset{\sim}{K})+\alpha_L^2N_L\upsilon^2P_L(\underset{\sim}{K})]^2 \\ &+ [\alpha_S^2C_S^{int}(\underset{\sim}{K},\tau)C_S^{ext}(\underset{\sim}{K},\tau)+\alpha_L^2C_L^{int}(\underset{\sim}{K},\tau)C_L^{ext}(\underset{\sim}{K},\tau)]^2 \quad ,\end{aligned} \tag{95}$$

where the first term of Eq.(95) represents the static contribution and the second term contains the time dependence of the autocorrelation function [cf., Eq.(26)].

For rigid rods undergoing rotational Brownian Motion, for flexible coils undergoing internal segment diffusion, and for ions on the surfaces of either rod-like or spherical colloids, the autocorrelation function $C_S^{int}(\underset{\sim}{K},\tau)$ for the internal motions is a sum of exponential decays with relaxation times that are independent of $\underset{\sim}{K}$, or scattering angle θ, but with amplitudes that do depend upon $\underset{\sim}{K}$, or θ. Furthermore, in all of these cases the longest relaxation time (associated with electrically neutral fluctuations in the case of the ions) is infinity, and the amplitudes of this stationary mode is just μ^2 times the interference factor that one would calculate for the equilibrium distribution of segments over the appropriate internal coordinates. Fluctuations about this uniform distribution produce additional scattered light, and also give rise to the non-stationary decays in $C_S^{int}(\underset{\sim}{K},\tau)$. For the molecules of dimension much smaller than C_m/ω_o the amplitude of the stationary mode is dominant at all angles, though it exhibits a maximum at zero scattered angle that may be quite sharply peaked for large molecules (cf., Fig. 4). The amplitudes of the non-stationary decays vanish at $\theta=0^o$.

For the special cases mentioned above, then, one may write

$$C_S^{int}(\underset{\sim}{K},\tau) = B_{S0} + B_{S1}\exp(-\tau/\tau_{S1}) + B_{S2}\exp(-\tau/\tau_{S2}) + \ldots, \qquad (96)$$

with a corresponding equation for the L molecules, and to an exceedingly high degree of accuracy, Eq.(95) becomes

Figure 4

Relative scattering envelops B_{SO} and B_{LO} for two different sizes of particles S and L.

Θ
B_{LO}
Θ
B_{SO}

$$\langle J(0)J(\tau)\rangle = A^2\Big\{[\alpha_S^2 N_S \mu^2 P_S(\underset{\sim}{K})+\alpha_L^2 N_L \upsilon^2 P_L(\underset{\sim}{K})]^2$$

$$+\alpha_S^4 N_S^2 V^2 \exp(-2K^2 D_S \tau)\,[B_{S0}^2+2B_{S0}B_{S1}\exp(-\tau/\tau_{S1})+B_{S1}^2\exp(-2\tau/\tau_{S1})+\ \ldots]$$

$$+\alpha_L^4 N_L^2 V^2 \exp(-2K^2 D_L \tau)\,[B_{L0}^2+2B_{L0}B_{L1}\exp(-\tau/\tau_{L1})+B_{L1}^2\exp(-2\tau/\tau_{L1})+\ \ldots]$$

$$+2\alpha_S^2\alpha_L^2 N_S N_L V^2 \exp[-K^2(D_S+D_L)\tau]\,[B_{S0}B_{L0}+B_{L0}B_{S1}\exp(-\tau/\tau_{S1})$$

$$+B_{S0}B_{L1}\exp(-\tau/\tau_{L1})+B_{S1}B_{L1}\exp(-\tau/\tau_{S1})\exp(-\tau/\tau_{L1})+\ \ldots]\ . \qquad (97)$$

When there are enough large particles so that B_{L0} greatly exceeds B_{S0} over the entire accessible range of scattering angles, then the experiment is doomed to fail. When B_{L0} is negligible compared to B_{S0} over the entire angular range, then the high molecular weight material will pose no problem. Owing to the much greater size of the L particles, B_{L0} will in general decrease much more rapidly with increasing θ than does B_{S0}. Thus, it is possible for B_{L0} to be significant compared to B_{S0} at small scattering angles, but to be also negligible compared to B_{S0} at larger scattering angles. It may be anticipated that this will be the usual experimental circumstance in studies on dilute solutions of macromolecules. Furthermore, since B_{S0} and B_{L0} are scattering factors for the equilibrium distribution of the molecules over their internal coordinates, B_{L0} and B_{S0} must be proportional to υ^2 and μ^2, respectively, provided that the geometry is kept constant. However, B_{S1} and B_{L1}, being scattering factors for mean square fluctuations from the uniform distribution are proportional to υ and μ, respectively, and thus may be expected to remain smaller than B_{L0} or B_{S0}, respectively, so long as the wavelength of light is longer than the radius of gyration R_G of the molecule. Since B_{S1} and B_{L1} vanish at $\theta = 0$, they must possess

maxima at larger scattering angles. Clearly, the products $B_{S0}B_{S1}$, $B_{L0}B_{L1}$, $B_{S0}B_{L1}$, and $B_{L0}B_{S1}$ have maxima at some scattering angle greater than $\theta = 0$. When B_{L0} is sharply peaked in the forward direction as would be the case for dust or very high molecular weight aggregates, then the products $B_{L0}B_{L1}$ and $B_{L0}B_{S1}$ must manifest their maxima at fairly small scattering angles, certainly at much smaller angles than those for $B_{S0}B_{S1}$ and $B_{S0}B_{L1}$.

IV. Description and Operation of the Apparatus

THE LASER

In order to analyze the time dependent component of the scattered light in terms of molecular motions, a continuous source of coherent incident radiation is necessary.

The 6328A line of a Spectra-Physics Model 125A He-Ne gas laser was employed in these experiments. As a precaution against possible fluctuations in the intensity of the incident beam due to temperature changes within the plasma tube, an arbitrary warm-up period of two hours was allotted before each experimental run. The operating power of the unattenuated beam was measured to be between 65-70 milliwatts. The r.f. field of the Model 261 RF/DC Exciter, which was the accompanying power supply for the laser was turned up to its maximum power in order to minimize the signal due to the oscillations in the laser beam. Even with this procedure, these oscillations gave a significant contribution to the zero-angle scattered light in the very dilute concentration range. It was also noticed that the laser produced a faint blue halo around the primary beam. This unpolarized blue light was eliminated by a filter which transmitted light of wavelengths longer than 5800A. The angle between the direction of propagation of the incident beam and the surface of the filter was at some angle other than 90^{o} in order to prevent reflection of the beam back into the plasma tube.

THE POLARIZERS

The 10mm low power polarizers were purchased from Special Optics of Cedar Grove, New Jersey. It was not possible to completely extinguish the incident beam with only one polarizer. This may, in part, be due

to the intrinsic .03% linear cross component of the laser. The phototube current resulting from this component was measured to be 1/30 of the current due to light scattered from a .055 mg/ml solution of DNA. At maximum transmission of one polarizer, the power of the transmitted beam was reduced by approximately 33%, probably due to reflection. The polarizers were each mounted in two concentric aluminum cylinders for easy adjustment, the outer cylinder being fixed to the optical bench. A set screw prevented the inner cylinder from slipping with respect to the outer cylinder in the course of an experiment. The orientation of the polarizers with respect to the polarization of the incident beam was determined by the phototube current since the power meter was not sufficiently sensitive to small rotations of the polarizer. Prior to mounting the sample and lenses, the second polarizer (cf., Figure 5) was adjusted to the minimum transmission as determined by the current. The first polarizer was then placed on the optical bench and rotated until a minimum current was obtained. In this configuration, the first polarizer was assumed to be positioned in such a way as to minimize the transmission of the cross component in the laser beam. This orientation of the first polarizer was not changed throughout an experimental run. The second polarizer was always adjusted to a minimum value before any data was collected in the depolarized experiments. In the polarized finite-angle Rayleigh scattering experiments, the second polarizer was set at a maximum transmission at the beginning of the experimental run and was not changed in the course of the run.

The aluminum cylinder mounts were built by Mr. Dick Kair of this department.

Figure 5

Schematic diagram of the apparatus. The component parts of this apparatus are discussed in detail in Section IV. The configuration presented in this diagram is for the zero-angle depolarized scattering experiment.

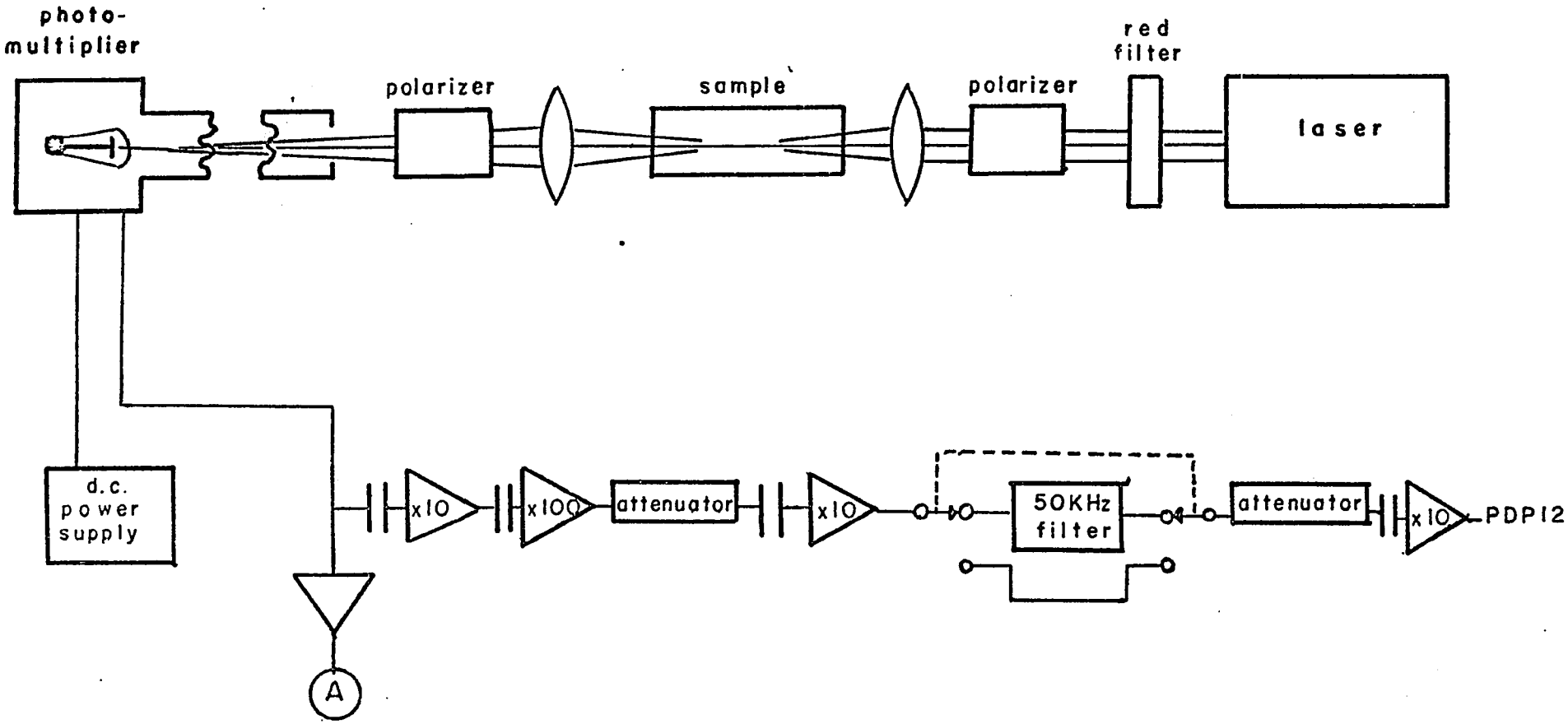
photo-
multiplier
polarizer
sample
polarizer
red
filter
laser
d.c.
power
supply
x10
x100
attenuator
x10
50KHz
filter
attenuator
x10
PDP12
A

THE LENSES

Two 10-cm focal length lenses were used in these experiments. The first lens was fixed in a mount that could be adjusted in three directions whereas the second lens could only be adjusted in the plane perpendicular to the propagation of the incident beam. The lenses were fixed in their mounts in such a way as to prevent reflection of light along the direction of propagation of the incident beam. The lenses were periodically cleaned between experimental runs by wiping their surfaces with lens paper moistened with spectroscopic grade acetone.

The lens mounts were built by Mr. Howard Fulton of this department.

THE SCATTERING CELLS

The cell used in the zero-angle experiments was a double jacketed cell with parallel optical quality pyrex windows. The capacity of the cell was approximately 50 ml. Prior to filling with the sample, the cell was flushed with approximately 3 liters of distilled water. The water was filtered directly with the aid of an aspirator into the cell through .22-3.0 micron Millipore filters. Since the sintered glass support in the commercial Millipore filter holder may contribute dust to the solution, the final two rinsings were done with the solvent by gravity-flow with unsupported Millipore filters. The sample to be used in the experiment was then filtered by gravity-flow through 3.0 micron Millipore filters.

The cylindrical cell used in the polarized Rayleigh experiments was made from low birefringence optical quality pyrex tubing. The capacity of the cell was approximately 25 ml. Since there was only one

Figure 6

Schematic diagrams of the sample cells used in the finite-angle Rayleigh scattering experiments (cell A) and the zero-angle depolarized scattering experiments (cell B). The arrows represent the direction of water flow.

A

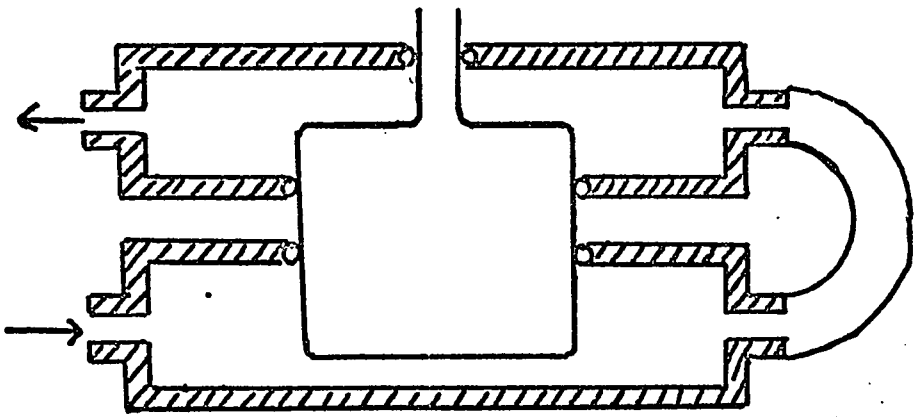

B

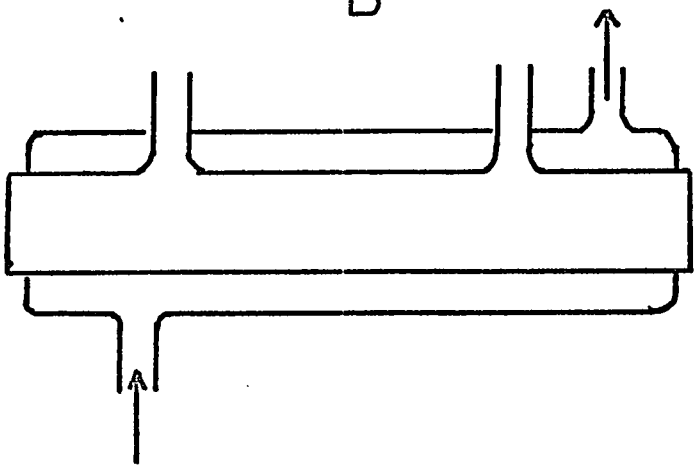

opening in the cell, the stem of the filter holder protruded into the cell in an attempt to circulate the water when rinsing the cell. Prior to filling the cell with the sample solution, the cell was placed in the laser beam to check for Tyndal scattering. The sample was then allowed to gravity-flow through a 3.0 micron Millipore filter directly into the cell. Temperature control was obtained by means of a specially designed water jacket. The water jacket consisted of two cylindrical metal containers which fit tightly over the top and bottom portions of the cell. "O" rings were used at the points of contact of the cell and water jackets to prevent leakage of the circulating water. When the cell was in place, there was apprxomately a 1-2mm spacing between the top and bottom inner surfaces of the water jacket.

In the experiments that were carried out on the I-beam (see below), water was circulated through the water jackets while data was being collected. This was not possible in earlier experiments because the optical bench was not completely decoupled from the external apparatus (i.e., water bath). Whenever the temperature was changed, approximately 15-30 minutes were allowed to establish equilibrium in the cell after the temperature attained the new valve.

The scattering cells were made by Mr. Ollin Barber and the cylindrical water jacket was built by Mr. Dick Kair of this department.

THE VIBRATION-DAMPING TABLE

The vibration-damping table was a 3000 pound I-beam which was decoupled from the floor by 16 springs. The springs were placed in groups of four on four sets of metal plates for stability and distribution of weight. The metal plates were then bolted to two smaller I-beams which,

in turn, supported the larger I-beam. The springs were selected to compress almost to solid when supporting the total weight. Each spring was stabilized to horizontal motion by being placed in a metal cap at each plate and then running a bolt through the center of the spring leading from the bottom plate to the upper plate. Each spring acted independently and was not fixed to either plate. It was estimated that the resonance frequency of the table was approximately 3/2 cycles per second.

To take advantage of the mass of the I-beam, the rotary milling table used in these experiments was bolted to the I-beam. The optical bench was fixed to the milling table and the scattering angles were read directly from the calibration on the milling table. All of the optical equipment used in the zero-angle depolarized experiments were mounted on the optical bench. In the finite-angle experiments, however, the sample cell, first lens, and first polarizer were mounted on a specially designed platform that was bolted to the vibration-damping table. This enabled the scattering angle to be changed without altering the initial alignment of the sample cell.

THE PHOTOTUBE

An RCA IP28 phototube and an ITT FW 130 phototube were used in these experiments. The ITT FW 130 with an S-20 photocathode surface was better suited for experiments with low intensity scattered light because of its low noise/signal ratio and optimum quantum efficiency at the laser frequency. Each phototube was housed in a specially designed aluminum case to shield it from external radiation. The phototube was then attached to a long brass tube which helped prevent extraneous light from reaching the sensitive portion of the phototube. Once the apparatus was aligned, the phototube housing was then clamped to the optical bench to prevent

vibrations and slippage. It was not found necessary to cool the ITT FW 130 phototube in the experiments described here.

The housing units were designed by Mr. Sheldon Danielson and built by Mr. Howard Fulton of this department.

ELECTRONICS

The electronic amplification and filtering system was designed and built by Mr. Sheldon Danielson with the help of Mr. Pete Wichern of this department. The d.c. component of the phototube current is continuously displayed on a long time-constant d.c. meter, while the fluctuating part is passed through a filter circuit with a response flat to within 1% from 3Hz to 50KHz and a cut-off was designed to prevent demodulation of high frequency components by the lower frequency rate of digitation. At the time this high frequency cut-off was first employed it definitely improved the signal quality. There were also two independent attenuator controls with a combined attenuation of 100. At zero settings, the attenuators reduced the built-in amplification of 10^5 to 10^3.

The filtered (a.c.) signal is relayed to the Analog-Digital converter of a PDP-12 computer by approximately 10 feet of coaxial cable. At designated times under program control the computer initiates the (18 microsecond) A-D conversion, and stores the resulting value of the voltage in one of 7168 successive locations in core. When the core is completely filled, the data-taking program is interrupted and the stored data is transferred to tape. Upon completion of the transfer the data-taking program resumes operation and collects voltages at another 7168 successive time intervals, which in turn are stored on the tape, etc. Though operating under program control, the actual initiation of the A-D

conversion is controlled by signals from a 400 KHz quartz crystal clock and associated buffer registers (KW12 Real Time Clock supplied with the computer by Digital Equipment Corporation).

The digitized signal could be monitored using the scope display of the computer. The phototube voltage was adjusted to an appropriate value using the scope display of the signal record. It was found that an oscilloscope with both external and line triggering modes was essential for the detection of coherent noise in a continuous display of the phototube signal.

V. Alignment and Focussing

The optical bench was mounted on the milling table and fixed at the zero-angle reading of the vernier scale. A movable target was then placed on the optical bench and raised to the level of the laser beam. The target was then translated from one end of the bench to the other. Both the laser and the optical bench were adjusted so that the beam was coincident with the target at both ends of the optical bench. Once this configuration was attained, the milling table was bolted to the I-beam and a target was fixed to the wall.

At the beginning of each experiment, the polarizers, lenses, and the sample cell were realigned and fixed in position. In the zero-angle experiments the front polarizer and filter were fixed in position first (cf., Figure 5). The first lens was then placed in position and adjusted until the laser beam was symmetric about the target on the wall. The second lens was then placed on the optical bench and adjusted until the laser beam was inside the target boundaries. The second polarizer was then placed in position. Finally, the sample was placed in a position such that the focal point of the first lens was at the center of the solution.

For the finite-angle scattering studies, the first polarizer and lens were mounted on a fixed platform together with the scattering cell. The scattering cell and water jacket were simply resting on the platform inside a specially designed well. The center of the well was placed directly above the center of the milling table. Due to its cylindrical shape, the scattering cell gives double images on the wall when not properly aligned. Alignment was performed by adjusting the position of the cell in the well until the two images were superimposed. The first

lens was then placed in position and translated until the focal point was at the center of the solution. Transverse adjustment of the lens was made to superimpose the two images on the wall. The remainder of the alignment procedure was the same as described above.

Since the ITT FW 130 phototube has a 2mm active spot, the initial position of the brass collimator is important in reducing the time required to find the maximum signal. If the tube is improperly aligned, the beam of scattered light may bounce off the walls of the tube and one may erroneously obtain a "maximum" in the signal. To help prevent stray light from reaching the phototube due to this bouncing effect, the walls of the tube were lined with black cloth. The presence of stray light was further minimized by using electrician's tape to reduce the front opening of the tube to a square of approximately 3mm on a side. The initial alignment was then made by placing a plug with a pin hole at its center in the far end of the collimator and adjusting the position of the brass tube until the laser light attains maximum intensity on the wall. The second lens is then adjusted until a sharp image appears on a card held at the point where the sensitive area of the phototube is expected to be when it is mounted on the back of the collimator. Since the lenses are mounted at an angle to prevent reflection along the path of the primary beam, it was necessary to readjust the transverse position of the lens in the focussing procedure. The focus was regularly checked prior to data collection at every temperature, since the quality of the signal was strongly dependent on how well the scattered beam was focussed. For the angular studies, a solution of polystyrene spheres was used to provide the image since the scattered light was more intense from this solution. The focus was initially checked at three or more angles.

Having aligned the apparatus and focussed the scattered light, the phototube was then placed in position. The vertical and horizontal positions of the phototube were adjusted until a maximum current was obtained. In the polarized Rayleigh scattering experiments, the second polarizer was then adjusted until a maximum current was obtained and then fixed in position with the set screw. This position was not changed throughout the experimental run. In the zero-angle depolarized experiments, the polarizer was always set to a minimum before collecting data. It was extremely important to minimize the current readings in these depolarized experiments since the primary beam can heterodyne-beat with the scattered light. Once the minimum was found, an oscilloscope was used to adjust the final position of the phototube. For some unknown reason, the a.c. signal on the oscilloscope appeared as cusps with superimposed grass, if the phototube was not properly aligned. Presumably these cusps were due to the plasma oscillations in the laser since they were observed to increase in magnitude when the power of the r.f. exitor was turned down. These cusps also appeared if the light was not focussed through the centers of the lenses. No cusps were observed in the polarized Rayleigh experiments.

Once the phototube had been positioned, it was then clamped to the optical bench to prevent slippage during the collection of data. Any fine adjustment for improving the signal after the phototube was fixed in position was carried out by readjustment of the horizontal and vertical positions of the second lens. The signal was then displayed on the scope of the PDP 12.

VI. Calf Thymus DNA

PREPARATION OF THE SAMPLE

The most expensive commercially available grade of highly polymerized calf thymus DNA (Lot No. AJ1) was purchased from Worthington Biochemical Corporation, Freehold, New Jersey. The fibrous material was introduced directly into a cellophane dialysis bag which contained approximately 50 ml of gravity-flow Millipore-filtered buffer solution. The buffer consisted of .0953 g/l of KH_2PO_4 and 1.1217 g/l of K_2HPO_4 dissolved in distilled water. The ionic strength was .02 and the pH was measured to be 7.6. The solution of DNA was then dialyzed against 500 ml of buffer solution with an EDTA concentration of .01M. The dialysis was carried out in a cold room ($5^{o}C$) with continuous agitation using a magnetic stirrer. The fibrous material was completely dissolved within 6 hours. The DNA was dialyzed twice against the EDTA solution, for 24 hours each time. The DNA solution was then dialyzed 5 or more times against 500 ml of the buffer solution without EDTA. The dialysis periods with the buffer solution varied from 8 to 24 hours, with the final dialysis always being 24 hours. The DNA solution was then placed in a volumetric flask and stored in the cold room until needed. Preparations of DNA solutions that were older than 5 weeks were not used in any of the experiments. The stock solution was diluted to the desired concentration with gravity-flow, Millipore-filtered buffer solution immediately before an experiment. Concentrations were obtained at room temperature using an optical density of $A_{260} = 20$ for a 1mg/ml solution.[20] The A_{280}/A_{260} ratio was found to be .370/.700 = .528, which is comparable to the value .55 obtained for the low-protein-contaminated sample of calf thymus DNA used by Liebe and Stuehr.[21]

ABSORBANCE-TEMPERATURE PROFILE

The transition temperature T_m was obtained from the temperature profile of the hypochromicity (Figure 7). The presence of sucrose (47 g/100 ml solution) did not significantly alter the T_m, though the transition seemed slightly broader (Figure 9). The absorbance-temperature profile of a DNA solution with an excess of Mg^{2+} per base was determined to test the effectiveness of the EDTA treatment (Figure 8). The T_m changed by almost 9° which indicates that an appreciable fraction of the phosphate groups cannot possess bound divalent ions after the EDTA treatment. The optical densities for these measurements are presented in Table I. The total weight lost due to evaporation in a complete temperature run (approximately 6 hours) was less than .03 grams.

VISCOSITY MEASUREMENTS

The flow times through an Ostwald viscometer for different aliquots of the same DNA solutions were measured concurrently with the light scattering experiment. The viscometer was cleaned by filling it with concentrated sulfuric acid and letting it stand overnight. After pouring out the acid, approximately 2 liters of distilled Millipore-filtered water were flushed through the viscometer with the aid of an aspirator. The rate of flow was adjusted so water completely filled the viscometer and no bubbles were trapped in the bulb. After rinsing, the viscometer was inverted and air was drawn through it until dry. The viscometer remained inverted until needed. The DNA solutions were first filtered once through a 3.0 micron Millipore filter under gravity flow and then 3 ml were pipetted directly into the viscometer. Between runs at different temperatures the ends of the viscometer were

Figure 7

Hypochromicity-temperature profile of calf thymus DNA in the phosphate buffer. The hypochromicity H was calculated from the optical absorbance $A_{260}(T)$ at the temperature $T(^{o}C)$ by the relationship

$$H = \frac{A_{260}(T) - A_{260}(49.6)}{A_{260}(81) - A_{260}(49.6)}$$

The T_m is approximately $67^{o}C$.

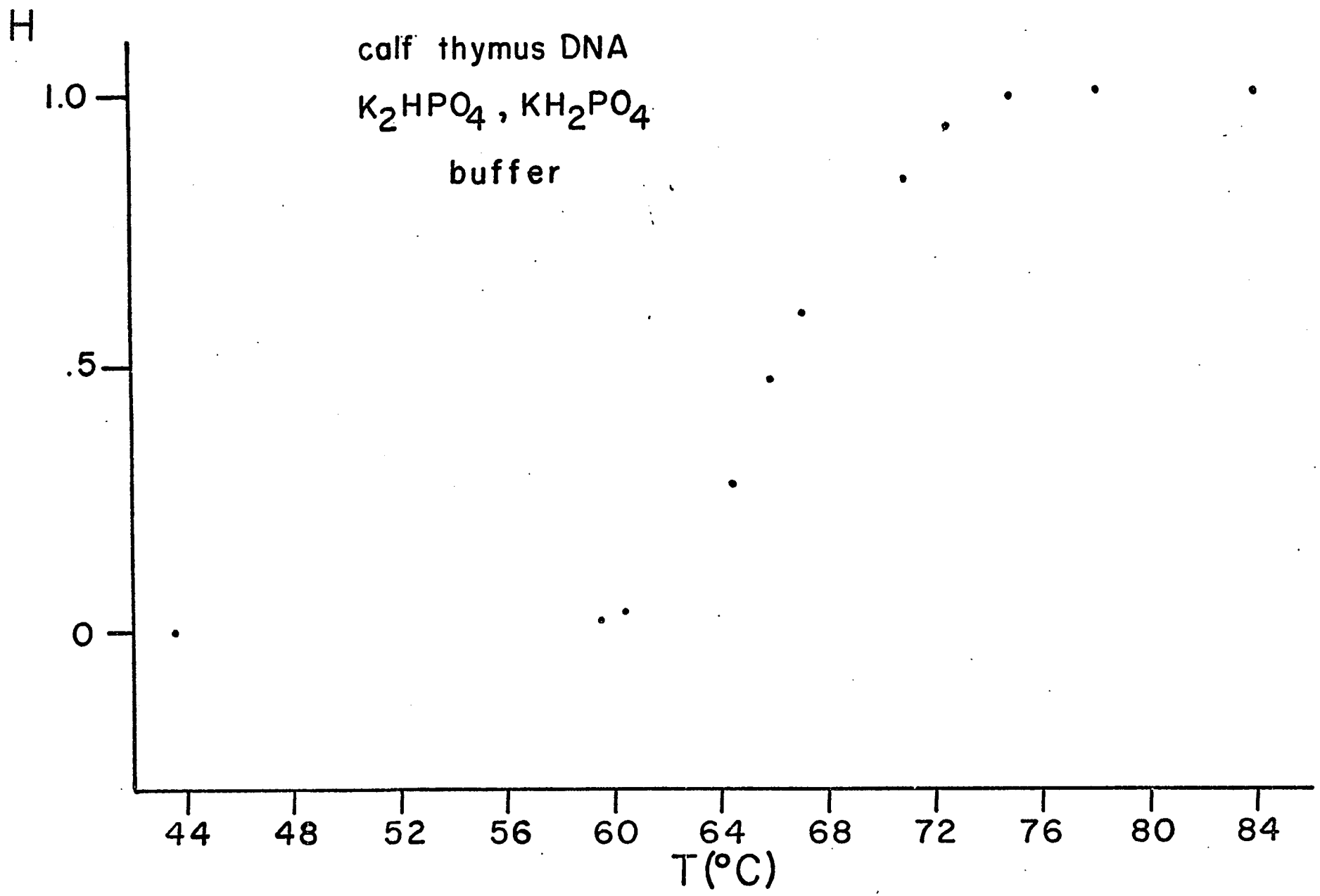
H
calf thymus DNA
K_2HPO_4, KH_2PO_4
buffer
1.0
.5
0
44
48
52
56
60
64
68
72
76
80
84
T(°C)

Figure 8

Hypochromicity-temperature profile of calf thymus DNA in the phosphate buffer with an excess of magnesium ions present (Mg^{2+}/phosphate ~4). A change of ~9° in the T_m (cf., Figure 7) infers that an appreciable fraction of the phosphate groups cannot possess bound divalent ions after the EDTA treatment.

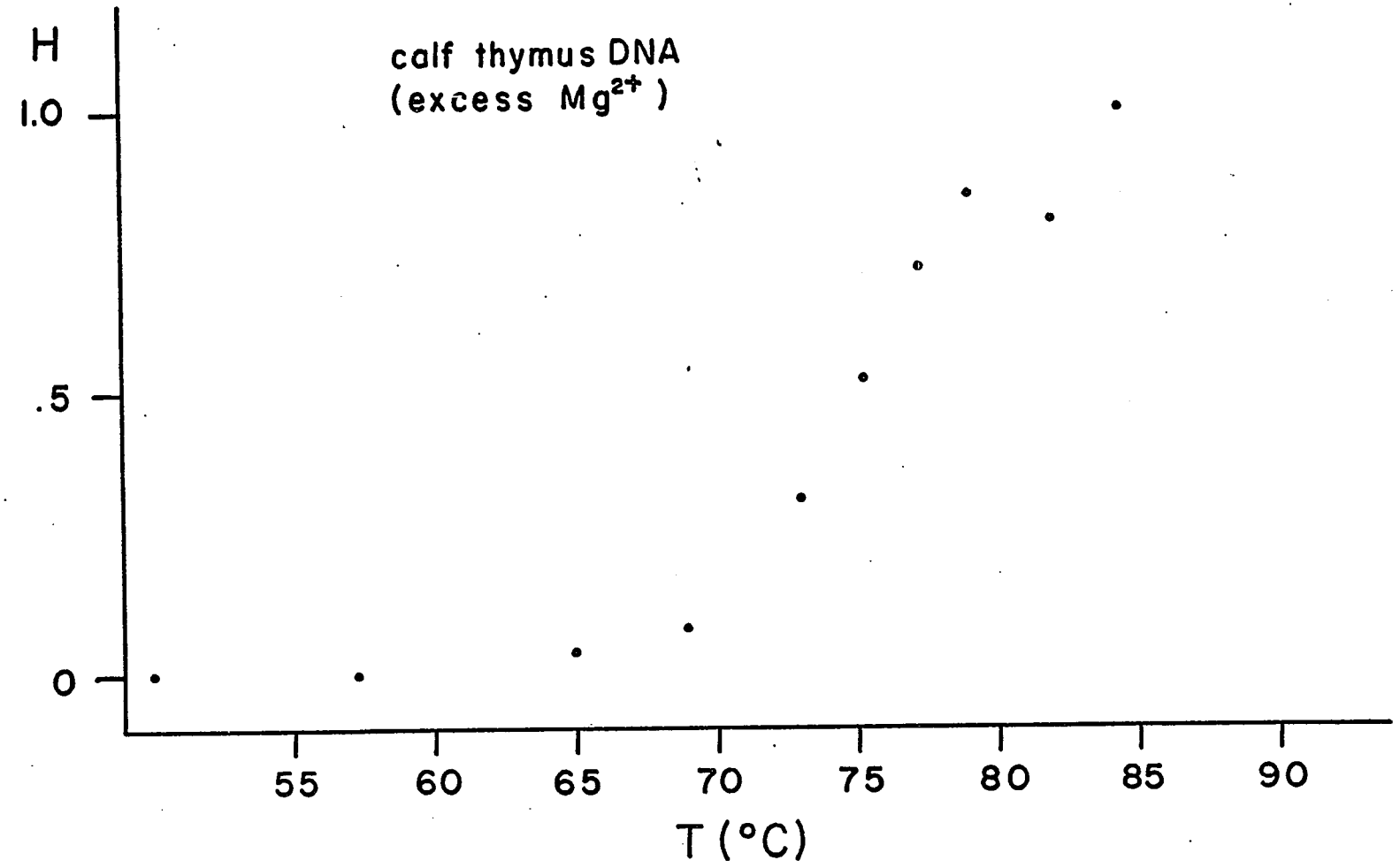
H
1.0
.5
0
calf thymus DNA
(excess Mg^{2+})
55
60
65
70
75
80
85
90
T (°C)

Figure 9

Absorbance-temperature profiles of calf thymus DNA in buffer (x) and sucrose + buffer (o). The concentration of the sucrose was approximately 47 g/100 ml of solution.

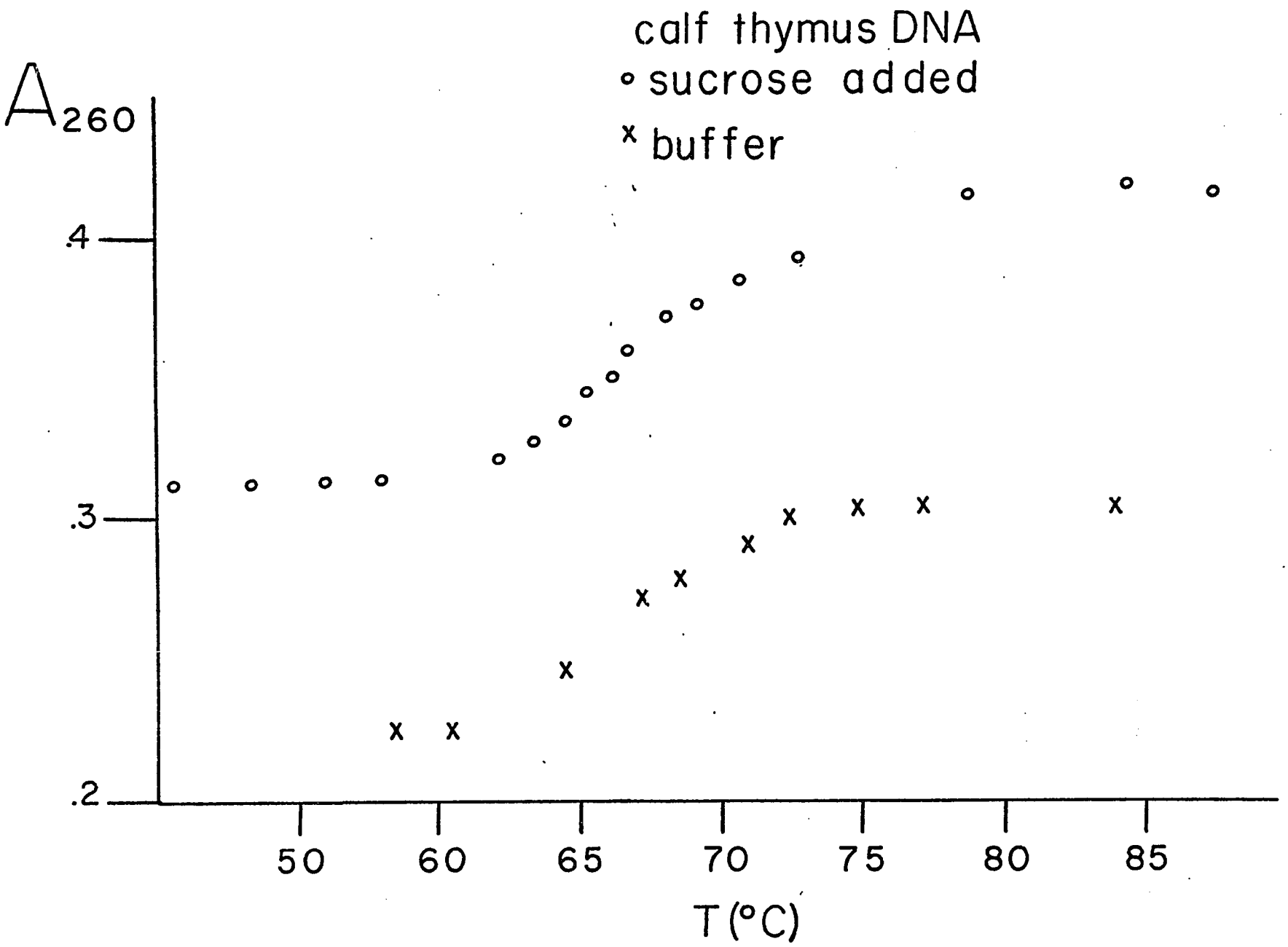
calf thymus DNA
sucrose added
buffer
A260
.4
.3
.2
50
60
65
70
75
80
85
T(°C)

connected by a rubber tube to form a closed loop in an attempt to prevent changes in concentration due to evaporation.

The temperature dependence of the viscometer proportionality constant A(T), defined by

$$\eta = A(T)t \quad , \tag{98}$$

where η is the viscosity in centipoise and t is in seconds, was determined from the known values of η for distilled water. Within an error of 1% of the known values of η for water A(T) was found to have the form

$$A(T) = .006884 + 1.4571/T \quad , \tag{99}$$

in the temperature range 20-80°C.

In the computation of the relative viscosity η_{rel}, the flow times were used directly, i.e.,

$$\eta_{rel} = \frac{t_{solution}}{t_{solvent}} \quad , \tag{100}$$

since Eq.(98) is not sufficiently accurate. The flow time for the K_2HPO_4, KH_2PO_4 buffer at a particular temperature was not measured concurrently with the experiment but was obtained from a smooth curve drawn through previously measured flow times at several temperatures. These flow times are presented in Table II. The computed values of the viscosity η and $\eta_{sp}/c = (\eta_{rel}-1)/c$ are listed in Table III. The temperature dependence of η_{sp}/c is illustrated in Figure 11.

To determine if the Millipore-filtering sheared the DNA, the flow times of unfiltered and filtered solutions of .035 mg/ml were determined. The DNA solution was filtered 5 times by gravity-flow through a 3.0 micron Millipore filter. The flow times of 81.84 and 81.92 seconds for the

TABLE I

Optical Absorbance A_{260}[a]
Temperature (^{o}C) in parenthesis

DNA + Mg^{2+}	DNA + Sucrose[b]	DNA
.255(25)	.311(26.4)	.223(26.9)
.257(41.7)	.315(32.1)	.223(41.7)
.250(50.7)	.312(41.0)	.225(57.5)
.250(57.3)	.312(50.8)	.226(60.4)
.254(65.0)	.312(53.4)	.246(64.5)
.258(69.5)	.314(56.0)	.262(65.0)
.281(73.5)	.314(58.0)	.272(67.2)
.304(75.3)	.321(62.1)	.279(68.5)
.313(76.5)	.328(63.4)	.292(71.0)
.322(77.4)	.335(64.4)	.300(72.5)
.335(79.1)	.344(65.2)	.304(74.8)
.330(81.0)	.350(66.2)	.305(77.1)
.350(64.5)	.360(66.8)	.305(84.0)
.350(95.4)	.371(68.1)	
	.375(69.1)	
	.385(70.8)	
	.393(72.8)	
	.415(78.9)	
	.418(84.4)	
	.415(87.5)	

a-loss of <.03 grams in course of these measurements.

b-.078 mg/ml + sucrose which was dilluted by 5 with sucrose solution.

$\frac{A_{280}}{A_{260}}$ = .528 at 20^{o}C.

TABLE II

Average Flow Times of 3 ml of Solution
(Seconds)

Temperature (^{o}C) in parenthesis

		DNA Solutions				
					Sucrose added	
Water	K_2HPO_4 KH_2PO_4 buffer	.018 mg/ml	.068 mg/ml	62 mg/ml	.078 mg/ml	.018 mg/ml
79.52(22.9)	73.89(26)	50.23(48.1)	67.97(38)	139.74(48)	290.88(37)	99.61(49.1)
67.39(30.8)	63.92(33)	46.23(53)	55.78(49)	127.94(53)	225.51(46)	79.64(60.5)
54.28(42.0)	58.18(38)	41.68(60.1)	53.73(52)	119.86(57)	202.82(49)	71.40(67.4)
44.12(55.0)	49.13(48)	37.31(67.9)	51.26(55)	106.50(63)	181.14(53.2)	65.69(72.5)
35.15(73.0)	42.86(57)	35.42(72.4)	47.39(60)	83.61(72.5)	139.41(65)	60.71(78.5)
	38.93(64)	30.85(84.6)	42.25(68)	75.09(76)	124.93(70)	
	37.07(68)		39.30(72)	65.14(80)	95.68(82)	
	35.27(72)		36.90(76)	57.45(85)		
	33.81(76)		35.41(79)			
	31.61(82)		33.82(82)			

Figure 10

Flow times of 3 ml of gravity-flow Millipore-filtered K_2HPO_4, KH_2PO_4 buffer. The flow times used in the calculation of η_{sp} were obtained from the smooth curve.

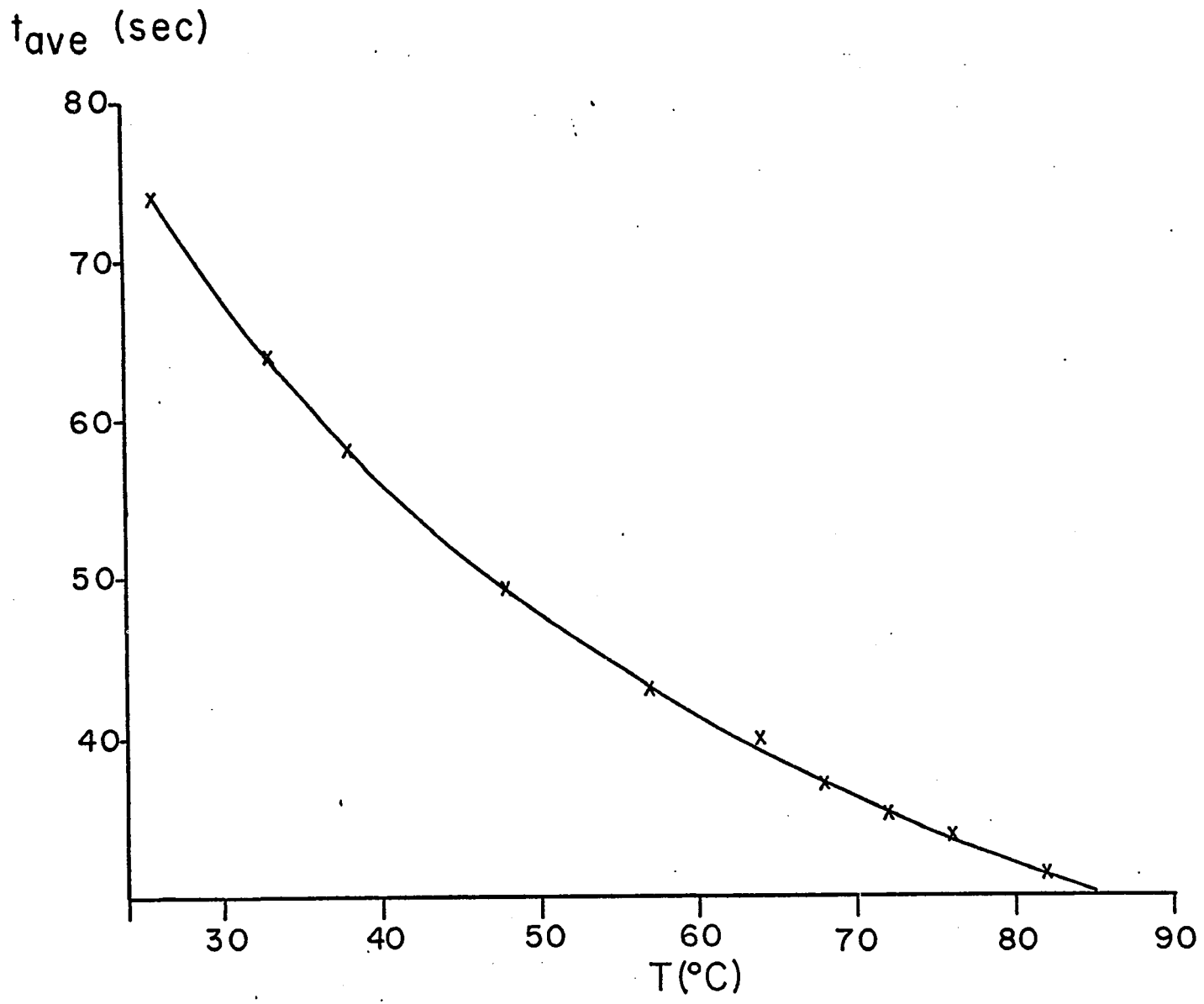
t_{ave} (sec)
80
70
60
50
40
30
40
50
60
70
80
90
T(°C)

TABLE III

Concentration (mg/ml)	η(Solution) (Centipoise)	$(\eta sp/c) \times 10^{-1}$ (dl/gm)	Temperature (°C)
.068	.6360	2.38	49.5
	.6108	2.40	52.0
	.5803	2.47	55.4
	.5333	2.33	60.4
	.4713	2.13	68.2
	.4365	1.69	72.0
	.4079	1.44	76.4
	.3904	1.22	78.8
.62	1.5884	2.96	48.0
	1.4460	2.90	53.0
	1.3422	2.86	57.0
	1.1608	2.61	63.0
	.8698	1.97	72.0
	.8562	2.09	76.0
	.7617	1.85	80.0
	.6623	1.57	85.0
.078+sucrose	2.5825	-	46.0
	2.0554	-	53.5
	1.5607	-	65.0
	1.3895	-	70.8
	1.0514	-	82.0
.018+sucrose	1.1363	-	49.1
	.9562	-	60.5
	.7971	-	67.4
	.7292	-	72.5

$[\eta] = 23.4$ dl/g

Figure 11

Reduced viscosity (η_{sp}/c) as a function of temperature for .62 mg/ml (x) and .068 mg/ml (o) solutions of calf thymus DNA in the phosphate buffer.

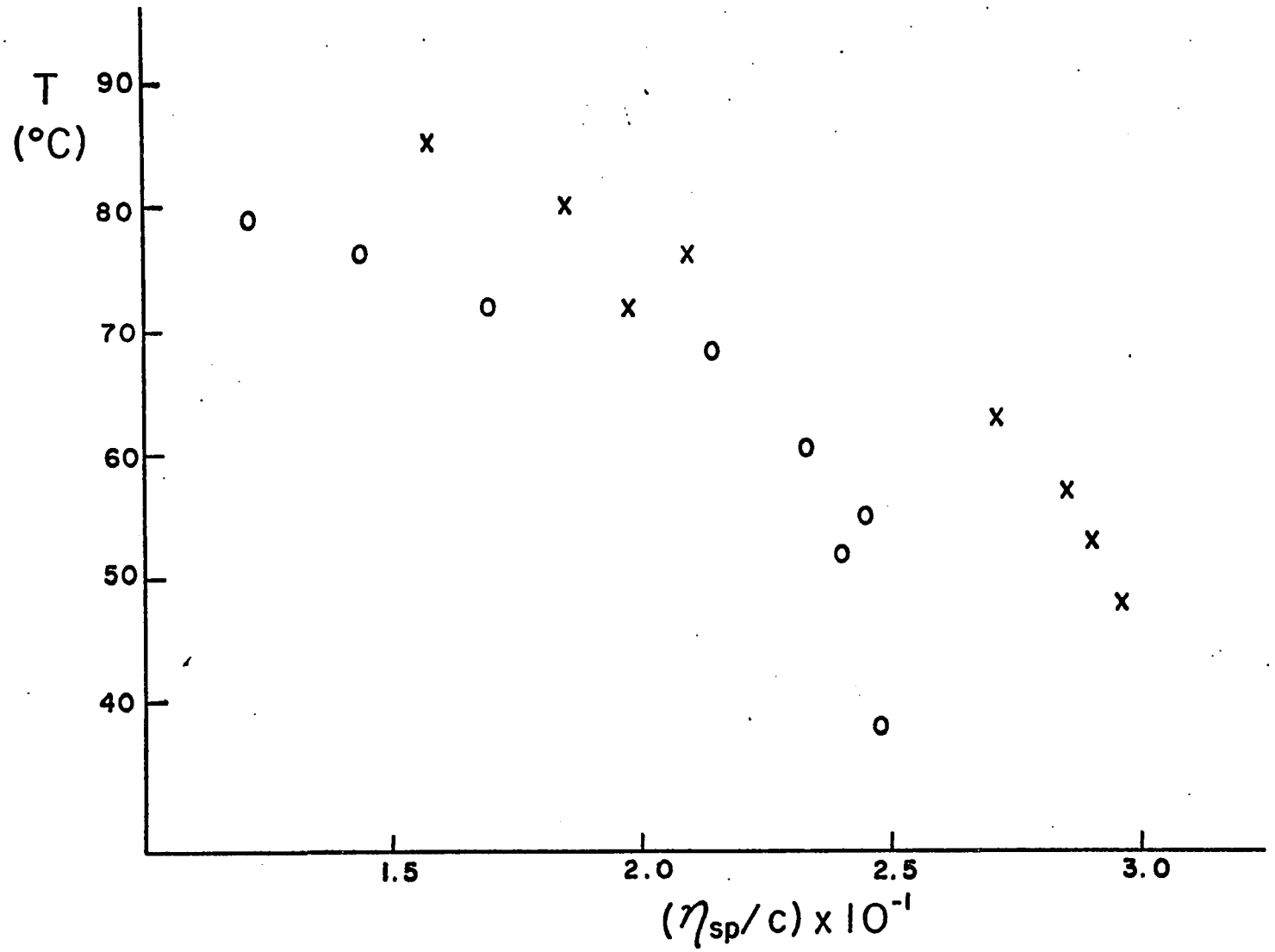
T
(°C)
90
80
70
60
50
40
1.5
2.0
2.5
3.0
$(\eta_{sp}/c) \times 10^{-1}$

unfiltered and filtered solutions, respectively, indicate that the DNA was not sheared in this process. Similar results were reported for slow flow rates of DNA solutions through a .22 micron Millipore filter.[20]

APPROXIMATE MOLECULAR WEIGHT

The intrinsic viscosity was determined from the specific viscosity by the relationship

$$\eta_{sp}/c = [\eta] + k[\eta]^2 c \quad , \tag{101}$$

where c is the concentration of DNA in g/dl. Using the specific viscosity computed at 48°C for the .62 and .068 mg/ml solutions of DNA and eliminating the term containing k, we find that

$$[\eta] \simeq 23.4 \text{dl/g} \quad . \tag{102}$$

Using the expression employed by Eigner and Doty[22]

$$[\eta] = 6.9 \times 10^{-4} M^{.7} \quad , \tag{103}$$

and also of Spatz and Crothers,[23]

$$M = 3.82 \times 10^{4} [\eta]^{1.4} \quad , \tag{104}$$

we obtain molecular weights of 3×10^6 and 2.4×10^6, respectively. Since the intrinsic viscosity of calf thymus DNA increases as the shear rate of the viscometer decreases,[24] 3×10^6 is an underestimate of the true molecular weight. A more accurate molecular weight is obtained if corrections for the rate of shear are taken into consideration (see Section IX).

VII. Calcuation of the Autocorrelation Function

Let us consider a time-varying amplitude A(t) that characterizes some property of a physical system (macroscopic) whose time-average is zero,

$$\langle A(t) \rangle_t = 0 \quad . \tag{105}$$

Since the macroscopic behavior of a system originates from the microscopic details of the system, it is clear that the time evolution of A(t) must be related to the motion of the microscopic particles. Since the motions of these particles are of finite velocity, one can always chose a time interval τ such that the value $A(t'+\tau)$ must, in some way, depend on the value $A(t')$, where t' is any arbitrary time. Therefore, the average value of the product $A(t')A(t'+\tau)$ does not have a zero average for a sufficiently small value of τ. We define the time-average autocorrelation function $\langle A(t)A(t+\tau) \rangle_t$ as

$$\langle A(t)A(t+\tau) \rangle_t \equiv \lim_{T\to\infty} \frac{1}{T} \int_0^T A(t)A(t+\tau)\,dt \quad , \tag{106}$$

where T is the period of observation. The equivalence between time and ensemble averages, together with the independence of origin of the ensemble average that is implied by such an ergodic assumption, is here invoked to obtain

$$\langle A(t)A(t+\tau) \rangle_t = \langle A(0)A(\tau) \rangle_{ENS} \equiv C(\tau) \quad . \tag{107}$$

The time average is obtained experimentally by observing the property A(t) in successive time intervals of duration b for a time period T. In a single record there are (T/b)+1 data points. The single record

autocorrelation function $S_j(nb)$, where j denotes the record index and n is an integer, is calculated according to the formula

$$S_j(nb) = \sum_{i=1}^{m} \frac{A_j(i)A_j(i+nb)}{m} \quad , \qquad (108)$$

where $m = (T/b)+1-n$ and $0 \leq n \leq T/b$. The autocorrelation function $C(\tau)$, where $\tau = nb$, is simply the average of the M single record autocorrelation functions, i.e.,

$$C(\tau) = \frac{1}{M} \sum_{i=1}^{M} S_i(\tau) \quad , \qquad (109)$$

where M = 18 for the calculations reported in this study.

According to Poincaré's Recurrence Theorem, all systems with finite volume and finite energy eventually return arbitrarily close to every state that is available to the system, provided a sufficient amount of time has elapsed (Poincaré Recurrence Time). The autocorrelation function should also be periodic if this condition is met. On the other hand, if the molecular processes are truly random and T is much less than the Poincaré Recurrence Time, then Eq.(109) should approach a well-defined curve that damps to zero at long times when $M \to \infty$.

It was a general procedure to collect data at two time intervals: 25 microseconds and either 250 microseconds or 500 microseconds. After the data was collected at a designated time delay, the autocorrelation function $S_1(nb)$ was computed for 1024 points. The computation time for this single record autocorrelation function was approximately 12 minutes. At the end of the computation, $S_1(nb)$ was displayed on the scope of the PDP-12. The data was saved if the magnitude of any ripples that were

present contributed less than 10% of the display. If the alignment was not nearly perfect, and if the second polarizer was not at a precise minimum, in the zero-angle depolarized experiments, the cusps in the signal introduced a periodic component into the autocorrelation function. Consequently, a typical time required to collect two good data tapes at one temperature for the zero-angle experiments was greater than 2 hours, compared to less than one hour for two tapes of data for finite-angle studies of the polarized Rayleigh component. The $C(\tau)$ calculated using all the data on the tape were calculated at a later date using the RK08 disk.

In the computation of $C(\tau)$, one had the option of calculating a single sequence of p points at q data point intervals, or two sequences of p and r points at intervals of q and s points. For example, most of the calculations performed in this study involved the computation of 71 points (point 1 indexed as 0) at every point and then 180 points at 10 point intervals, starting with point 81. The first computation was stored in tape blocks 4 and 5 while the second computation was stored in blocks 6 and 7. At the end of the computation, a contiguous display of both segments of $C(\tau)$ [i.e., not the entire contents of blocks 4 and 5 but only those locations storing $C(\tau)$] appeared on the scope of the PDP-12 at the end of the calculation. The values for p,q,r, and s were variable quantities that were read by the computer through the sense switches on its front panel.

VIII. Results

The calculated autocorrelation functions obtained from the zero-angle scattered light data are presented in Figures 12-18. A semi-log plot of a typical autocorrelation function is presented in Figure 19 for the data collected at 25 and 500 microsecond intervals. The low frequency ripples that appear in the 500 microsecond data are probably due to mechanical vibrations. To illustrate that the apparent linear portion of the 25 microsecond plot is not the longest relaxation time, the data is also plotted at 10 point intervals. It is inferred from Figure 19 that the autocorrelation function is composed of at least two, and probably several, exponential decay functions. If only the short and long times are to be considered, we can characterize the autocorrelation function by the general equation

$$C(\tau) = A\exp(-\tau/t_1) + B\exp(-\tau/t_2) + C \quad , \qquad (110)$$

where A,B,C are constants and t_1, t_2 are the two characteristic times at the extremes of the semi-log plot. It is shown in Appendix B that these extreme relaxation times are related to molecular relaxation times τ_{molec} by

$$t_c = \tau_{molec}/2 \quad , \qquad (111)$$

where t_c represents either extreme characteristic time. Several of these curves were subjected to a least-squares analysis (see Appendix A for the details).

The error in the parameters t_1 and t_2 obtained from any one particular curve is typically less than 15% with the majority of these curves having an error of approximately 10%. Since the error was computed from the

Figure 12

The autocorrelation function $C(\tau)$ for the K_2HPO_4, KH_2PO_4 buffer at room temperature. The relative magnitude of $C(\tau)$ for the buffer compared to $C(\tau)$ for a .068 mg/ml solution of DNA is approximately 1/4 as determined from the scaling factors in the programs which compute the autocorrelation function and remove the numerical values of the (normalized) autocorrelation function from the tape.

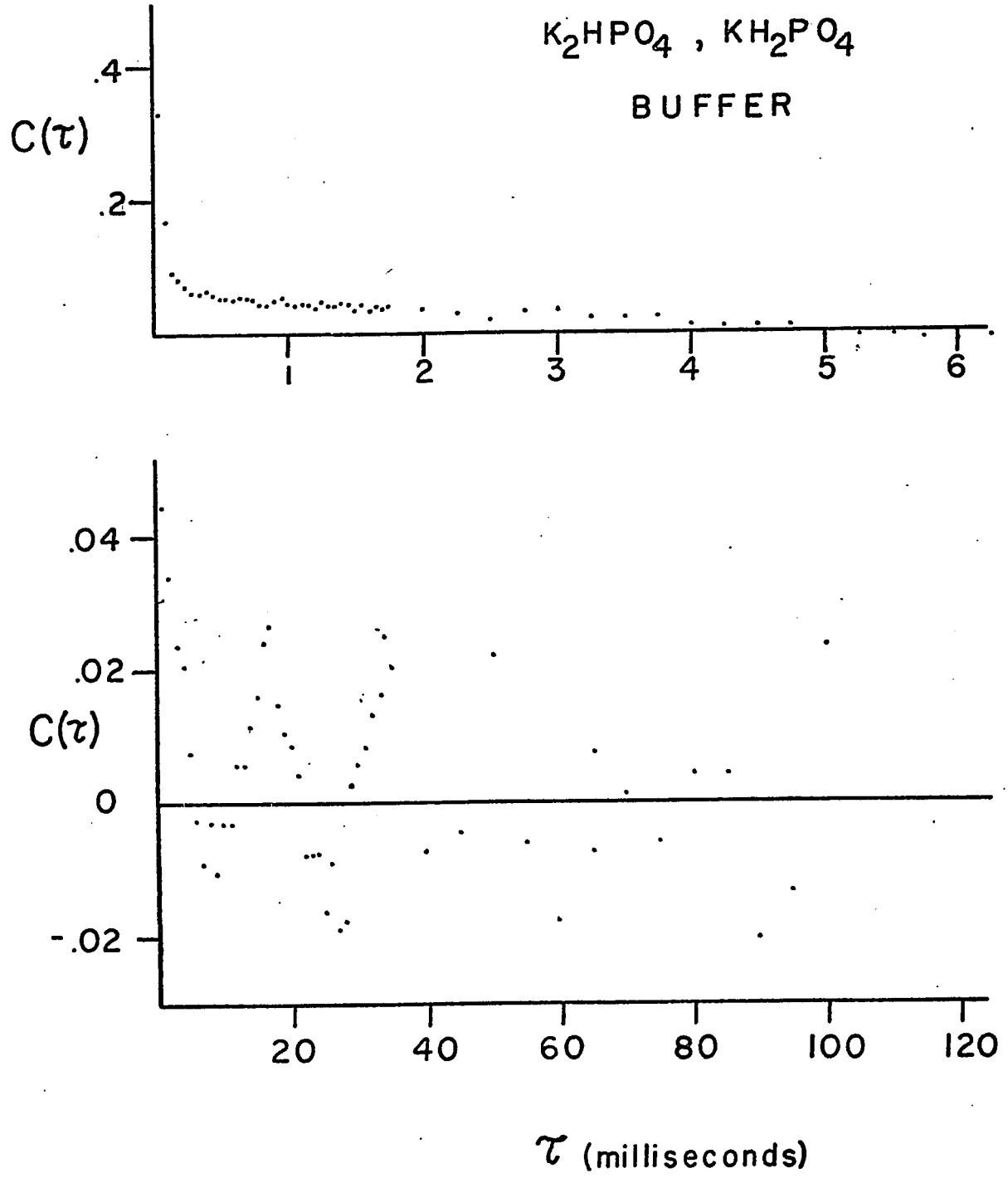
K_2HPO_4 , KH_2PO_4
BUFFER
C(τ)
.4
.2
1
2
3
4
5
6
.04
.02
C(τ)
0
-.02
20
40
60
80
100
120
τ (milliseconds)

Figure 13

Computed autocorrelation function for the .62 mg/ml solution of calf thymus DNA at 48°C. The scattered light was detected by the RCA IP28 phototube.

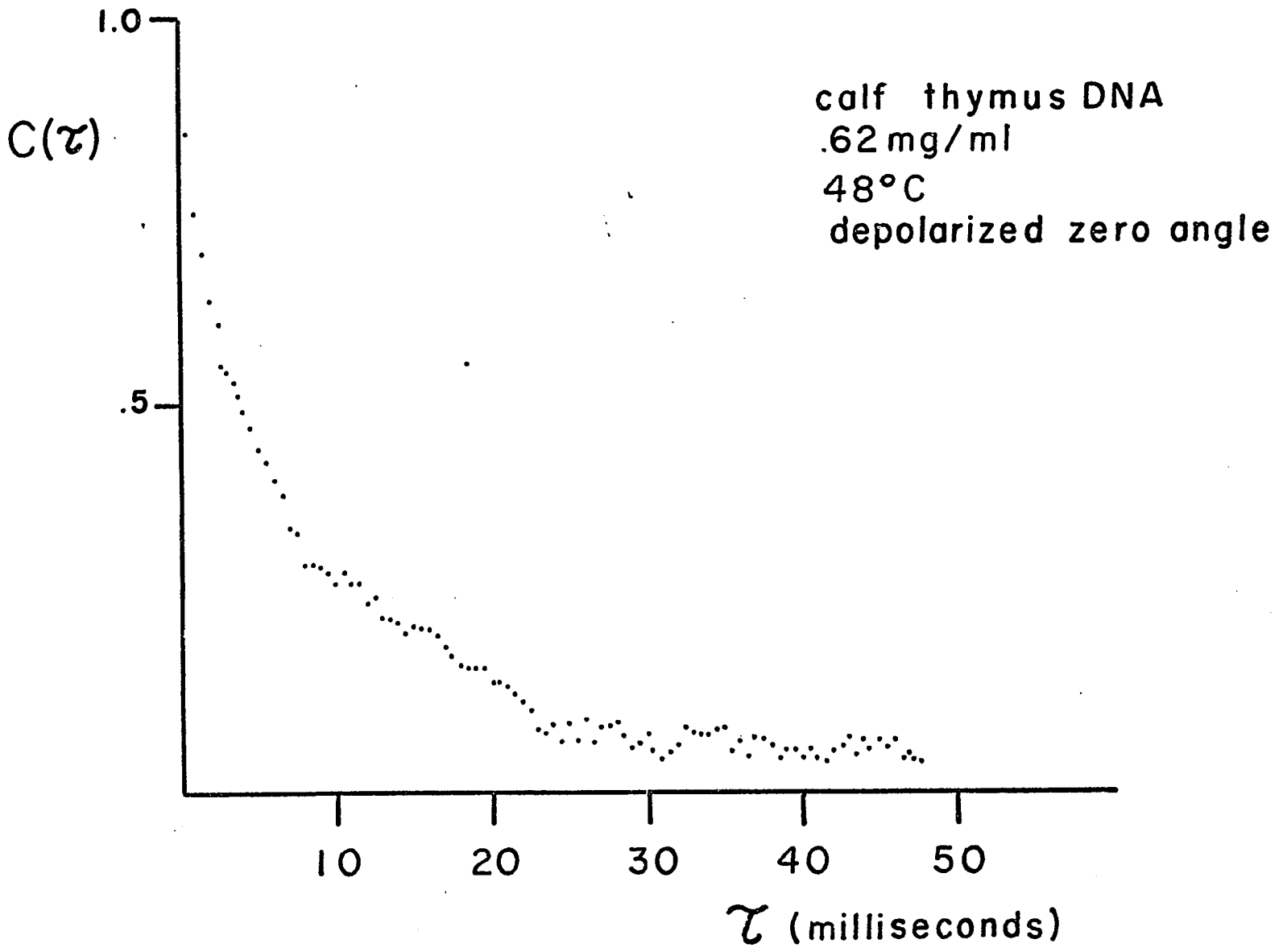
1.0
C(τ)
.5
calf thymus DNA
.62 mg/ml
48°C
depolarized zero angle
10
20
30
40
50
τ (milliseconds)

Figure 14

Computed autocorrelation function for the .068 mg/ml solution of calf thymus DNA at 49°C. The scattered light was detected by the ITT FW 130 phototube. Even though the concentration of DNA was 10 times smaller, the computed curve has less scatter than the curve in Figure 13. This is a result of the better quality of the phototube.

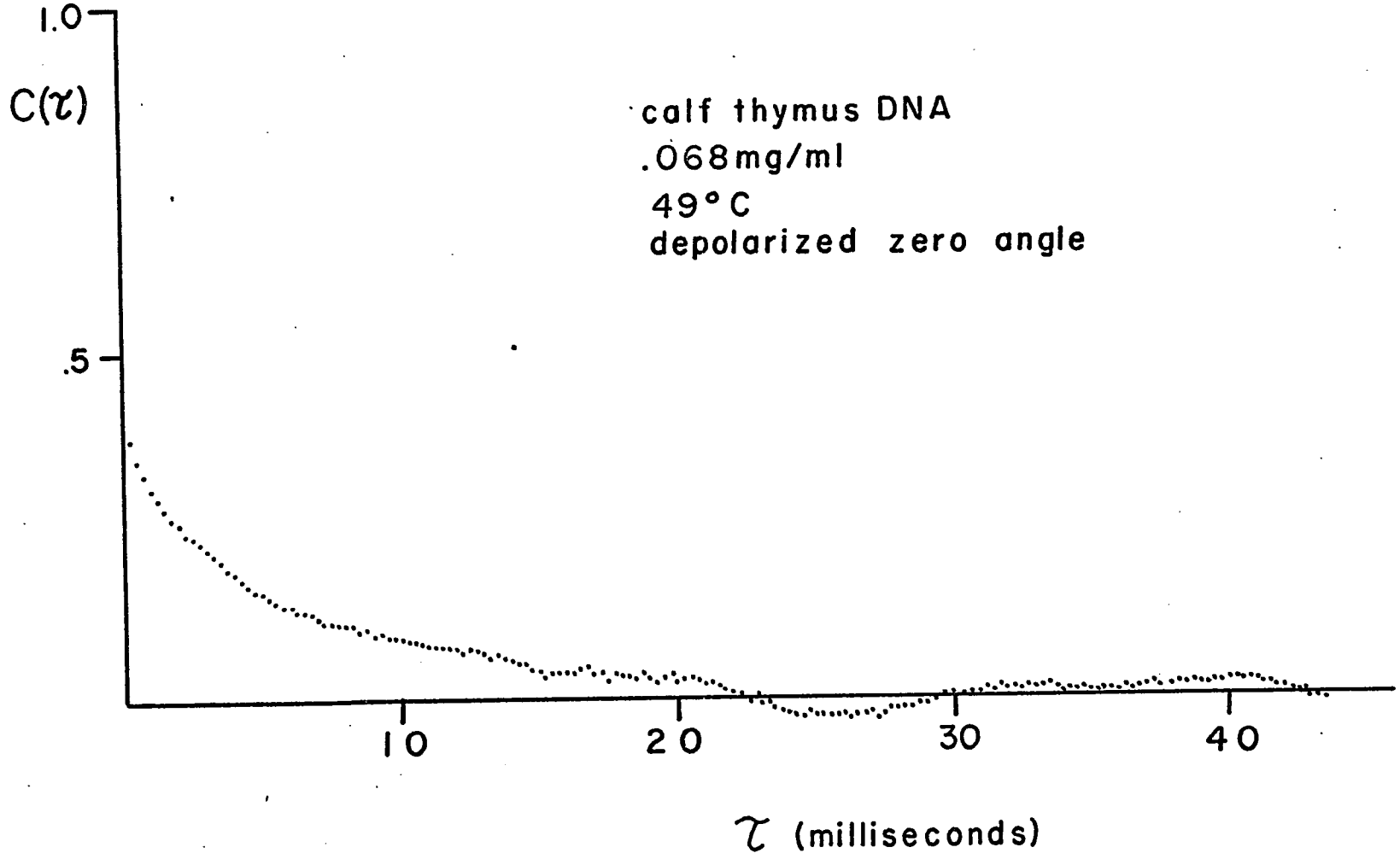
1.0
C(τ)
.5
calf thymus DNA
.068mg/ml
49°C
depolarized zero angle
10
20
30
40
τ (milliseconds)

Figure 15

Computed autocorrelation function for the .068 mg/ml solution of calf thymus DNA at 72°C. Note that the relaxation time at 72°C is longer than at 49°C (cf., Figure 14).

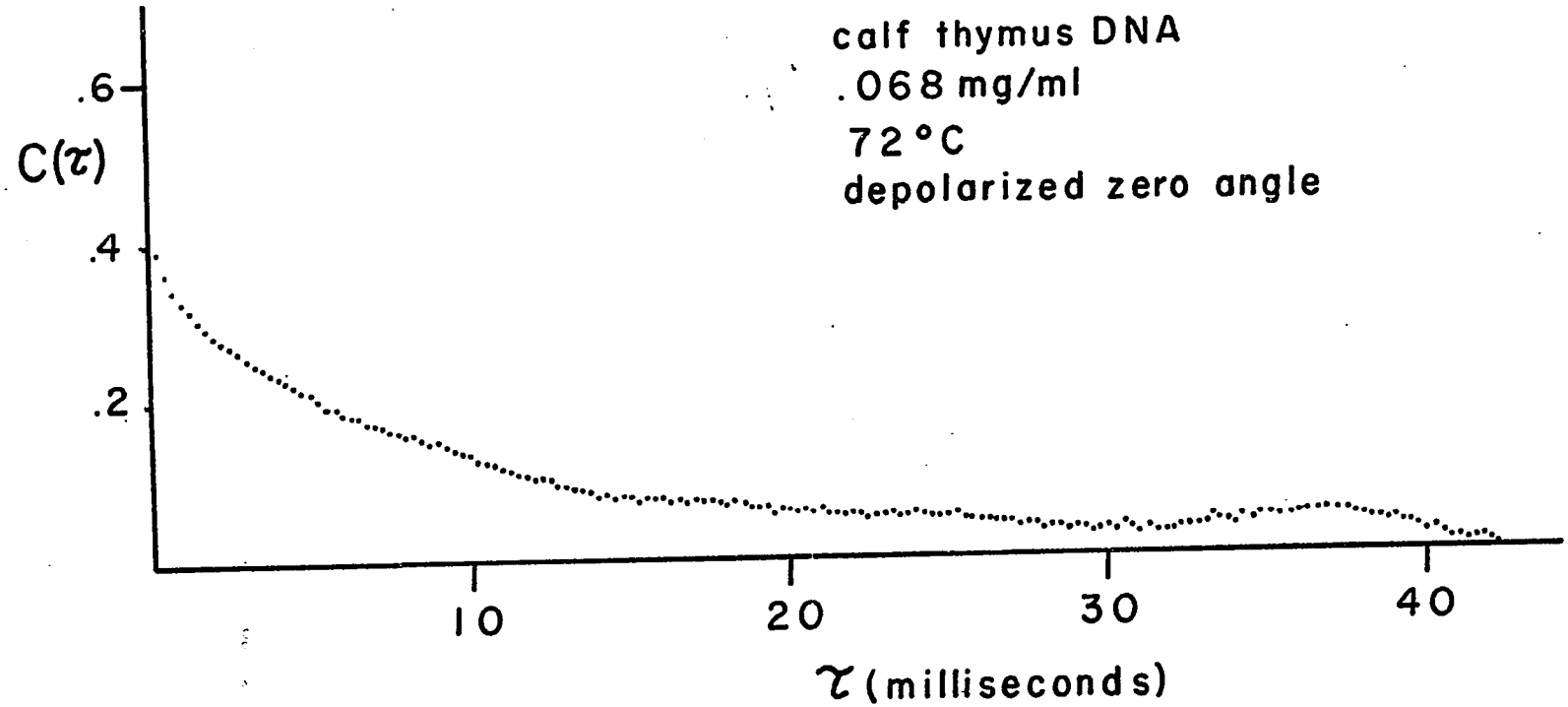
calf thymus DNA
.068 mg/ml
72 °C
depolarized zero angle
C(τ)
.6
.4
.2
10
20
30
40
τ (milliseconds)

Figure 16

Computed autocorrelation function for a .62 mg/ml solution of calf thymus DNA at 85°C. The ripples (approximately 120 Hz) are due to laser beam fluctuations and always occur in the zero-angle depolarized experiments if the second polarizer is not completely crossed to a minimum. The resulting relaxation times are twice as long for this heterodyne-beat signal than for the homodyne-beat signal (second polarizer set at a minimum).

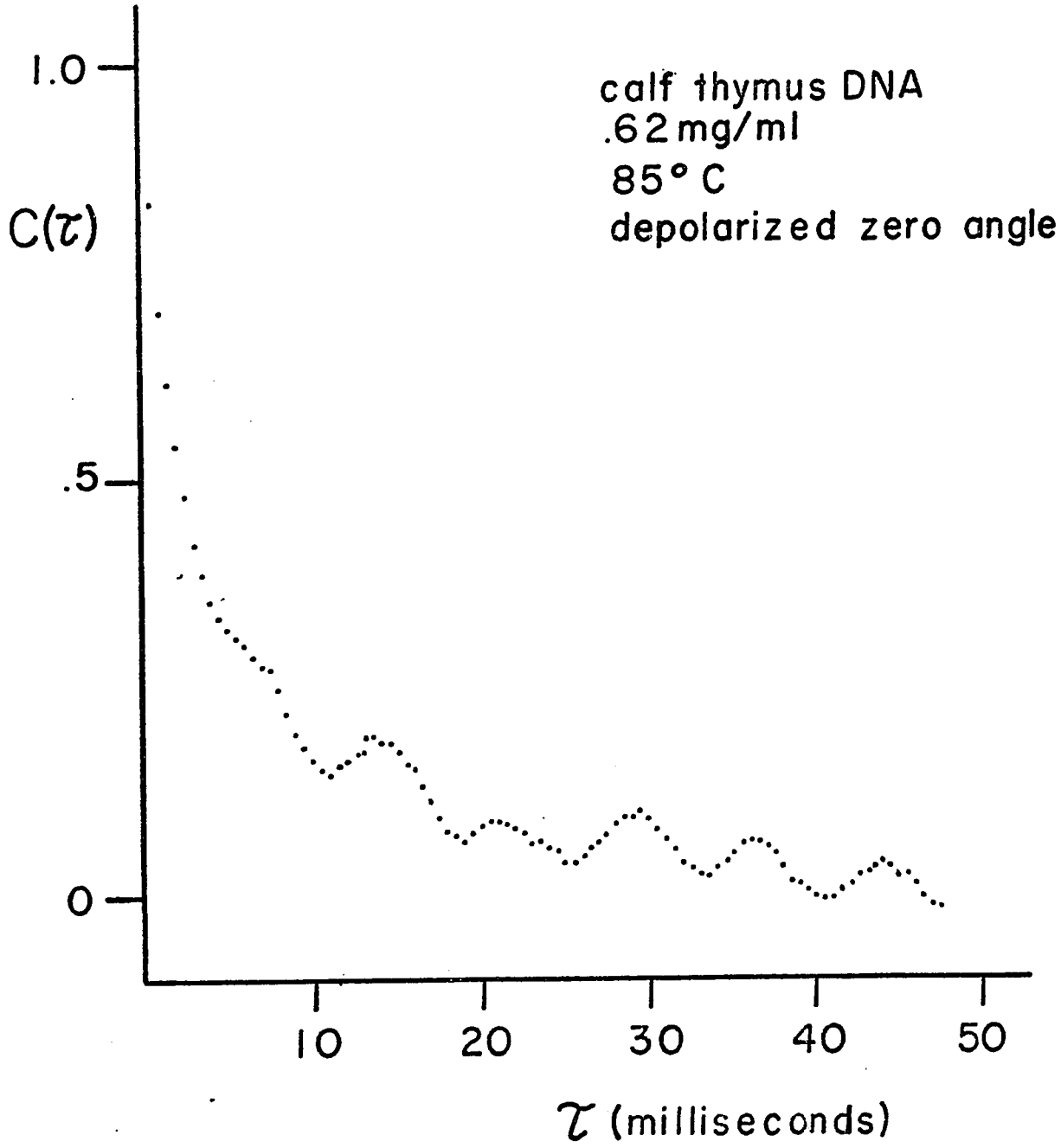
1.0
.5
0
C(τ)
calf thymus DNA
.62 mg/ml
85° C
depolarized zero angle
10
20
30
40
50
τ (milliseconds)

Figure 17

Computed autocorrelation function for a .078 mg/ml solution of calf thymus DNA in which 47 grams of sucrose/100 ml of solution were added.

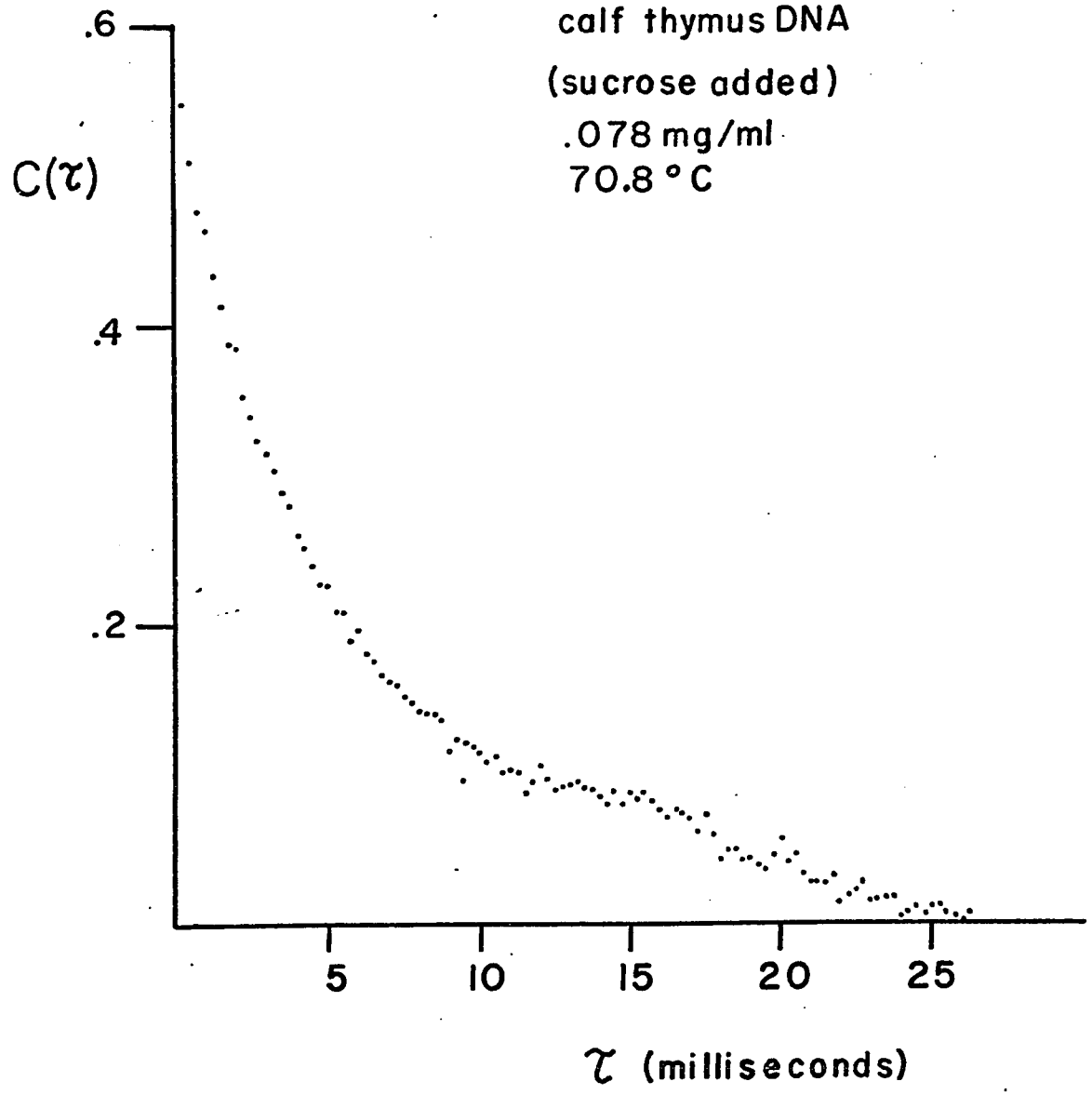
calf thymus DNA
(sucrose added)
.078 mg/ml
70.8 °C
C(τ)
.6
.4
.2
5
10
15
20
25
τ (milliseconds)

Figure 18

Computed autocorrelation function for a .078 mg/ml solution of calf thymus DNA in which 47 grams of sucrose/100 ml of solution were added.

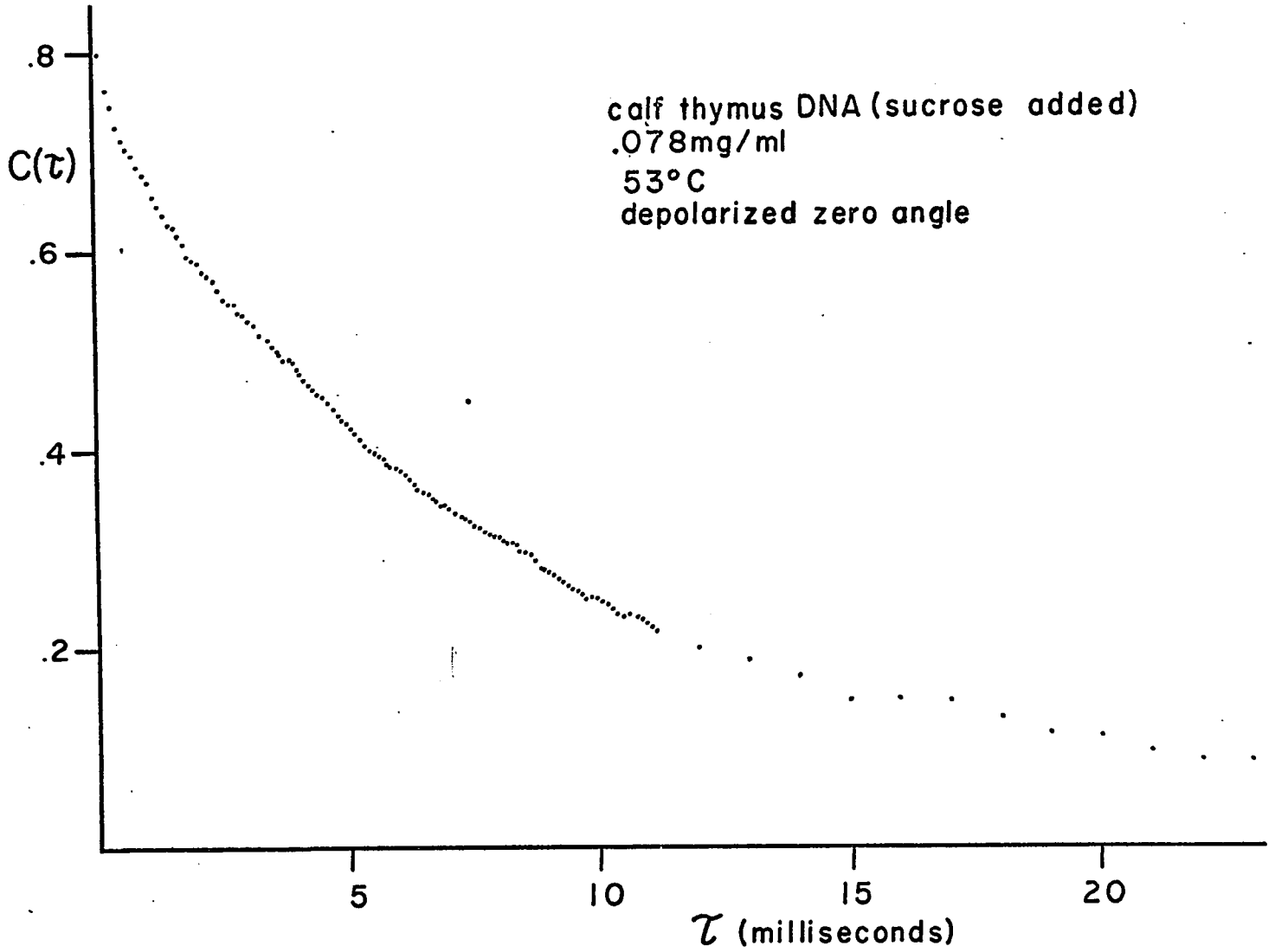
.8
C(τ)
.6
.4
.2
5
10
15
20
τ (milliseconds)
calf thymus DNA (sucrose added)
.078mg/ml
53°C
depolarized zero angle

Figure 19

Semi-log plot of $C(\tau)$ vs. the data point number for the .068 mg/ml concentration of calf thymus in the phosphate buffer at 49°C. The dots (•) represent the computed autocorrelation function from data collected at 25 microsecond intervals and displayed at one point intervals. The triangles (Δ) represent the same autocorrelation function as the dots, with every 10th point being displayed in this plot. The open circles (o) represent the computed autocorrelation function from data collected at 500 microsecond intervals. The ripple is due to mechanical vibration and introduces a periodic component to the autocorrelation.

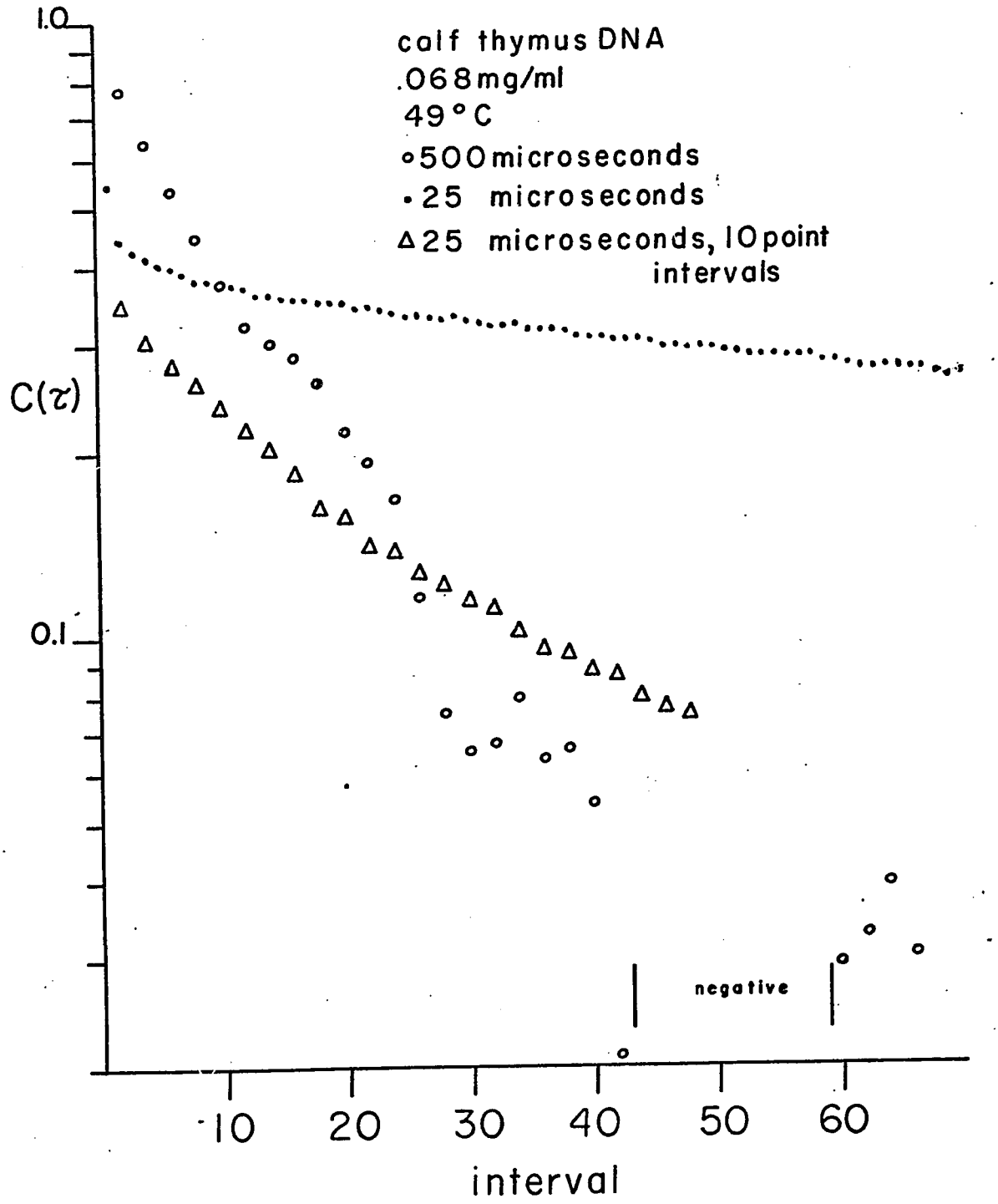
1.0
0.1
C(τ)
calf thymus DNA
.068 mg/ml
49 °C
o 500 microseconds
• 25 microseconds
Δ 25 microseconds, 10 point intervals
negative
10
20
30
40
50
60
interval

maximum and minimum slopes of the semi-log plot, the major source of the error is due to the superimposed mechanical vibration. The curve in Figure 16 has the largest error of the data reported in this study (approximately 60%). The higher frequency (~120 Hz) ripples occurring in this particular function are due to the intensity oscillations in the laser light and not due to the lower frequency vibrations. This is a typical result for the zero-angle depolarized experiment if the second polarizer is not crossed to a minimum. The scattered signal then heterodyne-beats with the primary beam and the characteristic relaxation time is then equivalent with the molecular relaxation time,

$$t_c = \tau_{molec} \tag{112}$$

Therefore, the characteristic times obtained from heterodyne-beat experiments are twice as long as those obtained from the homodyne-beat (self-beat) experiments (see Appendix B).

The characteristic times for the calf thymus DNA solutions used in these experiments are presented in Tables IV and V. The relaxation time-temperature profiles for these experiments are presented in Figures 20-22. Except for the .078 mg/ml solution with a high concentration of sucrose (47 g/100 ml of solution) a characteristic feature of these curves is the maximum which occurs approximately 4^{o} above the T_m. The data obtained on the sucrose samples are not as reliable as the .62 and .068 mg/ml samples because the former samples were filtered through the commercial Millipore filter holder under pressure, and it is not known if the DNA was sheared to a lower molecular weight. This is also the reason why no definite conclusions can be drawn about the viscosity dependence of the relaxation times. Comparing Figures 20 and 21,

TABLE IV

Worthington Calf Thymus DNA in

K_2HPO_4, KH_2PO_4 buffer

Concentration (mg/ml)	T(°C)	Characteristic Time (microseconds)					Data Collection Interval (microseconds)
		Graph		Least-Squares			
		t_1	t_2	t_1	σ	t_2	
.62	48	920	7400	1230		9548	25(a)
	48	(1800)	(11500)				500(d)
	53	910	11000				500(d)
	57	980	10900	580	5.8×10^{-2}	10900	25(a)
	57	1060	13000				500(d)
	63			733	4.5×10^{-3}	9800	25(a)
	63	950	11200				500(b)
	72	3120	17000				500(b)
	76			602		8700	25(b)
	76	1590	14000				500(a)
	80	1320	9800				500(a)
	85	600	6100	-	7×10^{-3}	1800	25(c)
	85	(1380)*	(12700)*				500(d)
.068	49.5	690	6500				25(b)
	52	1190	8120	-	6×10^{-3}	5452	25(b)
	55.4	410	5800				25(b)
	60.3	-	7100				25(b)
	68.2	-	7000				25(a)
	72	525	10000	605	1×10^{-2}	9007	25(a)
	76.4	840	10200	343	1×10^{-2}	7970	25(b)
	78.8	530	5710	-	8×10^{-3}	4444	25(c)
	49.5	-	7200				500(b)
	52	-	6700				500(c)
	55.4	-	7200				500(c)
	60.4	-	6000				500(c)
	68.2	-	11350				500(b)
	72	-	13200				500(b)
	76.4	-	10300				500(b)

( ) = unreliable data--error greater than 15%.

* heterodyne-beat

Data rating: (a) = negligible ripple to (d) = ripple is 10% of curve

TABLE V

Worthington Calf Thymus DNA in

K_2HPO_4, KH_2PO_4 buffer + sucrose

Concentration (mg/ml)	T (°C)	Characteristic Time (microseconds)				Solution Viscosity η	Data Collection Interval (microseconds)
		graph		least-squares			
		t_1	t_2	t_1	t_2		
.078 + sucrose	46	-	12760	2096	12214	2.583	25
	53.5	-	9350			2.055	25
	53.5	-	8740			2.055	500
	65	-	6880			1.561	25
	65	-	7800			1.561	500
	70.8	-	6750	-	6580	1.390	25
	70.8	-	7200			1.390	500
	82	-	4950			1.051	25
.018 + sucrose	49.1	590	10870			1.136	25
	60.5	1140	10870			.956	25
	60.5	-	7180			.956	250
	67.4	-	12270			.797	250
	72.5	-	6600			.729	250

Figure 20

Characteristic times as a function of temperature for the .068 mg/ml solution of calf thymus DNA in phosphate buffer. The open circles (o) are the longest relaxation times obtained from data collected at 500 microsecond intervals. The crosses (x) above the value of 6 milliseconds are the longest relaxation times obtained from data collected at 25 microsecond intervals while the crosses below 6 milliseconds are the shortest relaxation times obtained from the same data. The solid circles (●) are the values for the longest relaxation times obtained from a least-squares analysis of the 25 microsecond data.

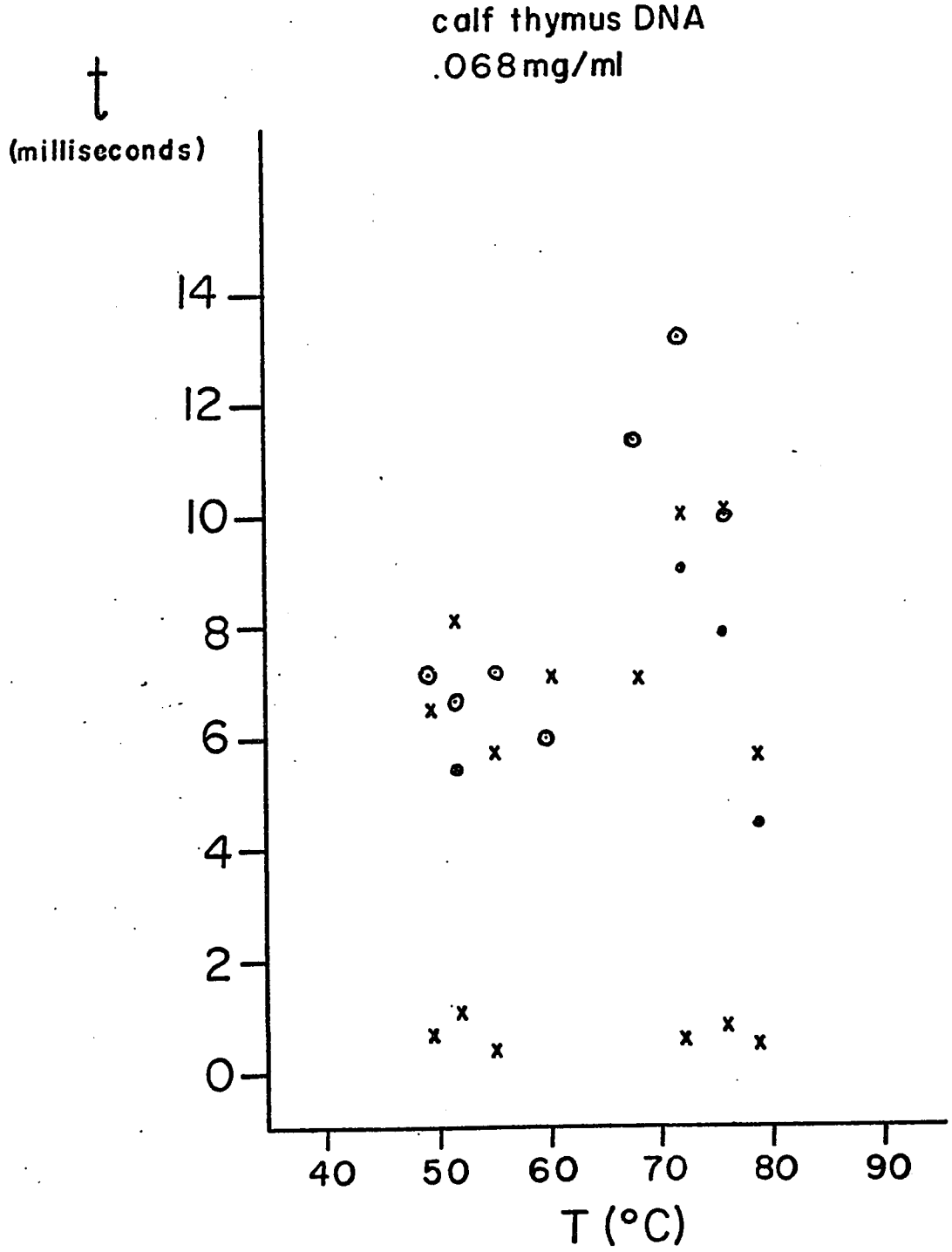
calf thymus DNA
.068 mg/ml
t
(milliseconds)
14
12
10
8
6
4
2
0
40
50
60
70
80
90
T (°C)

Figure 21

Characteristic times as a function of temperature for the .62 mg/ml solution of calf thymus DNA. The notation is the same as in Figure 20. The least-squares analysis of the 25 microsecond data at 85°C (represented by (S)) resulted in essentially one exponential function for $C(\tau)$. This is probably due to convergence of the least-squares analysis to a nearby minimum (but not the absolute minimum) in the function S since a semi-log plot clearly indicates at least two exponential functions.

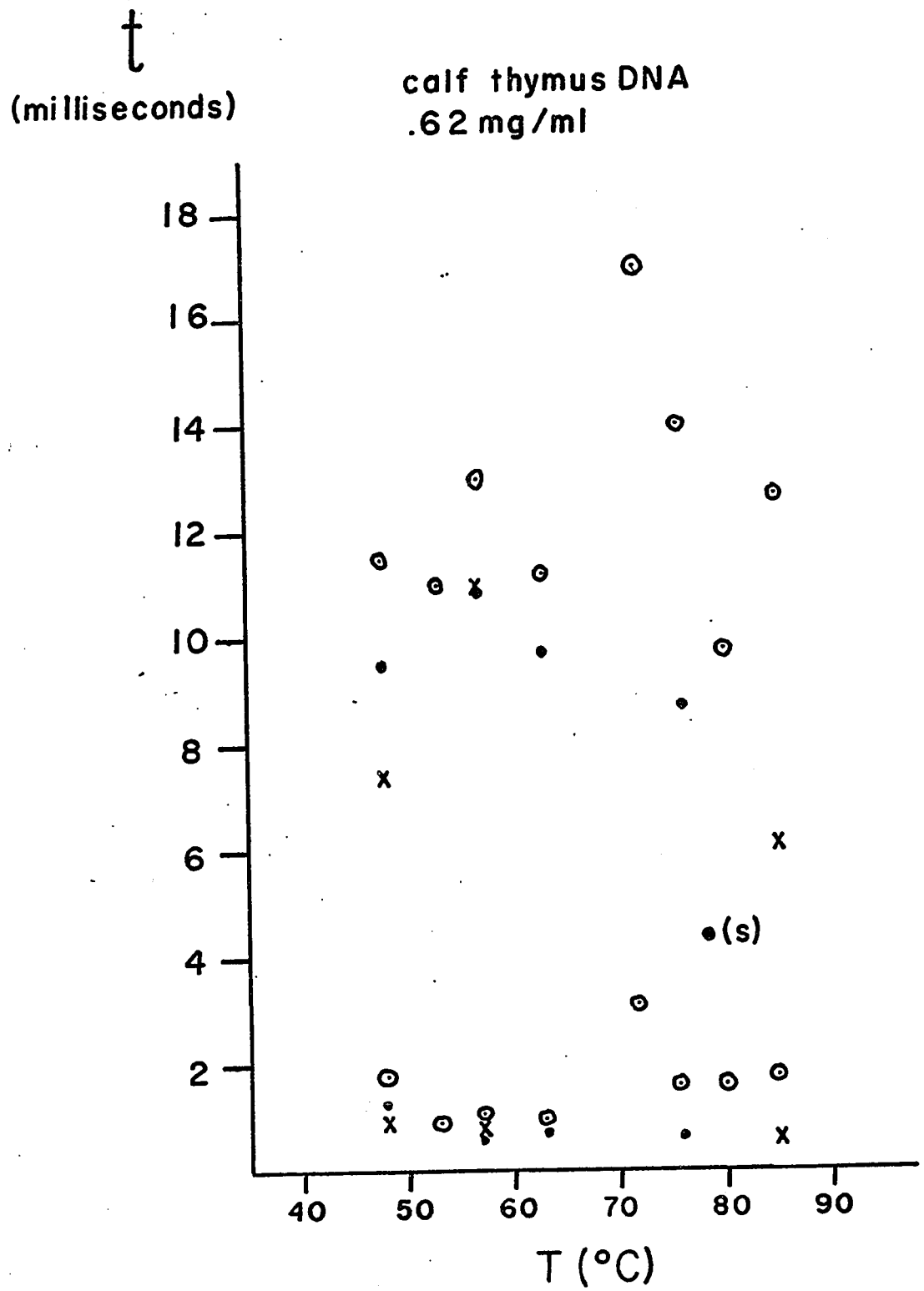
t
(milliseconds)
calf thymus DNA
.62 mg/ml
18
16
14
12
10
8
6
4
2
(s)
40
50
60
70
80
90
T (°C)

Figure 22

Longest characteristic relaxation times for calf thymus DNA dissolved in the phosphate buffer and then diluted with sucrose (in buffer) solutions. The triangles (Δ) are the values of the relaxation times obtained from data collected at 25 microsecond intervals while the inverted triangles (∇) are the values obtained from data collected at 250 microsecond intervals. The crosses (x) denote the values of the relaxation times obtained from data collected at 25 microsecond intervals and the open circles represent the values calculated from data collected at 500 microsecond intervals. It is not known if the higher concentrations of both DNA and sucrose (cf., Table V for the viscosities of these samples) are responsible for the suppression of the maximum that was observed in the other samples or if this apparent supporession results from shearing the DNA in the filtering process.

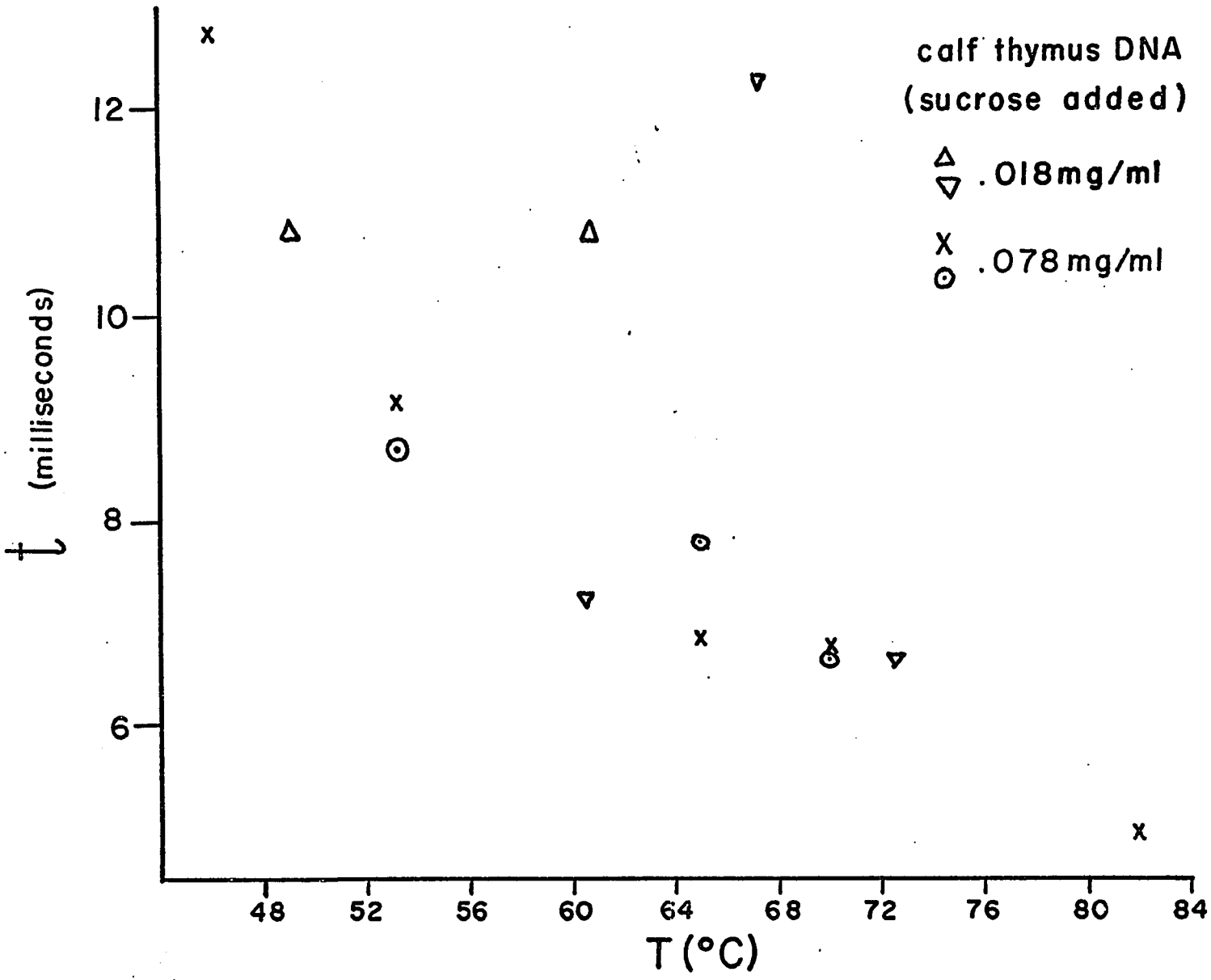
calf thymus DNA
(sucrose added)
.018mg/ml
.078mg/ml
12
10
8
6
(milliseconds)
48
52
56
60
64
68
72
76
80
84
T (°C)

there does appear to be a concentration dependence (also implying a viscosity dependence) in the relaxation times. If a viscosity dependence is present, then one might expect it to be a classical-type of dependence for these large molecules. The characteristic relaxation time should then have the general form

$$t_c = \eta F(r)/T \quad , \tag{113}$$

where η is the viscosity, T is the absolute temperature, and F(r) absorbs all of the constants and is a function of the molecular dimensions r. The temperature profiles of F(r) for the samples used in the present study are presented in Figures 23 and 24.

The temperature profile of the optical density A_{260} for DNA in the potassium phosphate buffer is presented in Figure 25 along with the temperature profiles of the longest relaxation time and η_{sp}/c for the .068 mg/ml samples.

The polarized finite-angle Rayleigh component of a .018 mg/ml solution of DNA was also investigated in the temperature regions immediately below the transition, at the maximum of F(r), and in a region where the specific viscosity had decreased by a factor of approximately 2 from the first region. Data was taken at several angles in the region prior to the transition in order to obtain the diffusion coefficient from the $\sin^2(\theta/2)$ dependence, which is illustrated in Figure 26. The results of the finite-angle study are summarized in Tables VIII and IX.

TABLE VI

Concentration (mg/ml)	Temperature °C	Characteristic Times (microseconds) t_1	Characteristic Times (microseconds) t_2	$F(r)_a = \frac{t_a T}{\eta}$ sec-deg / centipoise $F_1(r)$	$F(r)_a = \frac{t_a T}{\eta}$ sec-deg / centipoise $F_2(r)$	Data Collection Interval (microseconds)
.62	48	920	7400	.185	1.495	25
.62	48	(1800)	(11500)	.362	2.32	500
.62	48*	1230	9548	.248	1.930	25
.62	53	910	11000	.204	2.480	500
.62	57	980	10900	.239	2.689	25
.62	57*	580	10900	.142	2.680	25
.62	57	1060	13000	.260	3.196	500
.62	63*	733	9792	.212	2.834	25
.62	63	950	11200	.275	3.242	500
.62	72	3120	17000	1.235	6.743	500
.62	76*	600	8700	.245	3.546	25
.62	76	1590	14000	.648	5.707	500
.62	80	1320	9800	.612	4.541	500
.62	85	600	6100	.321	3.297	25
.068	49.5	690	6500	.347	3.296	25
.068	49.5	-	7174	-	3.637	500
.068	52	1190	8120	.633	4.323	25
.068	52*	-	5452	-	2.901	25
.068	52	-	6700	-	3.565	500
.068	55.4	410	5773	.231	3.267	25
.068	55.4	-	7200	-	4.074	500
.068	60.3	-	7100	-	4.436	25
.068	60.4	-	6000	-	3.751	500
.068	68.2	-	7000	-	5.068	25
.068	68.2	-	11350	-	8.217	500
.068	72	525	10000	.415	7.903	25
.068	72*	605	9007	.478	7.118	25
.068	72	-	13200	-	10.432	500
.068	76.4	840	10162	.723	8.704	25
.068	76.4*	343	7970	.294	6.827	25
.068	76.4	-	10300	-	8.823	500
.068	78.8	530	5710	.473	5.146	25
.068	78.8*	-	4444	-	4.004	25

*Least-squares values

Figure 23

Temperature dependence of $F(r) = tT/\eta$ for the longest-relaxation time of calf thymus DNA dissolved in the phosphate buffer. The time intervals used in collection data are: delta (Δ), 500 microseconds; theta ($\ominus$), 25 microseconds; crosses (x), 25 microseconds; open circles (o), 500 microseconds. The symbols (ϕ) and ($\bullet$) represent the least-squares computed values from the 25 microsecond data of the..62 mg/ml and .068 mg/ml solutions, respectively.

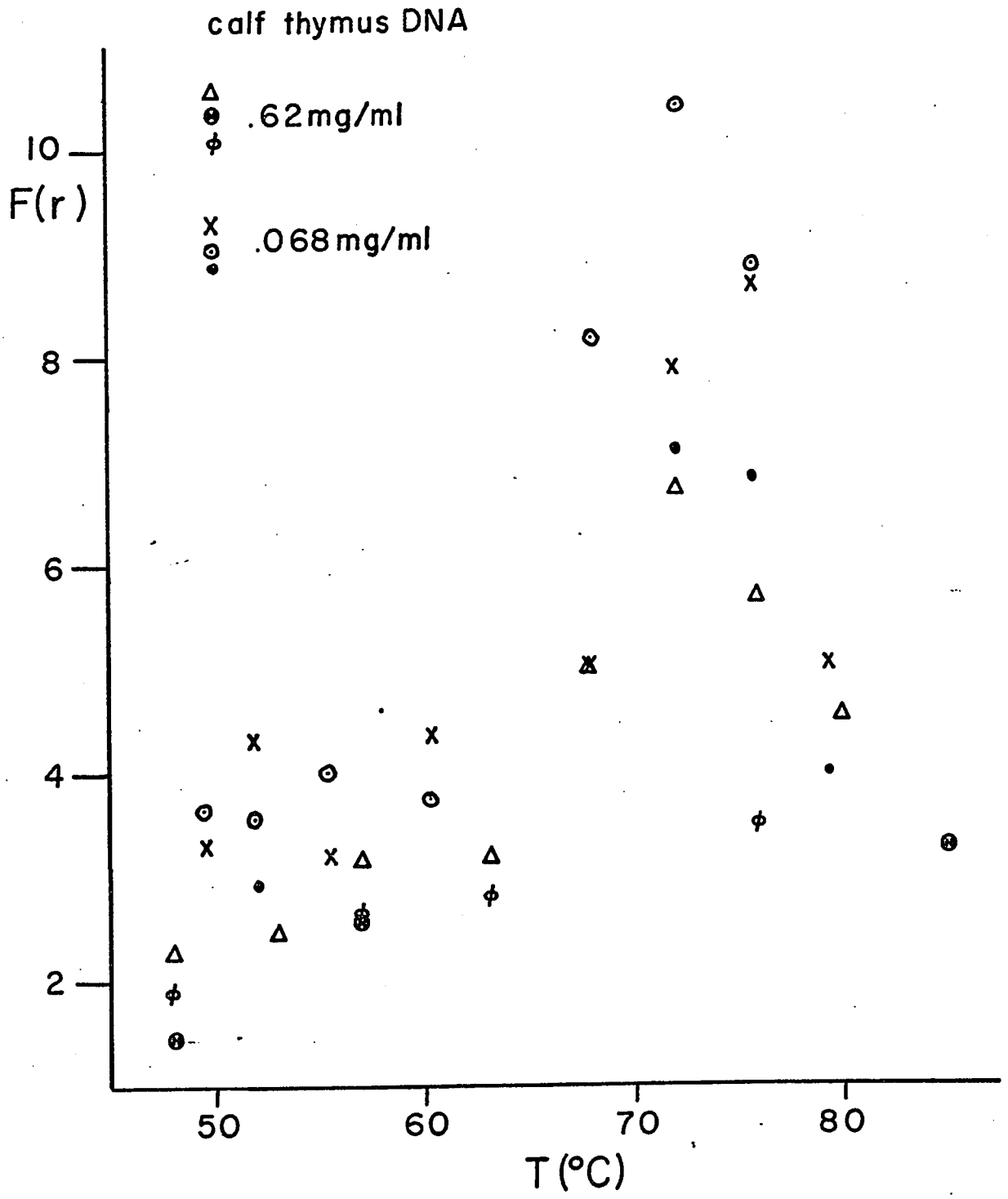
calf thymus DNA
.62mg/ml
.068mg/ml
F(r)
10
8
6
4
2
50
60
70
80
T(°C)

TABLE VII

Concentration (mg/ml)	Temperature °C	Characteristic time t_2 (microseconds)	$F_2(r) = \frac{t_2 T}{\eta}$	Data Collection Interval (microseconds)
.078+sucrose	46°	12755	1.5756	25
	46°*	12214	1.5087	25
	53.5	9346	1.4846	25
	65	6875	1.4889	25
	70.8	6750	1.6701	25
	70.8*	6580	1.6281	25
	82	4950	1.6714	25
	53.5	8740	1.3884	500
	65	7800	1.6893	500
	70.8	7200	1.7815	500
.018+sucrose	49.1	10871	3.0815	25
	60.5	10870	4.0450	25
	60.5	7102	2.6726	250
	67.4	12270	5.2396	250
	72.5	6600	3.1269	250

*Least-squares calculation

Figure 24

Temperature dependence of $F(r) = tT/\eta$ for the longest relaxation time of calf thymus DNA solutions diluted with concentrated sucrose solutions. The time intervals used in collecting data are: triangles (Δ), 250 microseconds; inverted triangles (∇), 25 microseconds; open circles (o), 500 microseconds; crosses (x), 25 microseconds.

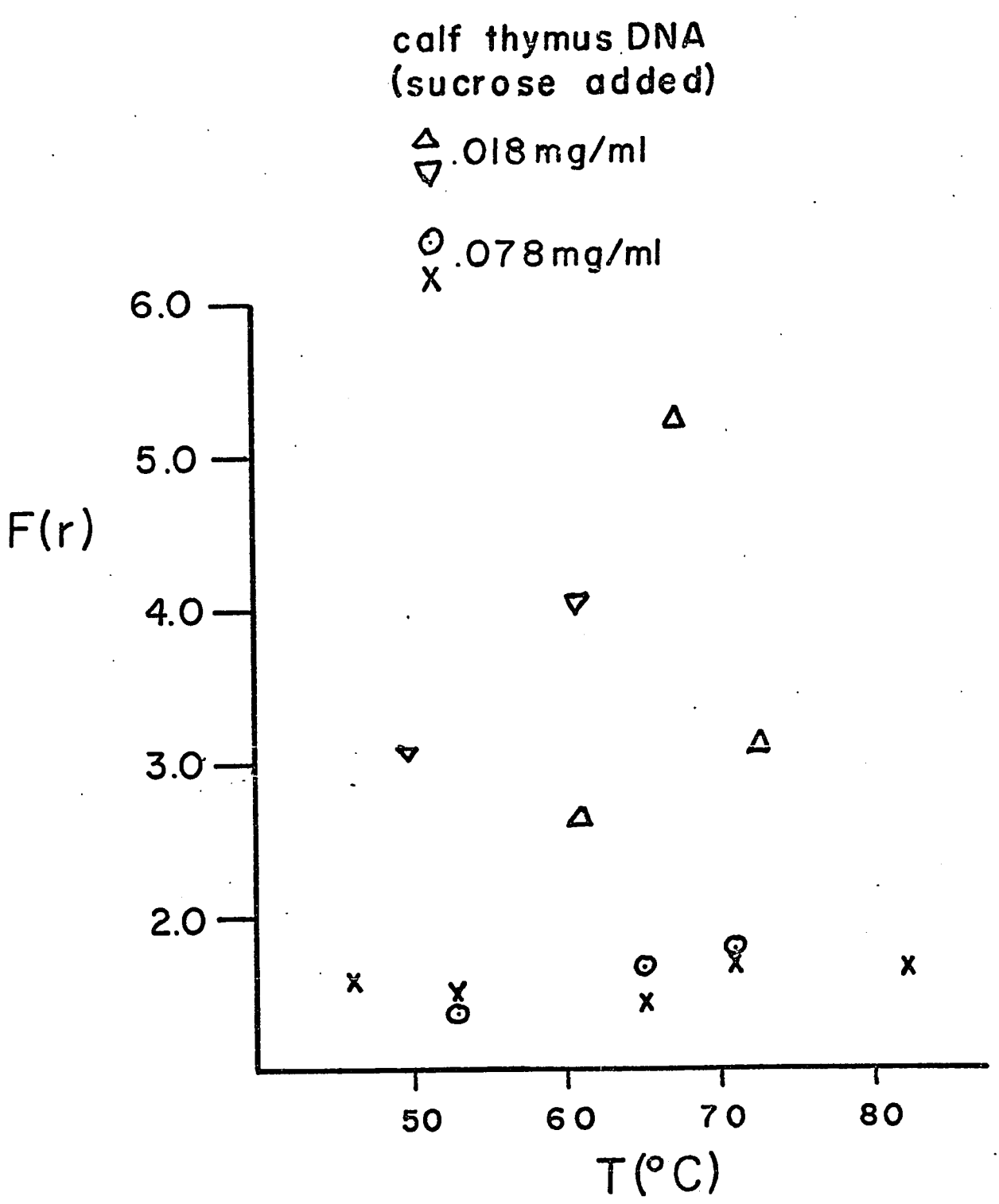
calf thymus DNA
(sucrose added)
.018 mg/ml
.078 mg/ml
6.0
5.0
4.0
3.0
2.0
F(r)
50
60
70
80
T(°C)

Figure 25

Temperature profiles of the reduced viscosity and longest relaxation time for the .068 mg/ml solution of DNA along with the optical absorbance of DNA in the phosphate buffer. The ordinate for the reduced viscosity (x) is in units of dl/g. The ordinate for the relaxation time (◎,⊙,o) is in units of milliseconds. The single open circles (o) are the characteristic times obtained from the 25 microsecond data. The double circles (◎) are the longest relaxation times obtained from data collected at 500 microseconds. The error was determined from the maximum and minimum slope of the semi-log plot of the autocorrelation function. The triple circles are the values obtained from a least-squares analysis of the 25 microsecond data.

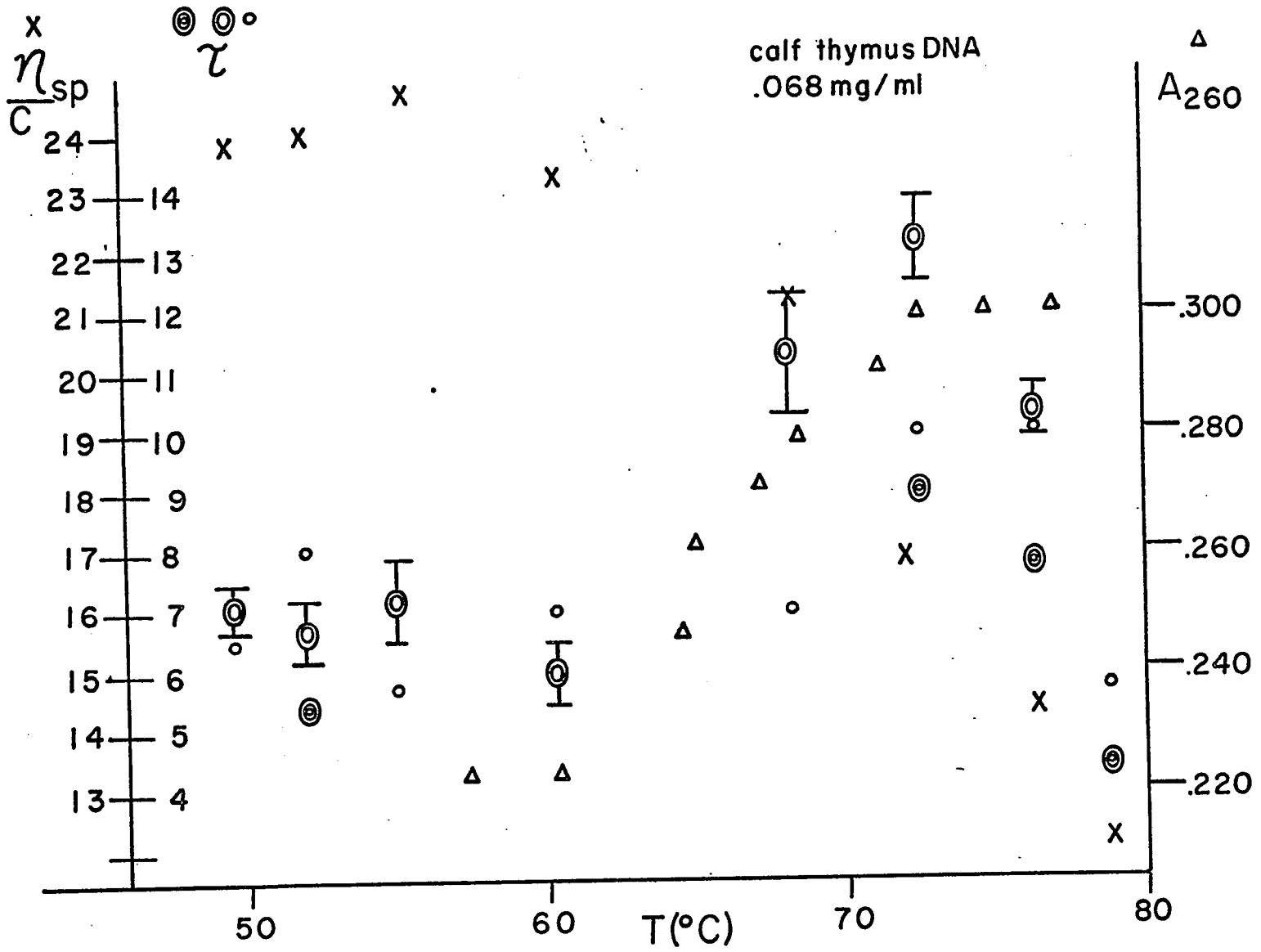
calf thymus DNA
.068 mg/ml
$\frac{\eta_{sp}}{C}$
τ
A_{260}
24
23
22
21
20
19
18
17
16
15
14
13
14
13
12
11
10
9
8
7
6
5
4
.300
.280
.260
.240
.220
50
60
70
80
T(°C)

Figure 26

$Sin^2(\theta/2)$ dependence of the reciprocal of the shortest (t_1) and longest (t_2) characteristic times obtained from finite-angle polarized Rayleigh scattering data. The long time component is probably due to aggregation or dust. The non-zero intercept is indicative of rotational (or internal) relaxation processes contributing to the scattered light in addition to the translational relaxation process. The diffusion coefficient obtained from the slope of $(1/t_1)$ vs. $\sin^2(\theta/2)$ is comparable to the value $.2 \times 10^{-7} cm^2/sec$ obtained by Dubin, Lunacek, and Benedek using self-beating light scattering techniques.

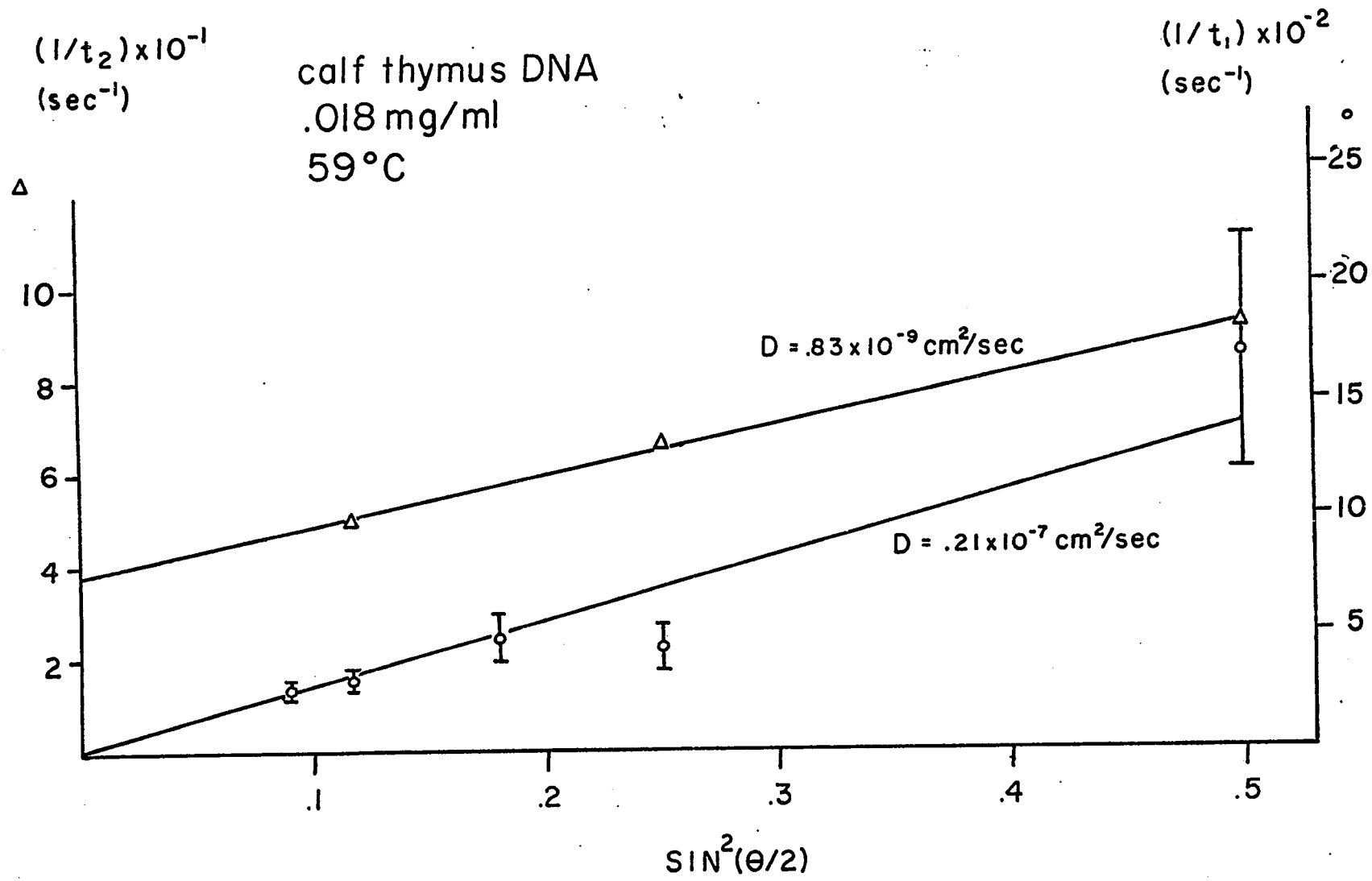
$(1/t_2)\times10^{-1}$
(sec^{-1})
calf thymus DNA
.018 mg/ml
59°C
$(1/t_1)\times10^{-2}$
(sec^{-1})
Δ
o
10
8
6
4
2
25
20
15
10
5
$D = .83\times10^{-9}\ cm^2/sec$
$D = .21\times10^{-7}\ cm^2/sec$
.1
.2
.3
.4
.5
$SIN^2(\theta/2)$

TABLE VIII

Finite-Angle Polarized Rayleigh Scattering

.018 mg/ml calf thymus DNA

(long times)

θ	$\sin^2(\theta/2)$	$\tau \times 10^2$ (sec)	$10^4 \tau \sin^2(\theta/2)$ (sec)	T ($^\circ$C)
35	.09	7.5	67	47.8
40	.117	3.0	35	47.8
40	.117	2.0	23	59.8
50	.179	5.1	96	59.8
60	.250	1.4	33	59.8
60	.250	1.6	39	59.8
90	.500	1.1	55	59.8
50	.179	1.7	31	72.5
60	.250	1.8	45	72.5
50	.179	1.4	26	77.4
50	.179	1.2	21	77.4

TABLE IX

Finite-Angle Polarized Rayleigh Scattering

.018 mg/ml Calf Thymus DNA

(short times)

θ	$\sin^2(\theta/2)$	$\tau \times 10^3$ (sec)	$1/\tau$ (sec^{-1})	$D \times 10^7$ cm^2/sec	T ^oC	% error[a]
35	.09	3.75	266	.22	59	3
40	.117	3.28	306	.20	59	7
50	.179	2.06	485	.21	59	24
60	.250	2.35	425	.13	59	11
90	.500	.58	1720	.26	59	27
60	.250	2.7	373	.11	72.5	
50*	.179	3.5	286	.12	72.5	
50	.179	1.66	602	.26	77.4	
50	.179	1.82	550	.23	77.4	

[a]estimated from maximum and minimum slope

*Least-squares calculation

IX. Discussion

On the basis of a comparison of the A_{280}/A_{260} ratio and the computed intrinsic viscosity (high shear rate) of the calf thymus DNA used in the present study with existing literature values, we infer that the DNA samples were of low protein contamination and were not unusually degraded. The total percent absorbance change $[A_{260}(84) - A_{260}(27)]/A_{260}(27) \simeq 37\%$ further suggests that all of the DNA was in the native form. A change in the T_m by almost 9^o (to a higher value) resulting from the addition of an excess of Mg^{2+} (Mg/P ≃ 4) implies that the phosphate groups of the EDTA treated DNA possess very few, if any, bound divalent ions. Comparison of Figure 12 with Figures 13-18 indicates that the Millipore-filtered solvent (i.e., dust particles present in the solvent) does not contribute significantly to the autocorrelation function. We must conclude, therefore, that the relaxation times obtained from the computed autocorrelation functions pertain to molecular relaxation processes in the DNA molecule.

A number of determinations of orientational relaxation times of native DNA's have been previously reported and the more recent of these are collected in Table X together with the method of measurement. Except for the dielectric dispersion figure all direct measurements were performed by stopped-flow techniques. The dieletric dispersion probably arises almost entirely from the ion-atmosphere polarization and provides essentially no hard information regarding orientational relaxation of the DNA itself. A number of estimates of the rotational diffusion coefficient based on steady-state flow-dichroism or birefringence measurements have also been made, and these results too are presented in Table X. It is necessary to assume that the molecules are rigid ellipsoids in order

TABLE X

Reported Literature Values for Related Molecules

Compound	(Orientation Relaxation) τ (sec)	D_Ω (sec^{-1})	Method
T4 DNA	.5(short)		stop-flow dichroism[a]
T4 DNA (dilute salt)0	.45		stop-flow dichroism[b]
calf thymus DNA (.19 mg/ml)		38	flow dichroism[c]
calf thymus DNA (.084 mg/ml)		35	flow dichroism[c]
T2 DNA (.031 mg/ml)		31	flow dichroism[c]
T2 DNA (at infinite dilution)	.45		stop-flow birefringence[d]
calf thymus DNA	.0013*		dielectric relaxation[e]
calf thymus DNA (.33 mg/ml) low salt		45	flow dichroism[f]
T2 DNA	.3		flow birefringence[g]

*time at which Mg^{2+} and Na^{+} conductivities were equal

a--P.R. Callis and N. Davidson, Biopolymers, 7, 335 (1969).
b--P.R. Callis and N. Davidson, Biopolymers, 8, 379 (1969).
c--A. Wada, Biopolymers, 2, 361 (1964).
d--D.S. Thompson and S.J. Gill, J. Chem. Phys., 47, 5008 (1967).
e--S. Takashima, Biopolymers, 5, 899 (1967).
f--L.F. Cavalieri, M. Rosoff, and B. Rosenberg, J. Am. Chem. Soc., 78, 5239 (1956)
g--R. Harrington, Biopolymers, 6, 105 (1968).

to obtain a value of the rotational diffusion coefficient from these measurements. The T2 and T4 DNA's used in the stopped-flow measurements had molecular weights of $1.2\text{-}1.3\times10^8$, much higher than the calf thymus used in this study. Callis and Davidson[25] found an empirical relation between the longest relaxation time and the molecular weight

$$\tau_1 = 5.0\times10^{-14}M^{1.6} \quad , \tag{114}$$

Using this relation one may estimate the time appropriate for calf thymus DNA of any particular molecular weight. The molecular weight of this calf thymus DNA was estimated from its viscosity. The Ostwald viscometer employed had a velocity-average shear-rate $\overline{|dv/dr|}_{vel} \equiv \Delta PR2/15\eta L$, (where ΔP = pressure drop, R = capillary radius, L = length of capillary, and η is the medium viscosity) of about 2060 sec^{-1}. At this shear rate, the observed η_{sp}/c is 23 dl/g, which lies somewhat above the curve of $\log(\eta_{sp}/c)$ vs. $(shear)^{\frac{1}{2}}$ found for calf thymus DNA by Frommer and Miller.[24] It may be inferred from their graph that this DNA has an η_{sp}/c at zero-shear in excess of 72.5 dl/g, perhaps as high as 90 dl/g. Using this estimate (72.5 dl/g) for η_{sp}/c at zero-shear, the molecular weight is estimated from the relation of Spatz and Crothers,[23]

$$M = 3.82\times10^4[\eta]_o^{1.4} \quad , \tag{115}$$

to be $M \simeq 15\times10^6$. Also the $S_{20,w}$ of Frommer and Miller's DNA is peaked at 26 corresponding to $M = 14.5\times10^6$. Taking the value $M = 15\times10^6$ for our calf thymus DNA, the estimated relaxation time is

$$\tau_1 = 14\times10^{-3}\,sec \quad , \tag{116}$$

which is slower by about a factor of two than was found here at 50°C.

Allowance for the higher temperature (50°C vs. 25°C) and concomitantly lower solvent viscosity (.56 cp vs. .89 cp) characterizing these studies (compared to those of Callis and Davidson) would be expected to bring the estimated τ quite close to the values observed here at 50°C. The lower ionic strength (.02 vs. .1) employed in the current studies might be expected to slow the rate of rotational relaxation as Wada has shown.[26] From Wada's results a slowing down by about 30% might be expected at 25°C, and presumably even less at higher temperatures. In view of the uncertainties involved in estimating the molecular weight and the different conditions prevailing in the two studies, the agreement between the relaxation times is satisfactory. Certainly, the dichroism (or birefringence) relaxation times are in principle the same as the ones appearing in the autocorrelation function of the depolarized component of the scattered light.

The two outstanding features of the T-dependence of the relaxation times are: (i) the maximum occurring in the relaxation times near T = 72°C and (ii) the failure of the relaxation times to decrease on the high T side of the transition to values well below those characterizing the native form on the low T side, despite a substantial decrease in the viscosity as T is raised through the transition. Such behavior clearly contradicts the predictions of the Rouse-Zimm[27,28] model as derived by Zimm. The expressions for the longest relaxation time in the "free-draining" and "non-free draining" limits are

$$\tau_1 = 6M\eta[\eta]_o/\pi^2RT \quad , \qquad (117a)$$

and

$$\tau_1 = M\eta[\eta]_o/.586RT(4.04) \quad , \qquad (117b)$$

respectively, where η is the solvent viscosity and R is the gas constant.

It is apparent that any decrease in either M or $[\eta]_o$ as the temperature is raised above T_M should lead to a decrease in τ_1, contrary to what was observed. Collapse of a rigid rod structure to random coils would also be expected to yield a much reduced relaxation time. Both the rigid rod and freely-jointed bead-spring models are inadequate to account for these data.

The near equality of rotational relaxation rates (above and below T_M) for molecules of such different character suggests that somewhat different mechanisms operate above and below T_M. On the high T side of the transition, the molecules might be expected to resemble closely the freely-jointed Kuhn segments of the Rouse-Zimm model. However, below T_M the rigidity to axial torsion of the molecule is not concordant with the free-jointing of the beads and springs essential to that model. It is probable that in a flexible, but still torsionally rigid, molecule the rotational Brownian motion about the long-axis of any segment is coupled to the end-over-end motion of the segments about their short-axes. Thus, the long-axial Brownian motion of a bent speedometer cable in a swimming pool will produce also some short-axis reorientations of some of the segments in the cable. The friction coefficient for spinning about the axis of the cable (or molecule) is rather low, and the motion is quite rapid. Some coupling of this rapid motion to the end-over-end reorientation of segments might be expected to enhance the rate of relaxation of the optical anisotropy (as the purely long-axis spinning will not do).

This torsional rigidity is distinct from flexibility or rigidity with respect to short axis bending. As the temperature is increased toward T_M the DNA melts locally, perhaps at bends, and the long-axis

Brownian motion is not propagated through those melted regions because they have lost their torsional rigidity. The rate of the long-axis diffusion will increase since the friction coefficients for the shortened rotating segments are smaller. Yet, because the torsional rigidity fails over a short distance, the long-axis rotations do not couple with the end-over-end short-axis rotations of distant segments, and it is therefore less effective in relaxing the fluctuations in segment orientations. At this point (near T_M) the rate of relaxation of the segment orientations has slowed to a minimum. Further melting completely decouples the long-axis from the end-over-end segment rotations, but the flexibility increase enables these latter motions to proceed slightly faster than before.

APPENDIX A: LEAST-SQUARES CALCULATION

The autocorrelation function for the experiments in this study is assumed to be of the general form,

$$C(nt) = A\exp(-an) + B\exp(-bn) + C \quad , \tag{A1}$$

where A,B,C are constants, n is an integer, t is the unit time interval, and $a = t/t_1$, $b = t/t_2$, where t_1, t_2 are the characteristic relaxation times. The weighted least-squares method then minimizes the function

$$\sum_{n=m}^{N} W_n[D_n - C(nt)]^2 \equiv S \quad , \tag{A2}$$

where W_n is the weighting factor of point n, D_n is the value of the nth point of the computed autocorrelation function, m,N are the initial and final points, respectively, in the region. To eliminate any complication arising from very fast relaxation processes, m was chosen such that mt > 250 microseconds.

If the initial guesses for the parameters A,B,C,a, and b are very close to the "true" values, we can expand Eq.(A1) in a Taylors series and retain only the first correction term,

$$C(nt) = C^o(nt) + \sum_{\alpha} \frac{\partial C(nt)}{\partial \alpha}\Big|_{\alpha=\alpha^o} \Delta\alpha \quad , \tag{A3}$$

where α is a generalized parameter, $C^o(nt)$ is C(nt) evaluated at the initial guess parameters, and $\Delta\alpha = \alpha' - \alpha^o$ is the difference between the initial guess and the first corrected value of the parameter. Substituting Eq.(A3) into Eq.(A2), minimizing the function S with respect to the

parameters α, and retaining only the first derivative terms, leads to the expression,

$$\sum_{n=m}^{N} W_n \left(D_n - C^o(nt) - \sum_{\alpha} \frac{\partial C(nt)}{\partial \alpha}\Big|_{\alpha=\alpha^o} \Delta\alpha \right) \left(\sum_{\beta} \frac{\partial C(nt)}{\partial \beta}\Big|_{\beta=\beta^o} \right) = 0 \quad . \tag{A4}$$

If we now define the vectors

$$(\underset{\sim}{R})_\alpha \equiv \Delta\alpha \quad , \tag{A5}$$

$$(\underset{\sim}{T})_\alpha \equiv \sum_{n=m}^{N} W_n [D_n - C^o(nt)] \frac{\partial C(nt)}{\partial \alpha}\Big|_{\alpha=\alpha^o} \quad , \tag{A6}$$

and the matrix

$$(\underset{\simeq}{G})_{\alpha\beta} \equiv \sum_{n=m}^{N} W_n \frac{\partial C(nt)}{\partial \alpha} \frac{\partial C(nt)}{\partial \beta}\Big|_{\substack{\alpha=\alpha^o \\ \beta=\beta^o}} \quad , \tag{A7}$$

we can write Eq.(A4) in the form

$$\underset{\sim}{T} = \underset{\simeq}{G}\underset{\sim}{R} \quad . \tag{A8}$$

Therefore, the value of the first corrected guess parameter α' is obtained by solving Eq.(A8) for $(\underset{\sim}{R})_\alpha$

$$\alpha^1 = \alpha^o + (\underset{\simeq}{G}^{-1}\underset{\sim}{T})_\alpha \quad . \tag{A9}$$

This procedure is repeated until the fractional change $\Delta\alpha/\alpha$ is less than some arbitrary value for all of the parameters.

Since A,B, and C are constants, we can obtain expressions for these parameters in terms of exp(-a) and exp(-b). Minimization of Eq.(A2) with respect to these parameters leads to the expressions,

$$A = \left[\sum_{n=m}^{N} W_n[D_n - B\exp(-bn) - C]\exp(-an)\right] \Big/ \sum_{n=m}^{N} W_n \exp(-2an) \quad , \tag{A10}$$

$$B = \left[\sum_{n=m}^{N} W_n[D_n - A\exp(-an) - C]\exp(-bn)\right] \Big/ \sum_{n=m}^{N} W_n \exp(-2bn) \quad , \tag{A11}$$

$$C = \left[\sum_{n=m}^{N} W_n(D_n - A\exp(-an) - B\exp(-bn)\right] \Big/ \sum_{n=m}^{N} W_n \quad . \tag{A12}$$

For given values of a and b, we can solve the set of simultaneous equations (A10) to (A12) for A, B, and C. On defining the quantities

$$F(1) \equiv \sum_{n=m}^{N} W_n \exp(-an) \quad , \tag{A13a}$$

$$F(2) \equiv \sum_{n=m}^{N} W_n \exp(-bn) \quad , \tag{A13b}$$

$$F(3) \equiv \sum_{n=m}^{N} W_n \quad , \tag{A13c}$$

$$F(4) \equiv \sum_{n=m}^{N} W_n D_n \quad , \tag{A13d}$$

$$F(5) \equiv \sum_{n=m}^{N} W_n \exp(-2nb) \quad , \tag{A13e}$$

$$F(6) \equiv \sum_{n=m}^{N} W_n D_n \exp(-an) \quad , \tag{A13f}$$

$$F(7) \equiv \sum_{n=m}^{N} W_n \exp(-na-nb) \quad , \tag{A13g}$$

$$F(8) \equiv \sum_{n=m}^{N} W_n \exp(-2na) \quad , \tag{A13h}$$

$$F(9) \equiv \sum_{n=m}^{N} W_n D_n \exp(-nb) \quad , \tag{A13i}$$

$$F(10) \equiv F(8)F(3) - [F(1)]^2 \quad , \tag{A13j}$$

$$F(11) \equiv F(8)F(9) - F(6)F(7) \quad , \tag{A13k}$$

$$F(12) \equiv F(4)F(8) - F(6)F(1) \quad , \tag{A13l}$$

$$F(13) \equiv F(1)F(7) - F(2)F(8) \quad , \tag{A13m}$$

and

$$F(14) \equiv F(8)F(5) - [F(7)]^2 \quad . \tag{A13n}$$

The quantities A, B, and C are

$$B = [F(10)F(11)+F(12)F(13)]/[F(14)F(10)-F(14)F(13)] \quad , \tag{A14}$$

$$A = [F(6)F(3)-F(4)F(1)]/F(10)-B[F(7)F(3)-F(2)F(1)]/F(10), \tag{A15}$$

and

$$C = [F(4)-AF(1)-BF(2)]/F(13) \quad . \tag{A16}$$

In the actual computation of the least-squares values of the parameters, the initial guess values for a and b were obtained from a semi-log plot of the computed autocorrelation function and the initial guess values for A, B, and C were computed from Eqs.(A14)-(A15). If the autocorrelation function appeared to be a single exponential, the rows and columns corresponding to the parameters B and b in Eq.(A9) were set equal to zero and, of course, B was set equal to zero in Eqs.(A15) and (A16).

It was found that some of the curves could not be fit to an equation of the form in Eq.(A1). After a few iterations, some of the parameters would obtain enormously large values. This is probably because the matrix $\underset{\sim}{G}$ was ill-conditioned.

For each curve that was fit by the least-squares method, the function

$$\sigma = [S/(N-m)]^{\frac{1}{2}} \quad , \qquad \text{(A17)}$$

was computed. The parameters obtained from the best least-squares fit were found to be reliable when $\sigma < 10^{-2}$.

APPENDIX B: MIXING WITH THE PRIMARY BEAM

When the analyzing polarizer is rotated away from the intensity minimum, then some of the primary beam is mixed with the scattered beam, resulting in an alteration of the correlation function of the phototube current. If ϕ is the angle by which the analyzer is rotated from the intensity minimum, then the transmitted electric field amplitude at the detector is just

$$E_\phi(R,t) = E_x(R,t)\cos\phi + E_z(R,t)\sin\phi \quad . \tag{B1}$$

The intensity is

$$I_\phi(t) = \frac{c}{4\pi}|E_\phi(R,t)|^2 =$$

$$\cos^2\phi I_x(t) + \sin^2\phi I_z(t) + \frac{2c}{4\pi}\cos\phi\sin\phi E_x^*(R,t)E_z(R,t) \quad , \tag{B2}$$

and its autocorrelation function is given by

$$\langle I_\phi(t)I_\phi(t+\tau)\rangle_t = \cos^4\phi\langle I_x(t)I_x(t+\tau)\rangle_t$$

$$+ \frac{4c^2}{16\pi^2}\cos^2\phi\sin^2\phi\langle E_x^*(R,t)E_x(R,t+\tau)E_z(R,t)E_z^*(R,t+\tau)\rangle_t$$

$$+ \sin^4\phi\langle I_z(t)I_z(t+\tau)\rangle_t + \cos^2\phi\sin^2\phi\langle I_x(t)I_z(t+\tau) + I_z(t)I_x(t+\tau)\rangle_t$$

$$+ \frac{2c}{4\pi}\cos^3\phi\sin\phi\langle I_x(t)E_x^*(R,t+\tau)E_z(R,t+\tau) + E_x^*(R,t)E_z(R,t)I_x(t+\tau)\rangle_t$$

$$+ \frac{2c}{4\pi}\cos\phi\sin^3\phi\langle I_z(t)E_x^*(R,t+\tau)E_z(R,t+\tau) + E_x^*(R,t)E_z(R,t)I_z(t+\tau)\rangle_t \quad . \tag{B3}$$

The last two averages rigorously vanish when the motions of the molecules responsible for the scattering are uncorrelated. Writing Eq.(66) as

$$I_x(t) = I_z(t)\frac{F}{(E_z^o)^2}\left(\sum_{J=1}^{N}\sum_{j=1}^{\mu}\cos\theta(t'_{Jj})\cos\chi(t'_{Jj})\right)^2 \quad , \tag{B4}$$

we find

$$I_\phi(t)I_\phi(t+\tau) = \cos^4\phi\langle I_z(t)I_z(t+\tau)\rangle_t\{A + \frac{8\pi}{30}F^2N(N-1)\mu^2M(\tau)^2\}$$

$$+ 4\cos^2\phi\sin^2\phi\langle I_z(t)I_z(t+\tau)\rangle_t\frac{FN\mu}{(E_z^o)^2}\frac{4\pi}{30}^{\frac{1}{2}}M(\tau)$$

$$+ \sin^4\phi\langle I_z(t)I_z(t+\tau)\rangle_t$$

$$+ 2\cos^2\phi\sin^2\phi\langle I_z(t)I_z(t+\tau)\rangle_t A^{\frac{1}{2}} \quad , \tag{B5}$$

where

$$M(\tau) \equiv \frac{4\pi}{30}^{\frac{1}{2}}\left\langle b^*_{2,1}(0)b_{2,1}(\tau)\right\rangle_{ens} - \mathrm{Re}\left\langle b^*_{2,1}(0)b_{2,-1}(\tau)\right\rangle_{ens} \quad . \tag{B6}$$

The term with $M(\tau)$ is the heterodyne term resulting from mixing the scattered beam with the primary beam, while the $M(\tau)$ term is the so-called homodyne term. When the molecular correlation function $M(\tau)$ is an exponential decay, then the heterodyne term will decay half as rapidly as the homodyne term.

REFERENCES

1. von Smoluchowski, Ann. d. Physik, 25, 205 (1908).
2. A. Einstein, Ann. d. Physik, 39, 789 (1912).
3. L. Brillouin, Compte Rend., 158, 1331 (1914).
4. L. Brillouin, Ann. Phys. (Paris), 17, 88 (1922)
5. R. Pecora, J. Chem. Phys., 40, 1604 (1964).
6. H.Z. Cummins, N. Knable, and Y. Yeh, Phys. Reve. LeHers, 12, 150 (1964).
7. F.T. Arecchi, M. Giglio, and V. Tartari, Phys. Rev., 163, 186 (1967).
8. M.J. French, J.C. Angus, and A.G. Walton, Science, 163, 345 (1969).
9. L. Blum and Z.W. Salsburg, J. Chem. Phys., 48, 2292 (1968).
10. J.M. Schurr, J. Phys. Chem., 73, 2820 (1969).
11. B.J. Berne, J.M. Deutsch, J.T. Hynes, and H.L. Frisch, J. Chem. Phys., 47, 3675 (1968).
12. Y. Yeh and R.N. Keeler, J. Chem. Phys., 51, 1120 (1969).
13. Y. Yeh, J. Chem. Phys., 52, 6218 (1969).
14. R. Pecora and W.A. Steele, J. Chem. Phys., 42, 1872 (1965).
15. A. Wada, N. Suda, T. Tsuda, and K. Soda, J. Chem. Phys., 50, 31 (1969).
16. S.B. Dubin, N.A. Clark, and G.B. Benedek, J. Chem. Phys., 54, 5158 (1971).
17. R. Pecora, J. Chem. Phys., 48, 4126 (1968).
18. T.J. Herbert, F.D. Carlson, and H.Z. Cummins, Biophys. J., 9, 518 (1969).
19. J.D. Jackson, Classical Electrodynamics, John Wiley and Son, Inc., N.Y., 1962, Chapt. 9.
20. J.A. Harpst, A.I. Krasna, and B.H. Zimm, Biopolymers, 6, 595 (1968).
21. D.C. Liebe and J.E. Stuehr, Biopolymers, 11, 167 (1972).
22. J. Eigner and P. Doty, J. Mol. Biol., 12, 549 (1965).

23. H. CH. Spatz and D.M. Crothers, J. Mol. Biol., 42, 191 (1969).

24. M.A. Frommer and I.R. Miller, Biopolymers, 6, 1461 (1968).

25. P.R. Callis and N. Davidson, Biopolymers, 8, 379 (1969).

26. A. Wada, Biopolymers, 2, 361 (1964).

27. P.E. Rouse, J. Chem. Phys., 21, 1272 (1953).

28. B.H. Zimm, J. Chem. Phys., 24, 269 (1956).